Cascade Hydrogenation of Carbon Dioxide to Methanol

by

Chelsea Ariane Huff

A dissertation submitted in partial fulfillment
of the requirements for the degree of
Doctor of Philosophy
(Chemistry)
in the University of Michigan
2014

Doctoral Committee:

Professor Melanie S. Sanford, Chair
Professor Adam J. Matzger
Assistant Professor Nathaniel K. Szymczak
Professor Levi T. Thompson

ACKNOWLEDGEMENTS

I am so fortunate to have been educated by such talented individuals while being a student at the University of Michigan. Melanie, you have been a constant source of encouragement for me. You have the unique ability to recognize each of your student's strengths and weaknesses, and you use that knowledge to inspire us to grow, truly bringing out the best in everyone that you mentor. I came to Michigan terrified of public speaking, but your unwavering belief in me has instilled me with the confidence I need to be successful not only in my career, but in life as well. Beyond this, having the chance to learn from your example on how to solve problems, present, write, and work with others has been an invaluable experience for me. I am so grateful for the past five years, and I know I could not have received a better education anywhere else. It's obvious that you care very much about all of your students, and I know that so much of your time goes towards helping us. So, I want to thank you, Melanie, for working so hard for all of us. You are a remarkable role model and truly exceptional at everything you do.

I would also like to thank my dissertation committee for their support, guidance, and time. Professor Matzger, thank you for letting me rotate in your group and bug you with questions about my research or job search every time I saw you in the hallway. You are always entertaining to talk to. Professor Szymczak, thank you for all of your helpful suggestions over the years. Professor Thompson, I appreciate all of your input on our collaboration—learning to think about chemistry from an engineer's perspective was very beneficial for me. I'd also like to thank Eugenio Alvarado for always taking the time to explain the details of the various NMR spectroscopy experiments that I ran. Jeff Kampf incredibly fast at solving X-ray crystal structures for me, and I want to thank him for all of his hard work. Roy Wentz spent many hours making all sorts of glass contraptions for my project that made my life much easier over the past five years, so I want to thank him for always being so friendly and willing to help me. I am also grateful to Tracy

Stevenson, Chris Peters, Laurie MacDonald, and Jon Boyd for their hard work in keeping the Chemistry building and the department running smoothly. The administrative staff has also helped me with various problems over the years, especially Margarita Bekiares, so I thank them for their help.

It has been a pleasure to work with everyone in the Sanford Lab. Marion, you were a mentor to me when I really needed guidance during my first years at Michigan. You helped me tremendously with setting up a challenging project and writing drafts for fellowship applications, candidacy documents, papers, etc. I am so grateful that you took an interest in mentoring me, and more than that, becoming one of my closest friends. Your continued encouragement and support even after you moved off to become a big professor means so much to me, so thank you for everything. Sharon, even though our research projects couldn't have been more different, I came to you time and again to discuss whatever problem I was having, and you always took the time to figure it out with me. You are one of the most logical and intelligent people that I have ever met—thank you for being an example of the kind of scientist I want to strive to be. Some of the best memories I have in Ann Arbor are from when we were just sitting in lab talking (or competing in nonexistent baking competitions), and I am grateful to be your friend. Deeps, I'm so thankful we somehow managed to overlap in the Sanford lab. You are one of the most genuinely kind, understanding, and funny people I know. You always make time for me when I need your help, and you are by far the best neighbor I have ever had :) Norman, even though you were constantly telling me puns, it was fun working with you on the same project this past year. You are a born problem solver and are always so generous with your time. I value your hard work, insights, and friendship, and I look forward to seeing all you will accomplish. Thomas, thank you for your input on my project and for always being cheerful in lab. Danielle and Yuan, it was a lot of fun working with both of you! I'd also like to acknowledge Brannon, Nick Deprez, Tom, Andrew, and Kara for being so welcoming and helpful to me when I first joined the group, as well as Kate, Anna, Tiffiny, Laura, Pablo, Naoko, and Amanda for always being there to talk to. I'd like to give additional thanks to Doug, BJ, and Jeff, as well as Dipa and Nomaan for editing thesis chapters. Lastly I want to thank a couple non-Sanfordians who have also been very instrumental in my progress—Jeff, I can't count the

number of times you have helped me over the past eight years. I don't think I would have passed thit brain class without you. You are loyal and generous, and I'm lucky to call you my friend. Thank you for always being there and for making me laugh. Sameer, thank you for always having time to talk about science and gossip with me. Let me know when you plan to move into the basement. Nathan, I think I still owe you a car for your fellowship services.

Prior to coming to Michigan, I was fortunate to have talented mentors who were instrumental in my scientific growth. Professor Zhang, working in your lab was such a positive early experience for me, and I have to thank you for giving me that opportunity and for inspiring me to further pursue chemistry as a career. Kimberly, I think I must have asked you at least one thousand questions while you were helping me figure out what I was doing in the lab. So thank you for being so patient and for being such a great teacher. Professor Veige, you always encouraged me to think independently, and I learned a lot of organometallic chemistry while working in your group. Thank you for letting me work in your lab and for not kicking me out after I flooded it. Matt, thank you being the best lab TA and for always believing in me and pushing me to be the best scientist I could be.

Finally, none of this would be possible without the love, concern, patience, and support of my family—my brother, Chad, and especially my parents, Carla and Dave. I know that I could not have come this far without the both of you. Mom, thank you for believing in me and for doing whatever you could to help me be successful. Dad, you were always a role model of remarkable work ethic and enthusiasm for solving problems. Thank you for instilling that attitude in me. Joe, you are always there for me when I need you and you have made our time in Ann Arbor a happy one. Thank you for being a part of my life and for always encouraging me to try new things.

TABLE OF CONTENTS

LIST OF SCHEMES

LIST OF FIGURES

LIST OF TABLES

LIST OF ABBREVIATIONS

18-crown-6	1,4,7,10,13,16-hexaoxacyclooctadecane
anisole	methoxybenzene
BET	Brunauer–Emmett–Teller
DMSO	dimethylsulfoxide
DMF	*N,N*-dimethylformamide
dppe	diphenylphosphinoethane
EF	ethyl formate
EtOH	ethanol
FA	formic acid
HMBC	heteronuclear multiple bond correlation)
HMDSO	hexamethyldisiloxane
HSQC	heteronuclear single quantum coherence spectroscopy
ICP	inductively coupled plasma
K_{eq}	equilibrium constant
KO*t*Bu	potassium *tert*-butoxide
HCOOMe	$HCOOCH_3$ or methyl formate
nacnac	β-diketiminate
NEt_3	triethylamine
$NHMe_2$	dimethylamine
NMR	nuclear magnetic resonance
NOE	Nuclear Overhauser effect
NOESY	Nuclear Overhauser effect spectroscopy
ORTEP	Oak Ridge thermal ellipsoid plot
OAc	acetate or CH_3COO

OTf	trifluoromethanesulfonate or CF_3SO_3
ppm	parts per million
PNN	6-(di-*tert*-butylphosphinomethylene)-2-(*N*,*N*-diethylaminomethyl)-1,6-dihydropyridine
PNP	2,6-bis(diisopropylphosphinomethylene)pyridine
RPM	rotations per minute
THF	tetrahydrofuran
TON	turnover number
TMS	tetramethylsilane
XRD	X-ray diffraction

ABSTRACT

CO_2 is an abundant C1 building block that has the potential to be utilized in the synthesis of many commodity chemicals and fuels that are currently derived from fossil feedstocks. Methanol in particular is produced annually on a multimillion metric ton scale, primarily from CO/H_2 at elevated temperatures (240–260 ºC). However, because the hydrogenation of CO_2 is entropically unfavorable, the ability to operate at lower reaction temperatures is expected to lead to an overall higher theoretical yield of methanol. Herein we report the use of homogeneous catalysts in tandem for the hydrogenation of CO_2 to CH_3OH at substantially lower temperatures (135 ºC).

Chapter 2 details the first system established for the direct homogeneous hydrogenation of carbon dioxide to methanol. A combination of ruthenium and scandium catalysts are employed to undergo the one pot stepwise reduction of CO_2 to formic acid, methyl formate, and finally methanol. Incompatibilities between catalysts and cascade system components are introduced and are further evaluated in detail in later chapters.

Chapter 3 describes potential deactivation pathways involving components of the cascade system with the Ru pincer ester hydrogenation catalyst applied in the cascade system. A new mode of activation of CO_2 and carbonyl compounds (esters, ketones, and aldehdyes) by this Ru pincer complex is discussed. Additionally, the relevance of these organometallic compounds under cascade catalysis conditions is studied.

Chapter 4 explores the idea of using a single catalyst for the cascade conversion of CO_2 to CH_3OH. A Ru pincer complex is tested for the CO_2 conversion to formate salts where the mechanism is investigated and catalytic conditions are established. Furthermore, these conditions are applied to a second-generation cascade system comprised of formate salt and amide intermediates, where the later is reduced to CH_3OH using a single catalyst.

Chapter 5 describes the application of heterogeneous catalysis for low temperature CO_2 conversion to methanol in the ester intermediate cascade system. In order to enhance the rate of the slow step while using heterogeneous catalysts at lower temperatures, homogeneous catalysts are added to the tandem system. Previously reported heterogeneous catalysts are explored, in addition to unprecedented Mo_2C based catalysts.

CHAPTER 1

Introduction

1.1 CO_2 Mitigation: A Challenge for the Twenty-First Century

Global demand for energy is increasing rapidly as a result of population and economic growth. Currently, the majority of energy in the United States is supplied by combustion of coal, crude oil, and natural gas as shown in Figure 1.1.[1] However, a consequence of burning fossil feedstocks for energy is that carbon dioxide (CO_2), the dominant combustion waste product, is emitted into the atmosphere. CO_2 emissions resulting from energy consumption alone (accounting for 70% of all CO_2 emitted)[2] increased from 2.2 to 5.5 million metric tonnes of CO_2 per year from 1949 in 2011,[1] and the atmospheric CO_2 concentration is currently about 400 ppm (parts per million), which is more than 100 ppm above the maximum values measured over the past 740,000 years.[3]

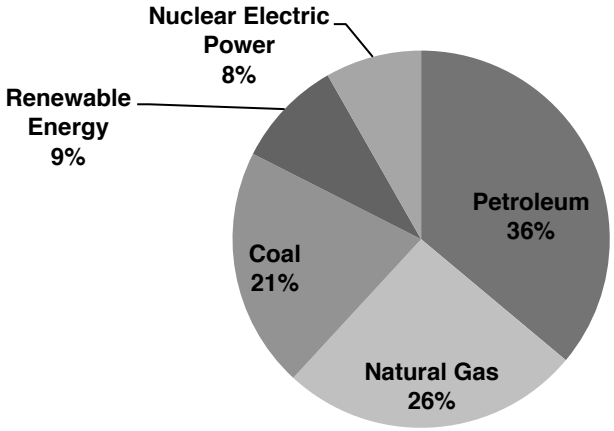

Source: U.S. Energy Information Administration (2011)

Figure 1.1. U.S. Energy Consumption Estimates by Source in 2011

One consequence of increased atmospheric concentrations of greenhouse gases (e.g. CO_2, CH_4) is a rise in the temperature at the Earth's surface due to the global

warming effect. This surface warming has resulted in an increase in the average ocean temperature by 0.74 ºC and in the sea level by 17 cm over the past 100 years.[4] Furthermore, over the past 200 years, or since pre-industrial times, seawater has absorbed approximately half of all anthropogenic CO_2 emissions.[5] As a result of the reaction between CO_2 and water to form carbonic acid (H_2CO_3), a reduction in seawater acidity by 0.1 pH units has been observed during the 20th century.[4] Effectively, this continued acidification is expected to severely decrease coral calcification and reef growth.[3] With energy-related global CO_2 emissions projected to increase from 31.6 Gt in 2011 to 62 Gt in 2050,[2] there is urgent need to reduce the concentration of CO_2 in the atmosphere. Developing more efficient ways to use our energy resources will play a role in mitigating CO_2 emissions, but more drastic measures to reduce atmospheric CO_2 on a large scale will be necessary. The leading approaches to achieve this are developing: i) carbon-neutral renewable energy technologies and ii) methods for CO_2 sequestration and storage.

1.2 Routes Toward Reducing CO_2 Emissions

1.2.1 Renewable Energy Economy

Of the total energy currently consumed in the U.S. every year, about 9% is produced by renewable energy sources (Figure 1.1). By the year 2040, renewable energy will play a larger role in energy generation, as this value is expected to increase to 13%, coupled with a 4% decrease in petroleum-derived fuel.[6] Leading examples of renewable energy technologies are solar, wind power, biomass, geothermal energy, and hydropower (Figure 1.2). For U.S. electricity generation specifically, solar generation[7] capacity is projected to lead to renewable energy growth, increasing by more than 1,000% by the year 2040. Wind capacity[8] is also expected to play an important role in expanding the renewable energy economy, accounting for 42 gigawatts of the energy capacity.[6]

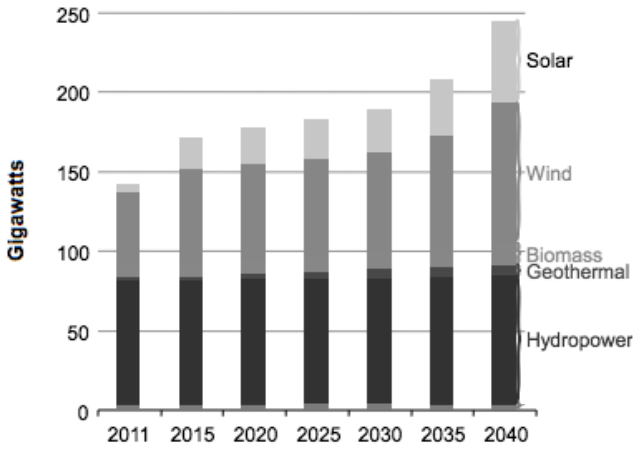

Figure 1.2. Renewable Electricity Generation Capacity by Energy Source in the U.S., 2011–2040. Preprinted with permission from U.S. Energy Information Association (2013).

Fundamental science is key in establishing technologies for energy production relying on solar energy. However, one challenge in shifting to a fundamentally different energy economy is that users and providers have a set of challenges in implementing the growing assortment of new renewable sources. For example, solar and wind energy are irregular and unpredictable; therefore, heavy reliance on these sources of energy would require a storage method for later use during times of intermittency.[9] Furthermore, with renewable energy developments comes the complimentary demand for technology to create new energy distribution methods and to integrate new energy sources into existing grids.[10] Progress is being made on all fronts, but the transition to renewable energy economy is expected to be gradual, due to the time required to develop and implement new technologies.

1.2.2 CO_2 Sequestration and Storage

While transitioning over to a renewable energy economy, energy-related CO_2 emissions, in addition to industrial CO_2 emissions (e.g. cement plants), will have to be managed. CO_2 capture from transportation emissions is costly since the atmospheric concentration is relatively low, so for this sector an alternative fuel that is carbon free (i.e. H_2) should be considered. A more practical sector to implement widespread CO_2 capture is electricity-generating power plants, which are responsible for 40% energy-related CO_2

emissions.

Chemical absorption is the most widely used technique for low pressure CO_2 capture, where CO_2-containing gas streams are passed over a liquid (amine or aqueous NaOH and Na_2CO_3 slurries) that forms chemical bonds with CO_2.[11] The primary challenge associated with these materials is that heating up to 200 ºC is required to break the bonds between CO_2 and the absorbent. Alternatively, solid absorbents like metal organic frameworks[12] typically have weaker interactions with CO_2 and are often treated with pressurized streams of CO_2 to yield effective interactions at the surface of the material. Alternatively, solid absorbents like zeolites[13] are operational at lower pressures of CO_2, however due to their hydrophilic nature, CO_2 capacity declines in the presence of water, and high regeneration temperatures are required.[14] Overall, CO_2 capture technologies require energy (either in the form of pressure or heating) that reduce the overall efficiency of a process and adds cost, where typical efficiency losses are around 6–12% for the CO_2 capture process.[2] To this end, to make these processes economically viable on a large scale, technology development for CO_2 sequestration and incentives for reducing CO_2 emissions will be necessary to offset the costs associated with these capture methods.

After CO_2 has been captured, storage of this gas must be considered as well. Cooling and compressing CO_2 for long-term underground storage is a technology that has already been implemented. Injection of liquid CO_2 into reservoirs in order to displace and mobilize oil is a process in Texas and currently consumes approximately 20 million tons/year of CO_2.[15] However, a series of earthquakes in Texas are thought to be linked to these CO_2 injections into the oil and gas wells.[16] Furthermore, the energy requirements to cool, compress, as well as transfer CO_2 from the site of generation to the storage site, are large. An alternative CO_2 "storage" approach is to retain CO_2 using chemical bonds. CO_2 can be thought of as a carbon building block to synthesize more valuable chemicals.[17] As an abundant and cheap C1 feedstock, exploring synthetic routes toward producing commodity chemicals and fuels on a wide scale could provide an economic driving force to capture CO_2, as well as solve storage issues. One such potential commodity chemical is CH_3OH, and the feasibility of this process will be discussed in detail herein.

1.3 Hydrogenation of CO_2 to CH_3OH

1.3.1 Potential for Industrial Synthesis

Methanol (CH_3OH) is a commodity chemical with a current annual global demand of 30 million metric tonnes, serving mainly as a chemical feedstock.[18] Predominately synthesized from methane-derived synthesis gas (syngas), or carbon monoxide (CO) and hydrogen (H_2), this reaction (equation 1) requires elevated temperatures between 220–270 ºC and pressures 50–100 bar with a Cu heterogeneous catalyst. The mechanism of this reaction is highly debated in the literature. One putative route is the direct hydrogenation of CO to CH_3OH (equation 1). Alternatively, CO_2 is debated to play an important mechanistic role in this reaction.[19] Cu catalysts used for this reaction also catalyze the water gas shift reaction (equation 2) at these temperatures, where CO and H_2O[20] are converted to CO_2 and H_2. Furthermore, the addition of 2–8% CO_2 to the synthesis gas feed has been found to improve the performance of the catalyst.[21]

$$CO + 2H_2 \rightarrow CH_3OH \quad (1)$$

$$CO + H_2O \rightarrow CO_2 + H_2 \quad (2)$$

$$CO_2 + 3H_2 \rightarrow CH_3OH + H_2O \quad (3)$$

There is also precedent for synthesizing CH_3OH from CO_2 and H_2 (equation 2) using similar Cu catalysts. A pilot plant based on this system was built for this reaction using a $Cu/Al_2O_3/ZnO/ZrO_2/Ga_2O_3$ heterogeneous catalyst at 250 ºC, thus demonstrating the viability for this process.[22] The primary obstacle in implementing this process is the current operational methanol synthesis method using syngas is more economically attractive compared to that using CO_2 as a starting material.

1.3.2 Alternative Approach: Homogeneous Catalysis

In considering ways to improve the efficiency of the CO_2 hydrogenation to CH_3OH, the thermodynamics of equation 2 were examined. This reaction is entropically disfavored with $\Delta S^o = -97.8$ calmol^{-1}K^{-1}. Therefore, operating at high temperatures with a negative entropy magnifies a negative $T\Delta S$ term, disfavoring the reaction overall, where $\Delta G^o = \Delta H^o - T\Delta S^o$. This unfavorable effect on the reaction can further be demonstrated

by considering the equilibrium constant at 250 ºC where K_{eq} = 1 x 10^{-8}. Therefore, it is desirable to conduct this reaction at lower temperatures in order to achieve an overall higher theoretical yield of methanol. Using reported heterogeneous catalysts, reducing the temperature below 220 ºC is kinetically undesirable.

In order to address this challenge, homogeneous catalysis can be considered for this reaction, as these systems often operate at lower temperatures. Additional advantages of homogeneous complexes as catalysts include their versatility and tunability through the use of diverse ancillary ligands as well as the ability to study the mechanism of reactivity on a molecular level. Toward this end, notable advances have been made to reduce CO_2 to CH_3OH at room temperature using homogeneous organocatalysts and metal complexes.[23–26] However, these catalytic methods typically require expensive reducing reagents such as hydrosilanes and boron hydrides that produce stoichiometric byproducts. In contrast, we were interested in developing a system using H_2 for this homogeneously catalyzed reaction. This dissertation will explore a cascade approach using homogeneous catalysis for CO_2 hydrogenation to methanol (Chapter 2),[27] and will demonstrate a mechanistic understanding of this system (Chapter 3 and 4)[28–30] where these findings are used to improve the overall cascade system (Chapter 4). Lastly, highlighting the benefits of using both homogeneous and heterogeneous catalysis, a cascade system utilizing both of these types of catalysts for low temperature methanol synthesis is explored (Chapter 5).

1.4 Potential Impact of CO_2 Conversion to CH_3OH and Other Chemicals

In addition to providing an environmentally safe outlet for CO_2 emissions, methanol produced from CO_2 could also function as a carbon neutral liquid fuel. If methanol was synthesized from CO_2 that is captured from the atmosphere and H_2 derived from solar[7] or wind-driven[8] water splitting, the overall process would be carbon-neutral.[31] Methanol is an energy-dense combustible liquid with a high octane number of 100, and is an excellent hydrogen storage material (containing 12.6 wt% H_2). In addition to being used as a transportation fuel, methanol can also be used in fuel cells where applicable low temperature aqueous methanol dehydrogenation catalysts have been reported.[32]

The current leading industrial process using CO_2 is the synthesis of urea, which consumes 70 million metric tonnes of CO_2 per year.[33] Moving forward, identifying more processes where CO_2 can be implemented as a feedstock, as in the production of CH_3OH, will be important for establishing more routes toward mitigating CO_2 emissions. Importantly, more companies are currently looking to make plastics, plasticizers, additives fuels and other chemicals;[34] specifically BASF and Linde are unveiling an industrial process to use CO_2 and CH_4 to synthesize CO and H_2 in 2015.[35]

1.5 References

1. Environment. Annual Energy Review 2011. U. S. Energy Information Administration, 2011, pp 302.

2. CO_2 capture and storage: A Key Carbon Abatement Option. International Energy Agency, 2008.

3. Hoegh-Guldberg, O.; Mumby, P. J.; Hooten, A. J.; Steneck; R. S.; Greenfield, P.; Gomez, E.; Harvell, C. D.; Sale, P. F.; Edwards, A. J.; Caldeira, K.; Knowlton, N.; Eakin, C. M.; Iglesias-Prieto, R.; Muthiga, N.; Bradbury, R. H.; Dubi, A.; Hatziolos, M. E. Coral Reefs Under Rapid Climate Change and Ocean Acidification. *Science* **2007**, *318*, 1737.

4. IPCC, Climate Change 2007: The Physical Science Basis. Contribution of Working Group I to the Fourth Assessment Report of the Intergovernmental Panel on Climate Change. Solomon, S. et al., Eds., Cambridge Univ. Press, Cambridge, UK, and New York, 2007.

5. Ocean Acidification Due to Increasing Atmospheric Carbon Dioxide. Raven, J. et al., Eds., Royal Society 2005.

6. International Energy Outlook 2013. U.S. Energy Information Administration, 2013.

7. (a) Kudo, A.; Miseki, Y. Heterogeneous Photocatalyst Materials for Splitting Water. *Chem. Soc. Rev.* **2009**, *38*, 253; (b) El Chaar, L.; Iamont, L. A.; El Zein, N. Review of Photovoltaic Technologies. *Renew. Sust. Energ. Rev.* **2011**, *5*, 2165.

8. Zervos, A.; Kjaer, B. "Pure Energy. Wind Energy Scenarios up to 2030," European Wind Energy Association, 2008.

9. Lewis, N. S.; Nocera, D. G. Powering the Planet: Chemical Challenges in Solar Energy Utilization. *P. Natl. Acad. Sci. USA*, **2006**, *103*, 15729.

10. Liserre, M.; Sauter, T.; Hung, J. Y. Future Energy Systems: Integrating Renewable Energy Sources into the Smart Power Grid through Industrial Electronics. March 2010 IEEE Industrial Electronics Magazine, **2010**, *4*, 18.

11. Spigarelli, B. P.; Kawatra, S. K. Opportunities and Challenges in Carbon Dioxide Capture. *J. CO_2 Util.* **2013**, *1*, 69.

12. Liu, J.; Thallapally, P. K.; McGrail, B. P.; Brown, D. R.; Liu, J. Progress in Adsorption-Based CO_2 Capture by Metal-Organic Framworks. *Chem. Soc. Rev.* **2012**, *41*, 2308.

13. Bae, T.-H.; Hudson, M. R.; Mason, J. A.; Queen, W. L.; Dutton, J. J.; Sumida, K.; Micklash, K. J.; Kaye, S. S.; Brown, C. M.; Long, J. R. Evaluation of Cation-Exchanged Zeolite Adsorbents for Post-Combustion Carbon Dioxide Capture. *Energy Environ. Sci.* **2013**, *6*, 128.

14. Yu, C.-H.; Huang, C.-H.; Tan, C.-S. A Review of CO_2 Capture by Absorption and Adsorption. *Aerosol Air Qual. Res.*, **2012**, *12*, 745.

15. Lackner, K. S. A Guide to CO_2 Sequestration. *Science* **2003**, *300*, 1677.

16. Gan, W.; Frohlich, C. Gas injection may have triggered earthquakes in the Cogdell oil field, Texas. *P. Natl. Acad. Sci. USA*, **2013**, *110*, 18786.

17. Sakakura, T.; Choi, J.-C.; Yasuda, H. Transformation of Carbon Dioxide *Chem. Rev.*, **2007**, *107*, 2365.

18. Methanol Utilisation Technologies. In *Methanol: The Basic Chemical and Energy Feedstock of the Future: Asinger's Vision Today.* Bertau, M.; Offermanns, H.; Plass, L.; Schmidt, F.; Wernicke, H.-J., Eds.; Wiley, 2014, pp. 327.

19. Grabow, L. C.; Mavrikakis, M. Mechanism of Methanol Synthesis on Cu through CO 2and CO Hydrogenation. *ACS Catal.* **2011**, *1*, 365.

20. Industrial grade synthesis gas contains H_2O as an impurity.

21. Lee, S. Methanol Synthesis from Syngas. In *Handbook of Alternative Fuel Technologies*. CRC Press, 2007, pp 297.

22. Ushikoshi, K.; Moria, K.; Watanabe, T.; Takeuchi, M.; Saito, M. A 50 kg/day Class Test Plant for Methanol Synthesis from CO2 and H2. *Stud. Surf. Sci. Catal.* **1998**, *114*, 357.

23. For examples of stoichiometric reduction of CO_2 to CH_3OH mediated by frustrated Lewis base pairs, see: (a) Ashley, A. E.; Thompson, A. L.; O'Hare, D. Non-Metal-Mediated Homogeneous Hydrogenation of CO_2 to CH_3OH. *Angew. Chem., Int. Ed.* **2009**,

48, 9839. (b) Ménard, G.; Stephan, D. W. Room Temperature Reduction of CO_2 to Methanol by Al-Based Frustrated Lewis Pairs and Ammonia Borane. *J. Am. Chem. Soc.* **2010**, *132*, 1796; For a review, see: (c) Stephan, D. W.; Erker, G. Frustrated Lewis Pairs: Metal-Free Hydrogen Activation and More. *Angew. Chem., Int. Ed.* **2010**, *49*, 46.

24. For catalytic reduction of CO_2 to CH_3OH with borane reducing agents, see: (a) Chakraborty, S.; Zhang, J.; Krause, J. A.; Guan, H. An Efficient Nickel Catalyst for the Reduction of Carbon Dioxide with a Borane. *J. Am. Chem. Soc.* **2010**, *132*, 8872. (b) Huang, F.; Zhang, C.; Jiang, J.; Wang, Z.-X.; Guan, H. How Does the Nickel Pincer Complex Catalyze the Conversion of CO_2 to Methanol Derivative? A Computational Mechanistic Study. *Inorg. Chem.* **2011**, *50*, 3816.

25. For catalytic reduction of CO_2 to CH_3OH with silane reducing agents, see: (a) Eisenschmid, T. C.; Eisenberg, R. The Iridium Complex Catalyzed Reduction of Carbon Dioxide to Methoxide by Alkylsilanes. *Organometallics* **1989**, *8*, 1822. (b) Riduan, S. N.; Zhang, Y.; Ying, J. Y. Conversion of Carbon Dioxide into Methanol with Silanes over *N*-Heterocyclic Carbene Catalysts. *Angew. Chem. Int. Ed.* **2009**, *48*, 3322; (c) Huang, F.; Lu, G.; Zhao, L.; Li, H.; Wang, Z.-X. The Catalytic Role of *N*-Heterocyclic Carbene in a Metal-Free Conversion of Carbon Dioxide into Methanol: A Computational Mechanism Study. *J. Am. Chem. Soc.* **2010**, *132*, 12388.

26. For other examples of homogeneous catalytic CO_2 reduction, see: (a) Laitar, D. S.; Müller, P.; Sadighi, J. P. Efficient Homogeneous Catalysis in the Reduction of CO_2 to CO. *J. Am. Chem. Soc.* **2005**, *127*, 17196. (b) Matsuo, T.; Kawaguchi, H. From Carbon Dioxide to Methane: Homogeneous Reduction of Carbon Dioxide with Hydrosilanes Catalyzed by Zirconium-Borane Complexes. *J. Am. Chem. Soc.* **2006**, *128*, 12362. For reviews, see: (c) Riduan, S. N.; Zhang, Y. Recent Developments in Carbon Dioxide Utilization under Mild Conditions. *Dalton Trans.* **2010**, *39*, 3347. (d) Darensbourg, D. J. Chemistry of Carbon Dioxide Relevant to Its Utilization: A Personal Perspective. *Inorg. Chem.* **2010**, *49*, 10765.

27. Excerpts of Chapter 2 reprinted with permission from Huff, C. A.; Sanford, M. S. Cascade Catalysis for the Homogeneous Hydrogenation of CO_2 to Methanol. *J. Am. Chem. Soc.* **2011**, *133,* 18122. Copyright 2011. American Chemical Society.

28. Excerpts of Chapter 3 reprinted with permission from Huff, C. A.; Kampf, J. W.; Sanford, M. S. Role of a Noninnocent Pincer Ligand in the Activation of CO_2 at (PNN)Ru(H)(CO). *Organometallics* **2012**, *31*, 4643. Copyright 2012. American Chemical Society.

29. Huff, C. A.; Kampf, J. W.; Sanford, M. S. Reversible Carbon-Carbon Bond Formation Between Carbonyl Compounds and a Ruthenium Pincer Complex. *Chem. Commun.* **2013**, *49*, 7147. – Reproduced by permission of The Royal Society of Chemistry. **http://pubs.rsc.org/en/content/articlelanding/2013/cc/c3cc43517b**

30. Excerpts of Chapter 4 reprinted with permission from Huff, C. A.; Sanford, M. S. Catalytic CO_2 Hydrogenation to Formate by a Ruthenium Pincer Complex. *ACS Catal.* **2013**, *3*, 2412. Copyright 2013. American Chemical Society.

31. Olah, G. A.; Goeppert, A.; Prakash, G. K. S. Chemical Recycling of Carbon Dioxide to Methanol and Dimethyl Ether: From Greenhouse Gas to Renewable, Environmentally Carbon Neutral Fuels and Synthetic Hydrocarbons. *J. Org. Chem.* **2009**, *74*, 487.

32. Nielsen, M.; Alberico, E.; Baumann, W.; Drexler, H.-J.; Junge, H.; Gladiali, S.; Beller, M. Low-Temperature Aqueous-Phase Methanol Dehydrogenation to Hydrogen and Carbon Dioxide. *Nature* **2013**, *495*, 85.

33. Joó, F. Activation of Carbon Dioxide. In Physical Inorganic Chemistry: Reactions, Processes, and Applications; Wiley-VCH: Weinheim, Germany, 2007; pp 252.

34. Scott, A. Carbon Dioxide-to-Chemical Processes Poised for Commercialization. *Chemical and Engineering News.* **2013**, *91*, 20.

35. Research Cooperation Develops Innovative Technology for Environmentally Sustainable Syngas Production from Carbon Dioxide and Hydrogen. BASF Press Release. July 2, 2013.

CHAPTER 2

Cascade Homogeneous Hydrogenation of Carbon Dioxide to Methanol

2.1 Introduction

Copper derived heterogeneous catalysts are well-known to promote the hydrogenation of CO_2 to CH_3OH at elevated temperatures ranging from 240–260 ºC.[1] However, since this reaction is entropically unfavorable ($\Delta S^o = -97.8$ calmol^{-1}K^{-1})[2], it would be desirable to carry out this transformation at lower reaction temperatures. This is expected to lead to an overall higher theoretical yield of CH_3OH.

Homogeneous catalysts typically operate at lower temperatures and are thus expected to realize more favorable reaction conditions. Additional advantages of homogeneous complexes as catalysts include: i) their versatility and tunability through the use of diverse ancillary ligands and ii) the ability to study the mechanism of reactivity on a molecular level. Toward this end, notable advances have been made in the reduction of CO_2 to CH_3OH at room temperature using homogeneous organocatalysts and Ni complexes, yielding turnover numbers (TONs) up to 1,840 (Scheme 2.1).[3–6] However, these catalytic methods typically require expensive reducing reagents such as hydrosilanes and boron hydrides that produce stoichiometric byproducts (Scheme 2.1, R). In contrast, exploration of the most atom-economical reductant, hydrogen (H_2), for this homogeneously catalyzed reaction has been limited.

Scheme 2.1. Catalytic Reduction of CO_2 to CH_3OH Using Silanes and Boranes

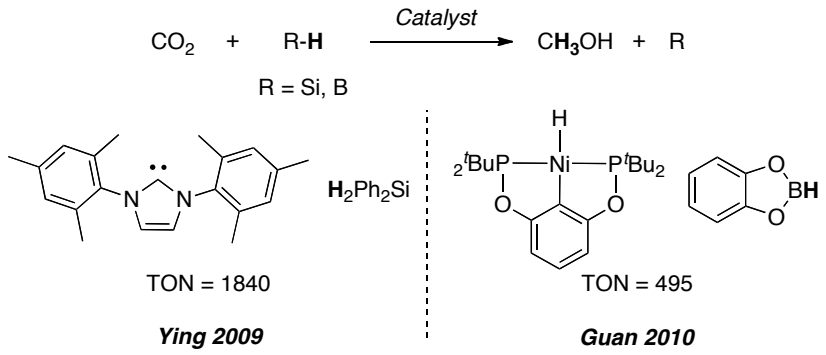

2.2 Multi-Catalyst Cascade System Design

Aiming to design a single homogeneous catalyst to facilitate the multi-step reduction of CO_2 to CH_3OH is a challenging goal such that the catalyst would have to perform numerous different proton and electron transfers throughout the reaction (Scheme 2.2). Instead, our approach was to investigate multiple catalysts for each individual step of the reaction. This would allow for catalyst design and optimization for each individual step in the reaction cascade.

Scheme 2.2. Multi-Step CO_2 Reduction to CH_3OH

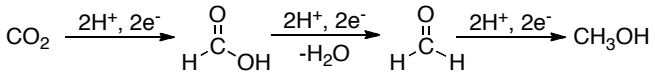

In order to implement this approach, we aimed to first devise a chemical route from CO_2 and H_2 to CH_3OH. As a first step, we envisioned hydrogenating CO_2 to formic acid (FA) using a metal catalyst (Scheme 2.3a). There are many metal catalysts reported for this reaction,[2,7] but because this reaction is thermodynamically uphill (ΔG^o = 7.8 kcalmol^{-1})[2], a base is required to drive the reaction to completion through the exothermic formation of a formate salt (Scheme 2.3b).[2] However, subsequent hydrogenation of the formate salt is not well precedented.

Scheme 2.3. CO_2 Hydrogenation to Formic Acid and Formate Salt

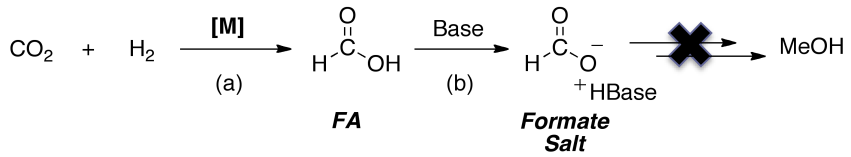

In order to address this challenge, we aimed to couple the hydrogenation of CO_2 to FA (Scheme 2.4, step i) with an exothermic esterification reaction catalyzed by **B** (Scheme 2.4, step ii), forming a formate ester. This ester could then be hydrogenated using catalyst **C** and H_2 to generate CH_3OH and the corresponding ester-derived alcohol (ROH, Scheme 2.4, step iii). This three-step reaction cascade should be carried out in one pot such that thermodynamically disfavored FA can be trapped and react further *in situ*. Importantly, this system should enable tuning of the rate and selectivity of each step simply by modifying catalyst **A**, **B**, and **C** independently.

Scheme 2.4. Cascade Hydrogenation of CO_2 to CH_3OH

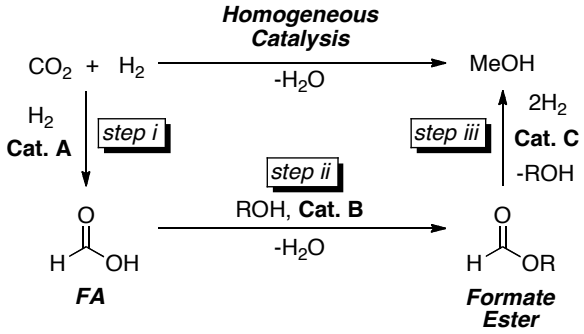

2.3 Optimization of Individual Steps

2.3.1 Steps i/ii: Cascade CO_2 Hydrogenation/Esterification

There are highly efficient established homogeneous catalysts for the conversion of CO_2 to methyl formate (HCO_2CH_3) (Scheme 2.4, steps i-ii) with TONs up to 13,000.[2] However, these systems require supercritical CO_2 (130 bar) as the solvent. Using relatively lower pressures of CO_2 in our system would be beneficial for mitigating potential incompatibilities of CO_2 with other components in the cascade system (see Section 2.3.2).

At 10 bar CO_2 and 30 bar H_2, the most active reported catalysts were selected and compared under identical conditions. As shown in Table 2.1, under neutral thermal esterification conditions, catalysts **A-1**–**A-3**[8–10] yielded modest quantities of methyl formate (entries 1–3). The TONs in these systems could be improved by the addition of triethylamine (NEt_3), a base that is commonly used to provide a thermodynamic driving force for CO_2 hydrogenation through the formation of the alkyl ammonium formate salt. Catalysts **A-2** and **A-3** worked the best under basic conditions, yielding a TON of 21 (entries 5–6). However, ester formation was slow under these thermal conditions, and **A-1**/NEt_3 and **A-3**/NEt_3 each afforded only two or three turnovers after 1 h (entries 7–8).

Table 2.1. Conversion of CO_2 to HCO_2CH_3: Thermal Esterification

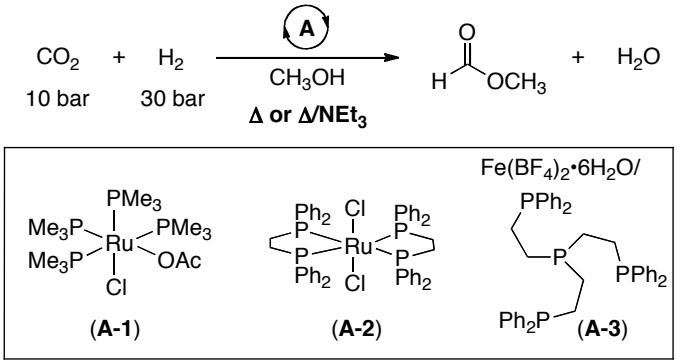

Entry[a]	Catalyst A/Additive	TON
1	**A-1**/none	3
2	**A-2**/none	1
3	**A-3**/none	10
4[b]	**A-1**/NEt_3	18
5[b]	**A-2**/NEt_3	21
6[b]	**A-3**/NEt_3	21
7[b,c]	**A-1**/NEt_3	3
8[b,c]	**A-3**/NEt_3	2

Conditions: [a]0.0126 mmol of catalyst **A**, 2 mL of CH_3OH, 16 h, 135 °C. [b]0.2 mL NEt_3 was added under otherwise identical conditions. [c]1 h.

It is well known that both Brønsted[11] and Lewis acid[12] catalysts can accelerate the esterification of carboxylic acids with alcohols. It follows that such catalysts might also prove advantageous for the formation HCO_2CH_3 from CO_2. A number of esterification

catalysts were tested for compatibly with catalysts for step i, including: $Sc(OTf)_3$, $Y(OTf)_3$, TsOH (*p*-toluenesulfonic), $SmCl_3$, $AlCl_3$, ZnO, ionic liquids,[13] and $CuCl_2$, where the most successful results re discussed below. As shown in Table 2.2, catalysts **A1**–**A3** were combined with TsOH (tosylic acid, **B-1**) and $Sc(OTf)_3$ (OTf = trifluoromethylsulfonate, **B-2**). Gratifyingly, the combination of $Ru(PMe_3)_4(Cl)(OAc)$ (**A-1**) and $Sc(OTf)_3$ (**B-2**) provided significantly enhanced TONs relative to the thermal and/or base-promoted reactions (TON = 40 vs 3 and 18, respectively). This **A-1**/**B-2** cascade reaction was also significantly faster than the NEt_3-promoted esterification, with a TON of 32 after 1 h at 135 ºC (entry 7).

Table 2.2. Conversion of CO_2 to HCO_2CH_3: Acid Catalyzed Esterification

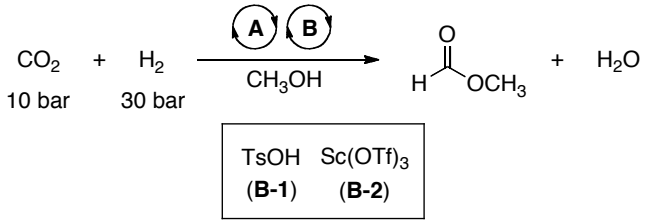

Entry[a]	Catalyst A/Additive	TON
1	**A-1/B-1**	11
2	**A-2/B-1**	10
3	**A-3/B-1**	13
4	**A-1/B-2**	40
5	**A-2/B-2**	16
6	**A-3/B-2**	5
7[b]	**A-1/B-2**	32

Conditions: [a]0.0126 mmol of catalyst **A** and **B**, 2 mL of CH_3OH, 16 h, 135 ºC. [b]1 h.

2.3.2 Step iii: Ester Hydrogenation

Having identified compatible catalysts for the first two steps of the reaction cascade, we next examined the hydrogenation of methyl formate, which would complete the overall transformation of CH_3OH from CO_2 (step iii, Scheme 2.4). Several homogeneous catalysts had been reported for the hydrogenation of challenging carbonyl containing substrates including amides and alkyl esters, although formate esters had not been examined prior to our study.[14–16] Thus, Ru complexes **C-1**–**C-3** (known ester or

amide hydrogenation catalysts) were tested in order to establish if they could catalyze the hydrogenation of HCO_2CH_3 to CH_3OH (Table 2.3). We found that both **C-1** and **C-2** catalyze the hydrogenation of the methyl formate efficiently at 135 ºC (entries 1–2). Notably, Milstein reported similar findings shortly before these results were published.[17]

With active formate ester hydrogenation catalysts in hand, the effect of introducing CO_2 into this reaction was studied, as this is a required component of the cascade system. While maintaining an overall pressure of 40 bar, a 5:35 ratio of H_2 to CO_2 resulted in low yields of CH_3OH while using **C-1** (Table 2.3, entry 4). We hypothesized that decreasing the partial pressure of CO_2 would allow for improved activity of the catalyst. Indeed, a 30:10 ratio of H_2:CO_2 provided a 97% yield of CH_3OH (entry 6) and this set of conditions was selected for cascade system experiments.

Table 2.3. Hydrogenation of HCO_2CH_3 in the Presence of CO_2

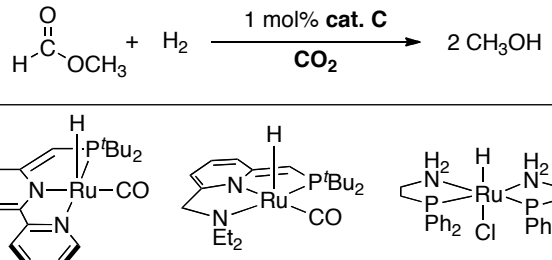

Entry[a]	Catalyst C	P_{H2}:P_{CO2}[b]	Conv. of HCO_2CH_3	Yield of CH_3OH
1	**C-1**	5:0	98%	98%
2	**C-2**	5:0	99%	>99%
3[c]	**C-3**	5:0	>99%	<3%[d]
4	**C-1**	5:35	54%	17%
5	**C-1**	20:20	85%	76%
6	**C-1**	30:10	97%	97%
7[b]	**C-2**	30:10	43%	16%

Conditions: [a]0.01 mmol of catalyst **C**, 1 mmol HCO_2CH_3, 1 mL of dioxane, 16 h, 135 ºC. [b]Pressures in bar. [c]1 mmol KO^{t}Bu was added under otherwise identical conditions. [d]KO^{t}Bu reacts directly with HCO_2CH_3, deprotonating the aldehydic H. The products of this reaction are HO^{t}Bu, CO, and KOMe.

2.4 Experimental Design and Detection

Before all components of the system were combined together to synthesize CH_3OH from CO_2 and H_2, experimental design was required so that methanol formed as a product in the reaction could be distinguished from the methanol added as a solvent. Initial evaluations were performed using ethanol (EtOH, Scheme 2.5a) as the solvent so that all CH_3OH detected by ^1H NMR spectroscopy analysis was definitively from CO_2. However, because ethanol is a bulkier alcohol in comparison with methanol, reduced yields in the esterification reaction (step ii) were observed. Therefore, deuterated methanol was explored, where CD_3OH (Scheme 2.5b) was selected instead of CD_3OD since it helped to reduce scrambling of CH_3OH (observed CH_2DOH/D, CHD_2OH/D due to exchange between M–**H** and CD_3O–**D**). To that end, using CD_3OH provided a system where CH_3OH could be detected by ^1H NMR spectroscopy, and the optimization reactions were conducted using this system. However, scrambling of the CD_3OH solvent (in some cases up to 50%) was still observed (Figure 2.1). Therefore, the optimized results obtained using the CD_3OH system were confirmed using $^{13}CO_2$ and ^{13}C depleted CH_3OH (Scheme 2.5c). This experiment allows for confirmation that all $^{13}CH_3OH$ detected by ^{13}C NMR spectroscopy is derived from $^{13}CO_2$ and not the $^{12}CH_3OH$ solvent.

Scheme 2.5. Experimental Design for the Cascade Hydrogenation of CO_2 to CH_3OH

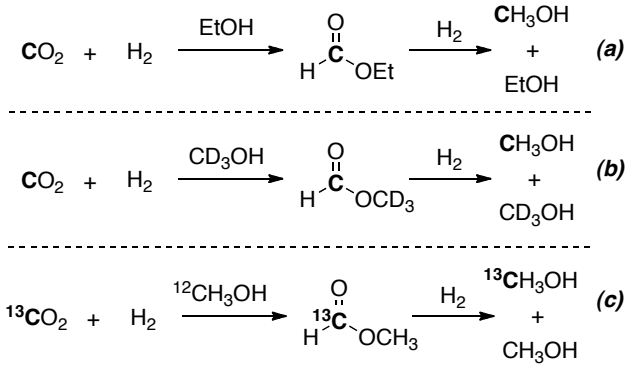

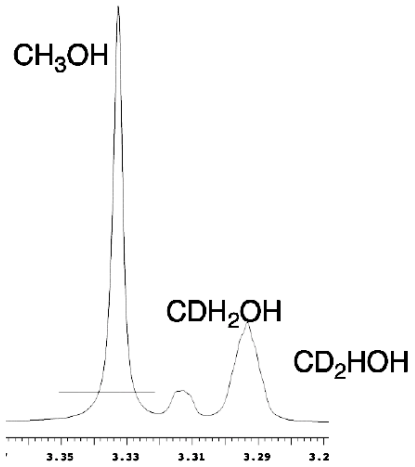

Figure 2.1. ^{1}H NMR Spectrum of CD_3OH Experiment

2.5 Cascade Conversion of CO_2 Hydrogenation to CH_3OH

2.5.1 One Pot CO_2 Conversion to CH_3OH

Before testing all catalysts together in one pot, experimental design was necessary in order to distinguish the methanol formed from CO_2 hydrogenation from the methanol added as a solvent/catalyst. Thus deuterated methanol (CD_3OH) was used as the solvent,[18] which would allow for the quantification of *in situ* produced CH_3OH by ^{1}H NMR spectroscopy. When combining all components together in one pot to hydrogenate CO_2 to CH_3OH, a TON of 3 was detected (Scheme 2.6). Importantly, there was a substantial amount of methyl formate remaining at the end of the reaction.

Scheme 2.6. One Pot Cascade CO_2 Conversion to CH_3OH

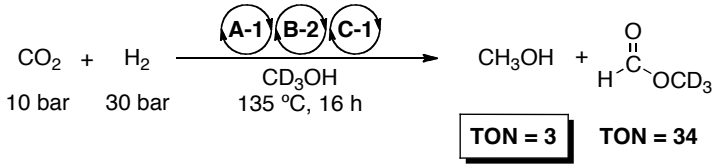

In order to determine why catalyst **C-1** was not fully reducing all of the methyl formate, exclusion reactions were carried out to determine what component(s) of the system were hindering **C-1**. By investigating the hydrogenation of methyl formate using **C-1** with and without **B-2**, it was clear that **B-2** and **C-1** are incompatible (Table 2.4). We

found that upon treating **C-2** with 1 equivalent of **B-2** ($Sc(OTf)_3$), 80% of the protonated triflate complex **1** was formed (Scheme 2.7), along with ~20% of 3 different Ru–H species as observed by ^1H NMR spectroscopy. The identity of this compound was confirmed through independent synthesis of **1** by treatment of **C-2** with triflic acid.

Table 2.4. Hydrogenation of HCO_2CH_3 in the Presence of **B-2**

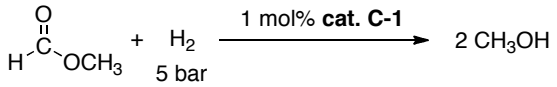

Entry[a]	Additive	Conv. of HCO_2CH_3	Yield of CH_3OH
1	none	>99%	>99%
2[b]	**B-2**	22%	31%

Conditions: [a]1mmol HCO_2CH_3, 0.0126 mmol **C-1**, 1 mL dioxane, 40 μL CD_3OH, 135 ºC, 16 h. Note: CD_3OH used to solvate **B-2**. [b]0.0126 mmol **B-2**.

Scheme 2.7. Reaction of **C-2** with $Sc(OTf)_3$

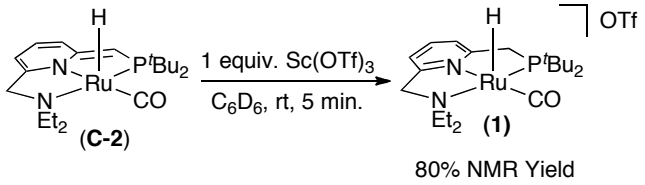

80% NMR Yield

2.5.2 Modified Reactor: Transfer System

To overcome the incompatibility between **B-2** and **C-1**, the catalysts were physically separated within the same high-pressure reactor. Catalysts **A-1**, **B-2**, and CH_3OH were placed in a vial inside the vessel, while **C-1** was dispensed into the outer well of the Parr vessel (Scheme 2.8). In this system, the volatile intermediate methyl formate (bp = 32 ºC at STP) can travel freely from the inner to the outer vessel, but the low volatility of the catalysts will keep them in their respective vessels. Gratifyingly, using this modified reactor yielded $^{13}CH_3OH$ in 25 turnovers from $^{13}CO_2$, where $^{13}CO_2$ and $^{12}CH_3OH$ were used to definitively track the produced methanol from CO_2.[19]

Scheme 2.8. Transfer System for the Cascade Catalytic Hydrogenation of CO_2

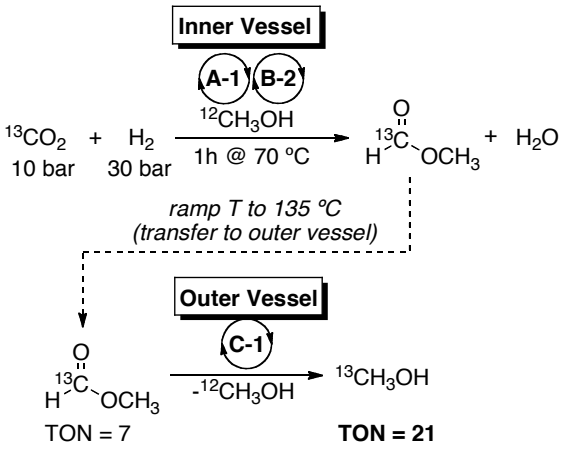

2.6 Conclusions

In summary, a cascade homogeneous catalytic approach toward the hydrogenation of CO_2 to CH_3OH has been demonstrated.[20] This serves as the first example, to our knowledge, of using homogeneous catalysts for the hydrogenation of CO_2 to CH_3OH. This multi-catalyst cascade system offers the unique advantage of allowing for optimization of individual steps of the overall reaction through catalyst design. Furthermore, it also allows for detailed analysis of catalyst incompatibilities and decomposition pathways on a molecular level. Using these aspects of the system to our advantage, we designed and optimized a setup that provides CH_3OH in 25 turnovers from CO_2. Chapters 3 and 4 will further explore more of the incompatibilities in this reaction cascade. Moreover, since this publication a similar cascade system that accesses an ester intermediate has been reported where, under analogous conditions the authors use a ruthenium phosphine complex and an acid catalyst to achieve CH_3OH in up to 86 TONs.[21]

2.7 Experimental Procedures and Characterization of Data

General Procedures

NMR spectra were obtained on a Varian MR 400 MHz (399.96 MHz for ^1H) or a Varian VNMRs 700 MHz (699.93 MHz for ^1H; 176.00 MHz for ^{13}C) spectrometer. All high-pressure reactions were carried out using a Parr Model 5000 Multiple Reactor system that includes six 50 mL vessels equipped with flat-gaskets and head mounting valves. The

system was operated with a 4871 process controller and SpecView version 2.5 software. A Swagelok SS Medium-Flow metering valve was used during the collection of volatile products from the pressurized reaction vessels.

Materials and Methods

The ruthenium catalysts **A-1**[9b], **A-2**[10b], **C-1**[14], **C-2**[15b], and **C-3**[16b] were prepared according to literature procedures. Pre-purified hydrogen (99.99%) and dry carbon dioxide (99.8%) were purchased from Metro Welding. Scandium triflate, iron tetrafluoroborate hexahydrate, and tris[2-(diphenylphosphino)ethyl]phosphine were purchased from Sigma Aldrich. Methyl formate and anhydrous dioxane were purchased from Alfa Aesar. Isotopically labeled compounds, including CD_3OH (99.95%), ^{13}C depleted CH_3OH (99.95%), $^{13}CO_2$ (99%), CD_3CN, and C_6D_6 (dried over sodium benzyl ketyl still) were purchased from Cambridge Isotope Laboratories. Methanol was dried over sodium and triethylamine was dried over CaH_2. Methyl formate was dried over calcium sulfate and distilled from phosphorus pentoxide. All experiments were conducted under a nitrogen atmosphere in either a glovebox or using standard Schlenk techniques.

Experimental Details

General Procedure for the Analysis of Volatile Products

After the reaction was complete, the pressure vessel was allowed to cool to room temperature. It was then slowly vented using a metering valve through a dry ice/acetone cooled trap. Once the vessel reached atmospheric pressure, the trap was placed in a LN_2-cooled bath and connected to a Schlenk line. The entire system was placed under vacuum and the liquid contents of the pressure vessel were then collected in the trap. The trap was disconnected from the Schlenk line and allowed to warm to room temperature. $CHCl_3$ was added as an NMR standard, the contents of the trap were added to in CD_3CN, and the mixture was analyzed by ^1H and/or ^{13}C NMR spectroscopy. Each reported TON represents an average of at least 2 trials.

General Procedure for the Hydrogenation of CO_2 to HCO_2CH_3 (Table 2.1 and Table 2.2)

In a N_2-filled glovebox, catalyst **A** (0.0126 mmol) and either NEt_3 (0.2 mL, 1.434 mmol) or catalyst **B-1**/**B-2** (0.0126 mmol) were dissolved in/added to CH_3OH (2 mL) in the well of a pressure vessel. A micro magnetic stirbar was added and the reactor was sealed and removed from the glovebox. The vessel was then pressurized with 10 bar CO_2, followed immediately within 1 minute with 30 bar H_2. The reaction was heated to 135 ºC for 16 h using SpecView software provided by Parr (a temperature of 125 ºC was initially entered into the SpecView program to prevent overshooting of 135 ºC) and then worked up using the general procedure for the analysis of volatile products above. $CHCl_3$ (30 µL, 0.3276 mmol) was added as the ^1H NMR standard and the reactions were analyzed by ^1H NMR spectroscopy. The TON corresponding to the yield of HCO_2CH_3 from CO_2 was calculated based on mmol of HCO_2CH_3/mmol catalyst A. See Figure 2.2 for a representative ^1H NMR spectrum.

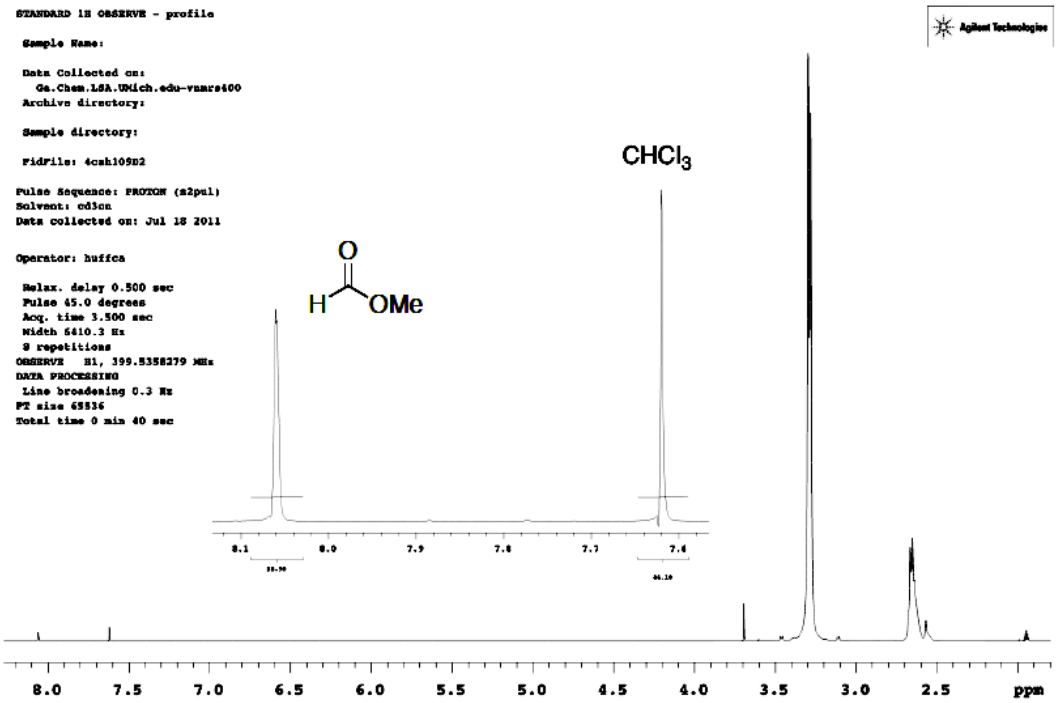

Figure 2.2. Representative ^1H NMR Spectrum for CO_2 Hydrogenation to HCO_2CH_3

General Procedure for the Hydrogenation of HCO_2CH_3 in the Presence of CO_2 (Table 2.3)

In a N_2-filled glovebox, catalyst **C** (0.01 mmol), HCO_2CH_3 (60 μL, 1 mmol), and dioxane (1 mL) were placed into the well of a pressure vessel. A micro magnetic stirbar was added and the reactor was sealed and removed from the glovebox. The vessel was then pressurized with CO_2, followed immediately within 1 minute with H_2. The reaction was heated to 135 ºC for 16 h using SpecView software provided by Parr. (A temperature of 125 ºC was initially entered into the SpecView program to prevent overshooting of 135 ºC.) The reaction was worked up using the general procedure for the analysis of volatile products. $CHCl_3$ (80 μL, 0.9938 mmol) was added as a ^{1}H NMR standard, and the reactions were analyzed by ^{1}H NMR spectroscopy. The yield of the reaction is based on the mmol of HCO_2CH_3 initially added.

General Procedure for the One Pot Cascade Conversion of CO_2 to CH_3OH in CD_3OH (Scheme 2.6)

In a N_2-filled glovebox, catalysts **A-1** (6.3 mg, 0.0126 mmol), **B-2** (6.2 mg, 0.0126 mmol), and **C-1** (5.6 mg, 0.0126 mmol) were dissolved in CD_3OH (2 mL) in the well of the pressure vessel. A micro magnetic stir bar was added and the reactor was then sealed and removed from the glovebox. The vessel was then pressurized with 10 bar CO_2, followed immediately within 1 minute with 30 bar H_2. The reactor was heated to 135 ºC for 16 h using SpecView software provided by Parr. (A temperature of 125 ºC was initially entered into the SpecView program to prevent overshooting of 135 ºC). $CHCl_3$ (30 μL, 0.3276 mmol) was added as the ^{1}H NMR standard and the reactions were analyzed by ^{1}H NMR spectroscopy. The TON corresponding to the yield of CH_3OH from CO_2 was calculated based on mmol of CH_3OH/mmol catalyst (**A**, **B**, or **C**). The reaction was worked up using the general procedure for the analysis of volatile products above. $CHCl_3$ (30 μL, 0.3276 mmol) was added as the ^{1}H NMR standard and the reactions were analyzed by ^{1}H NMR spectroscopy (Figure 2.3). Notably, a small amount of scrambling of the CD_3OH solvent occurred due to the reversibility of the hydrogenation of the ester at the reaction temperature (see inset of Figure 2.3).

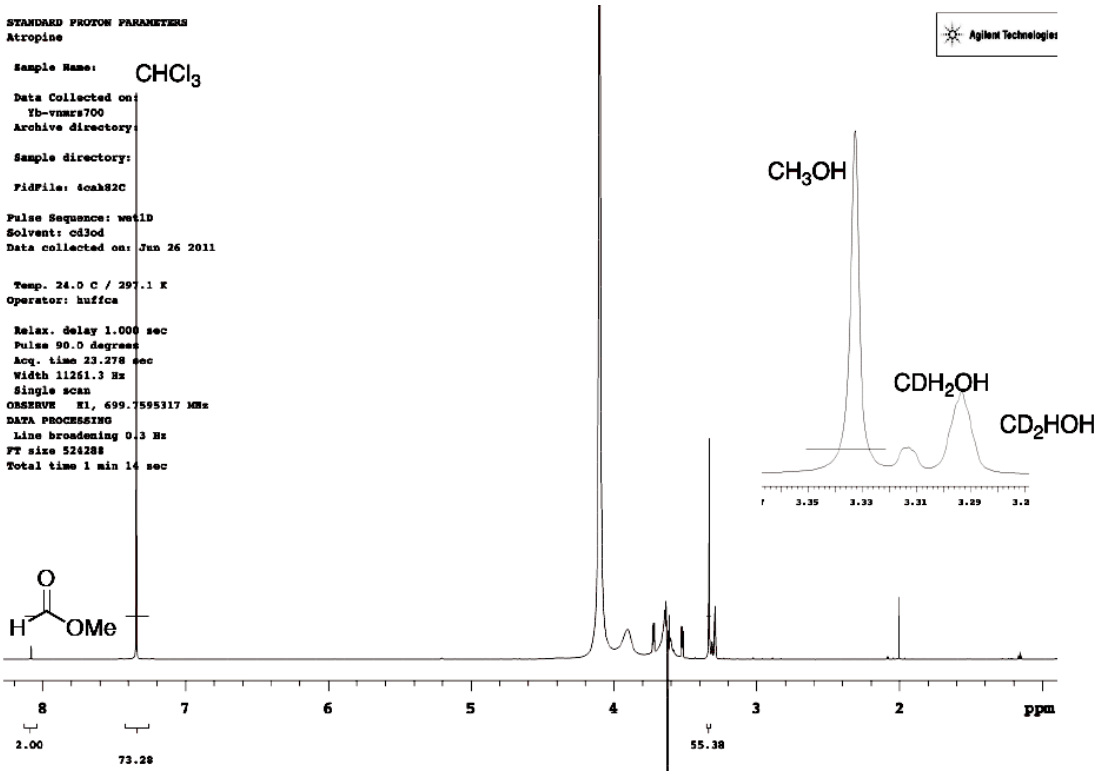

Figure 2.3. ^{1}H NMR Spectrum of Product Mixture Resulting from CD_3OH Experiment. Experimental details: Wet 1D, relaxation delay set at 25 s, pulse angle = 90º, solvent suppression for dioxane (delta = 13 Hz), 4 scans.

General Procedure for Hydrogenation of $^{13}CO_2$ to $^{13}CH_3OH$ using the Transfer Method (Scheme 2.8)

In a N_2-filled glovebox, catalysts **A-1** (6.3 mg, 0.0126 mmol) and **B-2** (6.2 mg, 0.0126 mmol) were dissolved in ^{13}C depleted CH_3OH in a 4 mL scintillation vial equipped with a micro magnetic stir bar. This vial was placed into the well of the pressure vessel. Catalyst **C-1** (5.6 mg, 0.0126 mmol) was dissolved in 1 mL of dioxane and dispensed into the well of the pressure vessel. The reactor was then sealed and removed from the glovebox. The vessel was pressurized with 10 bar $^{13}CO_2$, followed immediately within 1 minute with 30 bar H_2. The reactor was heated at 75 ºC for 1 h and the temperature was then ramped to 135 ºC and held at 135 ºC for an additional 15 h. (A temperature of 125 ºC was initially entered into the SpecView program to prevent overshooting 135 ºC). $CHCl_3$ (3 mL, 37.27 mmol, which corresponds to 0.4099 mmol $^{13}CHCl_3$) was added as a ^{13}C NMR standard, and the reactions were analyzed by ^{13}C NMR spectroscopy. The TON

corresponding to the yield of $^{13}CH_3OH$ from $^{13}CO_2$ was calculated based on mmol of $^{13}CH_3OH$/mmol catalyst (**A**, **B**, or **C**).

Experimental details for ^{13}C NMR experiment for the hydrogenation of $^{13}CO_2$ to $^{13}CH_3OH$: Decoupled without NOE, relaxation delay set at 60 s, pulse angle = 30º, 16 scans. A representative ^{13}C NMR spectrum is shown in Figure 2.4.

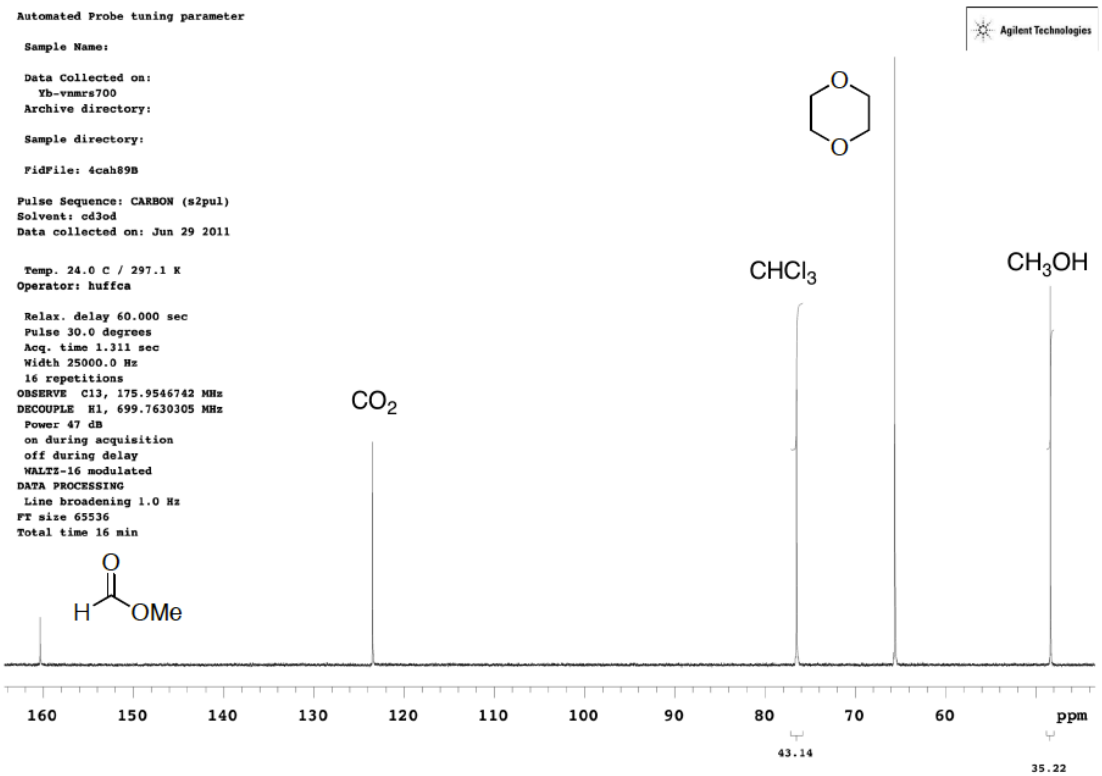

Figure 2.4. Representative ^{13}C NMR Spectrum of $^{13}CO_2$ Experiment

Procedure for the hydrogenation of HCO_2CH_3 in the presence of B-2 (Table 2.4)

Catalyst **C-1** (4.4 mg, 0.01 mmol) was dissolved in 1 mL dioxane and **B-2** (4.9 mg, 0.01 mmol) was dissolved in 40 µL of CD_3OH (Note: **B-2** is not soluble in dioxane, so CD_3OH was used to solvate it). These solutions were combined in the well of the pressure vessel. Methyl formate was then added (60 µL, 1 mmol), along with a micro magnetic stirbar. The reactor was sealed and removed from the glovebox and the vessel was pressurized with 5 bar H_2. The reaction was then heated to 135 ºC for 16 h using

SpecView software provided by Parr. (A temperature of 125 ºC was initially entered into the SpecView program to prevent overshooting 135 ºC.) The reaction was worked up using the general procedure for the analysis of volatile products. $CHCl_3$ (80 µL, 0.9938 mmol) was added as a ^{1}H NMR standard and the reactions were analyzed by ^{1}H NMR spectroscopy.

*Procedure for Synthesis and Characterization of Authentic Sample of **1***

Upon mixing a solution of **Cat. C-2** (2.5 mg, 5.5 µmol, 1 equiv.) in 0.45 mL dry C_6D_6 with triflic acid (1 µL, 0.011 mmol, 2 equiv.) in a J-Young NMR tube, a color change from dark brown to pale orange was observed. 90% NMR yield for **1** was determined by ^{1}H NMR spectroscopy (Figure 2.5), where the remaining 10% yield belongs to a second Ru species with a Ru-H shift at –20.09 ppm (J_{HP} = 25.1 Hz) (Figure 2.6).

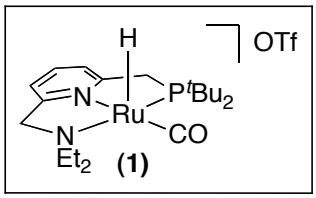

Diagnostic peaks:

^{1}H NMR (C_6D_6): δ –20.38 (d, J_{HP} = 27.2 Hz, 1H, Ru-*H*), aromatic peaks ranging from 6.4–6.9 ppm (indicates aromatized backbone).

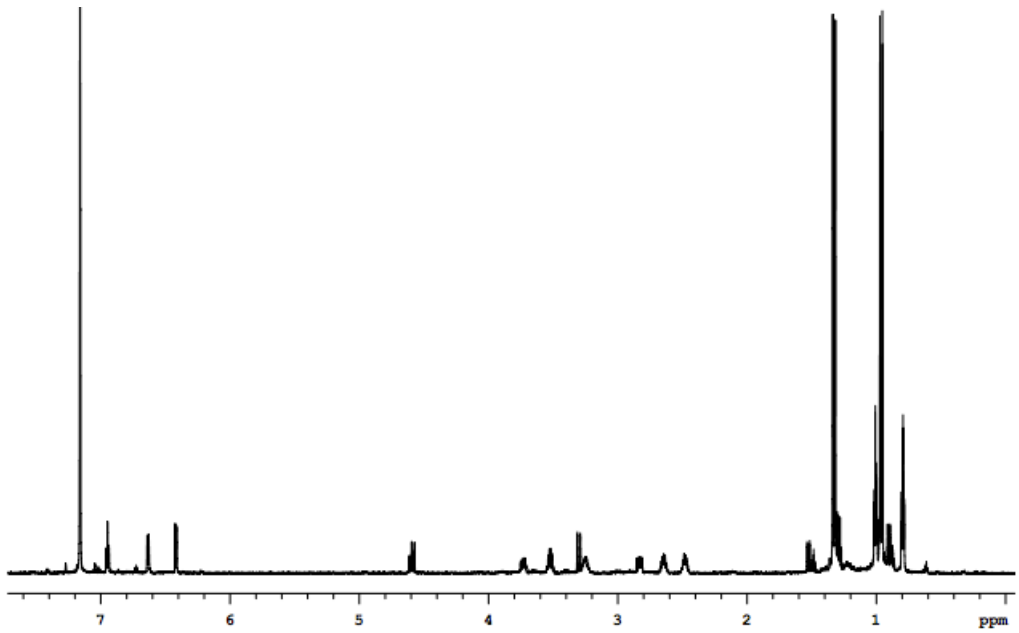

Figure 2.5. ^{1}H NMR Spectrum of **1**: Reaction of **C-2** with HOTf

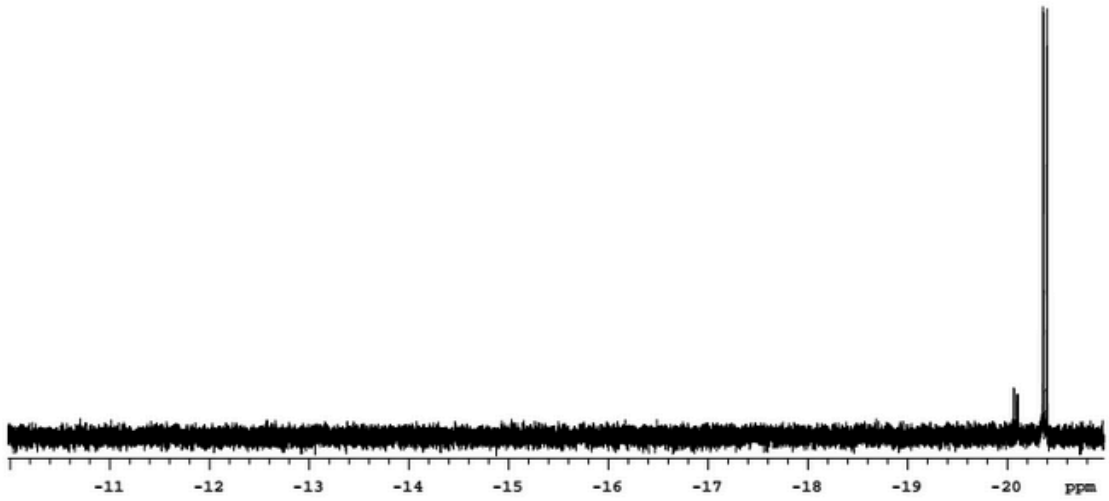

Figure 2.6. Hydride Region of ^{1}H NMR Spectrum of **1** from Reaction of **C-2** with HOTf

*Procedure for Reaction of **Cat C-2** with $Sc(OTf)_3$*

Scandium triflate (**B-2**, 3.3 mg, 6.6 µmol, 1 equiv.) was added to a solution of **Cat. C-2** (3 mg, 6.6 µmol, 1 equiv.) in 0.45 mL dry C_6D_6 in a J-Young NMR tube. Upon sonicating for 5 minutes a color change from dark brown to greenish yellow to orange was observed. 80% NMR yield for 1 was determined by ^{1}H NMR spectroscopy (Figure 2.7), where the remaining 20% yield belongs to a number of other Ru-H species as shown in the hydride region of the ^{1}H NMR spectrum (Figure 2.8).

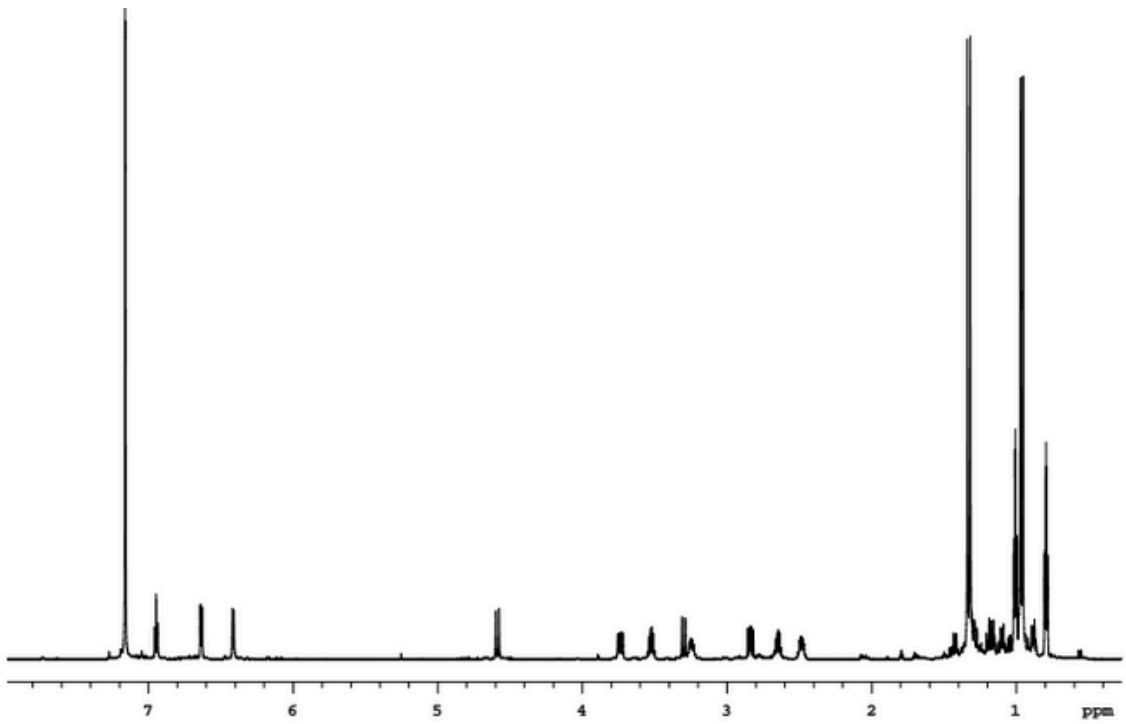

Figure 2.7. ^{1}H NMR spectrum of **1**: Reaction of **C-2** with **B-2**

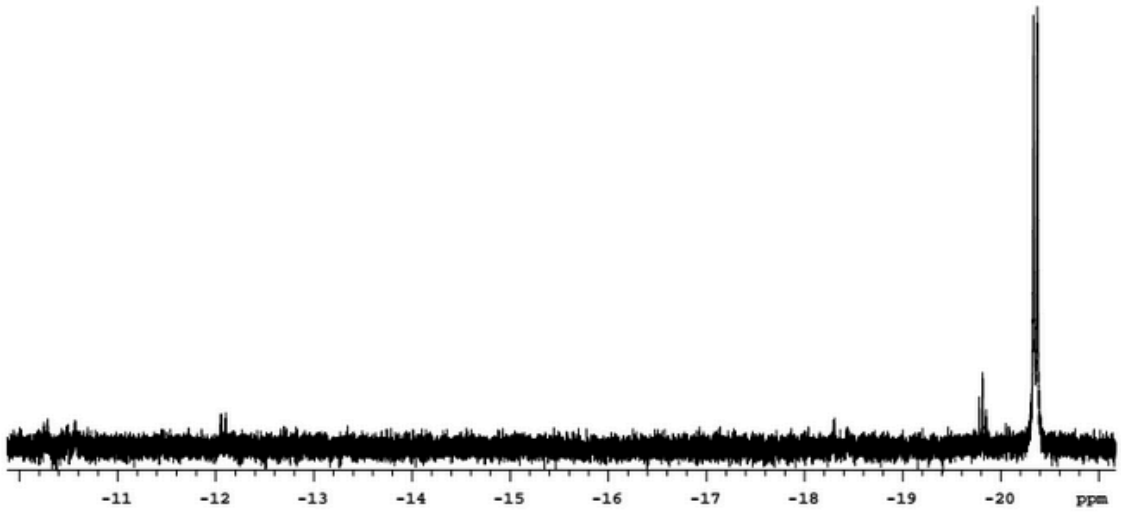

Figure 2.8. Hydride Region of ^{1}H NMR Spectrum of **1**: Reaction of **C-2** with **B-2**

2.8 References

1. (a) Ushikoshi, K.; Mori, K.; Watanabe, T.; Takeuchi, M.; Saito, M. A 50 kg/Day Class Test Plant for Methanol Synthesis from CO_2 and H_2. *Stud. Surf. Sci. Catal.* **1998**, *114*, 357. (b) Saito, M. R&D Activities in Japan on Methanol Synthesis from CO_2 and H_2. *Catal. Surv. Jpn.* **1998**, *2*, 175.

2. Jessop, P. G. Homogeneous Hydrogenation of Carbon Dioxide. *The Handbook of Homogeneous Hydrogenation* **2008**, 489.

3. For examples of stoichiometric reduction of CO_2 to CH_3OH mediated by frustrated Lewis base pairs, see: (a) Ashley, A. E.; Thompson, A. L.; O'Hare, D. Non-Metal-Mediated Homogeneous Hydrogenation of CO_2 to CH_3OH. *Angew. Chem., Int. Ed.* **2009**, *48*, 9839. (b) Ménard, G.; Stephan, D. W. Room Temperature Reduction of CO_2 to Methanol by Al-Based Frustrated Lewis Pairs and Ammonia Borane. *J. Am. Chem. Soc.* **2010**, *132*, 1796; For a review, see: (c) Stephan, D. W.; Erker, G. Frustrated Lewis Pairs: Metal-Free Hydrogen Activation and More. *Angew. Chem., Int. Ed.* **2010**, *49*, 46.

4. For catalytic reduction of CO_2 to CH_3OH with borane reducing agents, see: (a) Chakraborty, S.; Zhang, J.; Krause, J. A.; Guan, H. An Efficient Nickel Catalyst for the Reduction of Carbon Dioxide with a Borane. *J. Am. Chem. Soc.* **2010**, *132*, 8872. (b) Huang, F.; Zhang, C.; Jiang, J.; Wang, Z.-X.; Guan, H. How Does the Nickel Pincer Complex Catalyze the Conversion of CO_2 to Methanol Derivative? A Computational Mechanistic Study. *Inorg. Chem.* **2011**, *50*, 3816.

5. For catalytic reduction of CO_2 to CH_3OH with silane reducing agents, see: (a) Eisenschmid, T. C.; Eisenberg, R. The Iridium Complex Catalyzed Reduction of Carbon Dioxide to Methoxide by Alkylsilanes. *Organometallics* **1989**, *8*, 1822. (b) Riduan, S. N.; Zhang, Y.; Ying, J. Y. Conversion of Carbon Dioxide into Methanol with Silanes over *N*-Heterocyclic Carbene Catalysts. *Angew. Chem. Int. Ed.* **2009**, *48*, 3322; (c) Huang, F.; Lu, G.; Zhao, L.; Li, H.; Wang, Z.-X. The Catalytic Role of *N*-Heterocyclic Carbene in a Metal-Free Conversion of Carbon Dioxide into Methanol: A Computational Mechanism Study. *J. Am. Chem. Soc.* **2010**, *132*, 12388.

6. For other examples of homogeneous catalytic CO_2 reduction, see: (a) Laitar, D. S.; Müller, P.; Sadighi, J. P. Efficient Homogeneous Catalysis in the Reduction of CO_2 to CO. *J. Am. Chem. Soc.* **2005**, *127*, 17196. (b) Matsuo, T.; Kawaguchi, H. From Carbon Dioxide to Methane: Homogeneous Reduction of Carbon Dioxide with Hydrosilanes Catalyzed by Zirconium-Borane Complexes. *J. Am. Chem. Soc.* **2006**, *128*, 12362. For reviews, see: (c) Riduan, S. N.; Zhang, Y. Recent Developments in Carbon Dioxide Utilization under Mild Conditions. *Dalton Trans.* **2010**, *39*, 3347. (d) Darensbourg, D. J. Chemistry of Carbon Dioxide Relevant to Its Utilization: A Personal Perspective. *Inorg. Chem.* **2010**, *49*, 10765.

7. (a) Leitner, W. Carbon Dioxide as a Raw Material: The Synthesis of Formic Acid and Its Derivatives from CO_2. *Angew Chem Int. Ed.* **1995**, *34*, 2207; (b) Tanaka, R.; Yamashita, M.; Nozaki, K. Catalytic Hydrogenation of Carbon Dioxide Using Ir(III)-Pincer Complexes. *J. Am. Chem. Soc.* **2009**, *131*, 14168.

8. Catalyst **A-3**: Federsel, C.; et al. A Well-Defined Iron Catalyst for the Reduction of Bicarbonates and Carbon Dioxide to Formates, Alkyl Formates, and Formamides. *Angew. Chem., Int. Ed.* **2010**, *49*, 9777.

9. Catalyst **A-1**: (a) For catalytic results: Munshi, P.; Main, A. D.; Linehan, J. C.; Tai, C.-C.; Jessop, P. G. Hydrogenation of Carbon Dioxide Catalyzed by Ruthenium Trimethylphosphine Complexes: The Accelerating Effect of Certain Alcohols and Amines. *J. Am. Chem. Soc.* **2002**, *124*, 7963; (b) For synthetic procedure: Mainz, V. V.; Andersen, R. A. Preparation of $RuCH_2PMe_2(PMe_3)_3Cl$, $Ru(CH_2PMe_2)_2(PMe_3)_2$, and $Rh_2(CH_2PMe_2)_2(PMe_3)_4$ and Their Reactions with Hydrogen. *Organometallics* **1984**, *3*, 675.

10. Catalyst **A-2**: (a) For catalytic results: Kröcher, O.; Köppel, R. A.; Baiker, A. Highly Active Ruthenium Complexes with Bidentate Phosphine Ligands for the Solvent-Free Catalytic Synthesis of *N*, *N*-Dimethylformamide and Methyl Formate. *Chem. Commun*. **1997**, 453; (b) For synthetic procedure: Mason, R.; Meek, D. W.; Scollary, G. R. Polyphosphine Complexes of Ruthenium(II). *Inorg. Chim. Acta*, **1976**, *16*, L11.

11. Otera, J.; Nishikido, J. Esterification, 2nd ed.; 2009.

12. Barrett, A. G. M.; Braddock, D. C. Scandium(III) or Lanthanide(III) Triflates as Recyclable Catalysts for the Direct Acetylation of Alcohols with Acetic Acid. *Chem. Commun.* **1997**, 351.

13. Xiong, W.-M.; Zhu, M.-Z.; Deng, L.; Fu, Y.; Guo, Q.-X. Esterification of Organic Acid in Bio-Oil using Acidic Ionic Liquid Catalysts. *Energ. Fuels* **2009**, *23*, 2278.

14. Catalyst **C-1**: Balaraman, E.; Gnanaprakasam, B.; Shimon, L. J. W.; Milstein, D. Direct Hydrogenation of Amides to Alcohols and Amines under Mild Conditions. *J. Am. Chem. Soc.* **2010**, *132*, 16756.

15. Catalyst **C-2**: (a) For catalytic results: Zhang, J.; Leitus, G.; Ben-David, Y.; Milstein, D. Efficient Homogeneous Catalytic Hydrogenation of Esters to Alcohols. *Angew. Chem., Int. Ed.* **2006**, *45*, 1113. (b) For synthetic procedure: Zhang, G.; Leitus, Y.; Milstein, Ben-David, Y.; Milstein, D. Facile Conversion of Alcohols into Esters and Dihydrogen Catalyzed by New Ruthenium Complexes. *J. Am. Chem. Soc.* **2005**, *127*, 10840.

16. Catalyst **C-3**: (a) For catalytic results: Saudan, L. A.; Saudan, C. M.; Debieux, C.; Wyss, P. Dihydrogen Reduction of Carboxylic Esters to Alcohols under the Catalysis of Homogeneous Ruthenium Complexes: High Efficiency and Unprecedented Chemoselectivity. *Angew. Chem., Int. Ed.* **2007**, *46*, 7473. (b) For synthetic procedure: Abdur-Rashid, K.; Guo, R.; Lough, A. J.; Morris, R. H.; Song, D. Synthesis of Ruthenium Hydride Complexes Containing beta-Aminophosphine Ligands Derived from Amino Acids and their use in the H_2-Hydrogenation of Ketones and Imines. *Adv. Synth. Catal.* **2005**, *347*, 571.

17. Balaraman, E.; Gunanathan, C.; Zhang, J.; Shimon, L. J. W.; Milstein, D. Efficient Hydrogenation of Organic Carbonates, Carbamates, and Formates Indicates Alternative Routes to Methanol Based on CO_2 and CO. *Nat. Chem.* **2011**, *3*, 609.

18. CD_3OD was first employed but due to free D+ in the system, Ru-D was formed, yielding the deutero formate ester ($DCOCD_3$) in ~10% yield. This is an issue when using ^1H NMR to determine yields, thus CD_3OH was implemented to prevent this reaction from proceeding.

19. When using deuterated methanol for this reaction, a small amount of scrambling of the CD_3OH solvent occurred due to the reversibility of the ester hydrogenation at the reaction temperature. Thus $^{13}CO_2$ and $^{12}CH_3OH$ were in order to get a more accurate yield for the CO_2 hydrogenation reaction.

20. Excerpts of Chapter 2 reprinted with permission from Huff, C. A.; Sanford, M. S. Cascade Catalysis for the Homogeneous Hydrogenation of CO_2 to Methanol. *J. Am. Chem. Soc.* **2011**, *133,* 18122. Copyright 2011. American Chemical Society.

21. Wesselbaum, S.; Stein, vom, T.; Klankermayer, J.; Leitner, W. Hydrogenation of Carbon Dioxide to Methanol by using a Homogeneous Ruthenium–Phosphine Catalyst. *Angew. Chem., Int. Ed.* **2012**, *51*, 7499.

CHAPTER 3

Investigation of Side Reactions in the Cascade System

3.1 Introduction

As described in detail in Chapter 2, I developed a cascade catalytic sequence for converting CO_2 and H_2 to CH_3OH.[1] This cascade system is comprised of three steps, each of which requires a different homogeneous catalyst (Scheme 3.1). In the first step, CO_2 is hydrogenated to formic acid (FA) using a ruthenium catalyst. Subsequently, FA undergoes a scandium-catalyzed esterification reaction with CH_3OH to form methyl formate (step ii). This ester is then reduced with H_2 and (PNN)Ru(H)(CO) (**1**, PNN = 6-(di-*tert*-butylphosphinomethylene)-2-(*N*,*N*-diethylaminomethyl)-1,6-dihydropyridine)[2] to form two equivalents of CH_3OH (step iii). Overall, this system provides CH_3OH in up to 25 TONs.

Scheme 3.1. Cascade Homogeneous Hydrogenation of CO_2 to CH_3OH

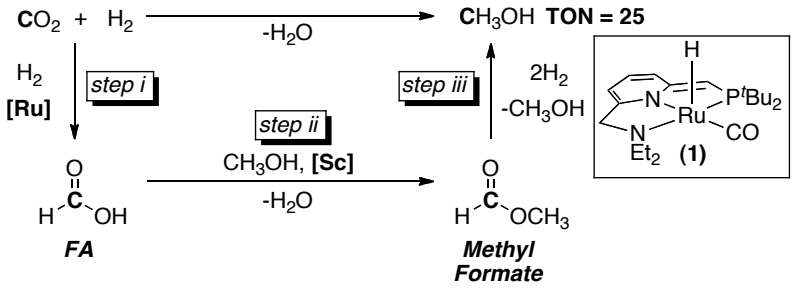

While this system was the first demonstration of using homogeneous catalysis to achieve the hydrogenation of CO_2 to CH_3OH, it is necessary to further improve the efficiency and thus the utility of this reaction. As a means to realize this objective, experiments were designed to uncover potential decomposition/inhibition pathways of

the employed catalysts. Specifically, these studies focus on undesired side reactions of **1** with other components of the cascade system.

3.2 Reactivity of Esters, Ketones, and Aldehydes with a Ru Pincer Complex

3.2.1 Methyl Formate

While exploring **1** as a methyl formate hydrogenation catalyst for its application in the cascade CO_2 hydrogenation system (Scheme 3.1, step iii), an unexpected color change from red/brown to yellow was observed upon mixing Ru complex **1** and methyl formate. This led us to hypothesize that a reaction occurs between these two compounds. Consistent with this finding, Milstein et al. recently reported the stoichiometric reaction of aldehydes with a related Ru PNP pincer complex, **2,** at –50 ºC (Scheme 3.2).[3] The resulting adduct, **3**, was characterized as a single stereoisomer and was determined to be unstable at room temperature.

Scheme 3.2. Reactivity of Ruthenium PNP Pincer Complex with Aldehydes[3]

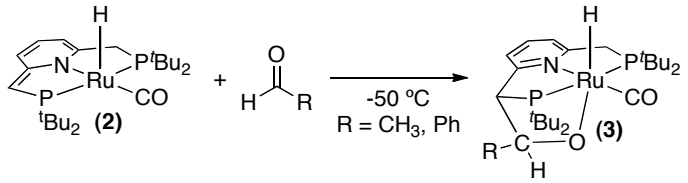

Our studies revealed that the treatment of **1** with 2.5 equivalents of methyl formate in C_6D_6 at 25 ºC results in complete conversion to a new Ru species with a Ru–H doublet at –15.25 ppm, as determined through ^{1}H NMR spectroscopic analysis (Scheme 3.3a). The newly formed Ru species was determined to be a Ru-methyl formate adduct (**4**), which is believed to form through the reaction of methyl formate with **1-Taut**. Characteristic features of **4**, such as the C–C bond between the carbonyl carbon of methyl formate and the nitrogen arm of the pincer ligand were confirmed through ^{1}H and ^{13}C HSQC (heteronuclear single quantum coherence spectroscopy) and HMBC (heteronuclear multiple-bond correlation) 2D NMR spectroscopic studies that verified the proximity between the methylene protons on the arm of the *N*-side of the ligand and the proton of methyl formate. Furthermore, NOESY (nuclear overhauser effect spectroscopy) NMR spectroscopic analysis showed cross-peaks between the protons in the *tert*-

butylphosphine and methoxy group, as well as between the diethylamine substituent with the proton of methyl formate, consistent with the stereoisomer depicted in Scheme 3.3. An X-ray crystal structure was also obtained by crystallizing **4** from a solution of **1** in methyl formate and pentane (Figure 3.1). This structure further confirmed the stereoisomer shown in Scheme 3.3. An analytically pure sample of **4** was obtained in 94% yield through slow evaporation of the volatiles from a solution of **1** in methyl formate. Moreover, removal of the volatiles from this reaction mixture resulted in complete regeneration of complex **1**, suggesting that the reaction is reversible (Scheme 3.3b).

Scheme 3.3. Reversible Reaction of **1** with Methyl Formate

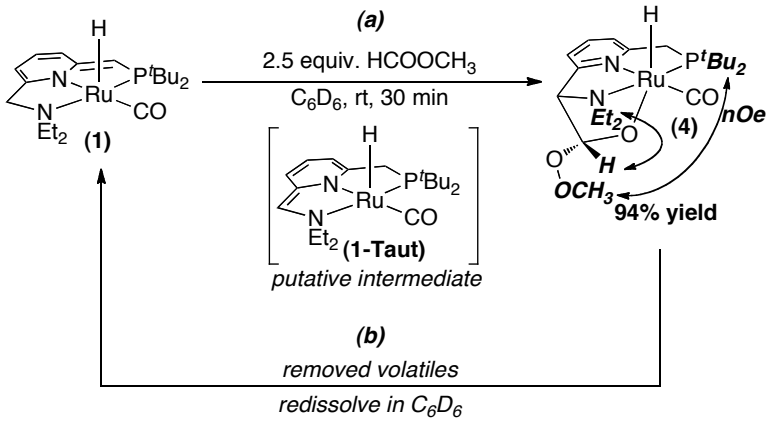

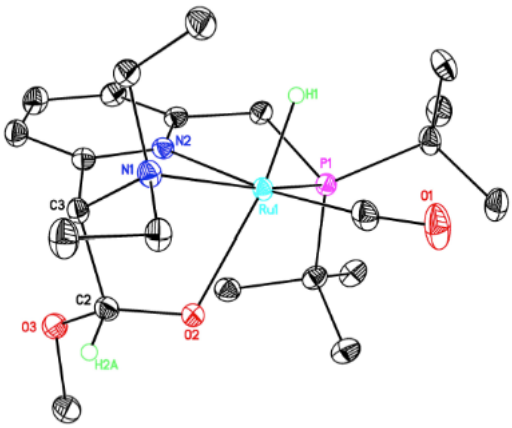

Figure 3.1. ORTEP diagram (50% probability level) of the molecular drawing of **4.** All H atoms (other than Ru−H and H–COOMe) have been omitted for clarity. Selected bond lengths (Å) and angles (deg): Ru1–O2 = 2.2022(9), C2–C3 = 1.5678(17), O2–C2 = 1.3409(15), Ru1–H1 = 1.526(19); Ru1–O2–C2 = 112.65(7), O2–C2–C3 = 112.50(10).

3.2.2 Other Carbonyl Compounds

A survey of different carbonyl compounds revealed that other formate esters (*e.g.*, ethyl formate), as well as aldehydes and ketones (*e.g.*, benzaldehyde and cyclopentanone), exhibit similar reactivity with **1** (Scheme 3.4). Products **5-7** were isolated in 65-88% yield and the structure of **6** was further characterized through X-ray crystallography (Figure 3.2). Like methyl formate, in most cases the coupling of the carbonyl compound to **1** was reversible (excluding benzaldehyde).

Scheme 3.4. Reactivity of **1** with Ethyl Formate, Cyclopentanone, and Benzaldehyde

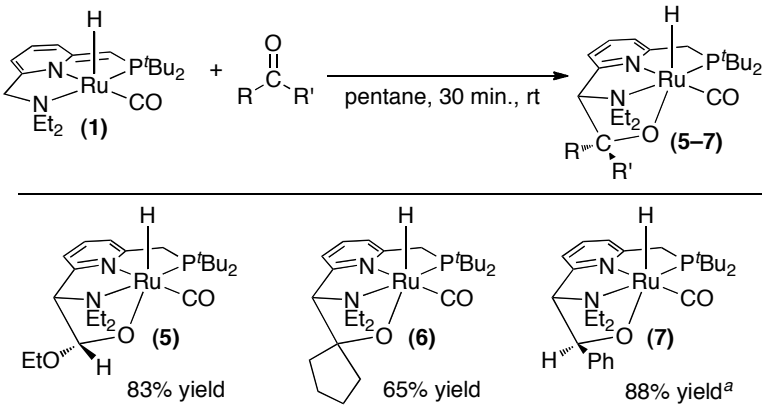

Conditions: (PNN)Ru(H)(CO) (**1**, 5 mg, 0.011 mmol), 1-11 equiv. carbonyl compound, 0.5 mL C_6D_6, rt, 30 min; [a]Mixture of diastereomers **7B-i** and **7B-ii** (see Scheme **3.6** for details).

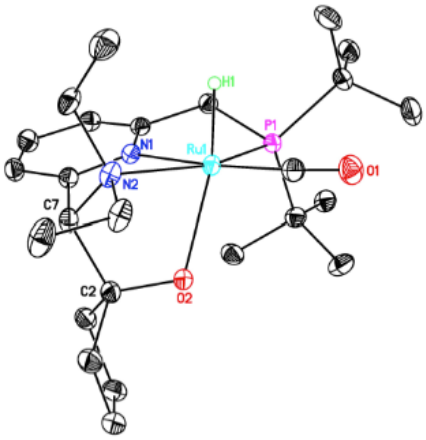

Figure 3.2. ORTEP diagram (50% probability level) of the molecular drawing of **6.** All H atoms (other than Ru–H) have been omitted for clarity. Selected bond lengths (Å) and

angles (deg): Ru1–O2 = 2.1991(9), C2–C7 = 1.5816(17), O2–C2 = 1.3867(14), Ru1–H1 = 1.534(19); Ru1–O2–C2 = 113.59(7), O2–C2–C7 = 109.79(9).

With most of the carbonyl compounds discussed thus far, a single isomeric product was detected at room temperature. This is particularly remarkable since the reaction of **1** with unsymmetrical carbonyl compounds could, in principle, lead to four products (Scheme 3.5). These include two pairs of regioisomers, where reactivity could occur on either the "*P*-side" (**A**) or the "*N*-side" (**B**) of the ligand. Furthermore, the *P*-side and *N*-side regioisomers could be comprised of a set of diastereomers, which will be referred to as **A-ii**/**A-ii** and **B-i**/**B-ii**, respectively.

Scheme 3.5. Four Potential Isomeric Products from the Reaction of **1** with Unsymmetrical Carbonyl Compounds

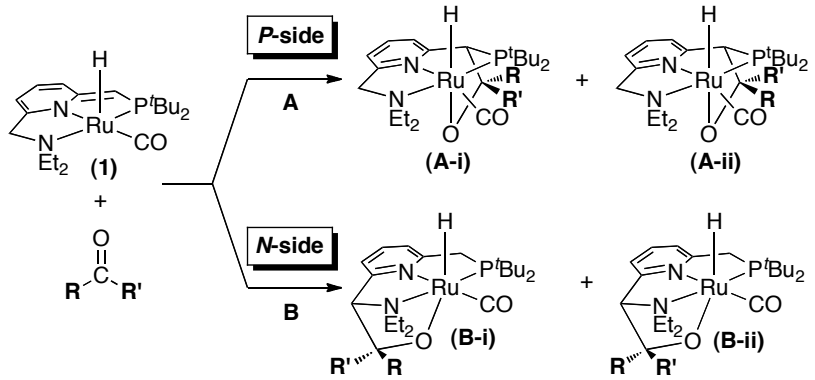

Despite this potential complexity, products **4-6** were formed as >95% of the isomer reported in Scheme 3.3 and Scheme 3.4 under the standard conditions (30 min, rt). However, benzaldehyde proved to be an exception, where a more complex product mixture was observed. The reaction of **1** with benzaldehyde under these conditions yielded **7** as a mixture of the two isomeric products **7B-i** and **7B-ii** in a 85:15 ratio. To further probe the reactivity of **1** with benzaldehyde, lower reaction temperatures were employed to allow for characterization of any kinetically favored isomers by NMR spectroscopy.

Reacting **1** and benzaldehyde at –50 ºC for five minutes in toluene-d_8 yielded the *P*-side complex **7A-i** as a single diastereomer with a diagnostic Ru-H shift at –15.35 ppm

(Scheme 3.6). As the mixture was warmed to room temperature and was allowed to equilibrate for five minutes, complete conversion of **7A-i** to a combination of the two *N*-side diastereomers **7B-i**:**7B-ii** (90:10) was observed, with Ru–H shifts at –14.84 and –15.16 ppm, respectively. Allowing this mixture to further equilibrate at room temperature for 24 hours resulted in a 15:85 ratio of **7B-i**:**7B-ii**. All isomers of **7** that were detected were fully characterized by NMR spectroscopy using HSQC and HMBC 2D NMR spectroscopic to verify if *N*-side or *P*-side regioisomers had formed, and NOESY NMR spectroscopic analysis to distinguish between diastereomers. Additionally, X-ray crystal structures of **7B-i** (Figure 3.3) and **7B-ii** (Figure 3.4) were obtained.

The *N*-side diastereomers are likely more thermodynamically stable than the observed *P*-side regioisomer as a result of the reduced sterics in the binding pocket. The NEt_2 group on the arm of the ligand is less sterically encumbering relative to the P^tBu_2 group, thus providing more stable *N*-side adducts. Notably, the C–C bond length between the benzaldehyde carbonyl carbon and the arm of the ligand for **7B-i** is 0.03 Å longer than **7B-ii** (C-2/C-9 and C-2/C-3, respectively). This likely is a reflection of the higher energy of **7B-i**.

Scheme 3.6. Reactivity of **1** with Benzaldehyde at Varied Temperatures

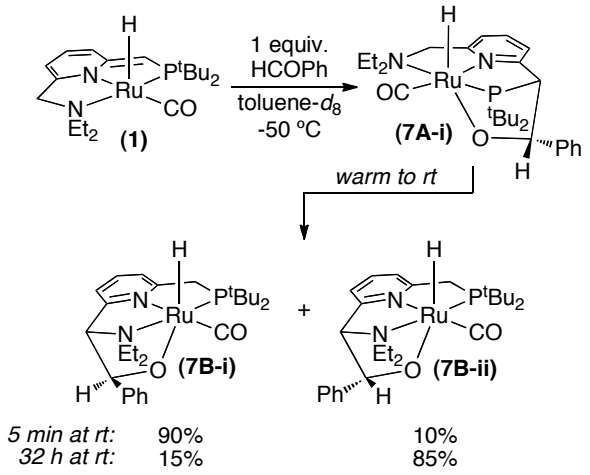

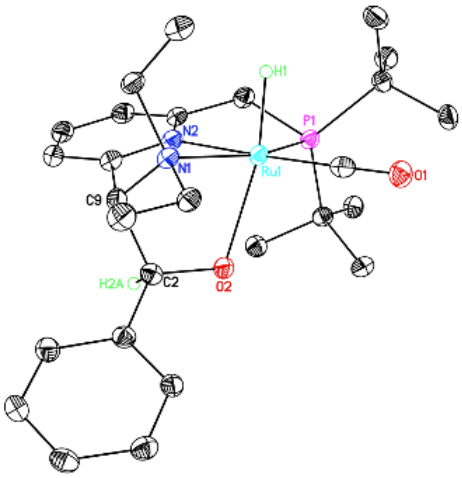

Figure 3.3. ORTEP diagram (50% probability level) of the molecular drawing of **7B-i.** All H atoms (other than Ru–H and H–COPh) have been omitted for clarity. Selected bond lengths (Å) and angles (deg): Ru1–O2 = 2.2293(16), C2–C9 = 1.588(3), O2–C2 = 1.374(3), Ru1–H1 = 1.58(3); Ru1–O2–C2 = 111.60(13), O2–C2–C9 = 110.71(18).

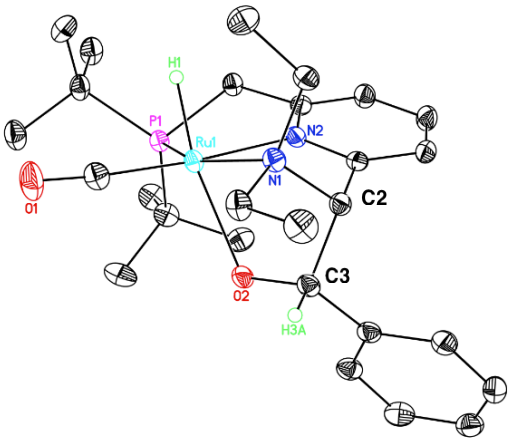

Figure 3.4. ORTEP diagram (50% probability level) of the molecular drawing of **7B-ii.** All H atoms (other than Ru–H and H–COPh) have been omitted for clarity. Selected bond lengths (Å) and angles (deg): Ru1–O2 = 2.2315(13), C2–C3 = 1.558(3), O2–C3 = 1.377(2), Ru1–H1 = 1.51(2); Ru1–O2–C3 = 112.27(11), O2–C3–C2 = 110.08(15).

Similarly, when **1** was reacted with 12 equivalents of symmetrical carbonyl compound cyclopentanone at –40 ºC, the *P*-side product **6A** was detected and fully characterized by NMR spectroscopy (Scheme 3.7). Upon warming to room temperature, complete conversion to the *N*-side isomer **6B** was observed. Benzaldehyde and cyclopentanone both demonstrate the potential isomeric complexity of the reaction of **1** with symmetrical and unsymmetrical carbonyl compounds.[4]

Scheme 3.7. Low Temperature Reaction of **1** with Cyclopentanone

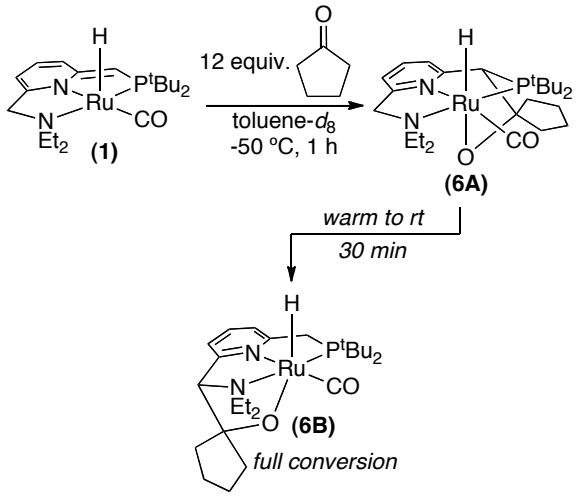

3.2.3 Reversibility Study for Carbonyl Compound Coupling with 1

In most cases, the reaction of **1** with carbonyl compounds was completely reversible. Thus we sought more quantitative data to evaluate the propensity for carbonyl compound coupling at **1**. Equilibrium constants (K_{eq}) for the reactions of **1** with varied carbonyl substrates were determined via ^{1}H NMR integration (Table 3.1). K_{eq} appears to be particularly sensitive to the steric properties of the carbonyl substrate. For example, K_{eq} decreases from 2.7 x 10^2 to 1.5 x 10^2 upon moving from methyl to ethyl formate, likely reflecting the increased size of the ethyl substituent. Electronic effects also play an important role in this equilibrium. For example, aldehydes are similar in size to formate esters but have a significantly more electrophilic carbonyl carbon. This results in a large value of K_{eq} for the reaction of **1** with benzaldehyde ($K_{eq} > 10^3$ at room temperature). Ketones are also more electrophilic than formate esters, but the carbonyl carbon is more sterically encumbered. With these substrates, steric factors appear to dominate the binding equilibrium. For example, K_{eq} for cyclopentanone is 5.0 x 10^1, while acetone (which has freely rotating the alkyl groups) has K_{eq} of $< 10^{-2}$ at room temperature. Similarly, no reaction of **1** with up to 20 equivalents of methyl acetate or *N*,*N*-dimethylformamide was observed, indicating that K_{eq} for these substrates is $< 10^{-3}$.

Table 3.1. K_{eq} for Reaction of **1** with Carbonyl Compounds

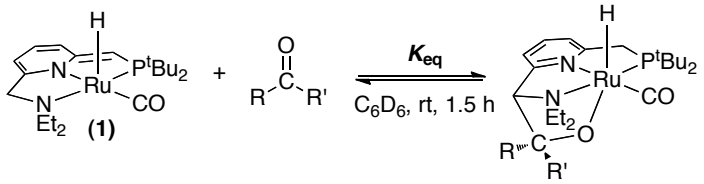

Carbonyl Compound	Major Product	K_{eq}
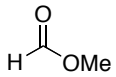	**4**	2.7×10^2
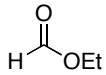	**5**	1.5×10^2
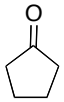	**6**	5.0×10^1
	**7B**[a]	$> 10^3$
	not det.[b]	$< 10^{-2}$
	not det.[b]	$< 10^{-3}$
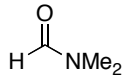	not det.[b]	$< 10^{-3}$

(a) Mixture of diastereomers **7B-i** and **7B-ii**. [b]not det. = products were not determined.

3.2.4 Implications for the Cascade System

Complex **1** catalyzes the hydrogenation of methyl formate (step iii of the cascade system, Scheme 3.1) via a metal-ligand bifunctional mechanism wherein H_2 is split by **1** to form Ru dihydride intermediate, **8** (Scheme 3.8a). Importantly, formation of the Ru methyl formate adduct (**4**) could inhibit hydrogenation catalysis as shown in Scheme 3.8b. In order to determine the extent of this inhibition, more in depth studies were carried out on the hydrogenation of methyl formate including: i) an order study in methyl formate; ii) determination of the catalyst resting state under the catalytic reaction conditions.

Scheme 3.8. Potential Reactivity of **1** under Methyl Formate Hydrogenation Conditions

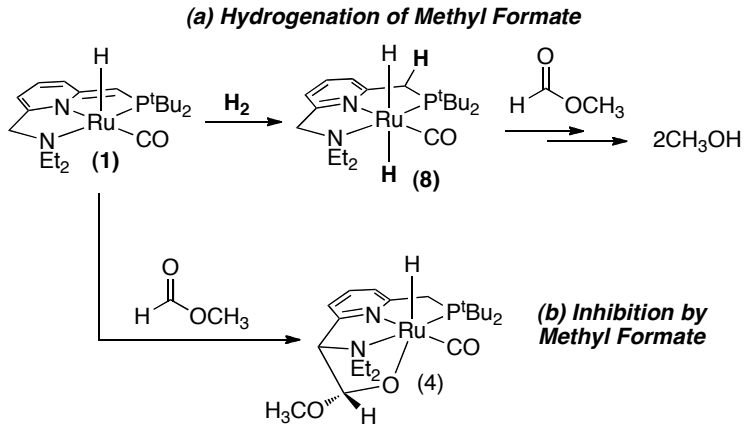

Order Study in Methyl Formate under Hydrogenation Conditions with 1

The order in methyl formate was measured to discern if substrate inhibition (*e.g.* formation of **4**) occurs during the hydrogenation of methyl formate to methanol. Under standard hydrogenation conditions, a J young NMR tube was charged with toluene-d_8, **1**, H_2, and methyl formate and was heated at 105 ºC over a two hour time period. A reaction profile was obtained during initial consumption of methyl formate (20-25% conversion) using ^{1}H NMR spectroscopy (Figure 3.5). Importantly, the rate of methyl formate conversion was measured for two different reactions where the initial concentration of methyl formate was 0.091 M and 0.18 M, 50 and 100 equivalents of methyl formate relative to **1**, respectively. If methyl formate were inhibiting the reaction, higher concentrations of methyl formate would be expected to slow the rate of hydrogenation. As shown in Figure 3.5, the concentration of methyl formate was plotted against time, and the slope of both lines (proportional to the rate) is identical. This indicates that the initial rate is not changing as a function of [HCOOMe], suggesting that the reaction is zero order in methyl formate under these conditions. Based on these data, the formation of **4** does not appear to inhibit ester hydrogenation catalysis.

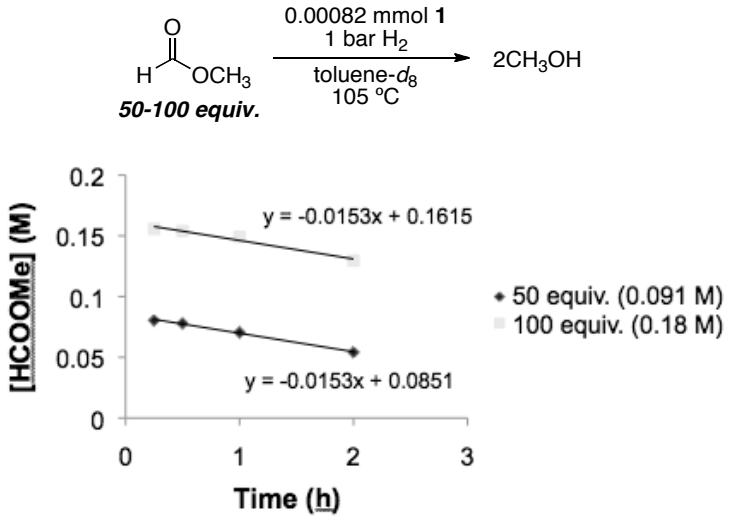

Figure 3.5. Hydrogenation of Methyl Formate: Order Study in Methyl Formate.

Determination of Catalyst Resting State for the Hydrogenation of Methyl Formate

To further test if **4** is forming during the catalytic hydrogenation of methyl formate, the catalyst resting state during the catalytic reaction was determined. Toluene-d_8, **1**, H_2, and 10 equivalents of methyl formate were added to a J-young tube and an initial ^{1}H NMR spectrum was acquired. As shown in Scheme 3.9a the major Ru species at room temperature was **4**.[5] The reaction was then heated at 70 ºC for 30 minutes during which time a 13% yield of methanol was obtained. While at this temperature, **8** was observed as the single Ru species (Scheme 3.9b), indicating that **4** is not present in significant quantities during catalysis.

Scheme 3.9. Hydrogenation of Methyl Formate: Observation of Catalyst Resting State

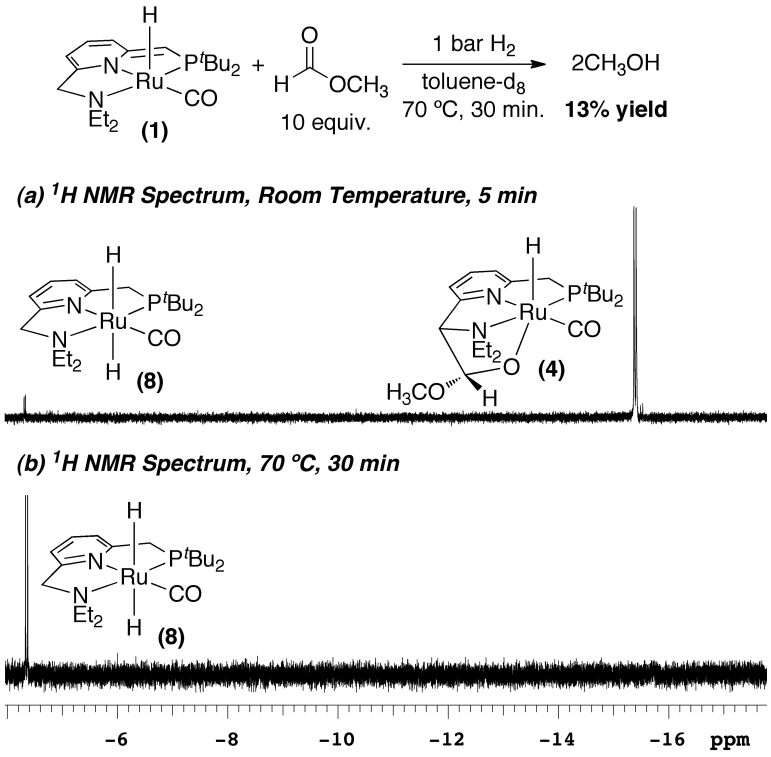

3.3 Reactivity of CO_2 with a Ruthenium Pincer Complex

3.3.1 Formation of Kinetic and Thermodynamic Products

Another component of the cascade system that could also directly react with Ru pincer complex **1** is CO_2. The most similar transformation found in the literature involves a β-diketiminate (nacnac) Sc complex.[6] This complex reacts with CO_2 to generate a Sc−O bond along with a C−C bond between CO_2 and the central carbon of the nacnac ligand. Moreover, ^{13}C labeling experiments show that CO_2 capture is reversible in this system.

Subjecting a C_6D_6 solution of **1** to 1 bar of CO_2 at room temperature resulted in an instantaneous color change from brown to yellow/orange, accompanied by a downfield shift of the ruthenium hydride ^1H NMR resonance from –26.45 ppm to –16.84 ppm. When the reaction mixture was allowed to stand overnight (or was heated to 70 ºC for 15 min), this new species (**9**) underwent complete conversion to a second product (**10**) with a Ru–H resonance at –16.18 ppm and was isolated in 87% yield (Scheme 3.10). 2D NMR spectroscopic experiments were carried out to fully characterize both complexes **9** and **10**, where the HMBC NMR spectroscopic experiment in particular provided information

on the proximity of the C–H on the arm of the ligand (adjacent to CO_2) to either P^tBu_2 or NEt_2, which was instrumental in verifying if the *P*-side or *N*-side isomer had formed.

Scheme 3.10. Reactivity of **1** with CO_2

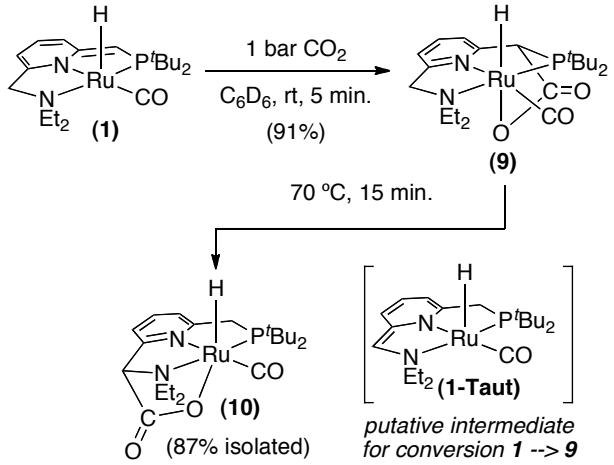

Additional support for the structural assignments of **9** and **10** was obtained by carrying out this sequence using $^{13}CO_2$. As shown in Figure 3.6, ^{1}H NMR spectroscopic analysis of the products of this reaction (**9-^{13}C** and **10-^{13}C**) showed ^{1}H-^{13}C coupling for H_A, which appears at 4.66 and 4.59 ppm, for **9-^{13}C** and **10-^{13}C** respectively. The observed two bond ^{1}H-^{13}C coupling constants are 4.2 Hz for **9-^{13}C** and 2.8 Hz for **10-^{13}C**.

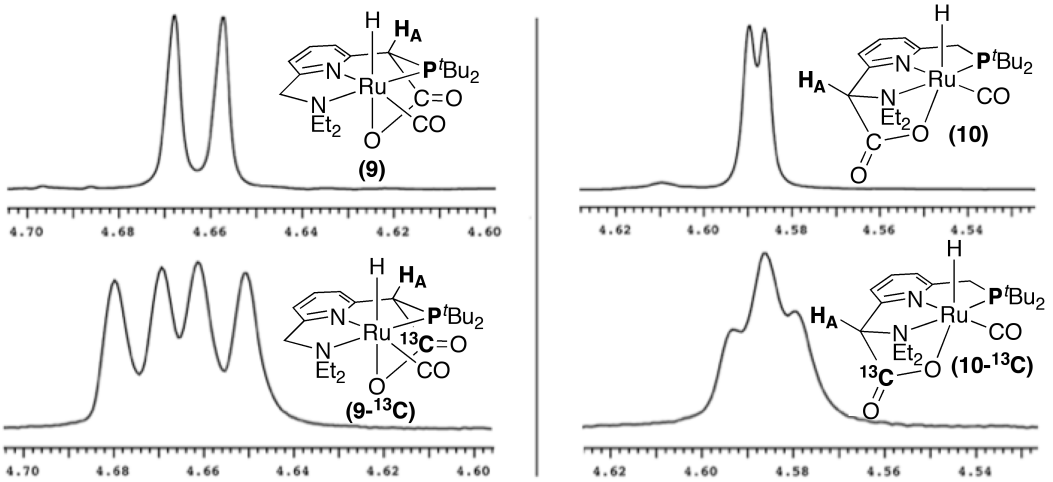

Figure 3.6. ^{1}H NMR signals for **9**, **9-^{13}C**, **10**, and **10-^{13}C**

The structure of complex **10** was further confirmed by X-ray crystallography. X-ray quality crystals were obtained by slow crystallization from a tetrahydrofuran (THF) solution of **10** at 25 ºC under 1 bar of CO_2 (Figure 3.7). The C–C distance for the bond formed between the pincer ligand and CO_2 (C2–C3 = 1.545 Å) is in the range of that observed for other ruthenium carboxylate complexes.[7] The constrained geometry of the metallacycle in **10** results in some bond angle distortion. For example, the N2–Ru1–O2 angle of 74.7º deviates significantly from the expected 90º for an ideal octahedral complex.

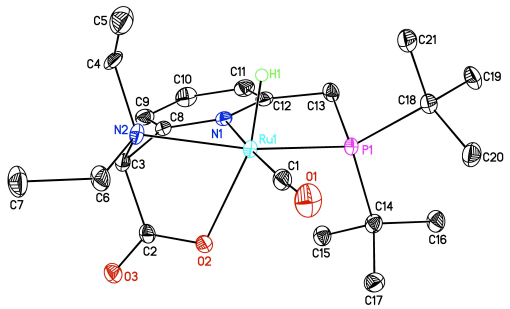

Figure 3.7. ORTEP diagram (50% probability level) of the molecular drawing of **10**. The packing solvent THF as well as all H atoms (other than the Ru–H) have been omitted for clarity. Selected bond lengths (Å) and angles (deg.): Ru1–H1 = 1.50(3), Ru1–N1 = 2.0902(18), Ru1–N2 = 2.2327(17), Ru1–O2 = 2.2524(15), Ru1–C1 = 1.834(2), Ru1–P1 = 2.2649(5), C2–C3 = 1.545(3), O2–C2 = 1.274(3), O3–C2 = 1.233(3), H1–Ru1–O2 =

163.6(11), N1–Ru1–C1 = 176.77(8), P1–Ru1–N2 = 159.02(5), N1–Ru1–O2 = 81.41(6), N2–Ru1–O2 = 74.72(6), C8–C3–C2 = 104.85(17).

3.3.2 Reversibility Study for CO_2 Coupling with 1 at Room Temperature

The facile conversion of **9** to **10** suggests that CO_2 activation is reversible for complex **9** (potentially followed by tautomerization of **1** to **1-Taut** (Scheme 3.10) and subsequent activation of CO_2 at **1-Taut** to generate **10**).[8] To further probe the reversibility of CO_2 activation, the solvent/CO_2 was removed from a C_6D_6 solution of complex **9** under vacuum, and the resulting residue was then redissolved in C_6D_6 under 1 bar of N_2. As shown in Scheme 3.11a, this procedure resulted in the formation of a 29% **1**, 17% **9**, and 45% **10** as determined by ^{1}H NMR spectroscopic analysis. In a second, independent experiment, a C_6D_6 solution of **9** was subjected to 1 bar of $^{13}CO_2$ for 1 hour at room temperature. This resulted in 26% **^{13}C** incorporation into **9** (Scheme 3.10b). Both of these experiments provide further evidence in support of the reversibility of C–C bond formation in **9**. Notably, shortly after this work was published, Milstein and coworkers reported similar findings with an analogous Ru PNP complex (**11**), where upon treatment with 1 bar CO_2, full conversion to CO_2 coupled product **12** was observed. Upon subjection to reduced pressure, the CO_2 coupling at **12** was reversible and **11** was recovered.[9]

Scheme 3.11. Reversibility Studies on Complex **9**

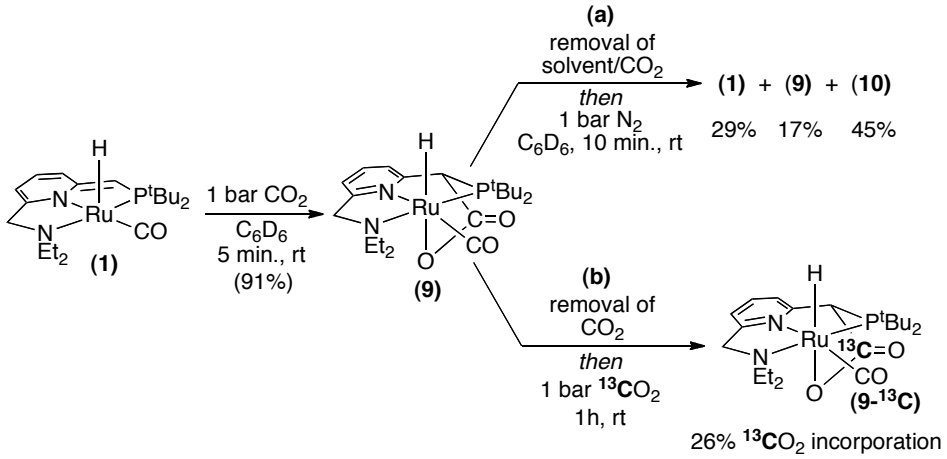

Scheme 3.12. Reversible Formation of **12** from **11** and CO_2[9]

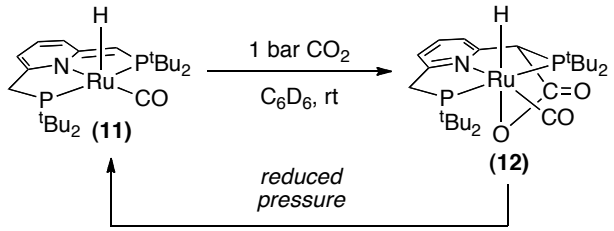

In marked contrast, at room temperature, complex **10** was stable to vacuum, and a solution of **10** under 1 bar of N_2 showed no reaction after 24 hours (Scheme 3.13a). Furthermore, complex **10** did not react with $^{13}CO_2$ over 16 hours (Scheme 3.13b), and in an independent experiment **10-^{13}C** underwent <5% $^{12}CO_2$ incorporation over 10 days in solution at room temperature. Collectively, these data indicate that at room temperature CO_2 activation is reversible at **9** but irreversible at complex **10**, likely a result of increased sterics on the *P*-side of the ligand relative to the *N*-side.

Scheme 3.13. Reversibility Studies on Complex **10**

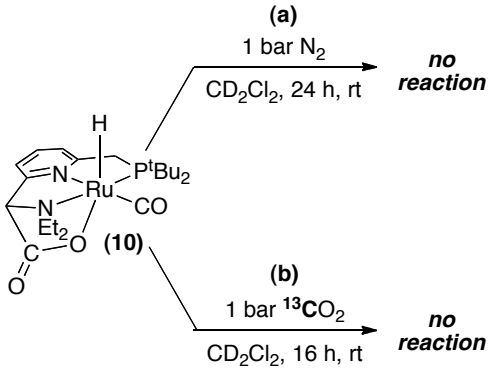

3.3.3 Implications for the Cascade System

The coupling of CO_2 with **1** at room temperature has been thoroughly studied; however, reactivity at elevated temperatures (analogous to required conditions for the cascade system) had not yet been evaluated. The formation of **10** during catalysis, would in theory, lower the amount of active hydrogenation catalyst, RuH_2 (**8**, Scheme 3.8) present in solution. In order to determine if CO_2 coupling with **1** is an issue in the cascade system, a number of experiments were conducted under catalytic reaction conditions to

determine the: i) extent of CO_2 inhibition for hydrogenation of methyl formate; ii) catalyst resting state; and iii) reversibility of the formation of **10** at elevated temperatures.

Hydrogenation of Methyl Formate in the Presence of CO_2

The **1**-catalyzed hydrogenation of methyl formate was carried out in the presence of CO_2 to determine the extent of CO_2 inhibition. CO_2 concentration was systematically varied from 0-25% of the total gas composition, and the effect on the yield was evaluated. As shown in Figure 3.8**,** charging the reactor with 40 bar H_2, yielded full conversion of methyl formate to methanol. However, upon adding a 35:5 mixture of H_2:CO_2, the yield decreased to 91%. This effect was further demonstrated by increasing the CO_2 content to a 30:10 mixture of H_2:CO_2, where the yield of methanol was less than 25%.

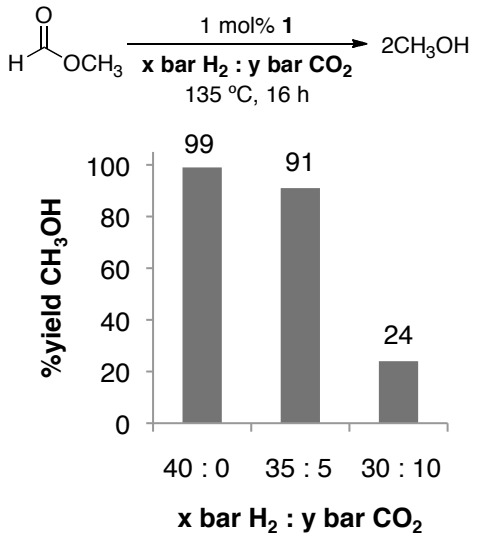

Figure 3.8. Hydrogenation of Methyl Formate using **1** in the Presence of CO_2

*Reactivity of **1** under CO_2 Hydrogenation Conditions*

Further studies were required to assess if the formation of **10** is responsible for reduced yields in the hydrogenation of methyl formate (Figure 3.8). Methoxybenzene-d_8 (anisole-d_8), **1**, and 1 bar of a mixture of H_2:CO_2 (4:1) were added to a J-young tube.

Heating this mixture at 120 ºC in the NMR spectrometer for 15 minutes, showed the formation of **10** in greater than 95% yield (Scheme 3.14).

Scheme 3.14. Observation of Resting State of **1** in the Presence of CO_2 and H_2

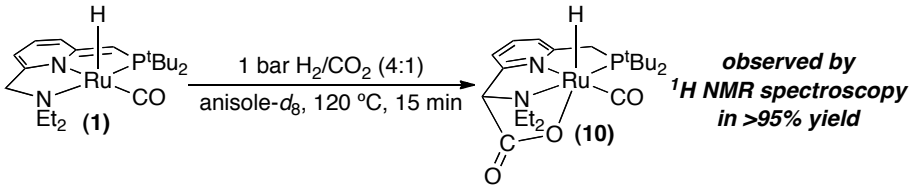

To gain a better understanding of the stability of **10** in the cascade hydrogenation system, a reversibility study was conducted at elevated temperatures similar to those utilized in the cascade system. A ^{13}C labeled sample of **10** was subjected to CO_2 in anisole and was heated at 70 – 120 ºC for 4 hours (Figure 3.9). After this time, the quantity of **10-^{13}C** was determined by quantitative ^{13}C NMR spectroscopic analysis in anisole. At 70 ºC, minimal exchange was observed; however, increasing the temperature to 100 and 120 ºC, significant ^{13}C incorporation was detected.

These experiments demonstrate that sufficiently high temperatures (>120 ºC) are required to render the formation of **10** reversible. Importantly, the overall objective for the homogeneously catalyzed cascade system is to operate at low reaction temperatures; however, reducing the temperature below 120 ºC is expected to reduce the rate of ester hydrogenation when using **1** (Scheme 3.1, step iii). Consequently, the temperature range is restricted to higher temperatures (>120 ºC) when using **1** in the cascade system.

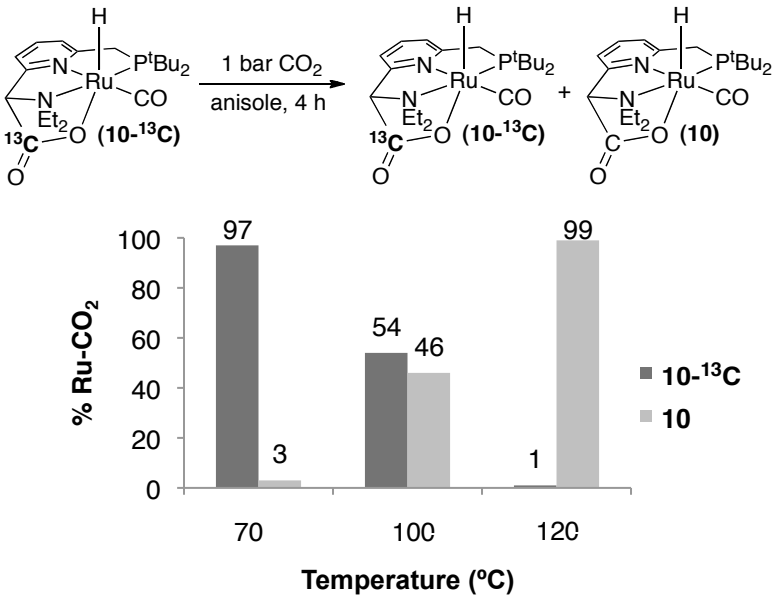

Figure 3.9. Reversibility Study for CO_2 Coupling with **1** at Varied Temperatures

3.4 Conclusions

In summary, a new mode of CO_2,[10] ester, ketone, and aldehyde[11] coupling with a Ru pincer complex was identified. The work described above shows that the reactivity of **1** with carbonyl compounds is more complex than was previously appreciated. While prior work focused primarily on **1** as a catalyst for the hydrogenation of C=O derivatives, it was found that **1** reacts with carbonyl compounds even in the absence of H_2. Furthermore, these reactions lead to numerous isomeric products that eventually equilibrate to a single major isomer. Additionally, at room temperature the reaction of **1** with esters and ketones is generally reversible. In contrast, benzaldehyde and CO_2 both react irreversibly.

This study also revealed that coupling between **1** and carbonyl compounds and CO_2 competes with H_2 addition. Specifically, the formation Ru-CO_2 adduct (**10**) and not the Ru-$HCOOCH_3$ adduct (**4**) was found to be a likely cause for reduced yields of methanol in the hydrogenation of methyl formate, a key step in the conversion of CO_2 to methanol. Furthermore, it was shown that with this ligand set, sufficiently high temperatures enable reversible coupling of CO_2 at **1**.

3.5 Experimental Procedures and Characterization of Data

General Procedures

NMR spectra were obtained on a Varian VNMRs 500 MHz (499.90 MHz for ^{1}H; 125.70 MHz for ^{13}C) or a Varian VNMRs 700 MHz (699.93 MHz for ^{1}H; 176.00 MHz for ^{13}C) spectrometer. Chemical shifts were referenced to an internal standard (tetramethylsilane or hexamethyldisiloxane for ^{1}H and ^{13}C; H_3PO_4 for ^{31}P).) or to residual solvent peaks (^{1}H, ^{13}C; C_6D_6: ^{1}H: 7.16 ppm, ^{13}C: 128.05 ppm; CD_2Cl_2: ^{1}H: 5.32 ppm, ^{13}C: 53.84 ppm). NMR signals were assigned based on the following 2D experiments: $^{1}H/^{1}H$ COSY, $^{1}H/^{13}C$ HMQC, $^{1}H/^{13}C$ HMBC, and $^{1}H/^{1}H$ NOESY. Abbreviations used in the NMR data: br, broad; s, singlet; d, doublet; t, triplet; q, quartet; m, multiplet. Elemental analysis was carried out at Atlantic Microlab in Norcross, GA. IR spectra were recorded on a Perkin-Elmer Spectrum BX FT-IR spectrometer using KBr pellets. High-resolution mass spectral data were obtained on an Agilent Q-TOF mass spectrometer in positive electrospray ionization mode. X-ray crystallographic data was collected on a Bruker SMART APEX-I CCD-based X-ray diffractometer.

Materials and Methods

All experiments were conducted under an oxygen-free atmosphere in either a glovebox or using Schlenk line technique, and all liquids were degassed using three freeze-pump-thaw cycles. (PNN)Ru(H)(CO) (**1**) was prepared according to a literature procedure.[12] Dry carbon dioxide (99.8%), ultra high purity hydrogen (99.999%), and a mix tank of 80% H_2/20% CO_2 were purchased from Metro Welding and $^{13}CO_2$ (99% ^{13}C) was purchased from Cambridge Isotope Laboratories. Methyl formate (Alfa Aesar) and ethyl formate (Acros) were purified by distillation from P_2O_5. Acetone (Fisher) was dried over $CaSO_4$. Benzaldehyde (Sigma Aldrich, 99.5%), acetaldehyde (Fluka, anhydrous >99.5%), and *N,N*-dimethylformamide (Alfa Aesar, 99.8%) were used without further purification. Cyclopentanone (Fisher) and methyl acetate (Aldrich) were dried over 4 Å sieves. Anisole (Aldrich) and anisole-d_8 were dried over sodium metal and degassed before use. Benzene-d_6, and toluene-d_8 were purchased from Cambridge Isotopes Laboratories and dried using benzophenone/ketyl stills. CD_2Cl_2 was dried by distillation from $CaSO_4$.

Hexamethyldisiloxane (HMDSO) was purchased from Sigma Aldrich and dried over 4 Å molecular sieves.

I. Reactivity Summary for Esters, Amides, Ketones, and Aldehydes with 1

A. Formation of Ru-Carbonyl Compound Adducts at Room Temperature for NMR Analysis (Scheme 3.3 and Scheme 3.4)

In an N_2 atmosphere dry box, (PNN)Ru(H)(CO) (**1**) (5 mg, 0.011 mmol) was dissolved in 0.5 mL C_6D_6 and added to a J-young NMR tube. The carbonyl compound was then added, resulting in a color change from dark red/brown to yellow over 30 min. The product of the reaction was determined by NMR analysis.

Table 3.2. Summary of Room Temperature Reactions of **1** with Carbonyl Compounds

Entry	Carbonyl Compound	Equiv. Added	Time (h)	Major Pdt.	Conver. of 1	Isolated Yield[a]
1	Methyl Formate	2.5	0.5	**4**	100%	94%
2	Ethyl Formate	4	0.5	**5**	100%	83%
3	Methyl Acetate	20	1	N/A	0%	NR
4	*N,N*-Dimethylformamide	20	1	N/A	0%	NR
5	Acetone	20	1	--[b]	13%	N/A
6	Cyclopentanone	11	0.5	**6B**	100%	65%
7	Acetaldehyde	1	0.1	--[b]	100%	N/A
8	Benzaldehyde	1	0.1	**7B-i**	100%	88%
9	Benzaldehyde	1	24	**7B-ii**	100%	88%

[a]Note: Where yields not given, the product was either not formed (NR) or was not characterized (N/A). [b]Multiple Ru-H species formed. [c]Yield reflects a mixture of diastereomers, **7B-i** and **7B-ii**.

*B. Isolation of Ru Carbonyl Compound Adducts (**4**, **5**, **6** and **7B-i**/**ii**) for Elemental Analysis and IR Characterization*

<u>Complex **4**</u>: In a N_2 atmosphere dry box, complex **1** (15 mg, 0.033 mmol) was dissolved in 0.2 mL of methyl formate. Over a period of 10 min at room temperature, a yellow crystalline material precipitated from solution. The remaining solvent was decanted, and the solid was dried *in vacuo*. Complex **4** was obtained as a yellow crystalline solid (16.3 mg, 94% yield). Anal. Calcd. for $C_{22}H_{39}N_2O_3PRu$: C, 51.65; H, 7.68; N, 5.4. Found: C, 51.45, H, 7.70; N, 5.42. NMR and IR characterization data are discussed in detail below.

Complex **5**: In an N_2 atmosphere dry box, complex **1** (15 mg, 0.033 mmol) was dissolved in 0.3 mL of pentane. Ethyl formate (5 μL, 0.062 mmol, 1.9 equiv) was then added. Over a period of 5-10 min at room temperature a yellow crystalline material precipitated from solution. The remaining solvent was decanted, and the solid was washed with pentane (2 x 0.1 mL). The solid was then dried *in vacuo*. Complex **5** was obtained as a yellow crystalline solid (14.4 mg, 83% yield). Anal. Calcd. for $C_{23}H_{41}N_2O_3PRu$: C, 52.56; H, 7.86; N, 5.33. Found: C, 52.37, H, 7.94; N, 5.17. NMR and IR characterization data are discussed in detail below.

Complex **6**: In an N_2 atmosphere dry box, complex **1** (15 mg, 0.033 mmol) was dissolved in 0.3 mL of pentane. Cyclopentanone (3 μL, 0.034 mmol, 1.0 equiv) was then added. Over a period of 5-10 min at room temperature a yellow crystalline material precipitated from solution. The remaining solvent was decanted, and the solid was washed with pentane (2 x 0.1 mL). The solid was then dried *in vacuo*. Complex **6** was obtained as a yellow crystalline solid (15.0 mg, 65% yield). Anal. Calcd. for $C_{25}H_{43}N_2O_2PRu$: C, 56.06; H, 8.09; N, 5.23. Found: C, 56.43, H, 8.22; N, 4.75. NMR and IR characterization data are discussed in detail below.

Complexes **7B-i/ii**: In an N_2 atmosphere dry box, complex **1** (15 mg, 0.033 mmol) was dissolved in 0.3 mL of pentane. Benzaldehyde (3.5 μL, 0.034 mmol, 1.0 equiv) was then added. Over a period of 5-10 min at room temperature a yellow crystalline material precipitated from solution. The remaining solvent was decanted, and the solid was washed with pentane (2 x 0.1 mL). The solid was then dried *in vacuo*. Complex **6** was obtained as a yellow crystalline solid (16.3 mg, 88% yield, approx. 7 : 3 mixture of **7B-I : ii**). Anal. Calcd. for $C_{27}H_{41}N_2O_2PRu$ (*mixture of isomers*): C, 58.15; H, 7.41; N, 5.02. Found: C, 58.26, H, 7.37; N, 4.94. NMR and IR characterization data are discussed in detail below.

C. Formation of Ru-Carbonyl Compound Adducts at Low Temperature for NMR Analysis (Scheme 3.6 and Scheme 3.7)

In an N_2-atmosphere dry box, complex **1** (5 mg, 0.066 mmol) was dissolved in 0.3 mL of toluene-d_8 and added to a J-Young NMR tube. The tube was placed in an LN_2 cooled cold well for 15 min. The carbonyl compound was then dissolved in 0.2 mL of toluene-d_8, and this solution was added to the NMR tube before returning it to the cold well for an additional 15 min. The tube was removed from the dry box and placed into a –78 ºC bath before inserting into precooled NMR instrument. A summary of low temperature experiments is shown in Table 3.3.

Table 3.3. Summary of Low Temperature Reactions of **1** with Carbonyl Compounds

Entry	Carbonyl Compound	Equiv. Added	Time (h)	Temp (ºC)	Conver. of 1	Major Pdt.
1	Methyl Formate	2.5	0.2	–70	0%	NR
2	Methyl Formate	2.5	13	–40	46%	not det.[a]
3	Cyclopentanone	12	1	–40	100%	**6A**
4	Benzaldehyde	1.5	0.08	–50	100%	**7A-i**

[a]1.7 : 1 : 3.2 ratio of undetermined species : 3 : 1 detected. We were unable to fully characterize the undetermined species; however, we speculate that it is the other *N*-side diastereomer of **4** (analogous to **7B-i**) with a Ru-H resonance at –15.48 ppm, based on the br s at 4.18 ppm (presumably C*H*N peak), the s at 4.70 ppm (presumably C*H*O peak), and other diagnostic resonances in the ^{1}H NMR.

D. Procedure for Equilibrium Constant Determination (Table 3.1)

In a N_2-atmosphere dry box, (PNN)Ru(H)(CO) (**1**, 0.5 mL of a 0.011 M solution in C_6D_6, 2.5 mg, 0.00554 mmol) and carbonyl compound (see table below; 1–5 equiv. added to allow for partial conversion of **1**) were combined in a J-young NMR tube. The tube then sat at room temperature for 1.5 h to allow the reaction to reach equilibrium. ^{1}H NMR spectroscopic analysis provided the ratios of **1**, free carbonyl compound and Ru-carbonyl product (**4**–**6**) formed.

Table 3.4. Optimization Studies for K_{eq} Determination

Entry	Carbonyl Compound	Equiv. Added	Time (h)	Major Pdt.	Average K_{eq}
1	Methyl Formate	1	1	**4**	$2.7 \times 10^2 \pm 0.4$
2	Methyl Formate	2	1.5	**4**	$3.0 \times 10^2 \pm 0.06$
3	Methyl Formate	2	2	**4**	$3.1 \times 10^2 \pm 0.2$
4	Ethyl Formate	2	1.5	**5**	$1.5 \times 10^2 \pm 0.02$
5	Cyclopentanone	5	1.5	**6**	$5.0 \times 10^1 \pm 0.2$
6	Cyclopentanone	5	4	**6**	$5.0 \times 10^1 \pm 0.1$

Note: For methyl and ethyl formate, a Ru-H peak at -4.74 ppm (3% relative to total Ru) forms after 2 h

E. Reaction Rate and Resting State Studies

A. Order Study in Methyl Formate (Figure 3.5)

In an N_2-atmosphere dry box, complex **1** (100 µL of an 8.2 mM solution in toluene-d_8, 0.37 mg, 0.00082 mmol), HCO_2CH_3 (100 µL of a 0.41 or 0.91 M solution in toluene-d_8, 0.041 or 0.082 mmol, 50 or 100 equiv.), tetramethylsilane (internal standard, 90 µL of a 0.23 mM solution in toluene-d_8, 0.143 µmol) and 220 µL of toluene-d_8 were added to a J-Young NMR tube. The samples were next subjected to 3 freeze pump thaw cycles before charging with 1 bar H_2. The tube was then placed into a preheated NMR spectrometer at 105 ºC. After allowing sample to equilibrate in the spectrometer for 10 minutes, a ^{1}H NMR spectrum was acquired at room temperature after 0.25, 0.5, 1, and 2 hours where the conversion of methyl formate to methanol was quantified. NMR experimental details: ^{13}C decoupled, 25 s relaxation delay, 2 scans acquired.

B. Hydrogenation of Methyl Formate: Observation of Catalyst Resting State (Scheme 3.9)

In an N_2-atmosphere dry box, complex **1** (2.5 mg, 0.0055 mmol), HCO_2CH_3 (3.5 µL, 0.55 mmol, 10 equiv.), tetramethylsilane (internal standard, 1.9 µL, 0.14 mmol, 2.5 equiv.), and 0.5 mL of toluene-d_8 were added to a J-Young NMR tube. The sample was next subjected to 3 freeze pump thaw cycles before charging with 1 bar H_2. An initial ^{1}H NMR spectrum was acquired (note: <5% **1** was observed in this spectrum), the tube was ejected while the spectrometer reached 70 ºC, and the tube was then placed into a preheated NMR spectrometer at 70 ºC. After allowing sample to equilibrate in the

spectrometer for 10 minutes, a ^{1}H NMR spectrum was acquired after 30 minutes yielding 13% CH_3OH. NMR experimental details: ^{13}C decoupled, 25 s relaxation delay, 2 scans acquired.

II. Reactivity Summary for CO_2 and 1

*A. Synthesis of Ru CO_2 Adducts (**9**, **9-^{13}C**, **10**, and **10-^{13}C**,* **Scheme 3.10** *and* **Figure 3.6***)*

Complex **9**: In an N_2-atmosphere dry box, (PNN)Ru(H)(CO) (**1**) (0.4 mL of a 5.5 mM solution in C_6D_6, 1 mg, 0.0022 mmol) and HMDSO (internal standard, 20 μL of a 15 mM solution of in C_6D_6, 0.00030 mmol) were combined in a J-young NMR tube. The tube was attached to a Schlenk line, and the N_2 atmosphere above the solvent was quickly removed under vacuum and then immediately replaced with CO_2. The tube was shaken, which resulted in an instantaneous color change from dark brown/red to orange. ^{1}H NMR spectroscopic analysis after 5 min at rt showed that **9** was formed in 91% yield (average of three experimental runs).

Complex **9-^{13}C**: In an N_2-atmosphere dry box, (PNN)Ru(H)(CO) (**1**) (9 mg, 0.020 mmol) and 0.4 mL C_6D_6 were added to a J-young NMR tube. The tube was attached to a Schlenk line, and the N_2 atmosphere above the solvent was quickly removed under vacuum and then immediately replaced with $^{13}CO_2$. The tube was shaken, which resulted in an immediate color change from dark brown/red to orange.

Complex **10**: In an N_2-atmosphere dry box, (PNN)Ru(H)(CO) (**1**) (50 mg, 0.11 mmol) was dissolved in benzene (4 mL) in a 25 mL Schenk flask. The flask was attached to a Schlenk line, and the N_2 atmosphere above the solvent was quickly removed under vacuum and then immediately replaced with 1 atm of CO_2. The reaction mixture was stirred at 70 ºC for 15 min, during which time a yellow precipitate began to form. The reaction was cooled to room temperature and then concentrated under vacuum to ~0.5 mL of benzene. Pentane (5 mL) was added to precipitate the product as a yellow solid. The solid was collected on a fritted filter, washed with pentane (2 x 3 mL), and dried under vacuum to afford **10** as a yellow solid (48 mg, 87% yield). X-ray quality crystals

(yellow needles) of **5** were formed via slow crystallization under an atmosphere of CO_2 in THF at room temperature.

<u>Complex **10-^{13}C**</u>: In an N_2-atmosphere dry box, (PNN)Ru(H)(CO) (**1**) (9 mg, 0.020 mmol) and 0.4 mL C_6D_6 were added to a J-young NMR tube. The tube was attached to a Schlenk line, and the N_2 atmosphere above the solvent was quickly removed under vacuum and then immediately replaced with $^{13}CO_2$. The tube was shaken, which resulted in an immediate color change from dark brown/red to orange. The sample was then heated to 70 ºC in the NMR probe for 5 minutes.

*B. CO_2 Reversibility Studies on **9**: Procedure for Removal of CO_2 (Scheme 3.11)*

In an N_2-atmosphere dry box, (PNN)Ru(H)(CO) (**1**) (0.4 mL of a 5.5 mM solution in C_6D_6, 1 mg, 0.0022 mmol) was added to a J-young NMR tube. The tube was attached to a Schlenk line, and the N_2 atmosphere above the solvent was quickly removed under vacuum and then immediately replaced with CO_2. The tube was shaken, which resulted in an immediate color change from dark brown/red to orange. ^{1}H NMR spectroscopic analysis after 5 min at rt showed full conversion of **1** to complex **4**. The sample was frozen in LN_2, and benzene/CO_2 were removed under vacuum via sublimation. The contents of the NMR tube were then redissolved in C_6D_6 (0.4 mL) and HMDSO (0.0003 mmol, 20 µL of a 15 mM solution in C_6D_6) was added as a standard. The reaction was immediately analyzed by ^{1}H NMR spectroscopy (after <10 min), which showed the presence of **1**, **9**, and **10** in a 1.7 : 1 : 2.6 ratio (Yield: 29% **1**, 17% **9**, 45% **10**).

*C. CO_2 Reversibility Studies on **9**: Procedure for Treatment with $^{13}CO_2$ (Scheme 3.11)*

In an N_2-atmosphere dry box, (PNN)Ru(H)(CO) (**1**) (0.2 mL of an 11 mM solution in C_6D_6, 1 mg, 0.0022 mmol), THF (0.137 mmol, based on 1.1% natural abundance of ^{13}C this corresponds to 0.0015 mmol $^{13}C_4H_8O$, 50 µL of an 2.7 M solution in C_6D_6) and C_6D_6 (0.2 mL) were combined in a J-young NMR tube. The tube was attached to a Schlenk line, and the N_2 atmosphere above the solvent was quickly removed under vacuum and then immediately replaced with CO_2. An immediate color change from dark brown/red to orange was observed after shaking the tube. ^{1}H NMR spectroscopic analysis after 5 min

at room temperature showed full conversion of **1** to complex **9**. The tube was then reattached to a Schlenk line and the CO_2 atmosphere above the solvent was quickly removed under vacuum and then immediately replaced with $^{13}CO_2$. The tube was shaken vigorously, and then the reaction was monitored as a function of time. The yields of each product are shown in the table below.

Table 3.5. Product Distribution for CO_2 Reversibility Experiment at **9**

Entry	Time (h)	9/9-^{13}C : 10/10-^{13}C (det. by ^{1}H NMR)	%9-^{13}C (det. by ^{13}C NMR)	%10-^{13}C (det. by ^{13}C NMR)
1	0.2	3 : 1	23%	<1%
2	1	3 : 2	26%	<5%
3	3	1 : 2	14%	10%
4	5	1 : 3	<5%	24%
5	24	Only **10**	<1%	40%

^{13}C NMR experimental details: Decoupled, no NOE, 30 s relaxation delay, 30º pulse angle, 30 scans collected.

*D. Reversibility Studies on **10** (Scheme 3.13)*

Complex **10** (1.3 mg, 0.0026 mmol) was dissolved in CD_2Cl_2 (0.15 mL) in a J-young NMR tube under an N_2 atmosphere. The sample was then allowed to stand for 24 h and was analyzed by ^{1}H NMR spectroscopy. No reaction was observed.

*E. Reversibility Studies on **10**: Procedure for Reaction of **10** with $^{13}CO_2$ (Scheme 3.13)*

In an N_2-atmosphere dry box, **10** (1.3 mg, 0.0026 mmol) and 200 µL CD_2Cl_2 were added to a thick walled J-young NMR tube. The tube was attached to a Schlenk line, and the N_2 atmosphere above the solvent was quickly removed under vacuum, and then immediately replaced with $^{13}CO_2$. The tube was shaken vigorously and the reaction was monitored by ^{13}C NMR spectroscopy as a function of time. No **10-^{13}C** was detected after 16 h. ^{13}C NMR experiment details: decoupled, no NOE, 30 s relaxation delay, 30º pulse angle, 16 scans acquired.

*F. Reversibility Studies on **10**: Procedure for Reaction of **10-^{13}C** with CO_2*

a. Room Temperature Study (Scheme 3.13)

Complex **10-^{13}C** (1.5 mg, 0.0030 mmol) was dissolved in CD_2Cl_2 (0.15 mL) in a J-young NMR tube. The tube was attached to a Schlenk line, and the N_2 atmosphere above the solvent was quickly removed under vacuum and then immediately replaced with CO_2. The tube was shaken vigorously, and the reaction was allowed to stand at room temperature for 10 days. The solvent was removed under vacuum and the resulting yellow solid was analyzed by positive electrospray ionization mass spectroscopy. The isotope envelope was compared to that of authentic samples of **10** and **10-^{13}C** (Figure 3.10 and Figure 3.11 below). These data indicate <5% incorporation of $^{12}CO_2$.

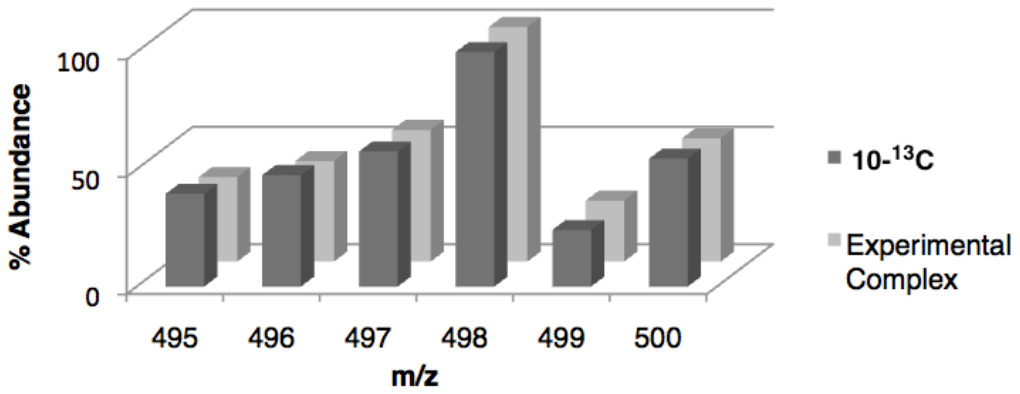

Figure 3.10. Comparison of Isotope Envelope for **10-^{13}C** and Reacted Complex

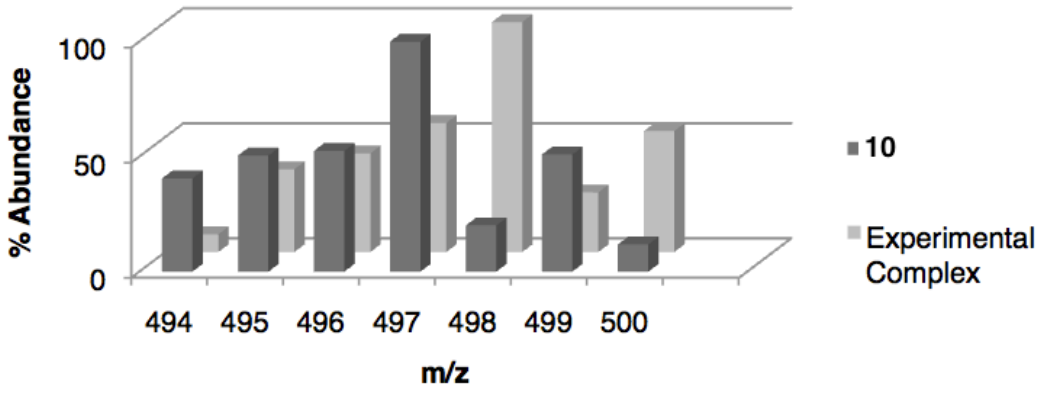

Figure 3.11. Comparison of Isotope Envelope for **10** and Reacted Complex

b. Variable Temperature Study (Figure 3.9)

Complex **10-^{13}C** (1.8 mg, 0.0036 mmol) was dissolved in anisole (0.45 mL, solvent and internal standard) in a J-young NMR tube. An initial ^{13}C NMR was acquired to determine the initial ratio of $^{13}CO_2$ in **10-^{13}C** relative to the internal standard, which is the 1.1% natural abundance of ^{13}C in anisole (specifically, the quaternary carbon of anisole was used). The tube was attached to a Schlenk line, and the N_2 atmosphere above the solvent was quickly removed under vacuum and then immediately replaced with CO_2. The tube was shaken vigorously, and the reaction heated at the specified temperature for 4 hours. After this time, the tube was cooled to room temperature and a ^{13}C NMR spectrum was acquired to determine the amount of **10-^{13}C** remaining. NMR experimental details: decoupled, no NOE, 0.1 s relaxation delay, 100 scans acquired.

*G. Observation of Catalyst Resting State for **1** in the Presence of CO_2 and H_2 (Scheme 3.14)*

In a N_2-atmosphere dry box, complex **1** (2 mg, 0.0044 mmol), hexamethyldisiloxane (internal standard, 1 µL, 4.7 µmol, 0.11 equiv.), and 0.45 mL of anisole-d_8 were added to a J-Young NMR tube. The N_2 atmosphere above the solvent was quickly removed under vacuum and then immediately replaced with 1 bar of pre-mixed 4:1 H_2:CO_2. An initial ^{1}H NMR spectrum was acquired to determine the relative ratio between Ru (summation of all diagnostic Ru-H peaks used, as they are all far upfield away from other peaks) and the internal standard. The tube was then placed into a preheated NMR spectrometer at 120 ºC and was allowed to react for 15 min. The ^{1}H NMR spectrum showed **10** to be the major product in 95% yield (minor product in <5% yield was the Ru-formate species to be discussed in the next chapter). NMR experimental details: ^{13}C decoupled, 10 s relaxation delay, 4 scans acquired.

III. NMR and IR Characterization of Ru-Carbonyl Compounds

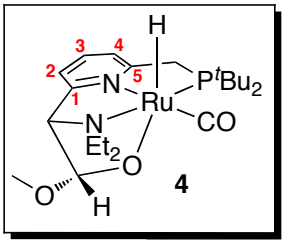

^{31}P{^{1}H} NMR (C_6D_6): 119.34 (s).

^{1}H NMR (C_6D_6): –15.25 (d, J_{HP} = 28.2 Hz, 1H, Ru-***H***), 0.84 (t, J_{HH} = 7.2 Hz, 3H, $NCH_2C\boldsymbol{H_3}$), 0.89 (t, J_{HH} = 6.9 Hz, 3H, $NCH_2C\boldsymbol{H_3}$), 1.25 (d, J_{HP} = 13.2 Hz, 9H, $PC(C\boldsymbol{H_3})_3$), 1.28 (d, J_{HP} = 13.0 Hz, 9H, $PC(C\boldsymbol{H_3})_3$), 2.20 (dqd, J_{HH} = 13.6 Hz, J_{HH} = 6.9 Hz, J_{HP} = 3.2 Hz, 1H, $NC\boldsymbol{H}HCH_3$), 2.37 (dq, J_{HH} = 13.6 Hz, J_{HH} = 6.9 Hz, 1H, $NC\boldsymbol{H}HCH_3$), 2.88 (dd, J_{HH} = 16.4 Hz, J_{HP} = 7.3 Hz, 1H, C***H***HP), 2.93 (dd, J_{HH} = 16.4 Hz, J_{HP} = 9.9 Hz, 1H, C***H***HP), 3.46 (s, $OC\boldsymbol{H_3}$), 3.52 (dq, J_{HH} = 14.4 Hz, J_{HH} = 7.2 Hz, 1H, $NC\boldsymbol{H}HCH_3$), 3.57 (m, 1H, $NC\boldsymbol{H}HCH_3$), 3.94 (t, $J_{HH/HP}$ = 2.7 Hz, 1H, C***H***N), 6.01 (d, J_{HH} = 2.7 Hz, 1H, C***H***O), 6.53 (d, J_{HH} = 7.5 Hz, 1H, Py-***H4***), 6.92 (d, J_{HH} = 7.7 Hz, 1H, Py-***H2***), 6.95 (t, J_{HH} = 7.6 Hz, 1H, Py-***H3***).

^{13}C{^{1}H} NMR (C_6D_6): 8.02 (s, $NCH_2\boldsymbol{C}H_3$), 11.15 (s, $NCH_2\boldsymbol{C}H_3$), 29.44 (d, J_{CP} = 4.6 Hz, $PC(\boldsymbol{C}H_3)_3$), 30.34 (d, J_{CP} = 2.3 Hz, $PC(\boldsymbol{C}H_3)_3$), 34.26 (d, J_{CP} = 22.8 Hz, $P\boldsymbol{C}(CH_3)_3$), 37.01 (d, J_{CP} = 20.6 Hz, $\boldsymbol{C}H_2P$), 37.63 (d, J_{CP} = 11.9 Hz, $P\boldsymbol{C}(CH_3)_3$), 46.82 (s, $N\boldsymbol{C}H_2CH_3$), 49.34 (s, $N\boldsymbol{C}H_2CH_3$), 53.10 (s, $O\boldsymbol{C}H_3$), 76.65 (s, ***C***HN), 102.85 (s, ***C***HO), 118.39 (d, J_{CP} = 8.7 Hz, Py-***C4***), 122.19 (s, Py-***C2***), 135.49 (s, Py-***C3***), 159.93 (d, J_{CP} = 3.9 Hz, Py-***C5***), 160.36 (s, Py-***C1***), 209.14 (m, Ru-***C***O).

Peaks corresponding to free methyl formate in spectra:

^{1}H NMR (C_6D_6): 3.16 (s, 1H, $OC\boldsymbol{H_3}$), 7.49 (s, 1H, ***H***CO).

^{13}C{^{1}H} NMR (C_6D_6): 50.03 (s, $O\boldsymbol{C}H_3$), 160.72 (s, ***C***=O).

IR (KBr pellet, cm^{-1}): 1982 (Ru-H), 1891 (CO).

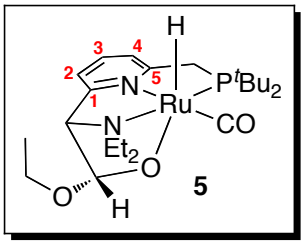

$^{31}P\{^1H\}$ NMR (C_6D_6): 119.42 (s).

^1H NMR (C_6D_6): –15.20 (d, J_{HP} = 28.1 Hz, 1H, Ru-***H***), 0.85 (t, J_{HH} = 7.0 Hz, 3H, $NCH_2C\boldsymbol{H_3}$), 0.89 (t, J_{HH} = 6.9 Hz, 3H, $NCH_2C\boldsymbol{H_3}$), 1.09 (t, J_{HH} = 7.1 Hz, 3H, $OCH_2C\boldsymbol{H_3}$), 1.23 (d, J_{HP} = 13.2 Hz, 9H, $PC(C\boldsymbol{H_3})_3$), 1.28 (d, J_{HP} = 12.9 Hz, 9H, $PC(C\boldsymbol{H_3})_3$), 2.22 (dqd, J_{HH} = 13.4 Hz, J_{HH} = 6.9 Hz, J_{HP} = 2.2 Hz, 1H, $NC\boldsymbol{H}HCH_3$), 2.39 (dq, J_{HH} = 13.4 Hz, J_{HH} = 6.9 Hz, 1H, $NC\boldsymbol{H}HCH_3$), 2.89 (dd, J_{HH} = 16.4 Hz, J_{HP} = 7.4 Hz, 1H, C***H***HP), 2.93 (dd, J_{HH} = 16.4 Hz, J_{HP} = 10.2 Hz, 1H, C***H***HP), 3.52 (dq, J_{HH} = 14.5 Hz, J_{HH} = 7.0 Hz, 1H, $NC\boldsymbol{HH}CH_3$), 3.59 (m, 2H, overlapping peaks: $NC\boldsymbol{HH}CH_3$ and $OC\boldsymbol{HH}CH_3$), 3.93 (t, $J_{HH/HP}$ = 2.5 Hz, 1H, C***H***N), 4.08 (dq, J_{HH} = 8.7 Hz, J_{HH} = 7.1 Hz, 1H, $OC\boldsymbol{HH}CH_3$), 6.12 (d, J_{HH} = 2.7 Hz, 1H, C***H***O), 6.56 (d, J_{HH} = 7.6 Hz, 1H, Py-***H4***), 6.94 (d, J_{HH} = 7.8 Hz, 1H, Py-***H2***), 6.98 (t, J_{HH} = 7.7 Hz, 1H, Py-***H3***).

$^{13}C\{^1H\}$ NMR (C_6D_6): 7.97 (s, $NCH_2\boldsymbol{C}H_3$), 11.12 (s, $NCH_2\boldsymbol{C}H_3$), 15.99 (s, $OCH_2\boldsymbol{C}H_3$), 29.39 (d, J_{CP} = 4.6 Hz, $PC(\boldsymbol{C}H_3)_3$), 30.28 (d, J_{CP} = 2.4 Hz, $PC(\boldsymbol{C}H_3)_3$), 34.17 (d, J_{CP} = 22.8 Hz, $P\boldsymbol{C}(CH_3)_3$), 36.96 (d, J_{CP} = 20.2 Hz, $\boldsymbol{C}H_2P$), 37.58 (d, J_{CP} = 11.8 Hz, $P\boldsymbol{C}(CH_3)_3$), 46.75 (d, J_{CP} = 1.3 Hz, $N\boldsymbol{C}H_2CH_3$), 49.27 (s, $N\boldsymbol{C}H_2CH_3$), 59.90 (s, $O\boldsymbol{C}H_2CH_3$), 76.93 (s, ***C***HN), 101.37 (s, ***C***HO), 118.15 (d, J_{CP} = 8.7 Hz, Py-***C4***), 122.16 (s, Py-***C2***), 135.05 (s, Py-***C3***), 159.70 (d, J_{CP} = 4.2 Hz, Py-***C5***), 160.53 (d, J_{CP} = 1.4 Hz, Py-***C1***), 209.27 (dd, $J_{PC/HC}$ = 15.2 Hz, $J_{PC/HC}$ = 7.2 Hz Ru-***C***O).

Peaks corresponding to free ethyl formate in spectra:

^1H NMR (C_6D_6): 0.83 (t, J_{HH} = 7.2 Hz, 3H, $OCH_2C\boldsymbol{H_3}$), 3.81 (q, J_{HH} = 7.2 Hz, 2H, $OC\boldsymbol{H_2}$), 7.56 (s, 1H, ***H***CO).

$^{13}C\{^1H\}$ NMR (C_6D_6): 13.95 (s, $OCH_2\boldsymbol{C}H_3$), 59.37 (s, $O\boldsymbol{C}H_2$), 160.30 (s, ***C***=O).

IR (KBr pellet, cm^{-1}): 1998 (Ru-H), 1885 (CO).

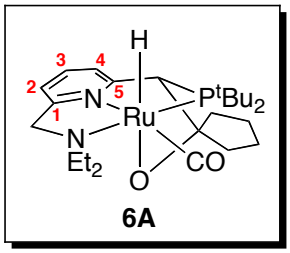

Spectra for complex 6A collected at –40 ºC

^{31}P{^{1}H} NMR (toluene-d_8): 109.07 (s).

^{1}H NMR (toluene-d_8): –15.51 (d, J_{HP} = 26.8 Hz, 1H, Ru-***H***), 0.81 (br t, J_{HH} = 6.9 Hz, 3H, NCH$_2$C***H$_3$***), 1.00 (br t, J_{HH} = 6.5 Hz, 3H, NCH$_2$C***H$_3$***), 1.17 (d, J_{HP} = 12.6 Hz, 9H, PC(C***H$_3$***)$_3$), 1.25 (d, *overlapping with excess cyclopentanone*, 9H, PC(C***H$_3$***)$_3$), 2.19 (m, 1H, NC***H***HCH$_3$), 2.28 (m, 2H, OCCH$_2$C***H$_2$***), 2.40 (m, 1H, NC***H***HCH$_3$), 2.47 (dq, J_{HH} = 7.4 Hz, 1H, OCC***H***H), 2.54 (dq, J_{HH} = 7.3 Hz, 1H, OCC***H***H), 2.61 (dd, J_{HH} = 16.6 Hz, J_{HH} = 7.2 Hz, 1H, OCC***H***H), 2.84 (dd, J_{HH} = 9.6 Hz, J_{HH} = 16.6 Hz, 1H, OCC***H***H), 2.95–2.98 (m, 3H, overlapping peaks: OCCH$_2$C***H$_2$*** and NC***H***H), 3.45–3.56 (m, 2H, NC***H$_2$***CH$_3$), 4.87 (d, J_{HP} = 6.7 Hz, 1H, C***H***P), 5.09 (d, J_{HH} = 13.6 Hz, 1H, C***H***HN), 6.22 (d, J_{HH} = 7.7 Hz, 1H, Py-***H2***), 6.43 (d, J_{HH} = 7.6 Hz, 1H, Py-***H4***), 6.76 (t, J_{HH} = 7.6 Hz, 1H, Py-***H3***).

^{13}C{^{1}H} NMR (toluene-d_8): 8.49 (s, NCH$_2$***C***H$_3$), 10.85 (s, NCH$_2$***C***H$_3$), 24.08 (s, OCCH$_2$***C***H$_2$), 29.29 (br s, PC(***C***H$_3$)$_3$), 30.28 (br s, PC(***C***H$_3$)$_3$), 30.74 (s, OCCH$_2$***C***H$_2$), 34.40 (d, J_{CP} = 24.4 Hz, P***C***(CH$_3$)$_3$), 37.13 (d, J_{CP} = 21.3 Hz, P***C***(CH$_3$)$_3$), 37.12 (s, OC***C***H$_2$), 38.72 (s, OC***C***H$_2$), 50.69 (s, N***C***H$_2$CH$_3$), 52.98 (s, N***C***H$_2$CH$_3$), 63.90 (s, ***C***H$_2$N), 85.96 (s, ***C***HP), 118.85 (s, Py-***C2***), 119.48 (d, J_{CP} = 9.3 Hz, Py-***C4***), 135.98 (s, Py-***C3***), 160.87 (s, Py-***C1***), 161.33 (d, J_{CP} = 3.9 Hz, Py-***C5***), 172.19 (s, O***C***C), 210.11 (d, J_{CP} = 16.5 Hz, Ru-***C***O).

Peaks corresponding to free cyclopentanone in spectra:

^{1}H NMR (toluene-d_8): 1.22 (m, 4H, OCCH$_2$C***H$_2$***), 1.62 (m, 4H, OCC***H$_2$***).

^{13}C{^{1}H} NMR (toluene-d_8): 23.16 (s, OCCH$_2$***C***H$_2$), 37.87 (s, O***C***H$_2$), 217.40 (s, ***C***=O).

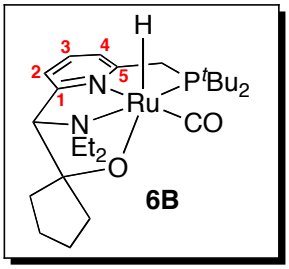

$^{31}P\{^1H\}$ NMR (C_6D_6): 119.49 (s).

^1H NMR (C_6D_6): –14.83 (d, J_{HP} = 28.9 Hz, 1H, Ru-***H***), 0.02 (dd, J_{HH} = 11.0 Hz, J_{HH} = 6.1 Hz, 1H, OCC$\boldsymbol{H_2}$), 0.78 (ddd, J_{HH} = 23.3 Hz, J_{HH} = 11.4 Hz, J_{HH} = 7.3, Hz, 1H, OCC$\boldsymbol{H_2}$), 0.95 (br t, J_{HH} = 5.9 Hz, 3H, NCH$_2$C$\boldsymbol{H_3}$), 1.01 (br t, J_{HH} = 6.3 Hz, 3H, NCH$_2$C$\boldsymbol{H_3}$), 1.26 (d, J_{HP} = 13.0 Hz, 9H, PC(C$\boldsymbol{H_3}$)$_3$), 1.27 (d, J_{HP} = 13.1 Hz, 9H, PC(C$\boldsymbol{H_3}$)$_3$), 1.51 (m, 1H, OCCH$_2$C$\boldsymbol{H_2}$), 1.62 (m, 1H, OCCH$_2$C$\boldsymbol{H_2}$), 1.94 (m, 1H, OCC$\boldsymbol{H_2}$), 2.09 (m, 1H, OCCH$_2$C$\boldsymbol{H_2}$), 2.29 (m, 2H, overlapping peaks: NC***H***HCH$_3$ and OCC$\boldsymbol{H_2}$CH$_2$), 2.33 (dqd, J_{HH} = 14.1 Hz, J_{HH} = 7.1 Hz, J_{HH} = 2.9 Hz, 1H, OCC$\boldsymbol{H_2}$), 2.54 (br m, 1H, NC***H***HCH$_3$), 2.88 (dd, J_{HH} = 16.9 Hz, J_{HP} = 7.1 Hz, 1H, C***H***HP), 3.00 (dd, J_{HH} = 16.9 Hz, J_{HP} = 9.6 Hz, 1H, C***H***HP), 3.61 (d, J_{HP} = 3.6 Hz, 1H, C***H***N), 3.76 (br s, 1H, NC***H***HCH$_3$), 3.88 (br s, 1H, NC***H***HCH$_3$), 6.59 (d, J_{HH} = 7.7 Hz, 1H, overlapping peaks: Py-***H2*** and Py-***H4***), 6.96 (t, J_{HH} = 7.8 Hz, 1H, Py-***H3***).

$^{13}C\{^1H\}$ NMR (C_6D_6): 9.99 (s, NCH$_2$***C***H$_3$), 11.06 (s, NCH$_2$***C***H$_3$), 23.15 (s, OCCH$_2$***C***H$_2$), 25.39 (s, OCCH$_2$***C***H$_2$), 29.70 (d, J_{CP} = 4.9 Hz, PC(***C***H$_3$)$_3$), 30.54 (d, J_{CP} = 2.8 Hz, PC(***C***H$_3$)$_3$), 34.54 (d, J_{CP} = 23.6 Hz, P***C***(CH$_3$)$_3$), 37.05 (d, J_{CP} = 19.9 Hz, ***C***H$_2$P), 37.99 (d, J_{CP} = 10.4 Hz, P***C***(CH$_3$)$_3$), 44.08 (s, OC***C***H$_2$), 44.17 (s, OC***C***H$_2$), 47.96 (s, N***C***H$_2$CH$_3$), 49.98 (s, N***C***H$_2$CH$_3$), 81.75 (s, ***C***HN), 84.94 (s, O***C***C), 118.40 (d, J_{CP} = 8.7 Hz, Py-***C4***), 119.98 (s, Py-***C2***), 135.31 (s, Py-***C3***), 160.65 (d, J_{CP} = 4.7 Hz, Py-***C5***), 163.38 (s, Py-***C1***), 209.73 (m, Ru-***C***O).

Peaks corresponding to free cyclopentanone in spectra:

^1H NMR (C_6D_6): 1.31 (m, 4H, OCCH$_2$C$\boldsymbol{H_2}$), 1.71 (m, 4H, OCC$\boldsymbol{H_2}$).

$^{13}C\{^1H\}$ NMR (C_6D_6): 23.15 (s, OCCH$_2$***C***H$_2$), 37.94 (s, O***C***H$_2$), 217.27 (s, ***C***=O).

IR (KBr pellet, cm^{-1}): 1995 (Ru-H), 1882 (CO).

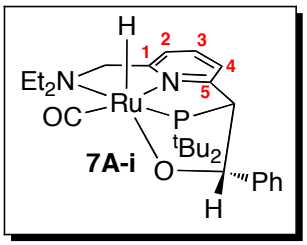

Spectra for complex 7A-i collected at –50 ºC

$^{31}P\{^{1}H\}$ NMR (toluene-d_8): 127.71 (s).

^{1}H NMR (toluene-d_8): –15.35 (d, J_{HP} = 16.7 Hz, 1H, Ru-***H***), 0.46 (br t, J_{HH} = 6.7 Hz, 3H, $NCH_2C\boldsymbol{H_3}$), 0.93 (br s, 9H, $PC(C\boldsymbol{H_3})_3$), 1.29 (d, J_{HP} = 11.8 Hz, 3H, $PC(C\boldsymbol{H_3})(CH_3)_2$), 1.39 (d, J_{HP} = 7.0 Hz, 3H, $PC(C\boldsymbol{H_3})(CH_3)_2$), 1.46 (br t, J_{HH} = 6.8 Hz, 3H, $NCH_2C\boldsymbol{H}_3$), 1.80 (br s, 1H, $NC\boldsymbol{H}HCH_3$), 2.20 (d, J_{HP} = 15.9 Hz, 3H, $PC(C\boldsymbol{H_3})(CH_3)_2$), 2.95 (d, J_{HH} = 11.0 Hz, 1H, NC***H***HPy), 2.97 (m, 1H, $NC\boldsymbol{H}HCH_3$), 3.30 (dq, J_{HH} = 13.8 Hz, J_{HH} = 6.7 Hz, 1H, $NC\boldsymbol{H}HCH_3$), 3.40 (d, J_{HH} = 11.0 Hz, 1H, NC***H***HPy), 3.60 (dq, J_{HH} = 13.8 Hz, J_{HH} = 6.7 Hz, 1H, $NC\boldsymbol{H}HCH_3$), 3.80 (d, J_{HH} = 7.0 Hz, 1H, C***H***P), 5.90 (d, J_{HH} = 7.7 Hz, 1H, Py-***H4***), 6.15 (d, J_{HH} = 7.5 Hz, 1H, Py-***H2***), 6.18 (s, 1H, C***H***O), 6.48 (t, J_{HH} = 7.9 Hz, 1H, Py-***H3***), 6.99–7.08 (m, *overlapping with benzaldehyde and residual toluene*, 5H, Ph-$\boldsymbol{H_{ortho/meta/para}}$).

$^{13}C\{^{1}H\}$ NMR (toluene-d_8): 7.37 (s, $NCH_2\boldsymbol{C}H_3$), 13.00 (s, $NCH_2\boldsymbol{C}H_3$), 25.07 (s, $PC(\boldsymbol{C}H_3)(CH_3)_2$), 29.73 (br s, $PC(\boldsymbol{C}H_3)_3$), 32.08 (s, $PC(\boldsymbol{C}H_3)(CH_3)_2$), 35.33 (d, J_{CP} = 8.9 Hz, $PC(\boldsymbol{C}H_3)(CH_3)_2$), 35.60 (d, J_{CP} = 13.6 Hz, $P\boldsymbol{C}(CH_3)_3$), 35.84 (d, J_{CP} = 16.5 Hz, $P\boldsymbol{C}(CH_3)_3$), 46.83 (s, $N\boldsymbol{C}H_2CH_3$), 55.61 (s, $N\boldsymbol{C}H_2CH_3$), 63.32 (d, J_{CP} = 14.2 Hz, ***C***HP), 66.08 (s, $N\boldsymbol{C}H_2Py$), 80.09 (s, ***C***HO), 116.66 (s, Py-***C2***), 122.19 (d, J_{CP} = 4.7 Hz, Py-***C4***), 126.28 (br s, $\boldsymbol{C_{Ph}}$***-ortho/meta***), 127.02 (br s, $\boldsymbol{C_{Ph}}$***-ortho/meta***), 134.66 (s, Py-***C3***), 136.41 (s, $\boldsymbol{C_{Ph}}$***-para***), 151.43 (d, J_{CP} = 5.2 Hz, H(OC)***C***) 156.29 (s, Py-***C1***), 161.21 (d, J_{CP} = 3.3 Hz, Py-***C5***), 211.21 (d, J_{CP} = 14.8 Hz, Ru-***C***O).

Peaks corresponding to free benzaldehyde in spectra:

^{1}H NMR (toluene-d_8): 7.06 (td, J_{HH} = 7.6 Hz, J_{HH} = 1.4 Hz, 2H, Ph-$\boldsymbol{H_{meta}}$), 7.14 (tt, J_{HH} = 7.5 Hz, J_{HH} = 1.3 Hz, 1H, Ph-$\boldsymbol{H_{para}}$), 7.52 (dd, J_{HH} = 7.9 Hz, J_{HH} = 1.3 Hz, 2H ,Ph-$\boldsymbol{H_{ortho}}$), 9.65 (s, 1H, ***H***CO).

$^{13}C\{^1H\}$ NMR (toluene-d_8): 128.86 (s, ***C_{Ph}-meta***), 129.56 (s, ***C_{Ph}-ortho***), 133.89 (s, ***C_{Ph}-para***), 137.04 (s, HCO***C***), 191.17 (s, ***C***=O).

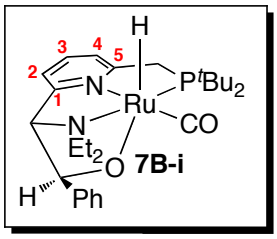

Spectra for complex 7B-i collected at –5 ºC

$^{31}P\{^1H\}$ NMR (toluene-d_8): 120.39 (s).

^1H NMR (toluene-d_8): –14.84 (d, J_{HP} = 28.1 Hz, 1H, Ru-***H***), 0.26 (br t, J_{HH} = 7.1 Hz, 3H, $NCH_2C\boldsymbol{H_3}$), 0.98 (br t, J_{HH} = 6.6 Hz, 3H, $NCH_2C\boldsymbol{H_3}$), 1.22 (br d, J_{HP} = 11.5 Hz, 9H, $PC(C\boldsymbol{H_3})_3$), 1.26 (d, J_{HP} = 13.0 Hz, 9H, $PC(C\boldsymbol{H_3})_3$), 2.20 (br s, 2H, $NC\boldsymbol{H_2}CH_3$), 2.82 (dd, J_{HH} = 16.2 Hz, J_{HP} = 6.9 Hz, 1H, C***H***HP), 2.89 (dd, J_{HH} = 16.2 Hz, J_{HH} = 9.9 Hz, 1H, C***H***HP), 3.35 (br m, 1H, NC***H***HCH_3), 3.76 (br s, 1H, NC***H***HCH_3), 4.07 (d, J_{HH} = 1.8 Hz, 1H, C***H***N), 4.70 (s, 1H, C***H***O), 6.52 (d, J_{HH} = 7.7 Hz, 1H, Py-***H4***), 6.61 (d, J_{HH} = 7.7 Hz, 1H, Py-***H2***), 6.96 (t, J_{HH} = 7.8 Hz, 1H, Py-***H3***), 6.95–7.18 (m, *overlapping with benzaldehyde and residual toluene*, 3H, Ph-$\boldsymbol{H_{meta}}$ and Ph-$\boldsymbol{H_{para}}$), 7.94 (d, J_{HH} = 7.6 Hz, 2H, Ph-$\boldsymbol{H_{ortho}}$***).***

$^{13}C\{^1H\}$ NMR (toluene-d_8): 6.93 (s, $NCH_2\boldsymbol{C}H_3$), 12.10 (s, $NCH_2\boldsymbol{C}H_3$), 29.06 (br s, $PC(\boldsymbol{C}H_3)_3$), 30.27 (br s, $PC(\boldsymbol{C}H_3)_3$), 34.17 (d, J_{CP} = 22.8 Hz, $P\boldsymbol{C}(CH_3)_3$), 36.87 (d, J_{CP} = 19.8 Hz, $\boldsymbol{C}H_2P$), 37.53 (d, J_{CP} = 11.8 Hz, $P\boldsymbol{C}(CH_3)_3$), 46.55 (s, $N\boldsymbol{C}H_2CH_3$), 49.82 (s, $N\boldsymbol{C}H_2CH_3$), 79.85 (s, overlapping peaks: ***C***HN and ***C***HO), 116.84 (s, Py-***C2***), 118.36 (d, J_{CP} = 8.9 Hz, Py-***C4***), 127.11 (s, ***C_{Ph}-ortho/meta***), 128.16 (s, Py-***C3***), 129.53 (s, ***C_{Ph}-ortho/meta***), 133.76 (s, ***C_{Ph}-para***), 151.39 (s, H(CO)***C***), 161.10 (d, J_{CP} = 4.4 Hz, Py-***C1***), 165.63 (s, Py-***C5***), 209.02 (d, J_{CP} = 15.4 Hz, Ru-***C***O).

Peaks corresponding to free benzaldehyde in spectra:

^{1}H NMR (toluene-d_8): 7.06 (td, J_{HH} = 7.6 Hz, J_{HH} = 1.4 Hz, 2H, Ph-$\boldsymbol{H_{meta}}$), 7.14 (tt, J_{HH} = 7.5 Hz, J_{HH} = 1.3 Hz, 1H, Ph-$\boldsymbol{H_{para}}$), 7.52 (dd, J_{HH} = 7.9 Hz, J_{HH} = 1.3 Hz, 2H ,Ph-$\boldsymbol{H_{ortho}}$), 9.65 (s, 1H, ***H***CO).

^{13}C{^{1}H} NMR (toluene-d_8): 128.86 (s, $\boldsymbol{C_{Ph}}$***-meta***), 129.56 (s, $\boldsymbol{C_{Ph}}$***-ortho***), 133.89 (s, $\boldsymbol{C_{Ph}}$***-para***), 137.04 (s, HCO***C***), 191.17 (s, ***C***=O).

IR data for mixture of 7B-i and 7B-ii:

IR (KBr pellet, cm^{-1}): 1991 (Ru-H), 1882 (CO).

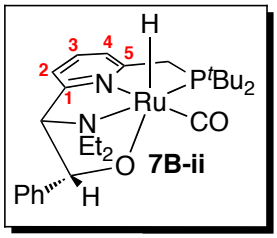

^{31}P{^{1}H} NMR (toluene-d_8): 118.19 (s).

^{1}H NMR (toluene-d_8): –15.16 (d, J_{HP} = 29.2 Hz, 1H, Ru-***H***), 0.89 (t, J_{HH} = 7.2 Hz, 3H, NCH$_2$C***H***$_3$), 1.08 (t, J_{HH} = 7.0 Hz, 3H, NCH$_2$C***H***$_3$), 1.28 (d, J_{HP} = 12.8 Hz, 9H, PC(C***H***$_3$)$_3$), 1.37 (d, J_{HP} = 13.2 Hz, 9H, PC(C***H***$_3$)$_3$), 2.30 (m, 2H, NC***H***$_2$CH$_3$), 2.89 (dd, J_{HH} = 16.6 Hz, J_{HP} = 7.2 Hz, 1H, C***H***HP), 2.96 (dd, J_{HH} = 16.6 Hz, J_{HP} = 9.8 Hz, 1H, C***H***HP), 3.61 (dq, J_{HH} = 14.4 Hz, J_{HH} = 7.2 Hz, 1H, NC***H***HCH$_3$), 3.93 (br s, 1H, NC***H***HCH$_3$), 4.01 (t, $J_{HH/HP}$ = 2.3 Hz, 1H, C***H***N), 6.07 (d, J_{HH} = 7.7 Hz, 1H, Py-***H2***), 6.08 (br s, 1H, C***H***O), 6.53 (d, J_{HH} = 7.7 Hz, 1H, Py-***H4***), 6.67 (t, J_{HH} = 7.7 Hz, 1H, Py-***H3***), 6.99–7.19 (m, *overlapping with benzaldehyde, **6B-i**, and residual toluene*, 5H, Ph***H-***$_{ortho/meta/para}$).

^{13}C{^{1}H} NMR (toluene-d_8): 7.49 (s, NCH$_2$***C***H$_3$), 12.44 (s, NCH$_2$***C***H$_3$), 29.99 (d, J_{CP} = 5.0 Hz, PC(***C***H$_3$)$_3$), 30.39 (d, J_{CP} = 2.8 Hz, PC(***C***H$_3$)$_3$), 34.60 (d, J_{CP} = 24.3 Hz, P***C***(CH$_3$)$_3$), 37.10 (d, J_{CP} = 19.0 Hz, ***C***H$_2$P), 37.84 (d, J_{CP} = 10.3 Hz, P***C***(CH$_3$)$_3$), 46.90 (s, N***C***H$_2$CH$_3$), 50.22 (s, N***C***H$_2$CH$_3$), 77.81 (s, ***C***HO), 80.54 (s, ***C***HN), 118.52 (d, J_{CP} = 8.6 Hz, Py-***C4***), 121.01 (s, Py-***C2***), 125.21 (s, ***C$_{Ph}$-ortho/meta***), 127.21 (s, ***C$_{Ph}$-ortho/meta***), 134.75 (s, Py-***C3***), 137.09 (s, ***C$_{Ph}$-para***), 150.17 (s, H(CO)***C***), 159.64 (s, Py-***C1***), 159.36 (d, J_{CP} = 4.8 Hz, Py-***C5***), 209.14 (d, J_{CP} = 16.0 Hz, Ru-***C***O).

Peaks corresponding to free benzaldehyde in spectra:

^{1}H NMR (toluene-d_8): 7.06 (td, J_{HH} = 7.6 Hz, J_{HH} = 1.4 Hz, 2H, Ph-***H$_{meta}$***), 7.14 (tt, J_{HH} = 7.5 Hz, J_{HH} = 1.3 Hz, 1H, Ph-***H$_{para}$***), 7.52 (dd, J_{HH} = 7.9 Hz, J_{HH} = 1.3 Hz, 2H ,Ph-***H$_{ortho}$***), 9.65 (s, 1H, ***H***CO).

^{13}C{^{1}H} NMR (toluene-d_8): 128.86 (s, ***C$_{Ph}$-meta***), 129.56 (s, ***C$_{Ph}$-ortho***), 133.89 (s, ***C$_{Ph}$-para***), 137.04 (s, HCO***C***), 191.17 (s, ***C***=O).

IR data for mixture of 7B-i and 7B-ii:

IR (KBr pellet, cm^{-1}): 1991 (Ru-H), 1882 (CO).

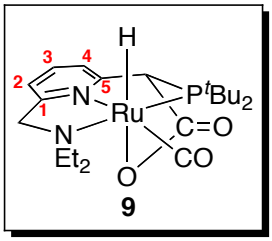

$^{31}P\{^1H\}$ NMR (C_6D_6): 126.88 (d, J_{PH} = 13.8 Hz).

^1H NMR (C_6D_6): –16.84 (d, J_{HP} = 16.7 Hz, 1H, Ru-***H***), 0.64 (t, J_{HH} = 7.1 Hz, 3H, $N(CH_2C\boldsymbol{H}_3)_2$), 0.92 (d, J_{HP} = 12.6 Hz, 9H, $P(C(C\boldsymbol{H}_3)_3)_2$), 1.09 (t, J_{HH} = 7.0 Hz, 3H, $N(CH_2C\boldsymbol{H}_3)_2$), 1.62 (d, J_{HP} = 13.1 Hz, 9H, $P(C(C\boldsymbol{H}_3)_3)_2$), 1.70 (m, 1H, $N(C\boldsymbol{H}HCH_3)_2$), 2.12 (dq, J_{HH} = 7.2 Hz, J_{HH} = 14.0 Hz, 1H, $N(C\boldsymbol{H}HCH_3)_2$), 3.10–3.15 (multiple peaks, 2H, $N(C\boldsymbol{H}HCH_3)_2$, C***H***HN), 3.27 (dq, J_{HH} = 7.1 Hz, J_{HH} = 13.9 Hz, 1H, $N(C\boldsymbol{H}HCH_3)_2$), 3.64 (d, J_{HH} = 14.0 Hz, 1H, C***H***HN), 4.66 (d, J_{HP} = 7.5 Hz, 1H, C***H***P), 6.39 (d, J_{HH} = 7.6 Hz, 1H, ***H2***), 6.98 (d, J_{HH} = 7.8 Hz, 1H, ***H4***), 7.03 (t app, J_{HH} = 7.6 Hz, J_{HH} = 7.7 Hz, 1H, ***H3***).

$^{13}C\{^1H\}$NMR (C_6D_6): 8.57 (s, $N(CH_2\boldsymbol{C}H_3)_2$), 11.82 (s, $N(CH_2\boldsymbol{C}H_3)_2$), 29.50 (d, J_{CP} = 3.52 Hz, $P(C(\boldsymbol{C}H_3)_3)_2$), 30.50 (d, J_{CP} = 3.76 Hz, $P(C(\boldsymbol{C}H_3)_3)_2$), 36.68 (d, J_{CP} = 15.0 Hz, $P(\boldsymbol{C}(CH_3)_3)_2$), 36.87 (d, J_{CP} = 14.7 Hz, $P(\boldsymbol{C}(CH_3)_3)_2$), 48.21 (s, $N(\boldsymbol{C}H_2CH_3)_2$), 55.40 (s, $N(\boldsymbol{C}H_2CH_3)_2$), 63.46 (d, J_{CP} = 9.7 Hz, ***C***HP), 66.21 (s, ***C***H_2N), 117.86 (s, ***C2***), 119.44 (d, J_{CP} = 7.8 Hz, ***C4***), 138.11 (s, ***C3***), 158.29 (s, ***C1***), 161.65 (s, ***C5***), 170.81 (d, J_{CH} = 5.2 Hz, ***C***O_2), 209.70 (dd, J = 5.9, 7.5 Hz, Ru-***C***O).

Diagnostic NMR Resonances for Complex 9-^{13}C:

$^{31}P\{^1H\}$ NMR (C_6D_6): 127.01 (dd, J_{PC} = 4.7 Hz, J_{HP} = 14.9 Hz).

^1H NMR (C_6D_6): 4.66 (dd, J_{HC} = 4.2 Hz, J_{HP} = 7.3 Hz, 1H, C***H***P).

$^{13}C\{^1H\}$NMR (C_6D_6): 63.56 (dd, J_{CC} = 38.3 Hz, J_{CP} = 9.1 Hz, ***C***HP), 170.88 (d, J_{CP} = 4.3 Hz, ***C***O_2).

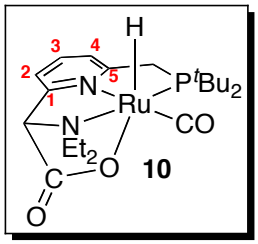

$^{31}P\{^1H\}$ NMR (C_6D_6): 119.4 (d, J_{PH} = 26.6 Hz).

^1H NMR (C_6D_6): –16.18 (d, J_{HP} = 28.8 Hz, 1H, Ru-***H***), 0.78 (t, J_{HH} = 7.1 Hz, 3H, $N(CH_2C\boldsymbol{H}_3)_2$), 0.92 (t, J_{HH} = 7.1 Hz, 3H, $N(CH_2C\boldsymbol{H}_3)_2$), 1.04 (d, J_{HP} = 13.1 Hz, 9H, $P(C(C\boldsymbol{H}_3)_3)_2$), 1.19 (d, J_{HP} = 13.3 Hz, 9H, $P(C(C\boldsymbol{H}_3)_3)_2$), 2.17 (m, 1H, $N(C\boldsymbol{H}HCH_3)_2$), 2.29 (dq, J_{HH} = 7.1 Hz, J_{HH} = 11.8 Hz, 1H, $N(C\boldsymbol{H}HCH_3)_2$), 2.78 (dd, J_{HH} = 16.5 Hz, J_{HP} = 7.4 Hz, 1H, C***H***HP), 2.92 (dd, J_{HH} = 16.5 Hz, J_{HP} = 10.2 Hz, 1H, C***H***HP), 3.34 (dq, J_{HH} = 7.1 Hz, J_{HH} = 11.8 Hz, 1H, $N(C\boldsymbol{H}HCH_3)_2$), 3.37 (dq, J_{HH} = 7.1 Hz, J_{HH} = 11.8 Hz, 1H, $N(C\boldsymbol{H}HCH_3)_2$), 4.59 (d, J_{HP} = 2.5 Hz, 1H, C***H***N), 6.69 (d, J_{HH} = 7.8 Hz, 1H, ***H2***), 7.05 (d, J_{HH} = 7.8 Hz, 1H, ***H4***), 7.12 (app. t, J_{HH} = 7.8 Hz, 1H, ***H3***).

$^{13}C\{^1H\}$NMR (C_6D_6): 9.13 (s, $N(CH_2\boldsymbol{C}H_3)_2$), 10.71 (s, $N(CH_2\boldsymbol{C}H_3)_2$), 29.40 (d, J_{CP} = 4.3 Hz, $P(C(\boldsymbol{C}H_3)_3)_2$), 30.32 (d, J_{CP} = 10.9 Hz, $P(C(\boldsymbol{C}H_3)_3)_2$), 34.52 (d, J_{CP} = 22.8 Hz, $P(\boldsymbol{C}(CH_3)_3)_2$), 37.14 (d, J_{CP} = 20.4 Hz, $\boldsymbol{C}H_2P$), 37.68 (d, J_{CP} = 12.0 Hz, $P(\boldsymbol{C}(CH_3)_3)_2$), 48.47 (s, $N(\boldsymbol{C}H_2CH_3)_2$), 49.18 (s, $N(\boldsymbol{C}H_2CH_3)_2$), 80.71 (s, ***C***HN), 119.55 (br s, ***C2***), 119.97 (d, J_{CP} = 27.0 Hz, ***C4***), 137.78 (d, J_{CP} = 29.3 Hz, ***C3***), 159.10 (s, ***C1***), 161.70 (s, ***C5***), 169.42 (br s, ***C***O_2), 207.96 (dd, J = 6.6, 9.3 Hz, Ru-***C***O).

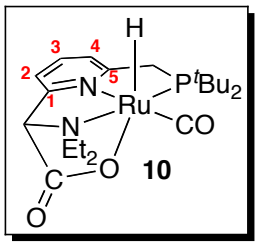

$^{31}P\{^1H\}$ NMR (CD_2Cl_2): 118.36 (d, J_{PH} = 26.6 Hz).

^1H NMR (CD_2Cl_2): –16.67 (d, J_{HP} = 29.4 Hz, 1H, Ru-***H***), 1.06 (d, J_{HP} = 13.3 Hz, 9H, $P(C(C\boldsymbol{H}_3)_3)_2$), 1.09 (t, J_{HH} = 7.1 Hz, 3H, $N(CH_2C\boldsymbol{H}_3)_2$), 1.23 (t, J_{HH} = 7.1 Hz, 3H, $N(CH_2C\boldsymbol{H}_3)_2$), 1.34 (d, J_{HP} = 13.5 Hz, 9H, $P(C(C\boldsymbol{H}_3)_3)_2$), 2.57 (m, 2H, $N(C\boldsymbol{H}HCH_3)_2$), 3.24 (dq, J_{HH} = 7.0 Hz, J_{HH} = 11.6 Hz, 1H, $N(C\boldsymbol{H}HCH_3)_2$), 3.31 (dd, J_{HH} = 16.6 Hz, J_{HP} = 7.5 Hz, 1H, C***H***HP), 3.36 (dq, J_{HH} = 7.1 Hz, J_{HH} = 11.8 Hz, 1H, $N(C\boldsymbol{H}HCH_3)_2$), 3.48 (dd, J_{HH} = 16.8 Hz, J_{HP} = 10.3 Hz, 1H, C***H***HP), 4.54 (d, J_{HP} = 2.6 Hz, 1H, C***H***N), 7.37 (d, J_{HH} = 7.9 Hz, 1H, ***H4***), 7.47 (d, J_{HH} = 7.7 Hz, 1H, ***H2***), 7.74 (app t, J_{HH} = 7.8 Hz, 1H, ***H3***).

$^{13}C\{^1H\}$NMR (CD_2Cl_2): 9.65 (s, $N(CH_2\boldsymbol{C}H_3)_2$), 10.53 (s, $N(CH_2\boldsymbol{C}H_3)_2$), 29.23 (d, J_{CP} = 4.7 Hz, $P(C(\boldsymbol{C}H_3)_3)_2$), 30.27 (d, J_{CP} = 2.8 Hz, $P(C(\boldsymbol{C}H_3)_3)_2$), 34.77 (d, J_{CP} = 23.7 Hz, $P(\boldsymbol{C}(CH_3)_3)_2$), 37.25 (d, J_{CP} = 20.6 Hz, $\boldsymbol{C}H_2P$), 37.45 (d, J_{CP} = 12.9 Hz, $P(\boldsymbol{C}(CH_3)_3)_2$), 48.36 (s, $N(\boldsymbol{C}H_2CH_3)_2$), 49.21 (s, $N(\boldsymbol{C}H_2CH_3)_2$), 79.76 (s, ***C***HN), 120.40 (s, ***C2***), 120.54 (d, J_{CP} = 8.3 Hz, ***C4***), 138.67 (s, ***C3***), 158.02 (s, ***C1***), 162.18 (d, J_{CP} = 4.0 Hz, ***C5***), 171.21 s, $\boldsymbol{C}O_2$), 207.82 (dd, J = 7.9 Hz, 14.9 Hz Ru-***C***O).

IR (KBr pellet, cm^{-1}): 2036 (ν(Ru-H)), 1893 (ν(CO)), 1647 (ν($O^{12}CO$));

Anal. Calcd. for $C_{21}H_{35}N_2O_3PRu$•0.5 C_4H_8O: C, 51.96; H, 7.39; N, 5.27. Found: C, 52.21, H, 7.51; N, 5.28. (*Note X-ray structure shows 0.5 equiv of THF per 1 equiv* ***5***).

Diagnostic NMR Resonances:

^1H NMR (C_6D_6): 4.59 (t app, $J_{HC/HP}$ = 2.8 Hz, 1H, C***H***N);

$^{13}C\{^1H\}$NMR (C_6D_6): 80.71 (d, J_{CC} = 47.7 Hz, ***C***HCO_2).

IV. NMR SPECTRA

^{1}H-^{1}H gCOSY NMR spectrum of 4 (C_6D_6)

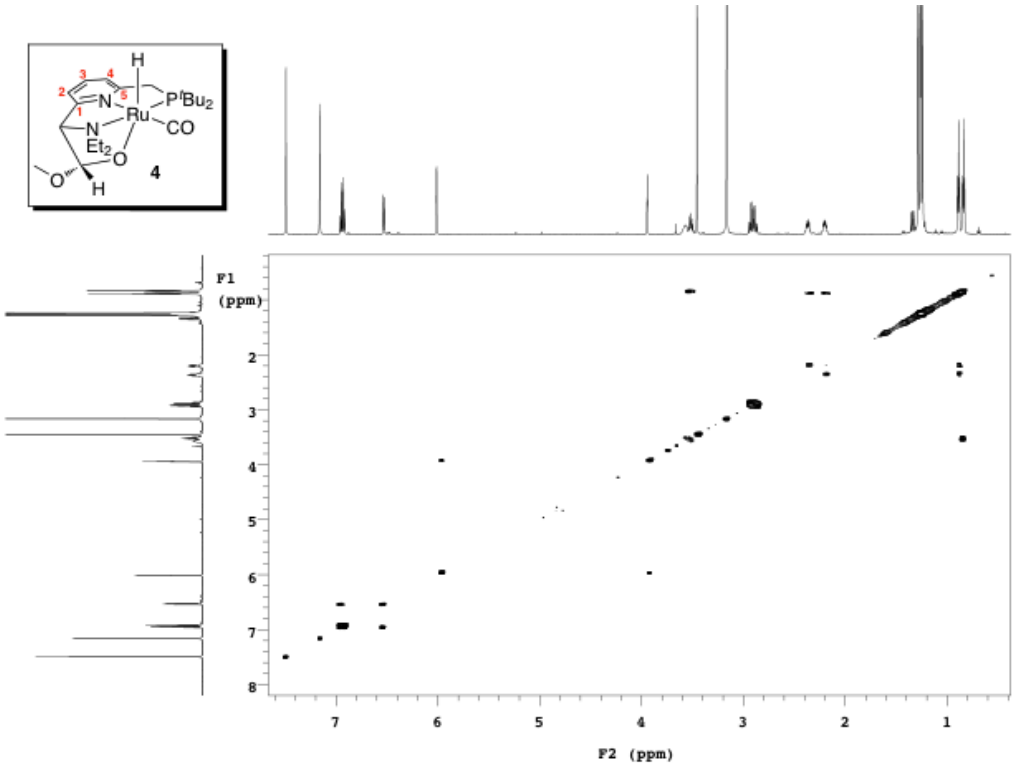

^{1}H-^{13}C gHSQC NMR spectrum of 4 (C_6D_6)

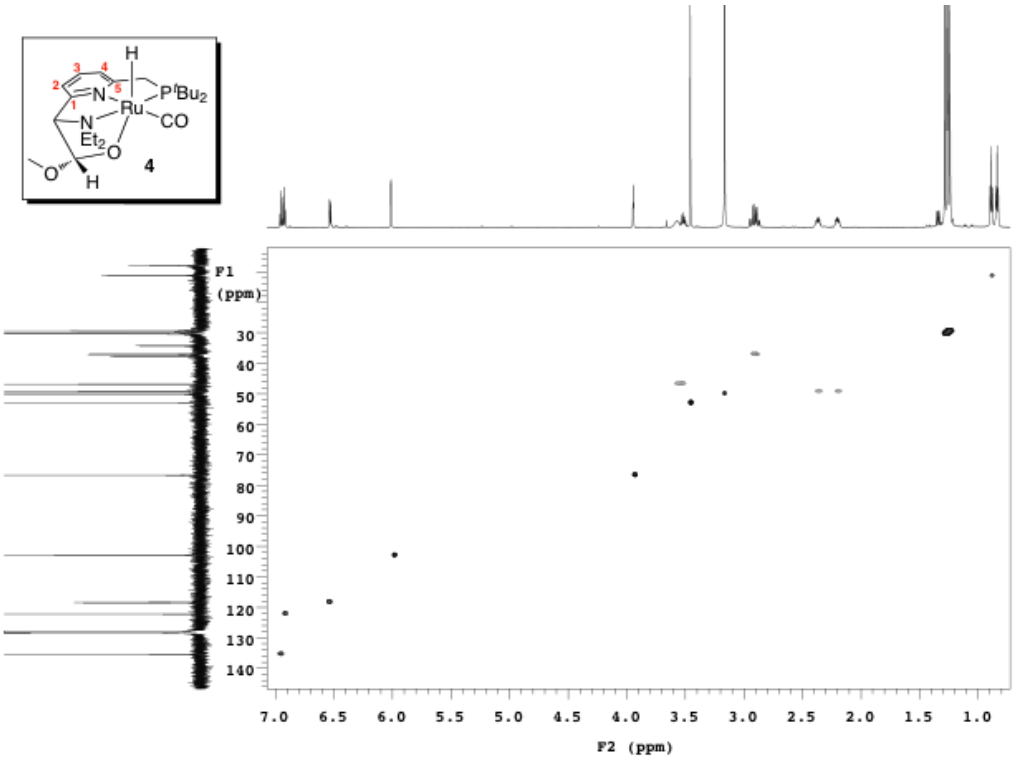

^{1}H-^{13}C gHMBC NMR spectrum of 4 (C_6D_6)

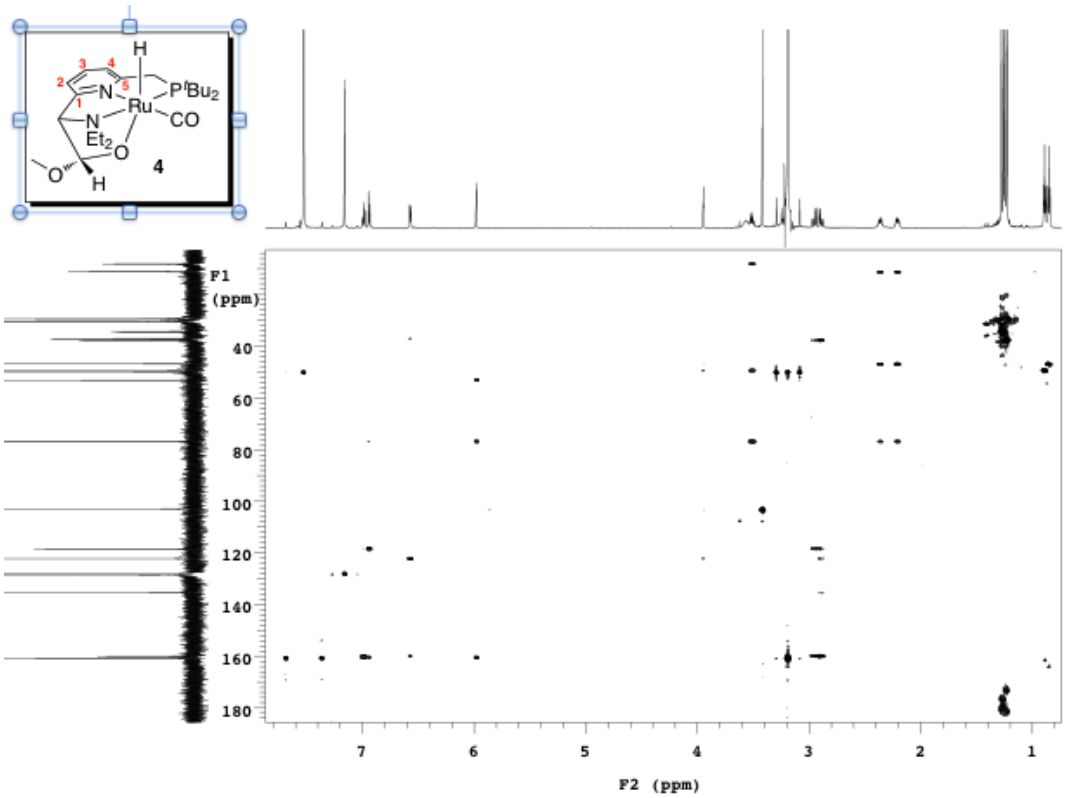

^{1}H-^{1}H NOESY NMR spectrum of 4 (C_6D_6)

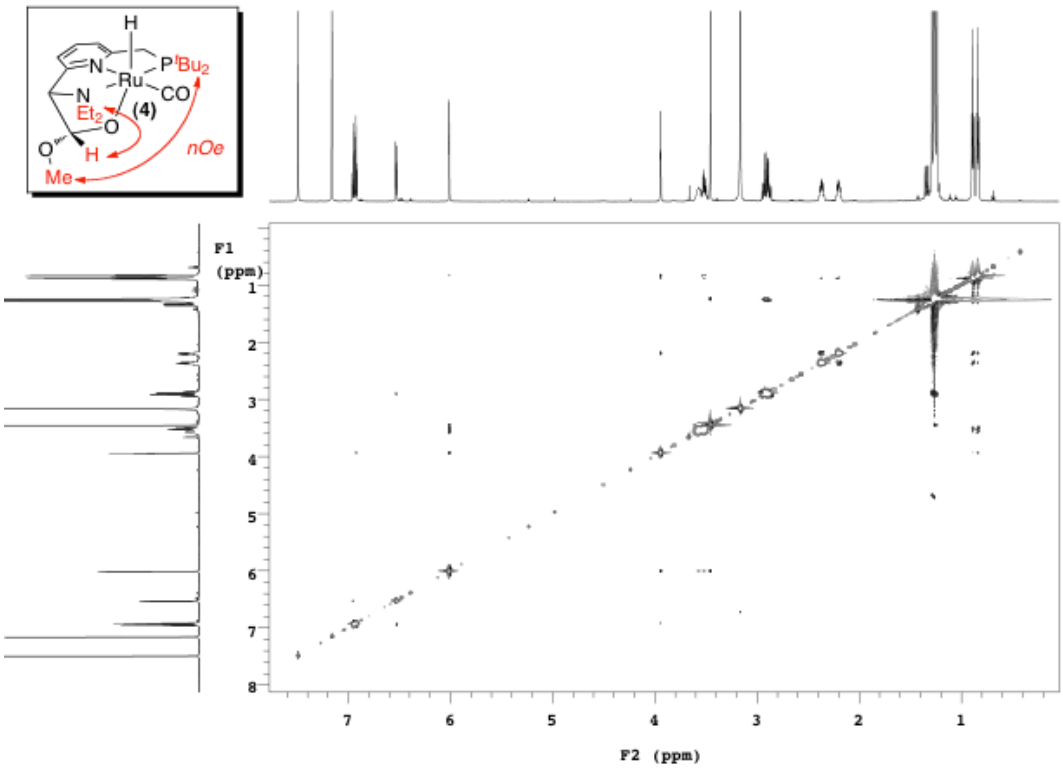

^{1}H-^{1}H gCOSY NMR spectrum of 5 (C_6D_6)

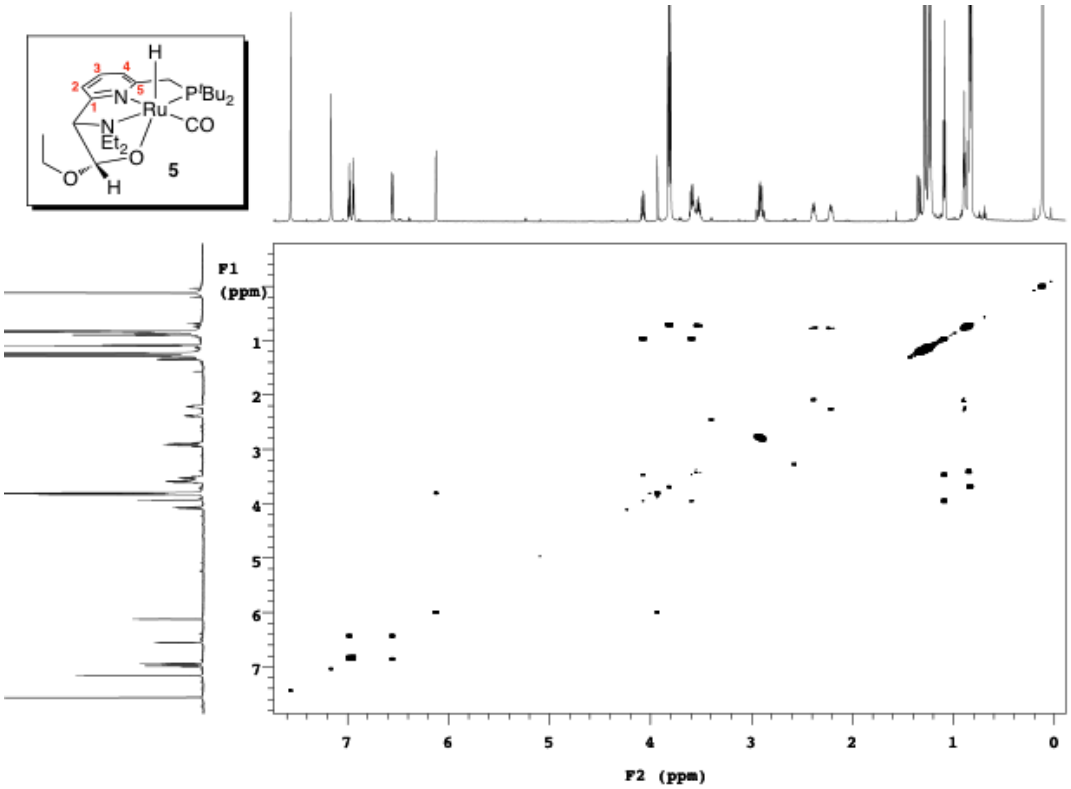

^{1}H-^{13}C gHSQC NMR spectrum of 5 (C_6D_6)

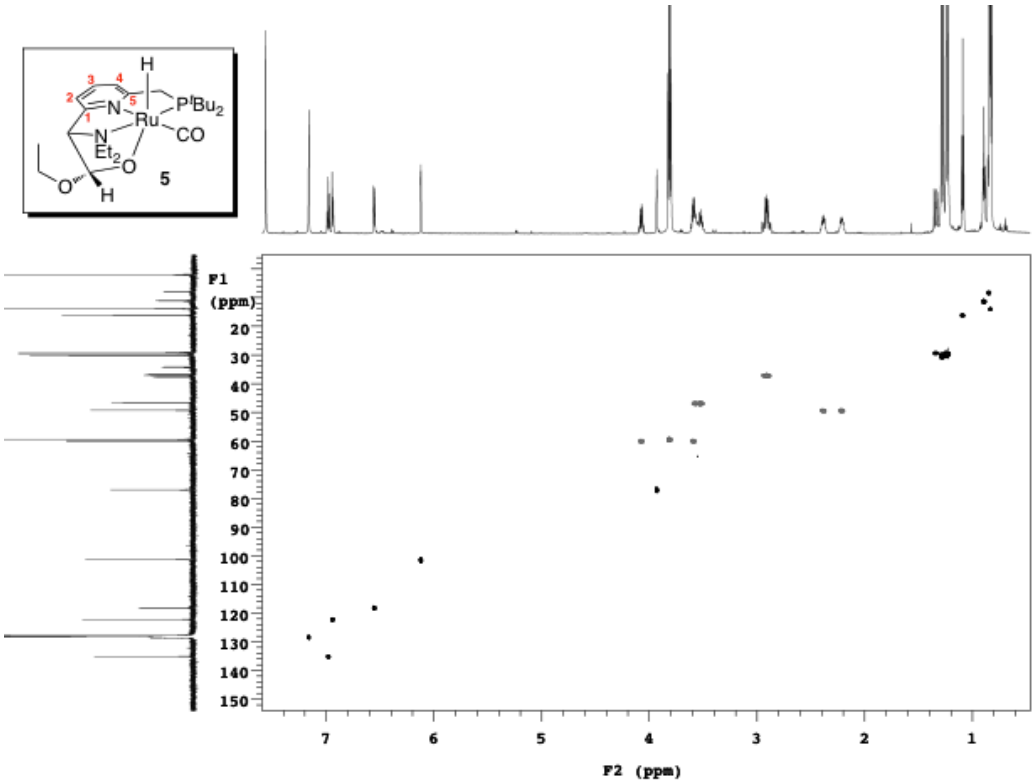

^{1}H-^{13}C gHMBC NMR spectrum of 5 (C_6D_6)

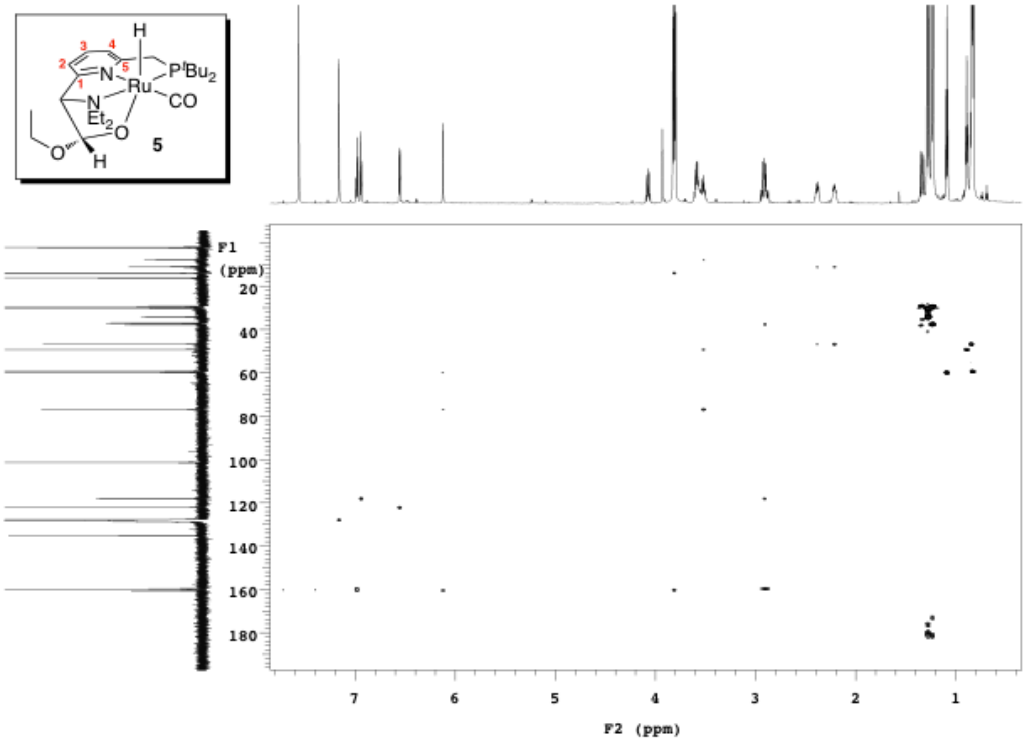

^{1}H-^{1}H NOESY NMR spectrum of 5 (C_6D_6)

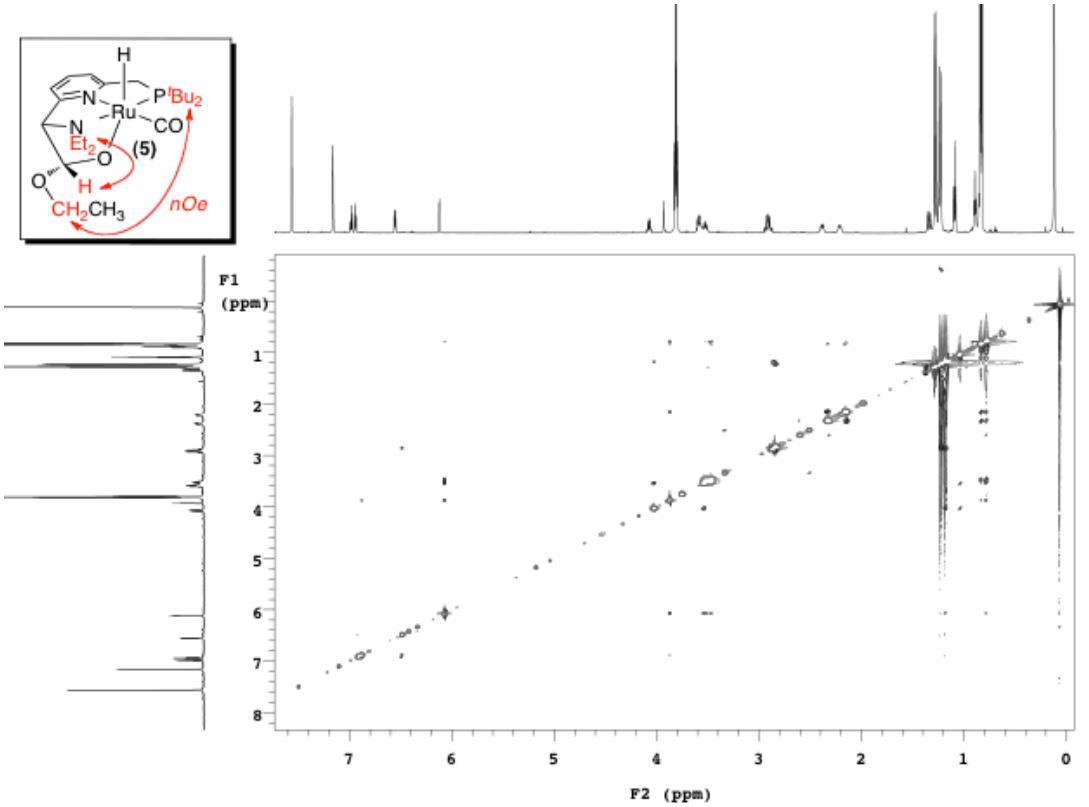

^{1}H-^{1}H gCOSY NMR spectrum of 6A (toluene-d_8, -40°C)

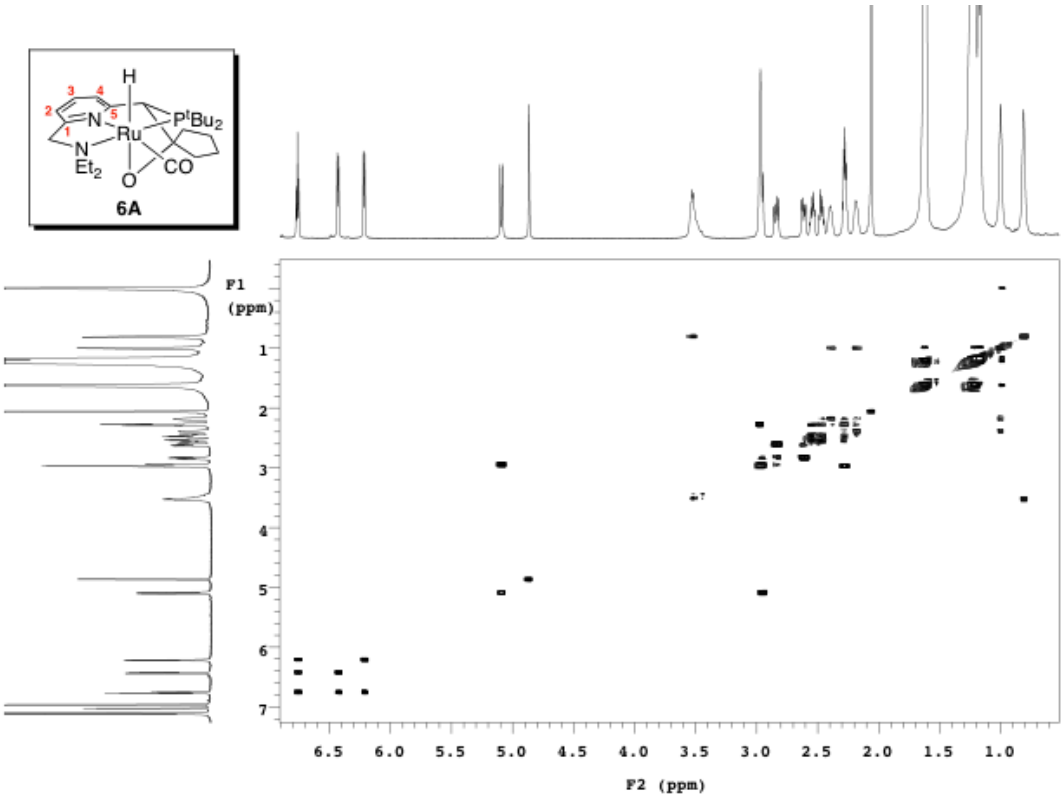

^{1}H-^{13}C gHSQC NMR spectrum of 6A (toluene-d_8, -40°C)

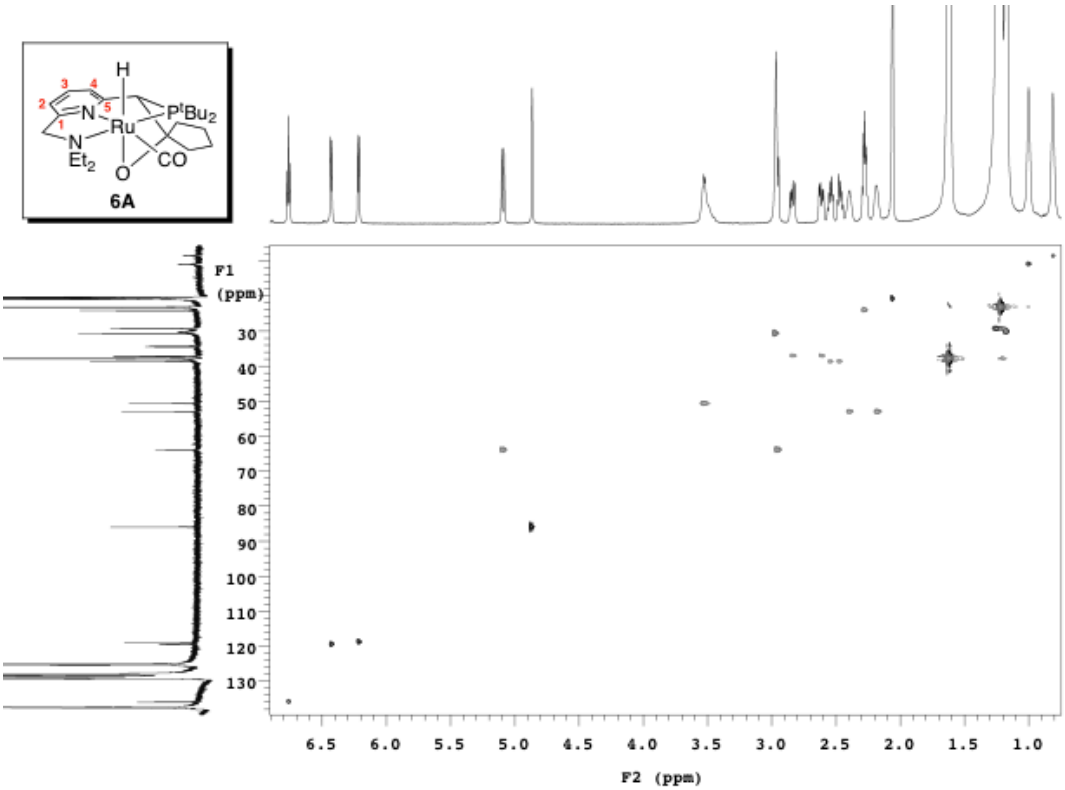

^{1}H-^{13}C gHMBC NMR spectrum of 6A (toluene-d_8, -40°C)

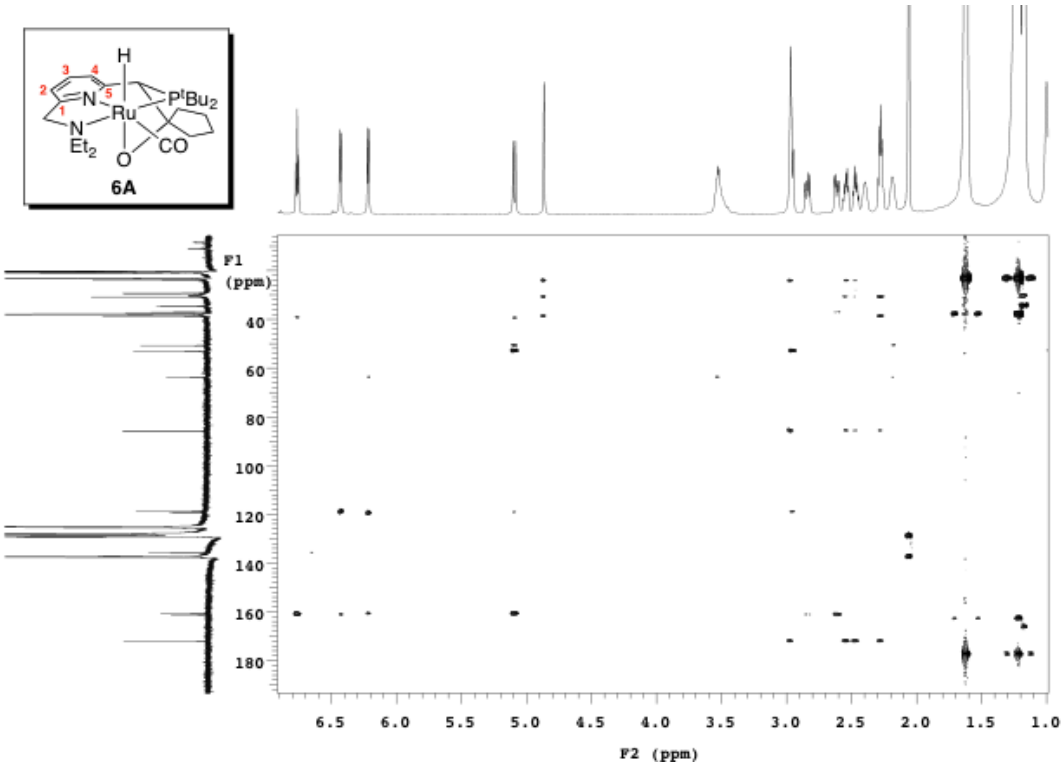

^{1}H-^{1}H gCOSY NMR spectrum of 6B (toluene-d_8)

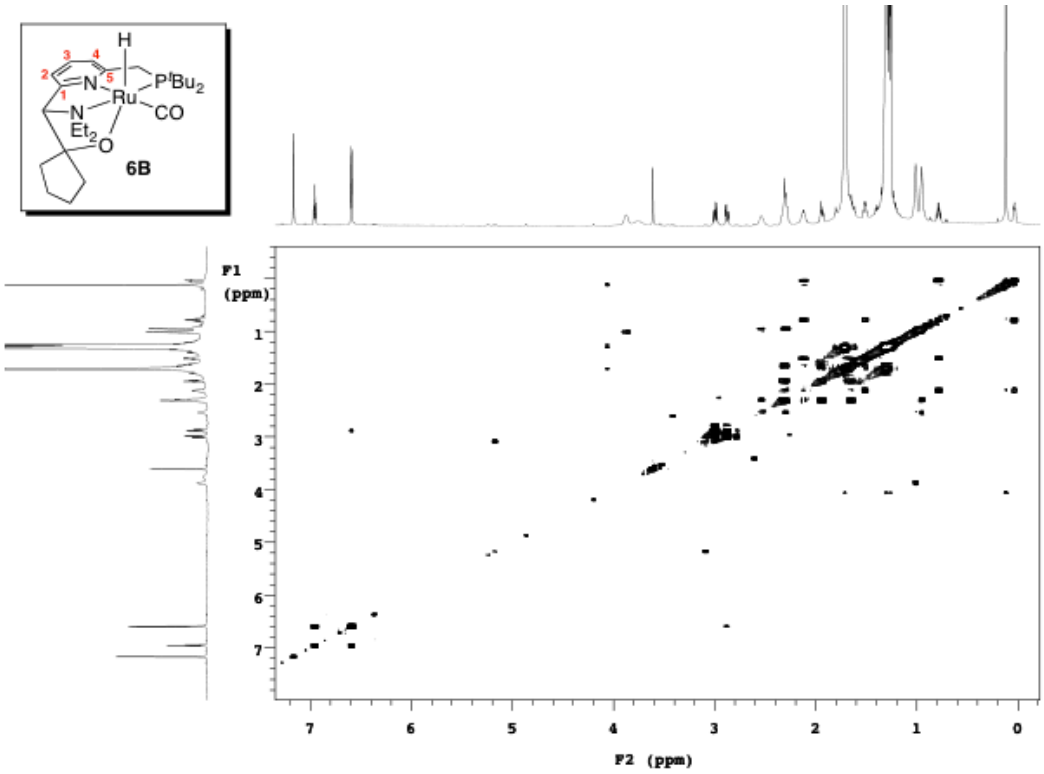

^{1}H-^{13}C gHSQC NMR spectrum of 6B (toluene-d_8)

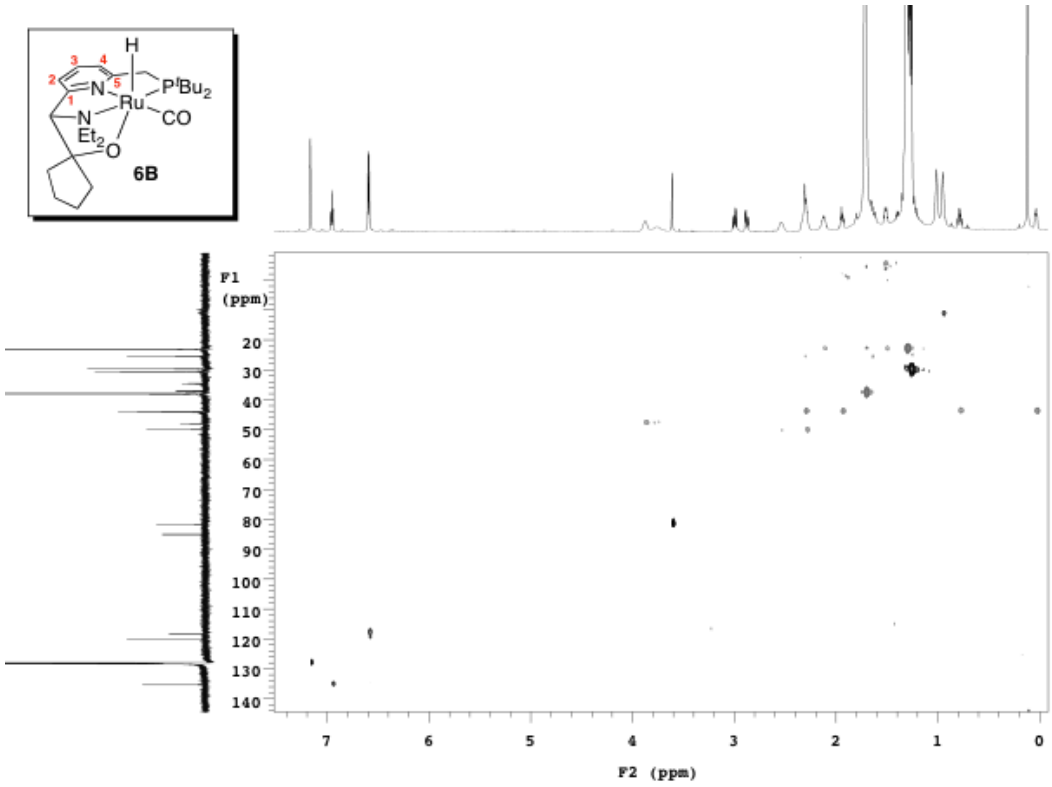

^{1}H-^{13}C gHMBC NMR spectrum of 6B (toluene-d_8)

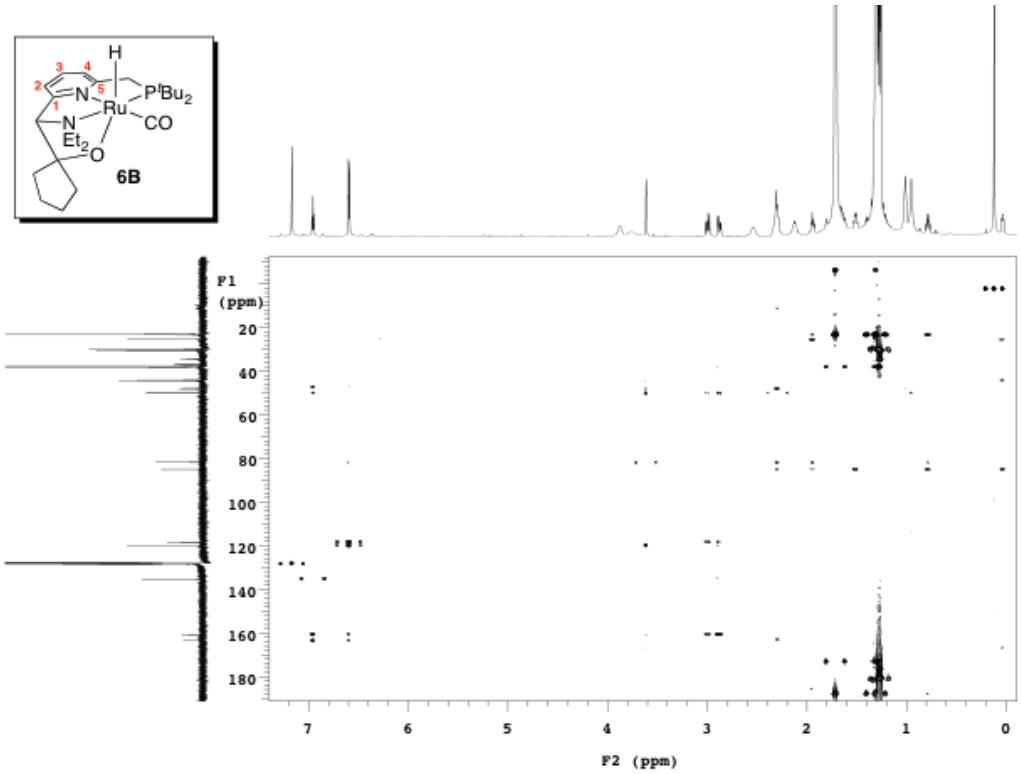

^{1}H-^{1}H gCOSY NMR spectrum of 7A-i (toluene-d_8, -50 ºC)

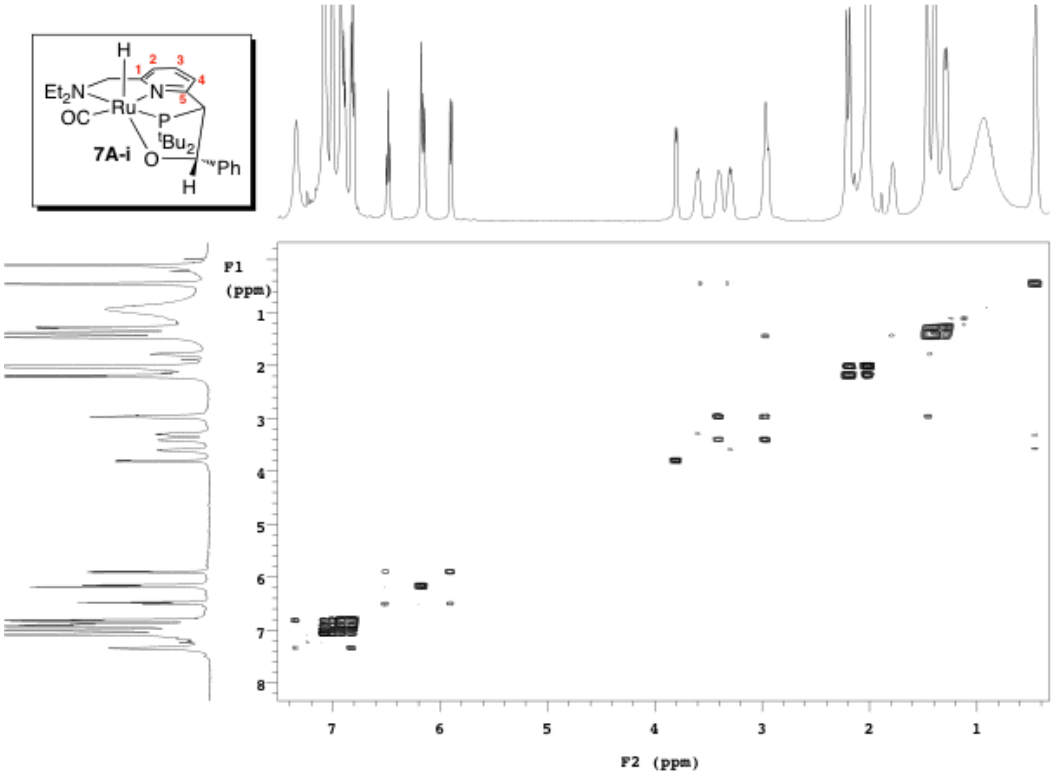

^{1}H-^{13}C gHSQC NMR spectrum of 7A-i (toluene-d_8, -50 ºC)

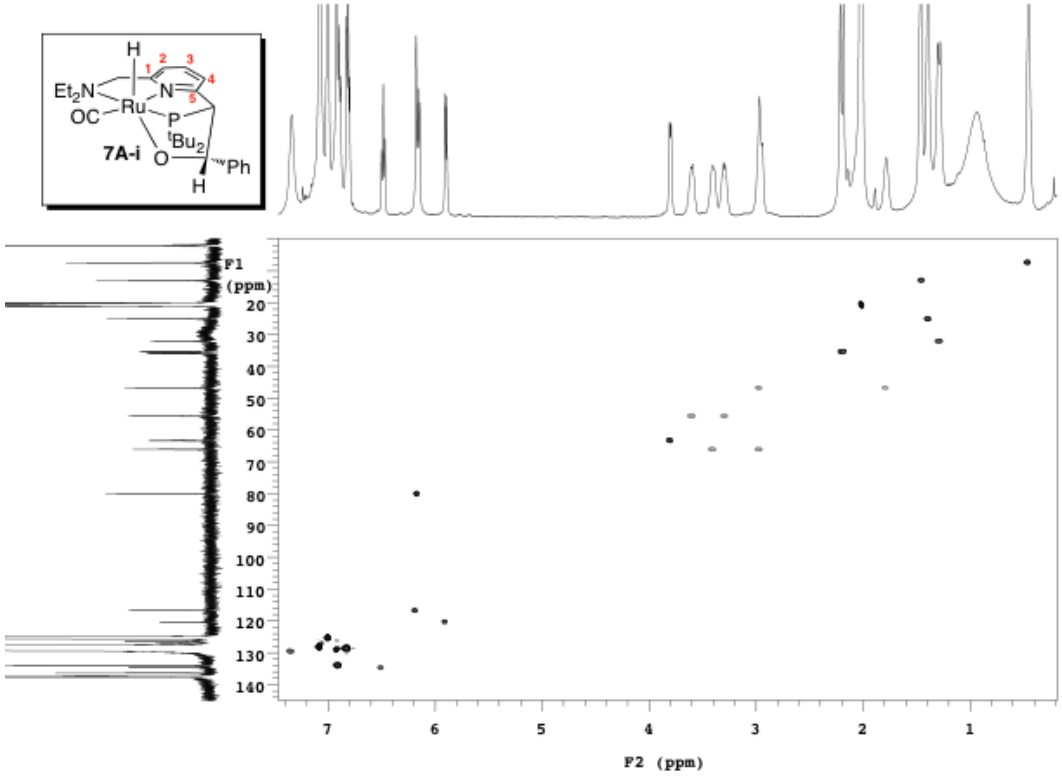

^{1}H-^{13}C gHMBC NMR spectrum of 7A-i (toluene-d_8, -50 ºC)

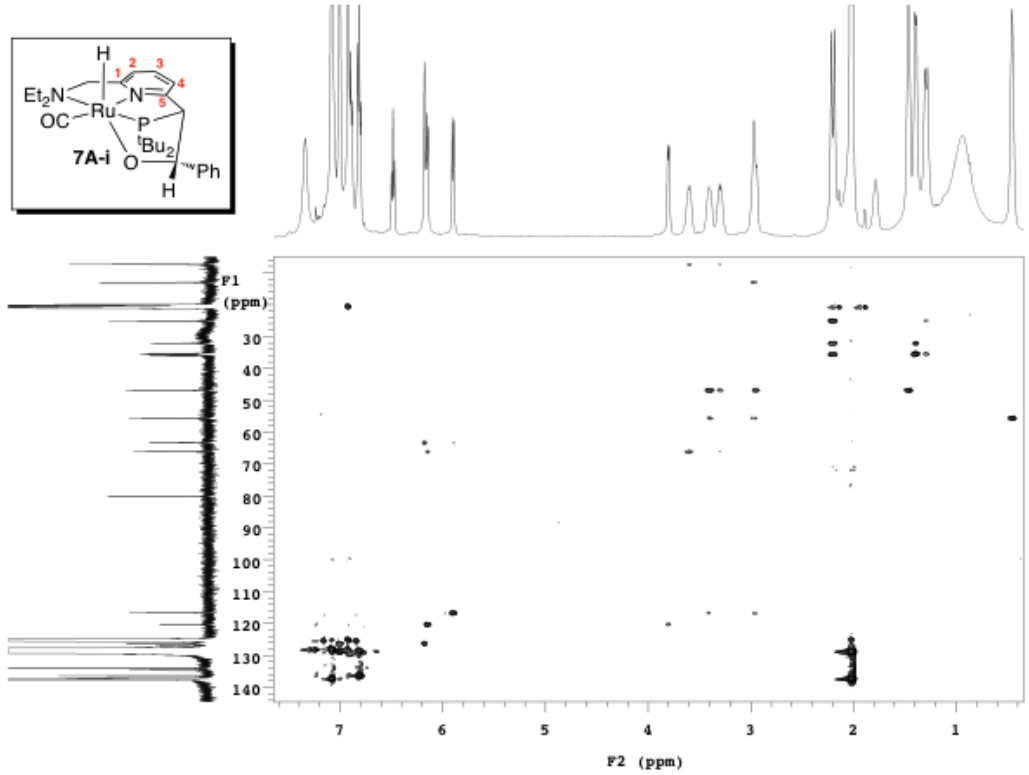

^{1}H-^{1}H NOESY NMR spectrum of 7A-i (toluene-d_8, -50 ºC)

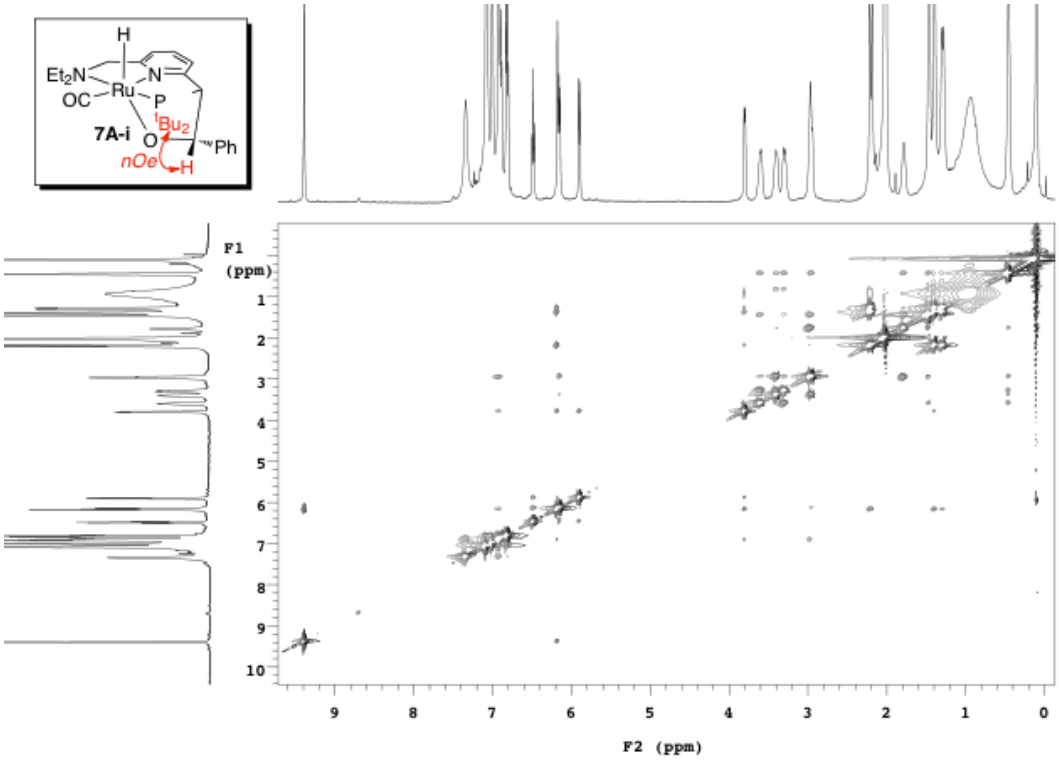

^{1}H-^{1}H gCOSY NMR spectrum of 7B-i (toluene-d_8, -5 °C)

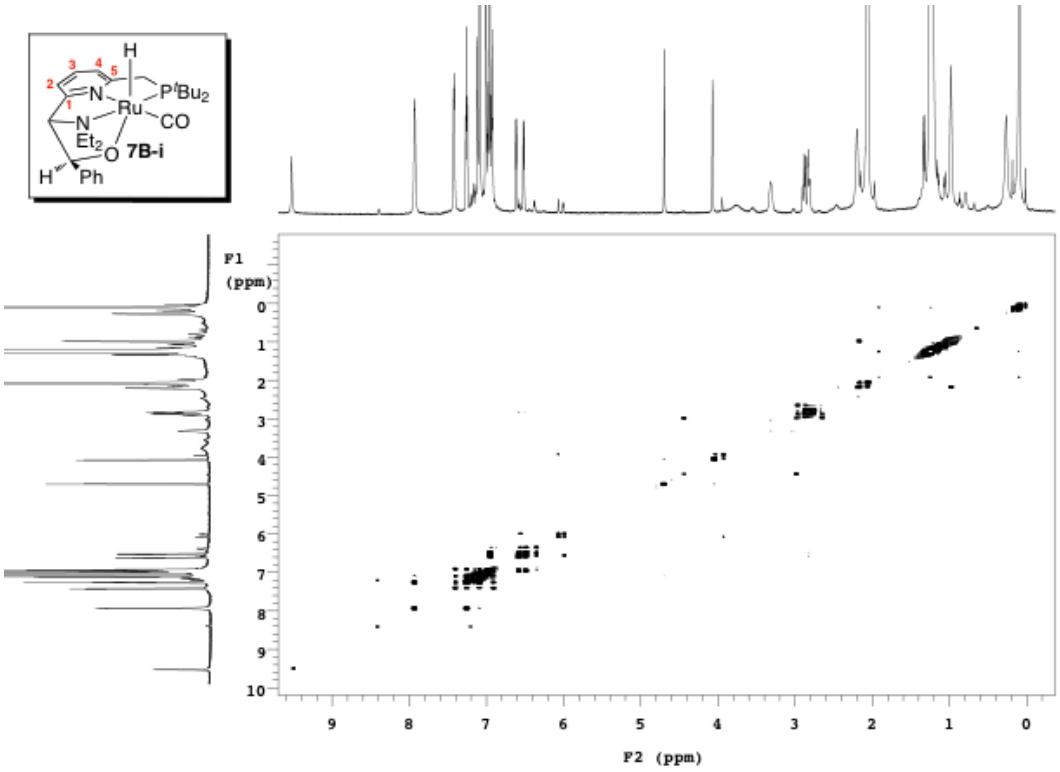

^{1}H-^{13}C gHSQC NMR spectrum of 7B-i (toluene-d_8, -5 °C)

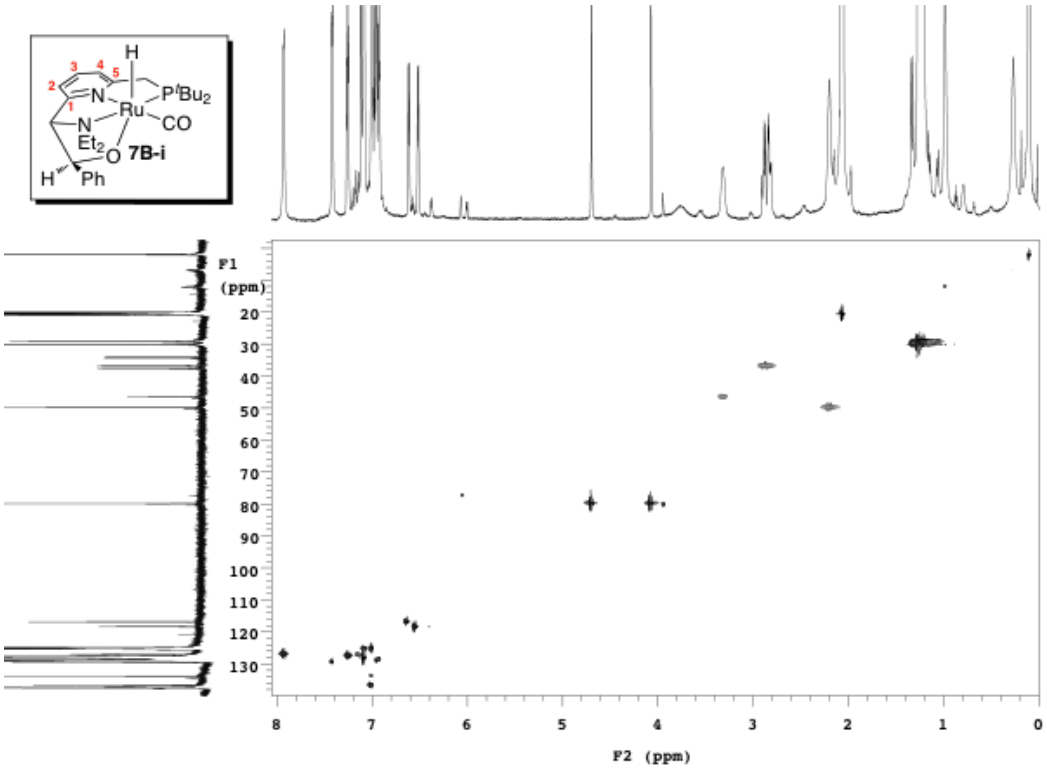

^{1}H-^{13}C gHMBC NMR spectrum of 7B-i (toluene-d_8, -5 °C)

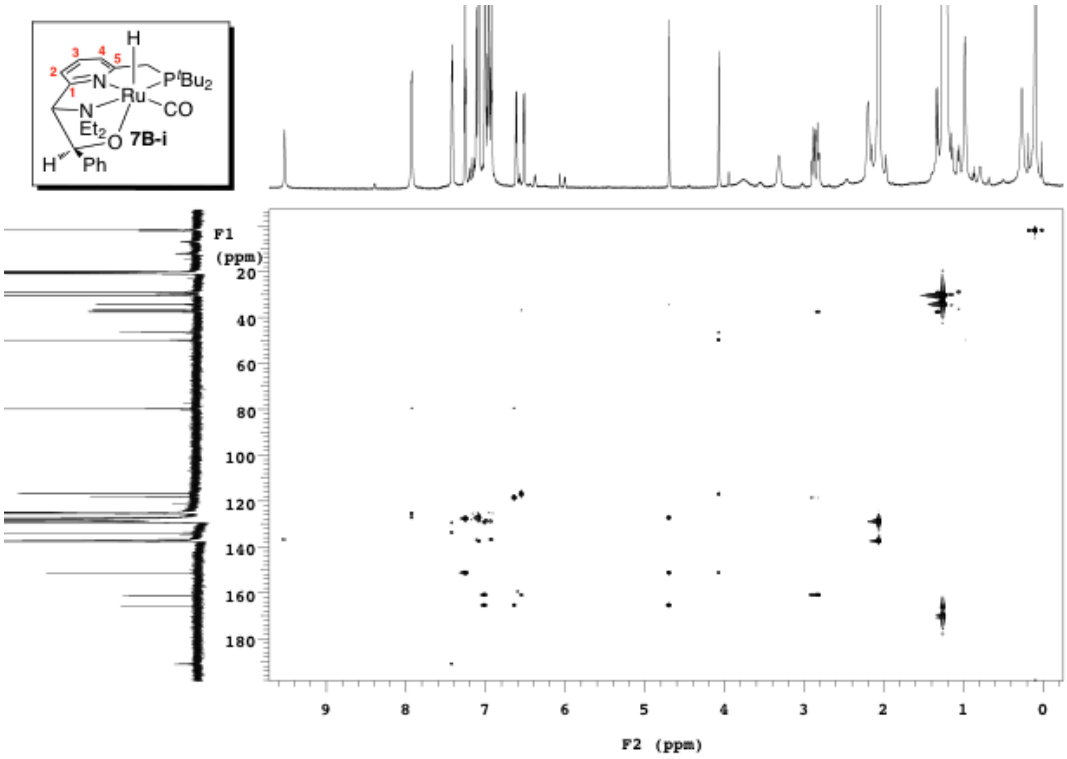

^{1}H-^{1}H NOESY NMR spectrum of 7B-i (toluene-d_8, -5 °C)

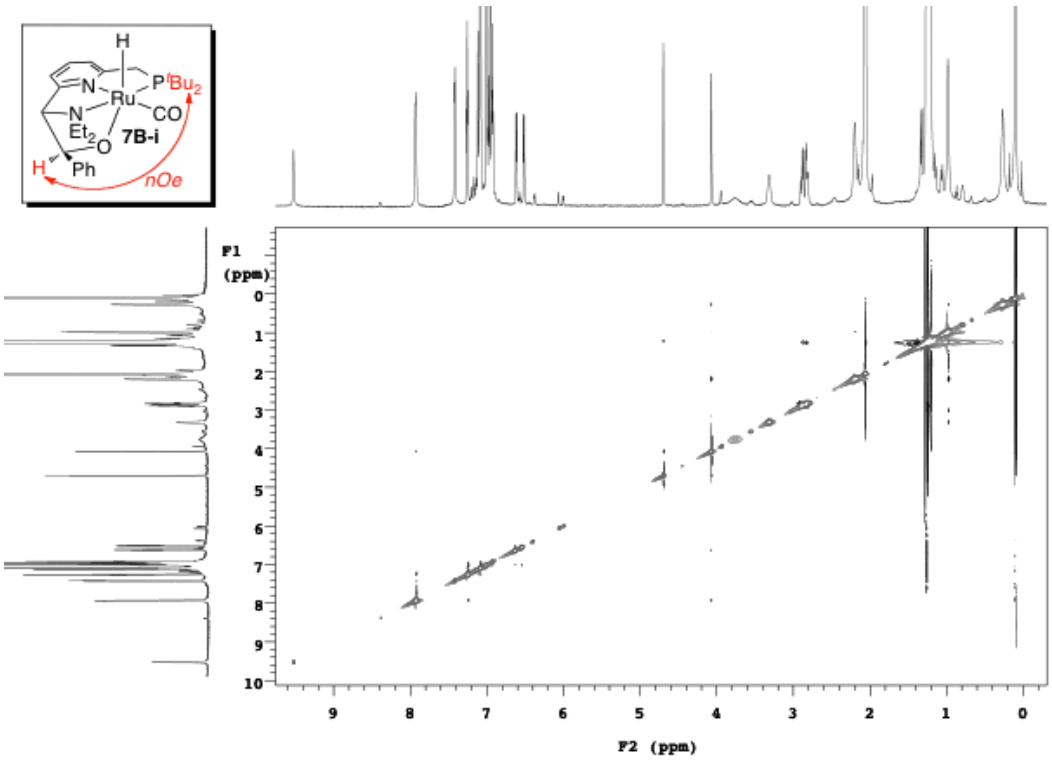

^{1}H-^{1}H gCOSY NMR spectrum of 7B-ii (toluene-d_8)

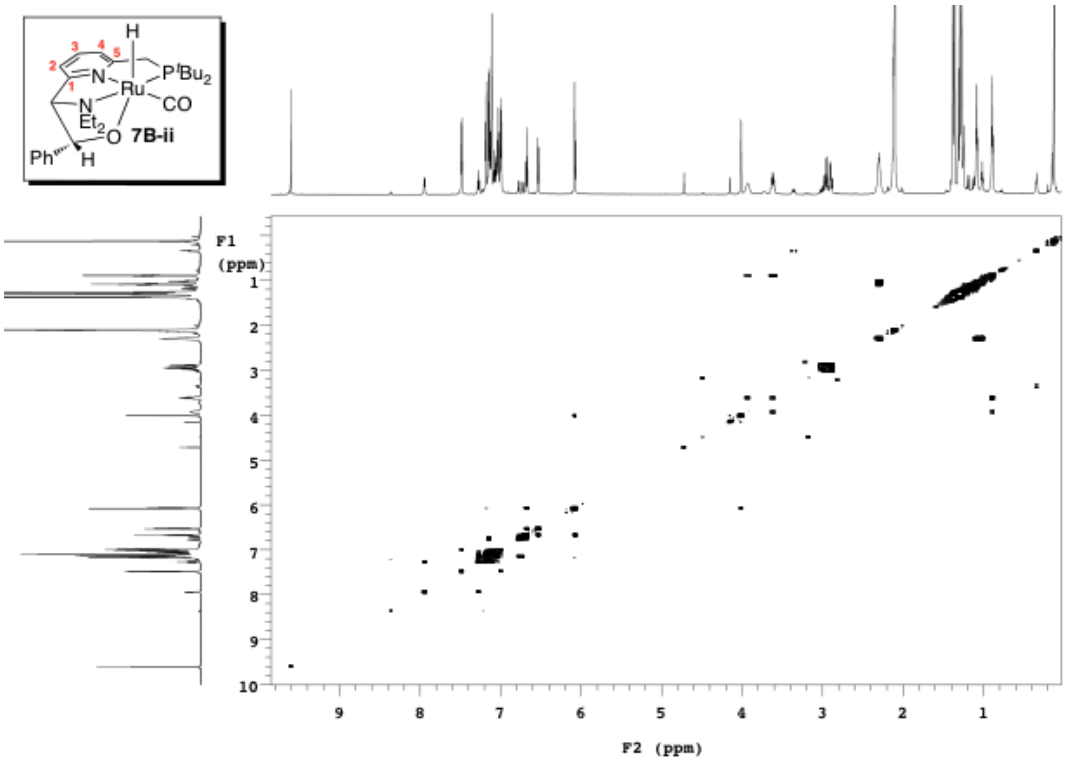

^{1}H-^{13}C gHMBC NMR spectrum of 7B-ii (toluene-d_8)

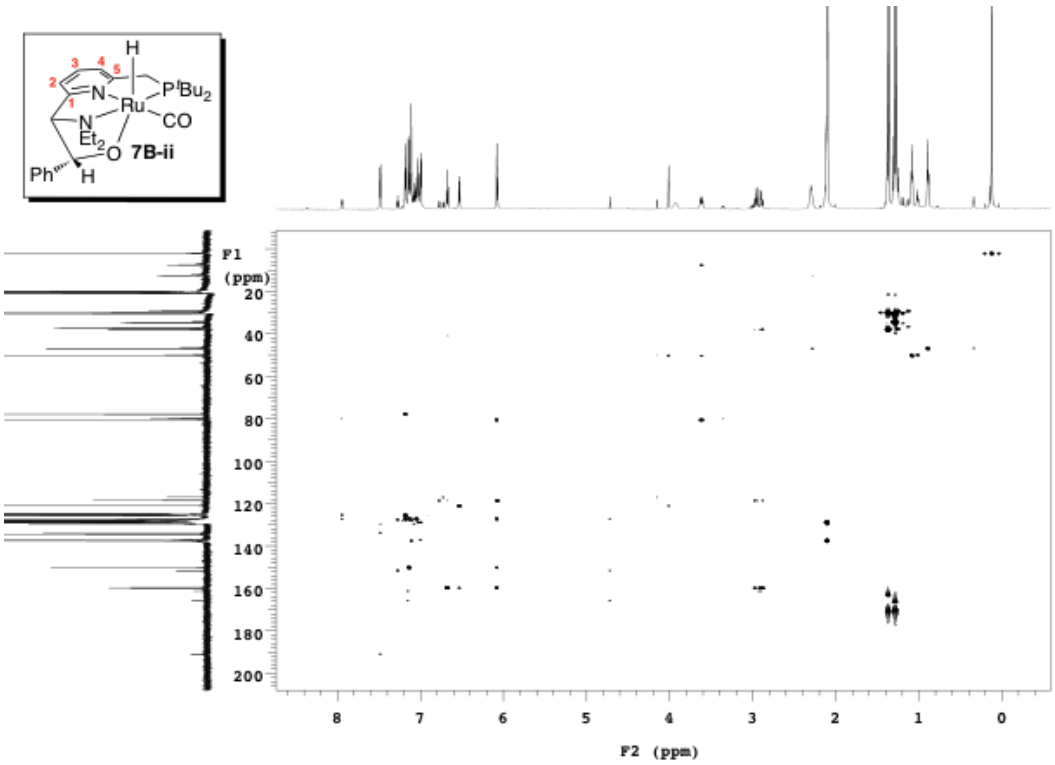

^{1}H-^{1}H NOESY NMR spectrum of 7B-ii (toluene-d_8)

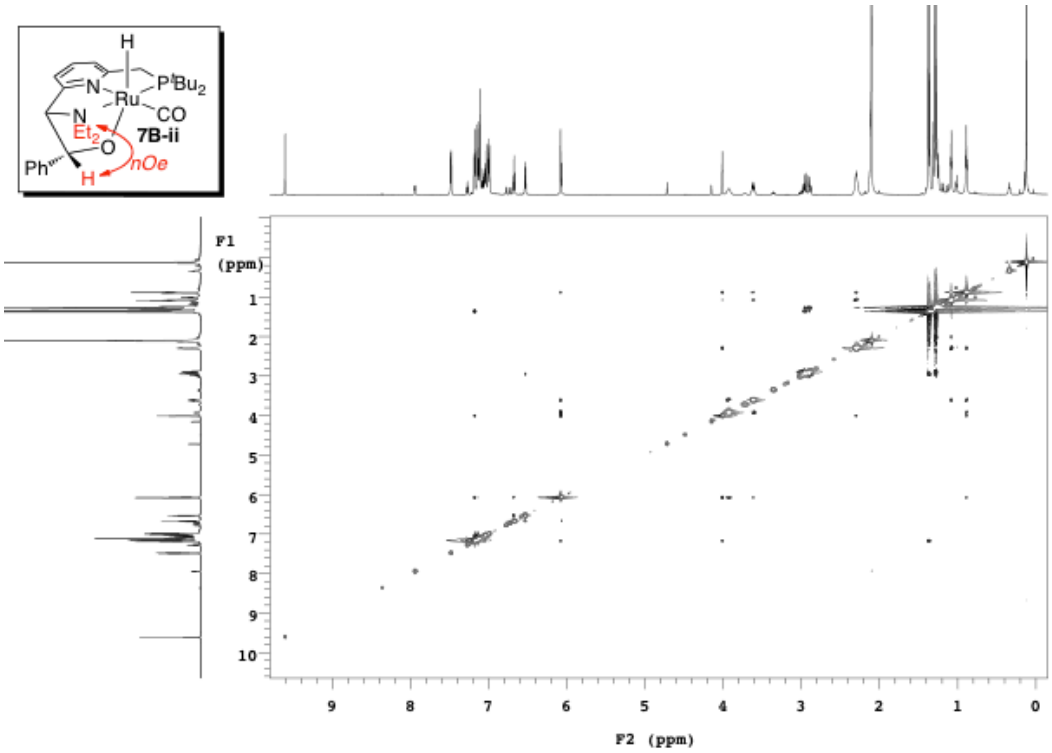

^{13}H{^{31}P} NMR spectrum of 9 (C_6D_6)

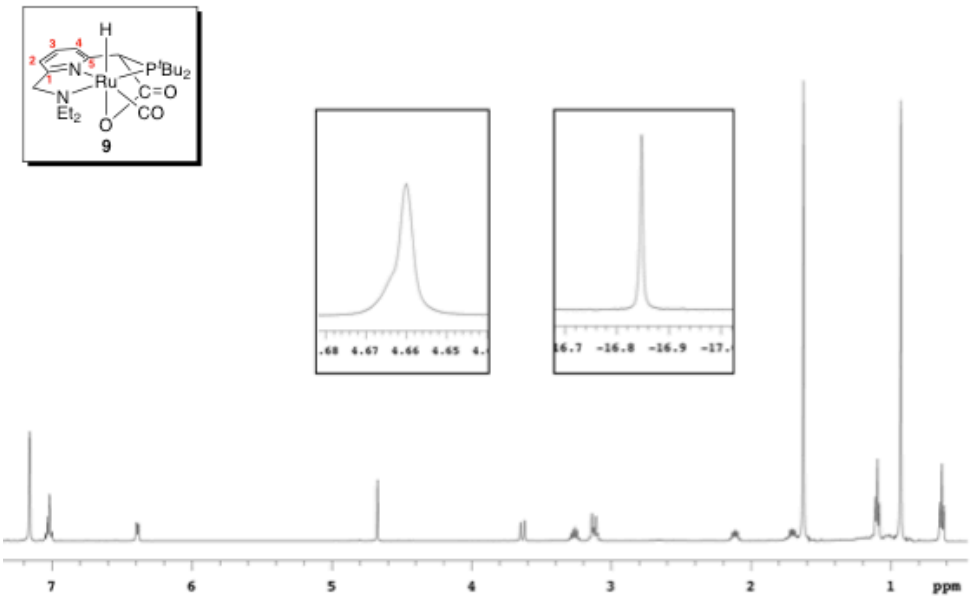

^{1}H-^{1}H COSY NMR spectrum of 9 (C_6D_6)

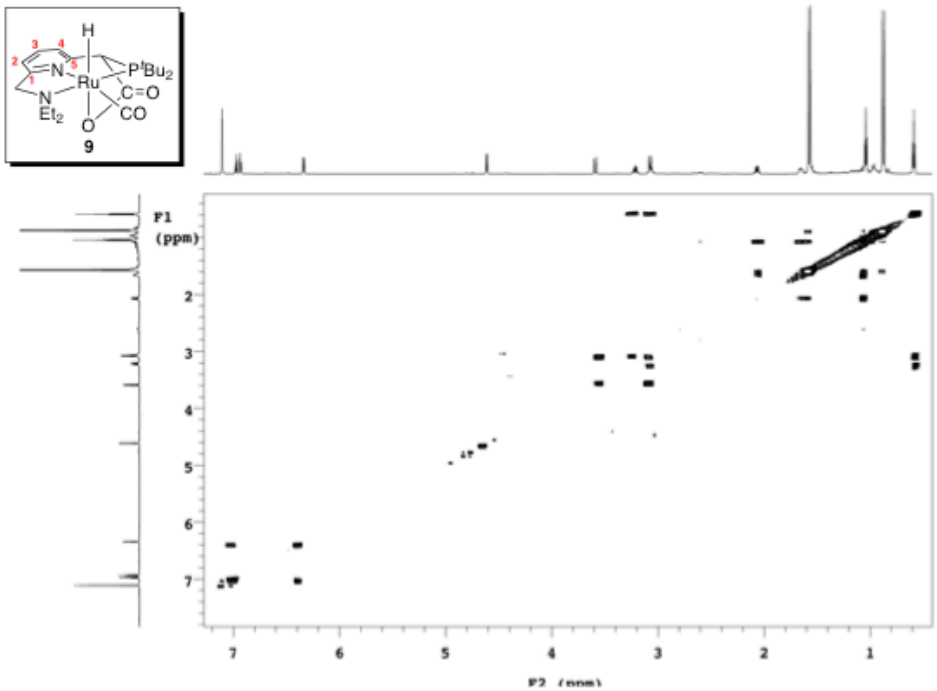

^{1}H-^{13}C HSQC NMR spectrum of 9 (C_6D_6)

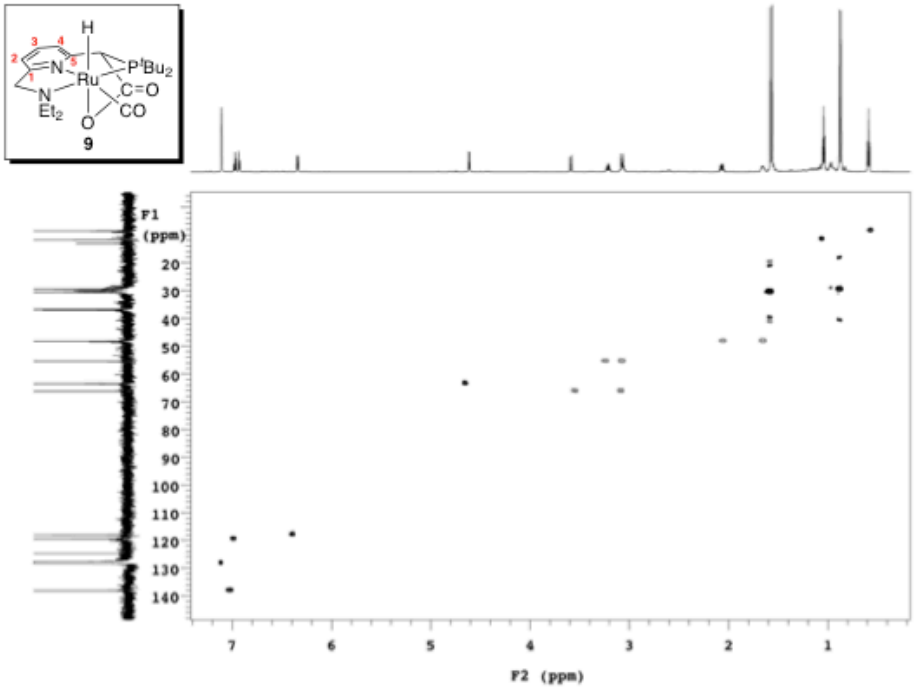

^{1}H-^{13}C CIGAR NMR spectrum of 9 (C_6D_6)

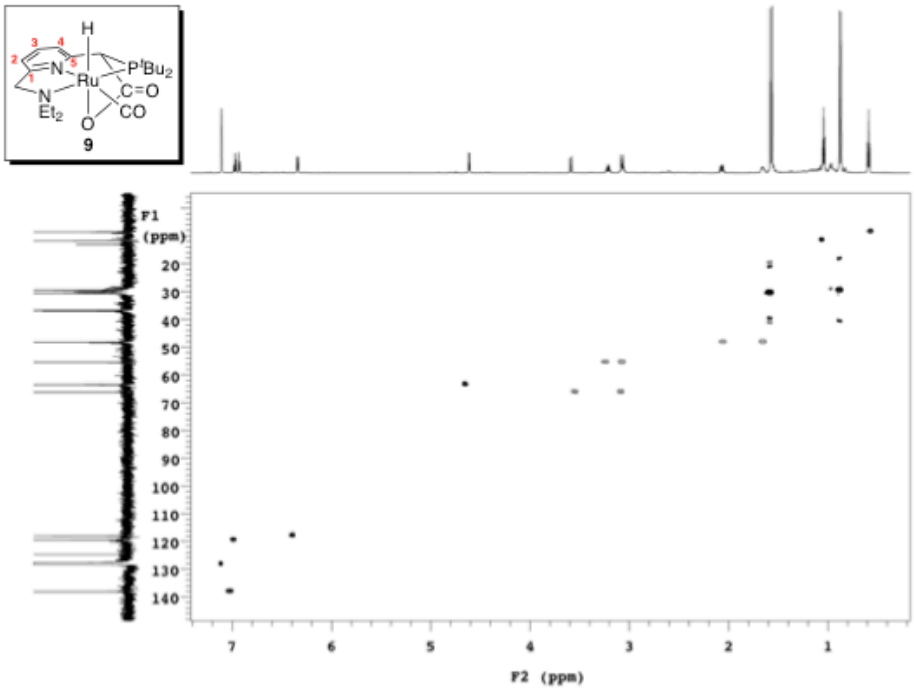

^{1}H-^{31}P HMBC NMR spectrum of 9 (C_6D_6)

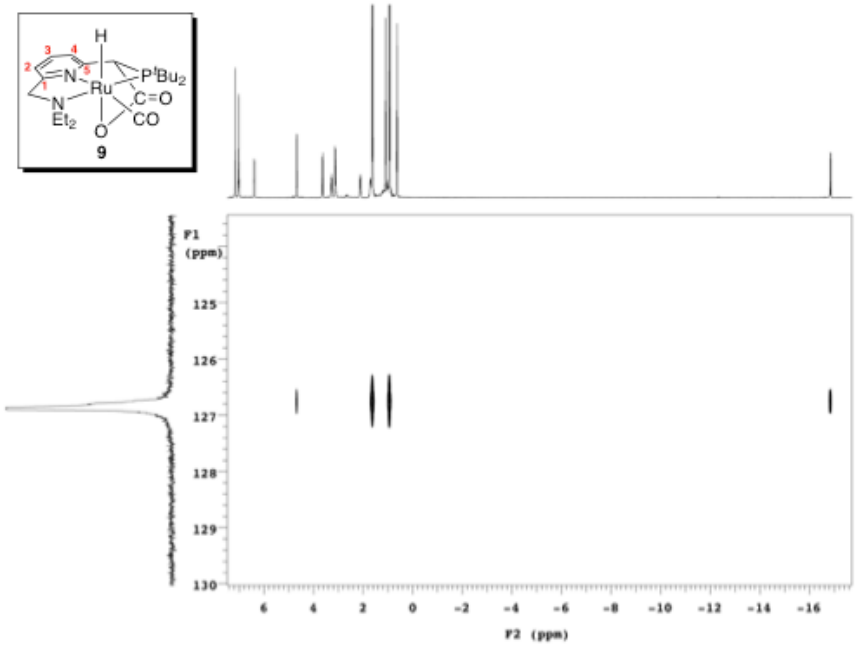

$^{13}H\{^{31}P\}$ NMR spectrum of 10 (C_6D_6)

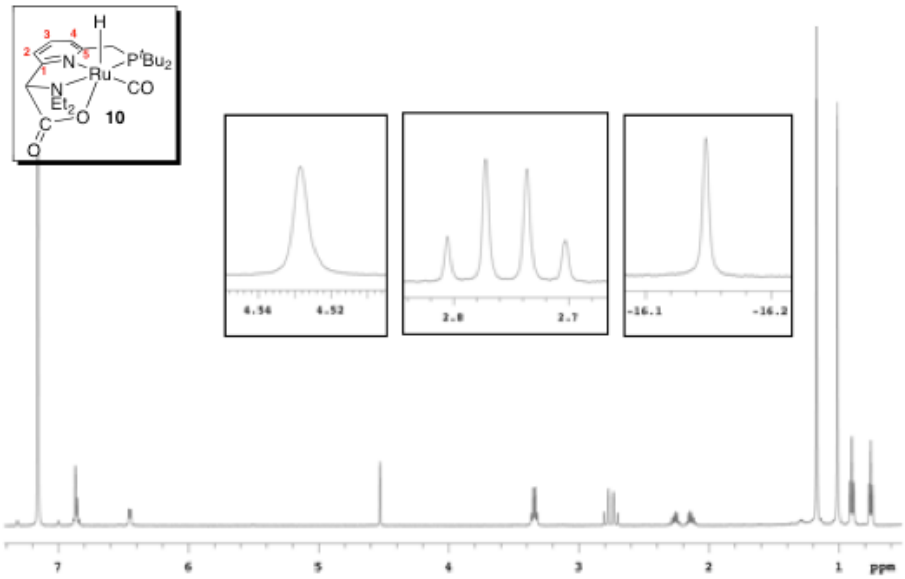

^{1}H-^{1}H COSY NMR spectrum of 10 (C_6D_6)

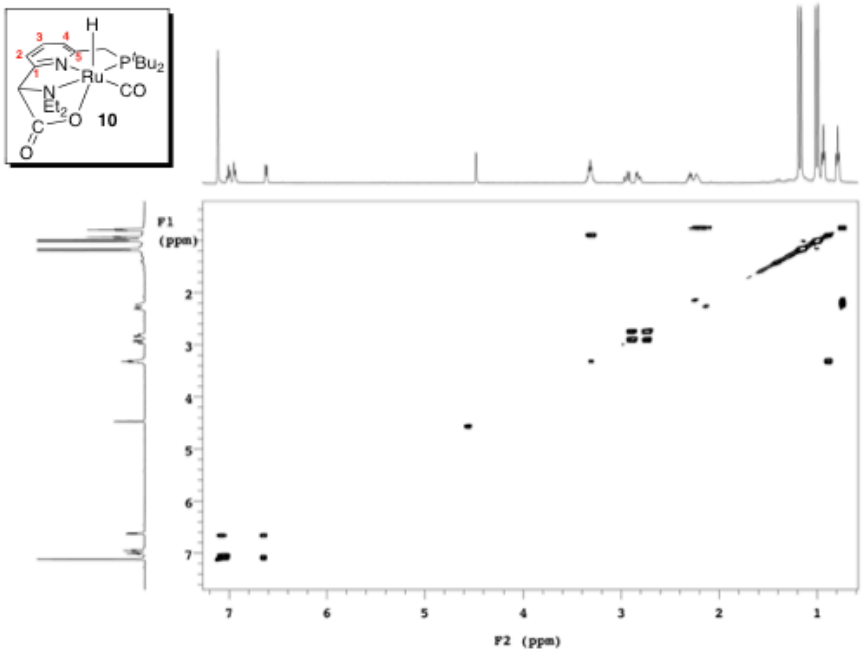

^{1}H-^{13}C HSQC spectrum of 10 (C_6D_6)

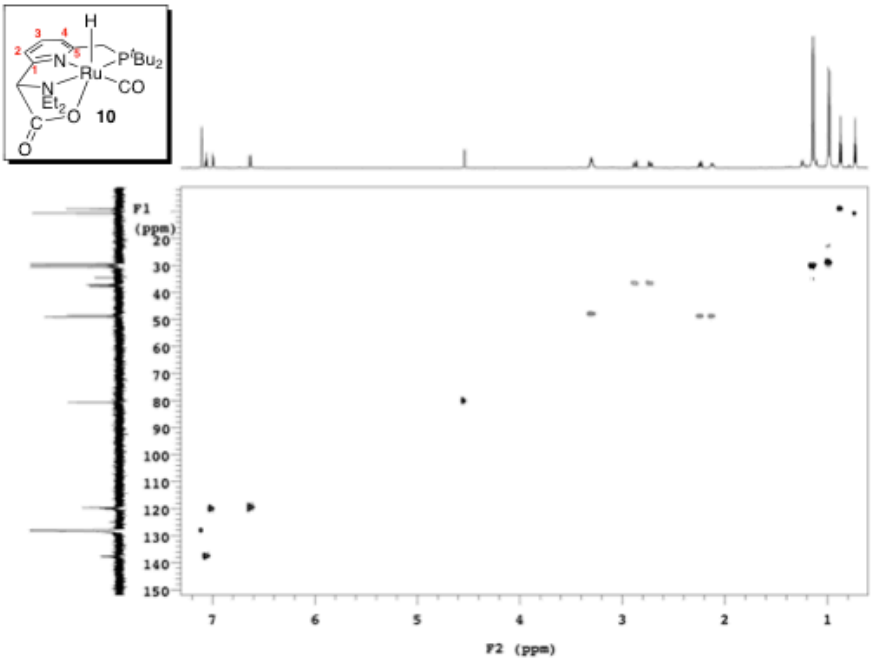

^{1}H-^{13}C HMBC spectrum of 10 (C_6D_6)

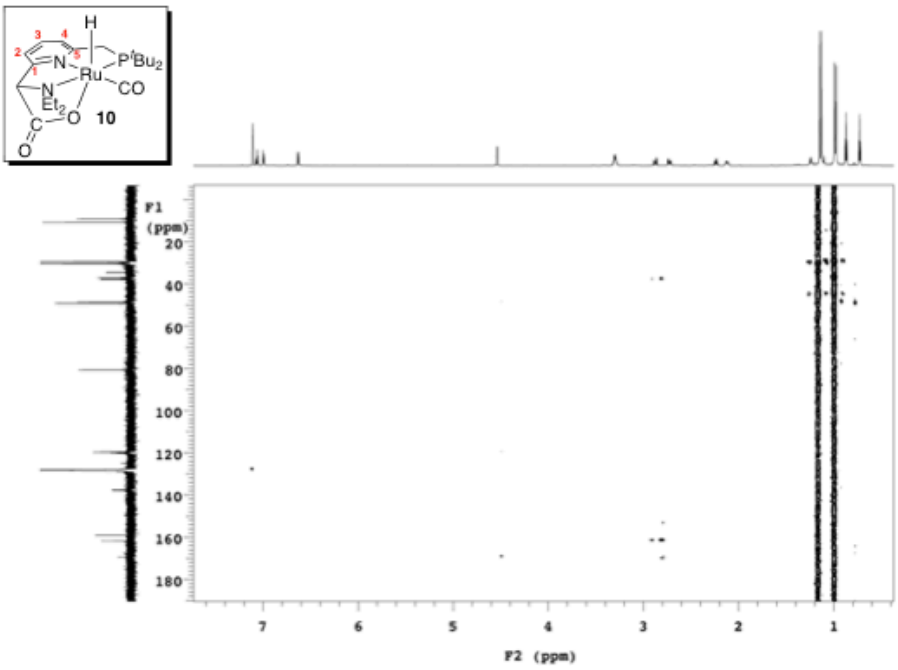

^{1}H-^{31}P HMBC spectrum of 10 (C_6D_6)

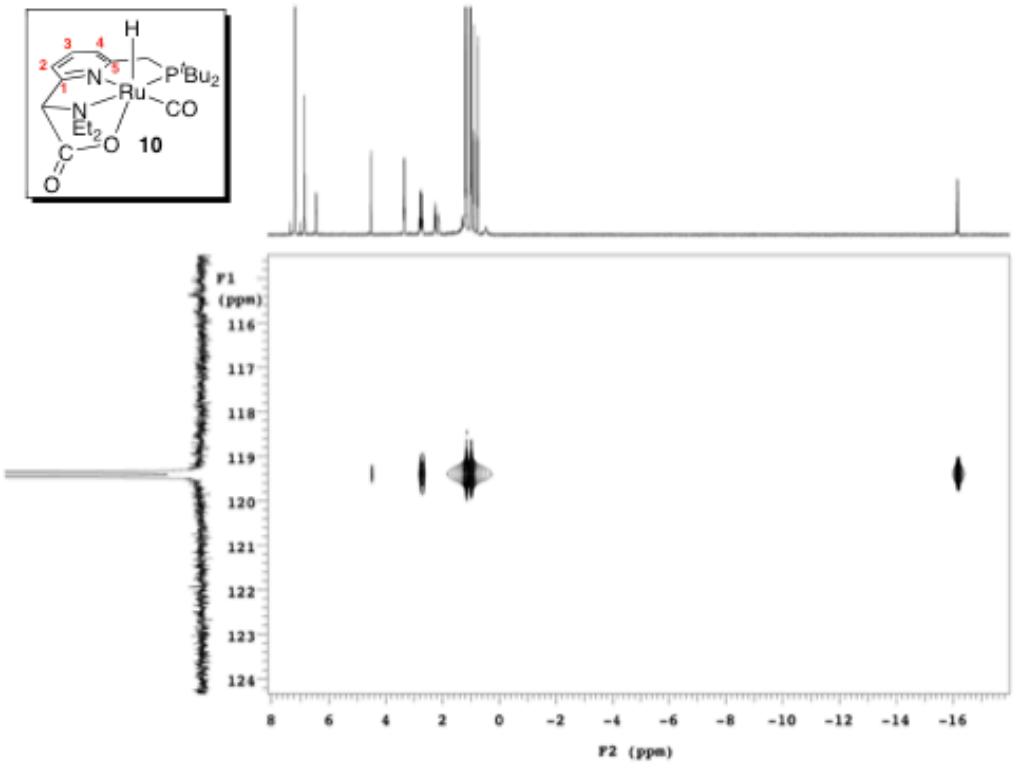

V. X-Ray Crystallography Experimental Data

In an N_2 atmosphere dry box, X-ray quality crystals of **4**, **6**, **7B-i**, and **7B-ii** were grown by dissolving **1** in a small amount of carbonyl compound that was then layered with pentane and cooled to -33 ºC. Yellow needles of **10** were grown from a tetrahydrofuran solution of the compound at 25 ºC. The crystals were mounted on a Bruker SMART APEX-I CCD-based X-ray diffractometer equipped with a low-temperature device and fine focus Mo-target X-ray tube (l = 0.71073 A) operated at 1500 W power (50 kV, 30 mA). The X-ray intensities were measured at 85(1) K; the detector was placed at a distance 5.070 cm from the crystal. Analysis of the data showed negligible decay during data collection; the data were processed with SADABS and corrected for absorption. The structure was solved and refined with the Bruker SHELXTL (version 2008/4) software package. All non-hydrogen atoms were refined anisotropically with the hydrogen atoms placed in a mix of idealized and refined positions.

*Crystal Data and Structure Refinement for **4***

Yellow blocks of **4** were grown from a pentane/methyl formate solution at -35 ºC. A total of 3000 frames were collected with a scan width of 0.5° in w and 0.45° in phi with an exposure time of 10 s/frame. The final cell constants (Table 3.6) were based on the xyz centroids of 1989 reflections above 10s(I). Disordered lattice solvates, presumably methyl were treated as contributing to diffuse scatter by the SQUEEZE subroutine of the PLATON program suite.

Table 3.6. Crystal Data and Structure Refinement for **4**

Empirical formula	$C_{22}H_{39}N_2O_3PRu$
Formula weight	571.64
Temperature	85(2) K
Wavelength	0.71073 Å
Crystal system	Monoclinic
Space group	$P2_1/c$
Unit cell dimensions	a = 17.9131(16) Å, a = 90º b = 10.7282(10) Å, b = 112.6070(10)º c = 15.6284(14) Å, g = 90º
Volume	2772.6(4) $Å^3$
Z	4
Calculated density	1.369 mg/mm^3
Absorption coefficient	0.657 mm^{-1}
F(000)	1200
Crystal size	0.26 x 0.25 x 0.25 mm^3
Theta range for data collection	2.26 to 28.34º
Limiting indices	$-23 \le h \le 23$, $-14 \le k \le 14$, $-20 \le l \le 20$
Reflections collected	73076
Independent reflections	6912 [R(int) = 0.0478]
Completeness to theta	28.34 (99.9 %)
Absorption correction	Semi-empirical from equivalents
Max. and min. transmission	0.8530 and 0.8477
Refinement method	Full-matrix least-squares on F^2

Data / restraints / parameters	6912 / 0 / 275
Goodness-of-fit on F^2	1.049
Final R indices [I>2s(I)]	$R_1 = 0.0215$, $wR_2 = 0.0552$
R indices (all data)	$R_1 = 0.0233$, $wR_2 = 0.0560$
Largest diff. peak and hole	0.674 and -0.347 e A^{-3}

*Crystal Data and Structure Refinement for **6***

Yellow plates of **6** were grown from a pentane/cyclopentanone solution at -35 ºC. A total of 4095 frames were collected with a scan width of 0.5° in w and 0.45° in phi with an exposure time of 20 s/frame. The final cell constants (Table 3.7) were based on the xyz centroids of 9915 reflections above 10s(I). The cyclopentanone solvate is disordered over two orientations.

Table 3.7. Crystal Data and Structure Refinement for **6** (with 1 equiv. cyclopentanone in crystal lattice)

Empirical formula	$C_{30}H_{51}N_2O_3PRu$
Formula weight	619.77
Temperature	85(2) K
Wavelength	0.71073 Å
Crystal system	Monoclinic
Space group	$P2_1/c$
Unit cell dimensions	a = 18.7853(6) Å, a = 90º b = 11.0118(3) Å, b = 102.4380(1)º c = 15.0703(4) Å, g = 90º
Volume	3044.27(15) $Å^3$
Z	4
Calculated density	1.352 mg/mm^3
Absorption coefficient	0.600 mm^{-1}
F(000)	1312
Crystal size	0.24 x 0.22 x 0.18 mm^3
Theta range for data collection	2.16 to 29.62º
Limiting indices	$-26 \le h \le 26$, $-15 \le k \le 15$, $-20 \le l \le 20$

Reflections collected	120048
Independent reflections	8551 [R(int) = 0.0437]
Completeness to theta	29.62 (99.8 %)
Absorption correction	Semi-empirical from equivalents
Max. and min. transmission	0.8997 and 0.8695
Refinement method	Full-matrix least-squares on F^2
Data / restraints / parameters	8551 / 13 / 400
Goodness-of-fit on F^2	1.010
Final R indices [I>2s(I)]	R_1 = 0.0235, wR_2 = 0.0630
R indices (all data)	R_1 = 0.0267, wR_2 = 0.0660
Largest diff. peak and hole	1.063 and -0.295 e A^{-3}

*Crystal data and structure refinement for **7B-i***

Yellow needles of **7B-i** were grown from a pentane/benzaldehyde solution at -35 ºC. A total of 2053 frames were collected with a scan width of 0.5° in w and 0.45° in phi with an exposure time of 90 s/frame. The final cell constants (Table 3.8) were based on the xyz centroids of 9969 reflections above 10s(I).

Table 3.8. Crystal Data and Structure Refinement for **7B-i**

Empirical formula	$C_{27}H_{41}N_2O_2PRu$
Formula weight	557.66
Temperature	85(2) K
Wavelength	0.71073 Å
Crystal system	Monoclinic
Space group	$P2_1/c$
Unit cell dimensions	a = 16.0967(8) Å, a = 90º b = 10.6978(5) Å, b = 108.5780º c = 16.1908(8) Å, g = 90º
Volume	2642.8(2) $Å^3$
Z	4
Calculated density	1.402 mg/mm^3
Absorption coefficient	0.680 mm^{-1}
F(000)	1168

Crystal size	0.19 x 0.05 x 0.02 mm^3
Theta range for data collection	2.32 to 27.32º
Limiting indices	$-20 \leq h \leq 20$, $-13 \leq k \leq 13$, $-20 \leq l \leq 20$
Reflections collected	39378
Independent reflections	5945 [R(int) = 0.0533]
Completeness to theta	27.32 (99.9 %)
Absorption correction	Semi-empirical from equivalents
Max. and min. transmission	0.9865 and 0.8817
Refinement method	Full-matrix least-squares on F^2
Data / restraints / parameters	5945 / 0 / 310
Goodness-of-fit on F^2	1.017
Final R indices [I>2s(I)]	$R_1 = 0.0301$, $wR_2 = 0.0660$
R indices (all data)	$R_1 = 0.0476$, $wR_2 = 0.0729$
Largest diff. peak and hole	0.857 and -0.324 e A^{-3}

*Crystal data and structure refinement for **7B-ii***

Yellow needles of **7B-ii** were grown from a pentane/benzaldehyde solution at 23 °C. A total of 4095 frames were collected with a scan width of 0.5° in w and 0.45° in phi with an exposure time of 15 s/frame. The final cell constants (Table 3.9) were based on the xyz centroids of 9951 reflections above 10s(I).

Table 3.9. Crystal Data and Structure Refinement for **7B-ii**

Empirical formula	$C_{27}H_{41}N_2O_2PRu$
Formula weight	557.66
Temperature	85(2) K
Wavelength	0.71073 Å
Crystal system	Orthorhombic
Space group	$P2_12_12_1$
Unit cell dimensions	a = 11.3568(3) Å, a = 90º b = 14.7861(4) Å, b = 90º c = 15.7682(4) Å, g = 90º
Volume	2647.84(12) $Å^3$
Z	4

Calculated density	1.399 mg/mm^3
Absorption coefficient	0.678 mm^{-1}
F(000)	1168
Crystal size	0.23 x 0.06 x 0.06 mm^3
Theta range for data collection	1.89 to 29.61°
Limiting indices	$-15 \leq h \leq 15$, $-20 \leq k \leq 20$, $-21 \leq l \leq 21$
Reflections collected	100960
Independent reflections	7441 [R(int) = 0.0653]
Completeness to theta	29.61 (100 %)
Absorption correction	Semi-empirical from equivalents
Max. and min. transmission	0.9604 and 0.8596
Refinement method	Full-matrix least-squares on F^2
Data / restraints / parameters	7441 / 0 / 310
Goodness-of-fit on F^2	1.068
Final R indices [I>2s(I)]	$R_1 = 0.0236$, $wR_2 = 0.0535$
R indices (all data)	$R_1 = 0.0266$, $wR_2 = 0.0553$
Largest diff. peak and hole	0.645 and -0.233 e A^{-3}

*Crystal data and structure refinement for **10***

Yellow needles of **10** were grown from a pentane/benzaldehyde solution at 23 °C. A total of 4095 frames were collected with a scan width of 0.5° in w and 0.45° in phi with an exposure time of 15 s/frame. The final cell constants (Table 3.10) were based on the xyz centroids of 9951 reflections above 10s(I).

Table 3.10. Crystal Data and Structure Refinement for **10**

Empirical formula	$C_{23}H_{39}N_2O_{3.5}PRu$
Formula weight	531.60
Temperature	85(2) K
Wavelength	1.54178 Å
Crystal system	Triclinic
Space group	P_{-1}
Unit cell dimensions	a = 8.04430(10) Å, a = 97.741(7)° b = 10.6437(2) Å, b = 91.333(6)°

	c = 14.8659(10) Å, g = 91.741(7)º
Volume	1249.74(9) $Å^3$
Z	2
Calculated density	1.413 mg/mm^3
Absorption coefficient	5.903 mm^{-1}
F(000)	556
Crystal size	0.17 x 0.09 x 0.05 mm^3
Theta range for data collection	4.84 to 68.24º
Limiting indices	$-9 \leq h \leq 9$, $-12 \leq k \leq 12$, $-17 \leq l \leq 17$
Reflections collected	32697
Independent reflections	4491 [R(int) = 0.0583]
Completeness to theta	68.24 (98.3 %)
Absorption correction	Semi-empirical from equivalents
Max. and min. transmission	0.7568 and 0.4336
Refinement method	Full-matrix least-squares on F^2
Data / restraints / parameters	4991 / 40 / 302
Goodness-of-fit on F^2	1.086
Final R indices [I>2s(I)]	$R_1 = 0.0295$, $wR_2 = 0.0809$
R indices (all data)	$R_1 = 0.0302$, $wR_2 = 0.0816$
Largest diff. peak and hole	0.618 and -0.791 e A^{-3}

3.6 References

1. Huff, C. A.; Sanford, M. S. Cascade Catalysis for the Homogeneous Hydrogenation of CO_2 to Methanol. *J. Am. Chem. Soc.* **2011**, *133,* 18122.

2. For catalytic results: Zhang, J.; Leitus, G.; Ben-David, Y.; Milstein, D. Efficient Homogeneous Catalytic Hydrogenation of Esters to Alcohols. *Angew. Chem., Int. Ed.* **2006**, *45*, 1113. (b) For synthetic procedure: Zhang, G.; Leitus, Y.; Milstein, Ben-David, Y.; Milstein, D. Facile Conversion of Alcohols into Esters and Dihydrogen Catalyzed by New Ruthenium Complexes. *J. Am. Chem. Soc.* **2005**, *127*, 10840.

3. Montag, M.; Zhang, J.; Milstein, D. Aldehyde Binding through Reversible C-C Coupling with the Pincer Ligand. *J. Am. Chem. Soc.* **2012** *134* 10325.

4. Low temperature studies on the reactivity of methyl formate with **1** were ambiguous and full characterization by low temperature NMR spectroscopy was not possible; however, it appears that regioisomer pair **4A-i**:**4A-ii** are both formed at –40 ºC.

5. Less than 5% **1** was also observed at room temperature.

6. LeBlanc, F. A.; Berkefeld, A.; Piers, W. E.; Parvez, M. Reactivity of Scandium β-Diketiminate Alkyl Complexes with Carbon Dioxide. *Organometallics* **2012**, *31*, 810.

7. (a) Severin, K.; Sünkel, K.; Beck, W. Synthesis, Stereochemistry and Reactions of Ruthenium(II) and Osmium(II) Complexes with α-Amino Carboxylates. *Chem. Ber.* **1994**, *127*, 615. (b) Kumar, P.; Singh, A. K.; Saxena, J. K.; Pandey, D. S. Synthesis and Characterization of Ruthenium(II) Polypyridyl Complexes Containing a-Amino Acids and its DNA Binding Behavior. *J. Organomet. Chem.* **2009**, *694*, 3570.

8. Other intermediates are possible on the pathway from **9** to **10**. These could include an O-bound CO_2 complex and/or a zero-valent Ru complex.

9. Vogt, M.; Gargir, M.; Iron, M. A.; Diskin-Posner, Y.; Ben-David, Y.; Milstein, D. A New Mode of Activation of CO_2 by Metal-Ligand Cooperation with Reversible C-C and M-O Bond Formation at Ambient Temperature. *Chem. Eur. J.* **2012**, *18*, 9194.

10. Huff, C. A.; Kampf, J. W.; Sanford, M. S. Reversible Carbon-Carbon Bond Formation Between Carbonyl Compounds and a Ruthenium Pincer Complex. *Chem. Commun.* **2013**, *49*, 7147. – Reproduced by permission of The Royal Society of Chemistry. **http://pubs.rsc.org/en/content/articlelanding/2013/cc/c3cc43517b**

11. Excerpts of Chapter 3 reprinted with permission from Huff, C. A.; Kampf, J. W.; Sanford, M. S. Role of a Noninnocent Pincer Ligand in the Activation of CO_2 at (PNN)Ru(H)(CO). *Organometallics* **2012**, *31*, 4643. Copyright 2012. American Chemical Society.

12. Zhang, G.; Leitus, Y.; Milstein, Ben-David, Y.; Milstein, D. Facile Conversion of Alcohols into Esters and Dihydrogen Catalyzed by New Ruthenium Complexes. *J. Am. Chem. Soc.* **2005**, *127*, 10840.

CHAPTER 4

Investigation of Ruthenium Pincer Complexes as Carbon Dioxide Hydrogenation Catalysts for Application to the Cascade System

4.1 Introduction

We have accomplished the development of a system for the catalytic reduction of carbon dioxide (CO_2) to methanol (CH_3OH) by a cascade sequence (see Chapter 2 for more details)[1] that begins with the conversion of CO_2 to formic acid (FA, Scheme 4.1, step i). This step is followed by Lewis-acid-catalyzed esterification to provide methyl formate (step ii), with subsequent methyl formate hydrogenation to liberate two equivalents of CH_3OH (step iii). The metal complexes utilized in this system were Ru complex **1**[2] for CO_2 hydrogenation step i, in concert with Milstein's Ru pincer complex Ru(PNN)(CO)(H) (**2**, PNN = 6-(di-*tert*-butylphosphinomethylene)-2-(*N*,*N*-diethylaminomethyl)-1,6-dihydropyridine)[3] as the catalyst for ester hydrogenation (step iii). The use of two different catalysts for these steps was necessary because neither one was individually effective for the entire cascade.

Scheme 4.1. Cascade Homogeneous Hydrogenation of CO_2 to Methanol

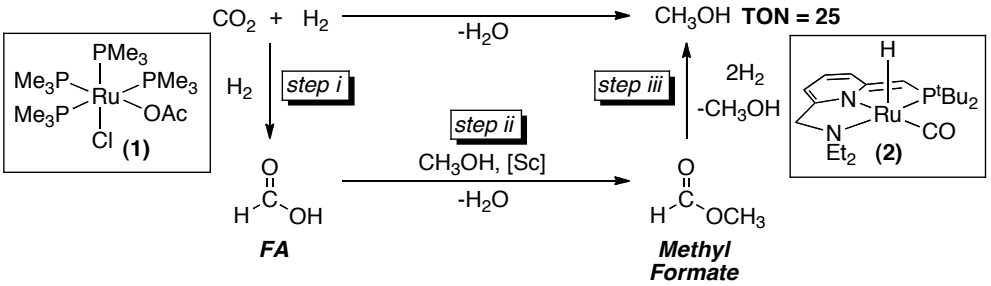

In an ideal system, a single catalyst would be used to promote each step in the reaction cascade in order to lower overall catalyst loading. However, when initially investigating homogeneous catalysts for this system, there were no known catalysts that could be implemented for multiple steps in the cascade. Revisiting the literature, there are many reported systems of the homogeneous hydrogenation of CO_2 to formic acid[4a–c] and formate salts,[4d–j] but far fewer for hydrogenation of esters.[5] Two of the most active homogeneous CO_2 hydrogenation catalysts reported to date are complex **1**[2] and Ir(PNP)$(H)_3$ (PNP = 2,6-bis(diisopropylphosphinomethylene)pyridine) pincer catalyst **3** (Scheme 4.2).[6] Both complexes provide formate from CO_2 in yields representing $>10^4$ catalytic turnovers and with turnover frequencies in excess of 10^4 h^{-1}. Noting that catalyst **3** closely resembles complex **2** in that they are both M–H complexes with a phosphino pyridine based pincer ligand, there is potential for **2** to serve as a CO_2 hydrogenation catalyst. As a method to determine if this objective is feasible, in depth studies into using **2** as a CO_2 hydrogenation catalyst were carried out. Additionally, a single metal complex was explored for the cascade conversion of CO_2 to methanol.

Scheme 4.2. Hydrogenation of CO_2 to Formate (a) Ru Catalyst **1** and (b) Ir Catalyst **3**

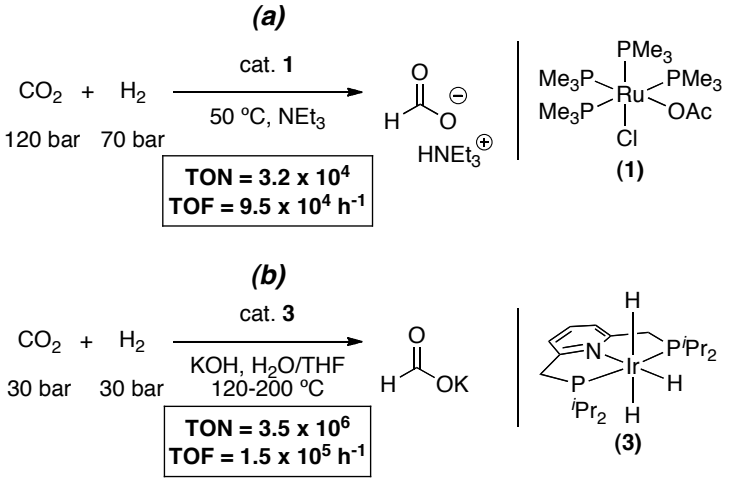

4.2 Ruthenium Pincer Complex as a CO_2 Hydrogenation Catalyst

By analogy to iridium catalyst **3**,[6] a possible catalytic cycle for reducing CO_2 to formate at complex **2** (Scheme 4.3) would involve (i) heterolytic cleavage of H_2 to form ruthenium dihydride **4**, (ii) insertion of CO_2 to generate formate complex **5**, and (iii)

deprotonation of the pincer ligand of **5** with concomitant release of formate to complete the catalytic cycle.[7,8] Step i of this cycle is well precedented, and has been studied in detail by Milstein and coworkers.[3] In contrast, the feasibility of steps ii and iii has not yet been established for this ruthenium system.

Scheme 4.3. Possible Catalytic Cycle for CO_2 Hydrogenation to Formate by Complex **2**

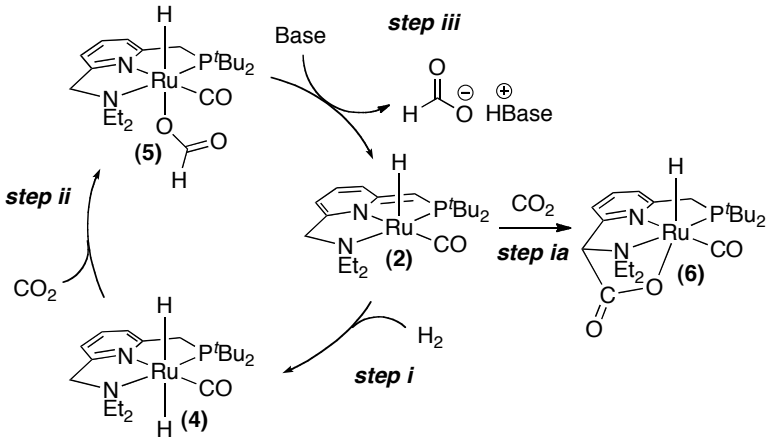

4.2.1 Stoichiometric Studies

We began our investigation by treating a solution of **2** in anisole-d_8 with a 4 : 1 mixture of H_2 and CO_2 (Scheme 4.4). This resulted in the conversion of **2** to formate complex **5** in 88% NMR yield after 24 hours at room temperature, as indicated by a Ru-H shift at –16.28 ppm (J_{HP} = 27.9 Hz).[9] This result established the feasibility of step ii of the catalytic cycle proposed in Scheme 4.3. Furthermore, the identity of **5** was confirmed by independent synthesis, and this complex was characterized using standard one- and two-dimensional NMR spectroscopic techniques as well as X-ray crystallography (Figure 4.1).[10] The CO_2 adduct **6** (formed by the direct reaction of **2** with CO_2, step ia of Scheme 4.3)[11–13] was detected as a minor side product in this reaction (12% yield, *vide infra* for further discussion).

Scheme 4.4. Reaction of **2** with CO_2 and H_2

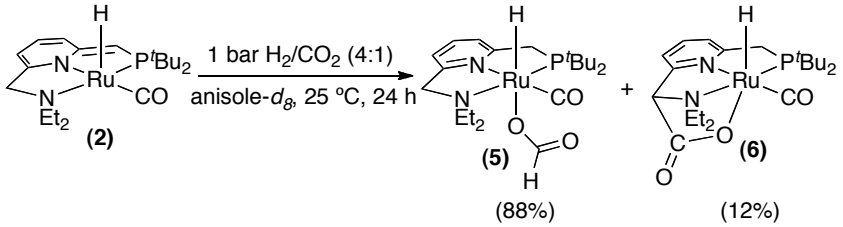

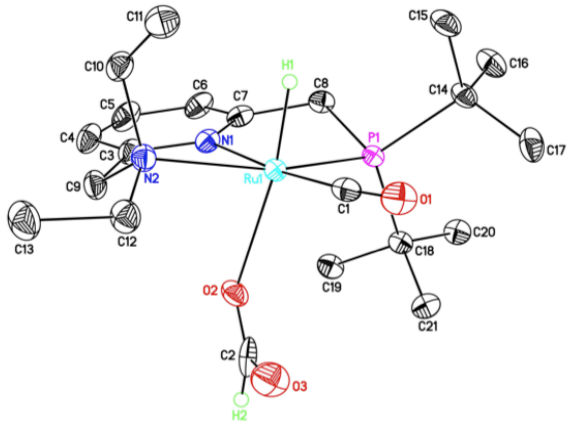

Figure 4.1. ORTEP diagram (50% probability level) of the molecular drawing of **5**. The packing solvent (benzene) as well as all H atoms (other than the Ru−H and H–COO) have been omitted for clarity. Selected bond lengths (Å) and angles (deg): Ru1−H1 = 1.45(3), Ru1–N1 = 2.0983(18), Ru1–N2 = 2.2535(18), Ru1–O2 = 2.2497(16), Ru1–C1 = 1.834(2), Ru1–P1 = 2.2626(5), O2–C2 = 1.203(3), O3–C2 = 1.283(3); H1–Ru1–O2 = 169.2(10); P1–Ru1–N2 = 158.83(5); N1−Ru1−O2 = 82.67(7), N2−Ru1−O2 = 83.88(6).

We next sought to identify conditions for promoting the final step (iii) of the proposed catalytic cycle. Based on precedent by Nozaki with Ir catalyst **3**,[6] we hypothesized that a strong base could deprotonate the pincer ligand of **5** and induce formate release. Indeed, the treatment of a solution of **5** in anisole-d_8 with 1 equivalent of potassium *tert*-butoxide (KO^{t}Bu) resulted in quantitative formation of **2** and potassium formate as determined by ^{1}H NMR spectroscopic analysis (Scheme 4.5).

Scheme 4.5. Deprotonation of **5** by KO^{t}Bu to Form **2** and HCOOK

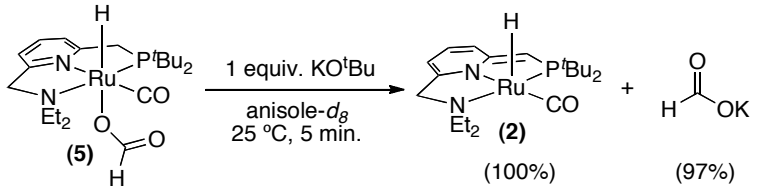

4.2.2 Catalytic Trials

The results in Scheme 4.4 and Scheme 4.5 demonstrate the feasibility of all three individual steps of the proposed **2**-catalyzed hydrogenation of CO_2 to formate. In order to combine these steps to achieve catalysis, **2** was initially treated with 10 bar CO_2 and 30 bar H_2 in the presence of 1200 equivalents of KO^{t}Bu in anisole at room temperature, conditions analogous to those of the stoichiometric reactions conducted above (Table 4.1, entry 1). The TON for this reaction was determined based on the yield of formate after 4 hours as a preliminary estimate of catalyst reactivity. Catalysis was sluggish under these initial conditions, and only 7 turnovers were observed after 4 hours (max possible TON = 1.2 x 10^3 based on equivalents of base). However, raising the temperature to 120 ºC resulted in a dramatic improvement in the performance of catalyst **2**, as it afforded 2.7 x 10^3 turnovers under otherwise analogous conditions (entry 2). We next replaced the non-polar solvent anisole with diglyme, reasoning that it would better solubilize KO^{t}Bu.[14] Gratifyingly, this resulted in a 3-fold improvement in TON (to 8.0 x 10^2) over the same period of time (entry 3).

A variety of different bases were next evaluated for the reaction in diglyme. K_2CO_3, KOH, K_3PO_4, and $KHCO_3$ were all effective in promoting this transformation, with TONs ranging from 5.1 x 10^2 to 1.1 x 10^3 (entries 4–7).[15] The best base for this reaction was K_2CO_3, yielding a TON of 1.1 x 10^3 and a TOF of 1.6 x 10^3 h^{-1}.[16,] These data stand in contrast to Nozaki's results with Ir pincer complex **3**. In that system, moving from KOH to a weaker base like K_3PO_4 resulted in a significant decrease in the TON (>7-fold).[6] The diversity of bases effective in the reaction of **2** suggests that deprotonation of intermediate **5** may be more facile than deprotonation of the analogous Ir formate intermediate. Notably, however, the neutral amine base NEt_3, which has been

frequently employed in CO_2 hydrogenation reactions,[2,4d–h,17] resulted in <5 turnovers in this system (entry 8).

Table 4.1. Hydrogenation of CO_2 to Formate Catalyzed by **2**

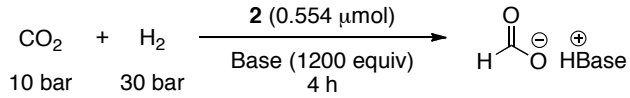

Entry[a]	Solvent	Temp (°C)	Base	TON Formate
1	anisole	25	KO^tBu	7.0×10^0
2	anisole	120	KO^tBu	2.7×10^2
3	diglyme	120	KO^tBu	8.0×10^2
4	diglyme	120	K_2CO_3	1.1×10^3
5[b]	diglyme	120	KOH	5.1×10^2
6	diglyme	120	K_3PO_4	9.0×10^2
7	diglyme	120	$KHCO_3$	5.5×10^2
8	diglyme	120	NEt_3	<5
9[b]	diglyme	120	K_2CO_3	6.6×10^2
10[b,c]	diglyme	120	K_2CO_3	1.4×10^3
11[b]	diglyme	100	K_2CO_3	9.0×10^3
12[b,d]	diglyme	120	K_2CO_3	2.3×10^4

[a] Conditions: CO_2 (10 bar), H_2 (30 bar), **2** (0.554 μmol, 1 equiv), base (0.6648 mmol, 1200 equiv), solvent (2 mL), 4 h. [b] With 100,000 equiv K_2CO_3, 5 mL diglyme. [c] 24 h. [d] 48 h.

Because the best results were obtained using K_2CO_3 as the base (entry 4), the effect of increasing the equivalents of K_2CO_3 was next examined, which would correspondingly increase the theoretical maximum TON of **3**. The use of 1.0×10^5 equivalents of K_2CO_3 at 120 ºC provided 6.6×10^2 turnovers after 4 h (entry 9) and 1.4×10^3 turnovers after 24 h. Notably, based on the stoichiometry of K_2CO_3, the maximum possible turnovers is 2.0×10^5.[16] Furthermore, increasing the temperature to 200 ºC provided 9.0×10^3 and 2.3×10^5 turnovers after 4 and 48 hours, respectively, with a TOF of 2.2×10^3 h^{-1} at this temperature.[18]

4.2.3 Mechanistic Studies

As discussed above, we originally envisioned the catalytic cycle in Scheme 4.3 as a plausible pathway for this transformation. If this mechanism is operative, formate

complex **5** should display similar catalytic activity as **2**. Indeed, under otherwise identical conditions, this catalyst provided comparable TON after 4 hours (compare Table 4.1, entry 4 and Table 4.2, entry 1).

Table 4.2. Complexes **2**, **5**, and **6** as Catalysts for CO_2 Hydrogenation

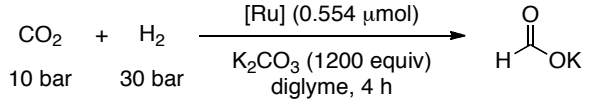

Entry[a]	[Ru]	Temp (°C)	TON Formate
1	**5**	120	1.0×10^3
2	**6**	120	1.1×10^3
3	**6**	70	<5
4	**2**	70	3.4×10^2
5	**5**	70	4.3×10^2

[a] Conditions: CO_2 (10 bar); H_2 (30 bar); Ru catalyst **2**, **5**, or **6** (0.554 μmol, 1 equiv), K_2CO_3 (0.6648 mmol, 1200 equiv), diglyme (2 mL), 4 h.

The mechanism as drawn in Scheme 4.3 implicates Ru-CO_2 complex **6** as an off-cycle side product. Previous studies from our group showed that the formation of **6** is irreversible at room temperature,[11] suggesting it may serve as a catalyst deactivation pathway. To test this possibility, we also examined the reactivity of **6** as a catalyst for CO_2 hydrogenation under our standard reaction conditions. Unexpectedly, we found that this Ru–CO_2 adduct afforded a TON of formate comparable to that of **2** and **5** after 4 hours at 120 ºC (Scheme 4.3, entry 2).

The observed catalytic activity of **6** can be explained by at least two mechanistic possibilities. A first is that CO_2 binding at **6** (step ia of Scheme 4.3) could be reversible at the elevated temperatures used for catalysis. This would enable the regeneration of **3**, which could then participate in CO_2 hydrogenation. Alternatively, **6** could potentially be capable of directly catalyzing CO_2 hydrogenation. As outlined in Scheme 4.6, a possible mechanism for this latter transformation could involve deprotonation of **6** to generate the unsaturated complex **7** (step i), followed by H_2 heterolysis (step ii), CO_2 insertion (step iii), and base-promoted product release (step iv).[19]

Scheme 4.6. Possible Catalytic Cycle for CO_2 Hydrogenation at Complex **6**

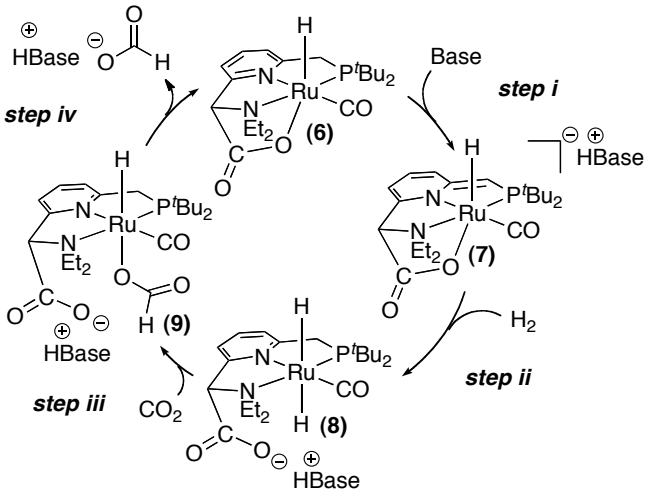

To test the first possibility (reversible formation of **2** from **6** at elevated temperatures), a $^{13}CO_2$-labeled sample of **6** was treated with 1 bar of $^{12}CO_2$ at 120 ºC. After 4 hours, >98% exchange was observed, indicating essentially complete reversibility under our standard catalysis conditions (Table 4.3, entry 1). Notably, the extent of exchange decreased sharply with temperature. At 100 ºC, <45% exchange was observed after 4 h, and minimal (3%) exchange was detected after 4 h at 70 ºC (entries 2–3). To probe the relevance of this reversibility to CO_2 hydrogenation catalysis, the **6**-catalyzed hydrogenation of CO_2 to formate at 70 ºC was examined (slow exchange conditions). As shown in Table 4.2, entry 3, less than 5 turnovers were observed after 4 hours. In contrast, **2** and **5** provided 3.4 x 10^2 and 4.3 x 10^2 turnovers under these conditions at 70 ºC (entries 4–5). The efficiency of **6** as a catalyst for hydrogenation at higher temperatures (fast exchange conditions), but not at lower temperatures (slow exchange conditions), suggests that the reversible binding of CO_2 is likely relevant to catalysis by **6** at elevated temperatures.

Table 4.3. Quantification of Reversible Binding of CO_2 at **6-^{13}C** at Varied Temperatures

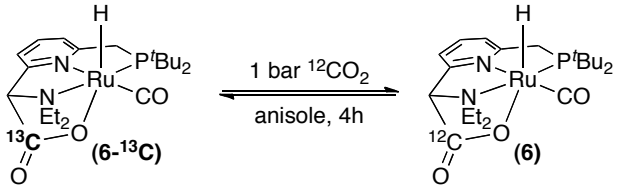

Entry[a]	Temp (ºC)	%6-^{13}C Remaining
1	120	<5
2	100	54
3	70	97

[a] Conditions: CO_2 (1 bar), **6-^{13}C** (1.8 mg, 3.63 μmol), anisole (0.45 mL), 4 h.

Importantly, the reversible formation of **2** from **6** under the conditions for catalysis does not rule out the possibility of direct CO_2 hydrogenation at **6** (catalytic cycle shown in Scheme 4.6). To explore this latter possibility, we first examined the stoichiometric reaction of **6** with 1 equivalent of KO^{t}Bu in dimethylsulfoxide (DMSO) at 25 ºC. After 5 min, a color change from yellow to bright orange was observed, accompanied by the complete conversion of **6** to a new Ru–H species, **7** (Scheme 4.7). This complex proved challenging to isolate in high purity,[20] as it is extremely moisture sensitive; however, an *in situ*-generated sample of **7** was fully characterized by ^{1}H and ^{13}C NMR spectroscopy.

Scheme 4.7. Formation of Anionic Ru Complex **7** by Deprotonation of **6**

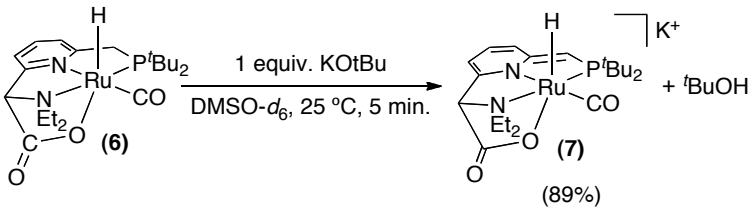

To probe whether **7** can participate in steps ii and iii of the catalytic cycle proposed in Scheme 4.6, a sample of **7**[20] was heated in DMSO-d_6 in the presence of 1 bar of a 4 : 1 mixture of H_2 : CO_2 at 120 ºC for 1 hour in the absence of exogenous base (Scheme 4.8). Under these conditions, 15% yield of HCOOK was detected.[21] This result

suggests that the **6**-catalyzed hydrogenation of CO_2 (Scheme 4.6) is a potentially viable route to formate, albeit a likely minor pathway relative to that depicted in Scheme 4.3.

Scheme 4.8. Reaction of **7** with CO_2 and H_2

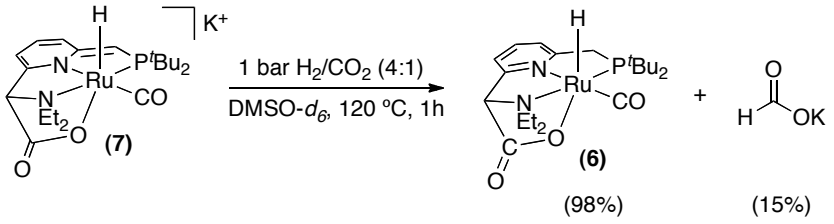

4.3 Second-Generation Cascade System: Amide Intermediate Pathway

4.3.1 Introduction

As discussed above, complex **2** is an effective catalyst for CO_2 hydrogenation to formate salt (Table 4.1)— an analogous reaction to step i (CO_2 conversion to free formic acid) in the cascade system for CO_2 conversion to CH_3OH (Scheme 4.1). Importantly, this finding could allow for complex **2** to serve as a single catalyst for both steps i and iii of the cascade system, thus reducing the total Ru catalyst loading required. However, a significant challenge toward accomplishing this goal is that the cascade system operates under Lewis acidic conditions (use of $Sc(OTf)_3$ for step ii), whereas stoichiometric base is required for **2**-catalyzed CO_2 hydrogenation (Table 4.1). In order to merge these two sets of reaction conditions, a modified cascade system that operates under basic conditions was developed.

In this second-generation cascade system, shown in Scheme 4.9, step i is the same as in the first-generation system (Scheme 4.1), where CO_2 is converted to FA. However, instead of being coupled with a Lewis-acid catalyzed esterification reaction, an amidation reaction is instead implemented. Using the Brønsted base dimethylamine ($NHMe_2$) provides *N*,*N*-dimethylformamide (DMF) as a cascade intermediate in step ii, which is hydrogenated to CH_3OH and $NHMe_2$ in the final step. Importantly, there is literature precedent for performing step ii in high yields without a catalyst.[22] Furthermore, under basic conditions, a single catalyst (i.e. complex **2**) could be used for both steps i and iii.

Scheme 4.9. Second-Generation Cascade System for CO_2 Hydrogenation to CH_3OH via an Amide Intermediate

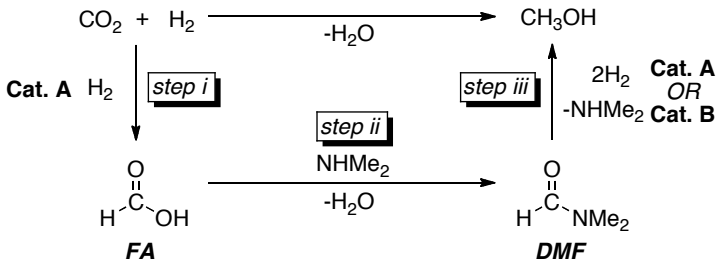

4.3.2 Step iii: DMF Hydrogenation

The overall objective in achieving the second-generation cascade system is to identify a single catalyst for both steps i and iii; therefore, catalyst activity for the more challenging step, hydrogenation of DMF, was first investigated. Following these studies, successful catalysts were then evaluated for CO_2 hydrogenation. In contrast to the many reported CO_2 hydrogenation catalysts,[4] analogous complexes for catalytic amide hydrogenation have remained elusive until recently.[23,24,25]

Complexes shown in Figure 4.2 include reported catalysts for the hydrogenation of carboxylic acid derivatives and carbamates to alcohols. Among these, **10**[23,26] and **12**[24] have been demonstrated as amide hydrogenation catalysts, whereas **2**[3b] and **11**[27] have been employed for ester hydrogenation catalysis. Amides, compared with esters, have a less electrophilic carbonyl carbon, and are thus generally a more challenging substrate to reduce;[28] however, since **2** and **11** are both highly effective ester hydrogenation catalysts (TON > 4000), they were still selected for initial evaluation.

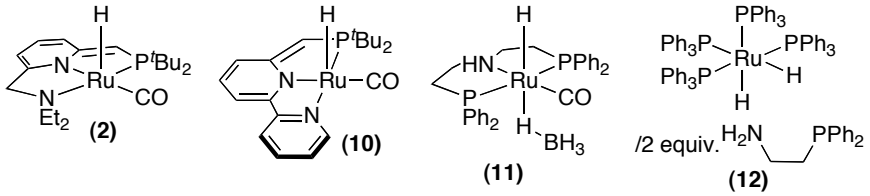

Figure 4.2. Reported Catalysts for Hydrogenation of Carboxylic Acid Derivatives to Alcohols

As shown in Table 4.4, known amide hydrogenation catalyst, **10**, as well as reported ester hydrogenation catalysts **2** and **11,** are all highly active catalysts for the

hydrogenation of DMF to CH_3OH (entries 1–3). Full conversion was achieved (or nearly 100 TONs) at 135 ºC at 50 bar H_2 after 19 hours. However, catalyst **12**, which was originally reported for hydrogenation of secondary and tertiary alkyl amides,[24] yielded low activity for this tertiary formamide (entry 4).[29]

Table 4.4. DMF Hydrogenation to CH_3OH

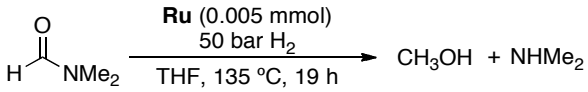

Entry[a]	Catalyst	Conv. of DMF	Yield of CH_3OH
1	**2**	>99%	>99%
2	**10**	>99%	>99%
3	**11**	>99%	>99%
4	**12**	<5%	<5%

[a] Conditions: DMF (0.5 mmol, 1 equiv.), H_2 (50 bar); Ru catalyst **2**, **10**, **11**, or **12** (0.005 mmol, 1 mol%), THF (1 mL), 19 h.

4.3.3 Hydrogenation of DMF in the Presence of CO_2

CO_2, a component of the cascade system (Scheme 4.9), was previously demonstrated to inhibit **2**-catalyzed ester hydrogenation.[1] Based on this finding, the effect of CO_2 on the hydrogenation of DMF was evaluated. Using 50 bar H_2 and just 1 bar CO_2, complex **2** provided <5% CH_3OH (Table 4.5, entry 1). However, complexes **10** and **11** provided higher yields of CH_3OH ranging from 20–40% yield (entries 2–3). Interestingly, complexes **2** and **10** are similar in structure with a difference of just eight wavenumbers for carbonyl stretch values for each complex (**2**: ν_{CO} = 1899 cm^{-1}; **10**: ν_{CO} = 1907 cm^{-1}) , but provided strikingly varied catalytic activity for this reaction. Furthermore, the yield of CH_3OH could be increased to 65% by addition of an alkali metal base, K_2CO_3 (Table 4.5, entry 4). Therefore, a closer examination of the origin of the difference in reactivity between **2** and **10**, as well as the effect K_2CO_3 has on CO_2 hydrogenation conditions, was considered.

Table 4.5. DMF Hydrogenation to CH_3OH in the Presence of CO_2

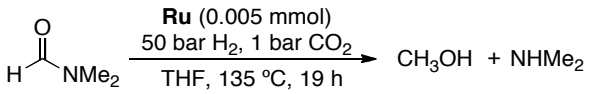

Entry[a]	Catalyst	Modified Conditions	Conv. of DMF	Yield of CH_3OH
1	**2**	--	<5%	<5%
2	**10**	--	60%	40%
3	**11**	--	30%	20%
4[b]	**10**	K_2CO_3	75%	65%

[a] Conditions: DMF (0.5 mmol, 1 equiv.), H_2 (50 bar), CO_2 (1 bar); Ru catalyst **2**, **10**, or **11** (0.005 mmol, 1 mol%), THF (1 mL), 19 h; [b] K_2CO_3 (0.5 mmol, 1 equiv.) added.

As mentioned previously in Chapter 3, treatment of **2** with 1 bar of a mixture of CO_2 and H_2 at 120 ºC for 15 minutes affords the Ru-CO_2 adduct **6** as the major product. Importantly, analogous to the cascade system via an ester intermediate, the formation of **6** could be responsible for low turnovers in the **2**-catalyzed hydrogenation of DMF (Table 4.5, entry 8). In contrast to the reaction with **2**, a similar experiment with **10** did not lead to a CO_2-catalyst adduct. Upon adding 1 bar of a mixture of CO_2 and H_2 to a solution of **10** in toluene-d_8, an initial ^{1}H NMR spectrum was acquired at room temperature revealing consumption of starting material, which has a diagnostic Ru-H doublet at –25.79 ppm, and the appearance of two new Ru-H species (Ru–H peaks: –15.76 ppm, br d; –16.52 ppm[30], br s), where all peaks in this spectrum were broad. The tube was then heated to 45 ºC in the NMR spectrometer, and cooled back to room temperature,[31] wherein a single Ru-H species remained with a doublet at –15.76 ppm (J_{HP} = 25.2 Hz) (Scheme 4.10a). This species was determined to be **13** (putative CO_2 hydrogenation intermediate analogous to **5**—see Scheme 4.3 for representative catalytic cycle) and its identity was confirmed through comparison with an authentic sample of **13**, prepared through treatment of **10** with formic acid (Scheme 4.10b).[32] The identity of **13** was further confirmed through conducting an HSQC 2D NMR spectroscopy experiment, which demonstrated that the singlet at 8.97 ppm is bound to a carbon with a shift at 172.58 ppm, in the range where H***C***OO is expected.

Scheme 4.10. Formation of **13** through Treatment of **13** with H_2/CO_2 or Formic Acid

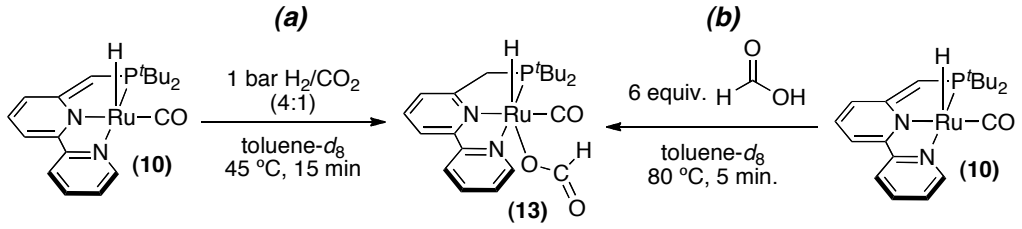

The absence of CO_2 coupling product on the *N*-side of **10** (Scheme 4.10a) can be attributed to the inability of CO_2 to bind due to the bipyridine substitution of the ligand. Most notably, the absence of CO_2 coupling with complex **10** could be the reason for higher catalyst turnover in the hydrogenation of DMF with this complex under CO_2 atmosphere in comparison with **2** (Table 4.5, entries 1 and 2). Furthermore, increased TON for the **10**-catalyzed hydrogenation of DMF in the presence of K_2CO_3 (Table 4.5, entry 4) is likely due to the base-promoted liberation of formate from complex **13** (Scheme 4.11).

Scheme 4.11. Putative Reactivity between **13** and K_2CO_3

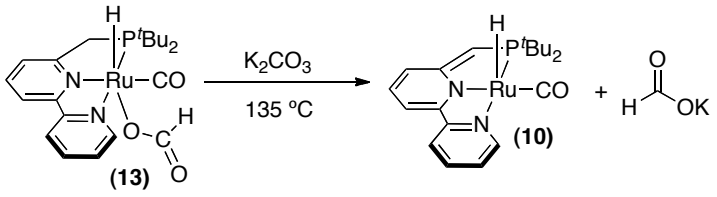

4.3.4 Step i/ii: CO_2 Conversion to DMF

Complexes previously reported for step i were first considered for the conversion of CO_2 to DMF. Complex **1** (Table 4.6) has been demonstrated to yield a TON of up to 420,000 for CO_2 conversion to DMF using $NHMe_2$ under supercritical CO_2 conditions (130 bar CO_2, 80 bar H_2).[22a] Using significantly lower pressures of 1 bar CO_2 and 50 bar H_2 with 1600 equivalents of $NHMe_2$ relative to catalyst provided a TON of 35 after 1 hour at 135 ºC (Table 4.6, entry 1). Moreover, reducing the temperature to 70 ºC resulted in an improved TON of 45 after 30 minutes and 140 after 1 hour. As the overall goal for the second-generation cascade system was to identify a single catalyst for the conversion of CO_2 to CH_3OH via an amide intermediate, catalysts efficient at DMF hydrogenation

were evaluated. As discussed above, **10** serves as an effective catalyst for conversion of DMF to CH_3OH in the presence of CO_2. Next we investigated whether complex **10** could catalyze the conversion of CO_2 to DMF, the first step of the proposed cascade (Scheme 4.9). As shown in entry 5, a TON of 90 was achieved after 1 hour at 70 ºC. Interestingly, other Ru complexes **2** and **11** (known primarily for hydrogenation of carboxylic acid derivative) also afforded DMF with a TON of 110 and 80, respectively under these optimal conditions (entries 4 and 6). These data demonstrate that under amidation conditions, CO_2 can be converted to DMF with a variety of Ru phosphine complexes.

Table 4.6. CO_2 Conversion to DMF

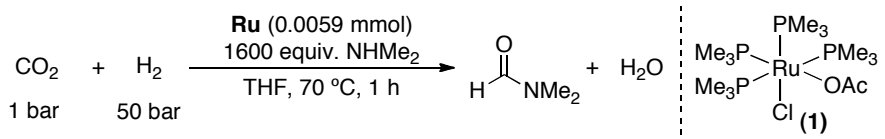

Entry[a]	Catalyst	Modified Conditions	TON DMF
1	**1**	135 ºC	35
2	**1**	30 min.	45
3	**1**	--	140
4	**2**	--	110
5	**10**	--	90
6	**11**	--	80

[a] Conditions: H_2 (50 bar), CO_2 (1 bar); Ru catalyst **1**, **2**, **10**, or **11** (0.0059 mmol), $NHMe_2$ (9.2 mmol, 1600 equiv., added as a solution in THF), 19 h.

4.3.5 Cascade Conversion of CO_2 to CH_3OH

With established conditions for steps i/ii and step iii with Ru complex **10**, all components of the system were combined. The following conditions were selected based on studies described above: 50 bar H_2, 1 bar CO_2, 1600 equivalents of $NHMe_2$, and a temperature scheme of 70 ºC for 1 hour prior to ramping the temperature to 135 ºC for 18 hours. A combination of complex **1** (serving as catalyst for step i) and **10** (serving as catalyst for step iii) yielded a TON of 100 for DMF and CH_3OH in less than a turnover (Table 4.7, entry 1). Upon adding 100 equivalents of K_2CO_3, the yield of CH_3OH was improved to TON = 24. Furthermore, removing catalyst **1** from the system and solely

using **10** for both steps i and iii yielded a TON of 15, thus satisfying the goal to identify a single catalyst for the second-generation cascade system

Table 4.7. CO_2 Hydrogenation to CH_3OH

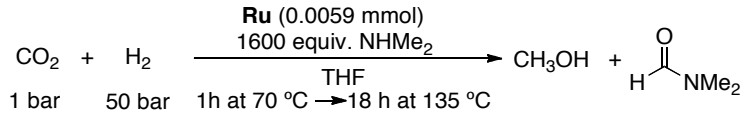

Entry[a]	Catalyst(s)	Modified Conditions	TON CH_3OH	TON DMF
1	**1 and 8**	--	<1	100
2[b]	**1 and 8**	K_2CO_3	25	65
3[b]	**8**	K_2CO_3	15	100

[a] Conditions: H_2 (50 bar), CO_2 (1 bar); Ru catalyst **1** and/or **8** (0.0059 mmol, 1 mol%), $NHMe_2$ (9.2 mmol, 1600 equiv., added as a solution in THF), 19 h. [b] K_2CO_3 (0.5 mmol, 100 equiv. relative to Ru) added.

4.4 Conclusions

In summary, Ru(PNN)(CO)(H) (**2**), a known ester hydrogenation catalyst, was demonstrated to also catalyze the hydrogenation of CO_2 to formate in the presence of a base. The transformation is proposed to proceed through a mechanism involving (i) heterolytic cleavage of H_2 at **2** to form a Ru–dihydride species, (ii) CO_2 insertion to generate a Ru–formate complex, and (iii) base-promoted release of formate. The feasibility of each of these proposed mechanistic steps has been demonstrated through stoichiometric studies of organometallic intermediates.[33]

These findings were applied to a second-generation cascade CO_2 hydrogenation to methanol system, wherein an amide intermediate was accessed. Through capitalizing on our newfound CO_2 hydrogenation conditions using a Ru pincer complex that is also capable of catalyzing amide hydrogenation, as well as employing a modified pincer ligand structure to further optimize the reaction, cascade system incompatibilities outlined in Chapters 2 and 3 were overcome. Additionally, this system demonstrated the feasibility of using a single catalyst that provides a TON of 15 for methanol using just 1 bar CO_2. Investigations are currently underway to further optimize this system.

4.5 Experimental Procedures and Characterization of Data

General Procedures

NMR spectra were obtained on a Varian VNMRs 500 MHz (500 MHz for ^{1}H; 126 MHz for ^{13}C; 202 MHz for ^{31}P) or a Varian VNMRs 700 MHz spectrometer (700 MHz for ^{1}H; 176 MHz for ^{13}C, 283 MHz for ^{31}P). Elemental analysis was carried out at Atlantic Microlab lab in Norcross, GA. IR spectra were recorded on a Perkin-Elmer Spectrum BX FT-IR spectrometer using KBr pellets. All high-pressure reactions were carried out using a Parr Model 5000 Multiple Reactor system that includes six 50 mL vessels equipped with flat-gaskets and head mounting valves. The system was operated by a 4871 process controller and SpecView version 2.5 software. Chemical shifts are reported in parts per million and are referenced to an internal standard, HMDSO (hexamethyldisiloxane; δ in anisole-d_8 = 0.11 ppm) relative to TMS. When needed, NMR assignments were performed with the help of $^{1}H/^{1}H$ COSY, $^{1}H/^{13}C$ HMQC, and $^{1}H/^{13}C$ HMBC experiments. Abbreviations used in the NMR experiments: br, broad; s, singlet; d, doublet; t, triplet; q, quartet; m, multiplet. ^{13}C NMR experiments were all proton decoupled, except for the upfield proton associated with Ru–H.

Materials and Methods

1[34], **2**,[3b] **6**,[11] **6-^{13}C**,[11] **10**,[23a] and $Ru(PPh_3)_4H_2$[35] were prepared according to the corresponding literature procedures. Carbonylchlorohydrido[bis(2-(diphenylphosphinoethyl)amino] ruthenium(II) or Ru-MACHO (**11**) and 2-(diphenylphosphino)ethylamine were purchased from Strem. Research grade carbon dioxide (99.999%), ultra high purity hydrogen (99.999%), and a mix tank of 80% H_2/20% CO_2 were purchased from Metro Welding. All experiments were conducted under an oxygen-free atmosphere in either a glovebox or on a Schlenk line. All solid bases were ground with a mortar and pestle before use. Anisole-d_8 (CDN Isotopes) was dried over sodium metal and degassed. D_2O and CD_3OD were purchased from Cambridge Isotope Laboratories and used as is. 2-Methoxyethyl ether (diglyme, Acros, 99+%), *N,N*-dimethylformamide (Alfa Aesar, 99.8%), 1,3,5-trimethoxybenzene (Acros), dimethyl sulfoxide (Aldrich, 99.9+%), KO^tBu (Alfa Aesar), 18-crown-6 (Acros), K_2CO_3

(Fisher, anhydrous powder), $KHCO_3$ (Acros), K_3PO_4 (Aldrich, 98+%), and KOH (Fisher) were used without further purification. Anisole (Aldrich) was dried over sodium metal and degassed before use, triethylamine (Acros) was dried over calcium hydride and degassed before use, HMDSO (hexamethyldisiloxane, Fluka) was dried over 4 Å sieves and degassed before use, and THF (tetrahydrofuran) was purified using an Innovative Technologies (IT) solvent purification system consisting of a copper catalyst, activated alumina, and molecular sieves. Dimethylamine (Aldrich, anhydrous >99%) and was condensed in dry THF using standard schlenk line technique to yield a 4.6 M solution. DMSO-d_6 (dimethylsulfoxide) was purchased from Cambridge Isotopes and used as is.

I. Stoichiometric and Catalytic Evaluation of 2-Catalyzed CO_2 Hydrogenation to Formate

*A. Reaction of **2** or **7** with CO_2 and H_2 (Scheme 4.4 and Scheme 4.8)*

In an N_2-atmosphere dry box, **2** or **7** (3.32 μmol), HMDSO (internal standard, 10 μL of a 0.753 M solution in anisole-d_8, 7.53 μmol), and 0.45 mL of anisole-d_8 were added to a J-young tube. An initial ^{1}H NMR spectrum was acquired in order to obtain the integral ratio of the Ru complex to HMDSO. The solution was frozen in LN_2, the N_2 atmosphere was removed, the tube was sealed while the solution thawed, and 1 bar H_2/CO_2 (4:1) was then introduced. The tube was then shaken before heating in an oil bath for the specified time and temperature (see Table 4.8 for variable temperature studies with **2**). Products **5** and **6** were detected and quantified by ^{1}H NMR spectroscopy as depicted in Figure 4.3.

Table 4.8. Reactivity of **2** with CO_2 and H_2 at Varied Temperatures

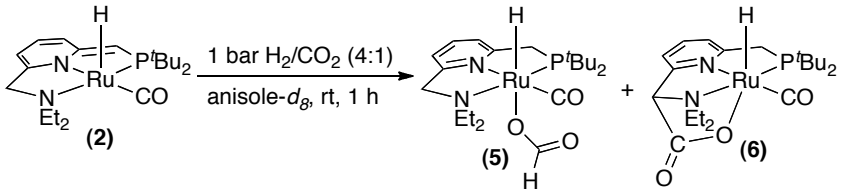

Entry	Temp (°C)	%5	%6
1[a]	25	88	13
2	70	34	64
3	120	15	75

[a] Reaction time: 24 h.

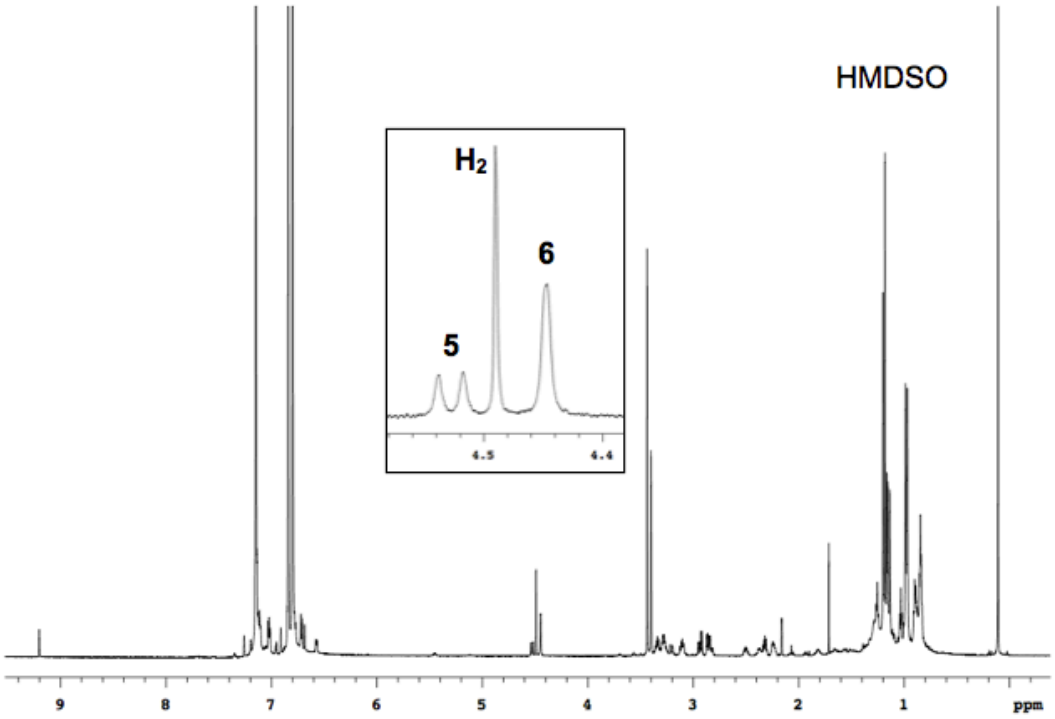

Figure 4.3. ^{1}H NMR Spectrum in Anisole-d_8 for the Quantitative Analysis of **5** & **6**

*B. Reaction of **5** with KOtBu (Scheme 4.5)*

In an N_2-atmosphere dry box, **5** (1.8 mg, 3.62 μmol), HMDSO (internal standard, 10 μL of a 0.753 M solution in anisole-d_8, 7.53 μmol), and 0.45 mL of anisole-d_8 were added to a J-young tube. An initial ^{1}H NMR spectrum was acquired in order to obtain the initial integral ratio of **5** to HMDSO. The tube was then brought back into the dry box and 1 equiv. KO^{t}Bu (0.4 mg, 3.62 μmol, 1 equiv) was added. Upon sonicating the tube for 1 min., the solution changed from pale yellow to dark red brown. A ^{1}H NMR was then acquired to determine the yield of **3** (Figure 4.4). The tube was then brought back into the dry box a second time where 1 mL of CD_3OD was added to solubilize HCOOK that was formed. The tube was then sonicated for 5 min. and a final ^{1}H NMR was acquired to determine the yield of potassium formate (Figure 4.5).

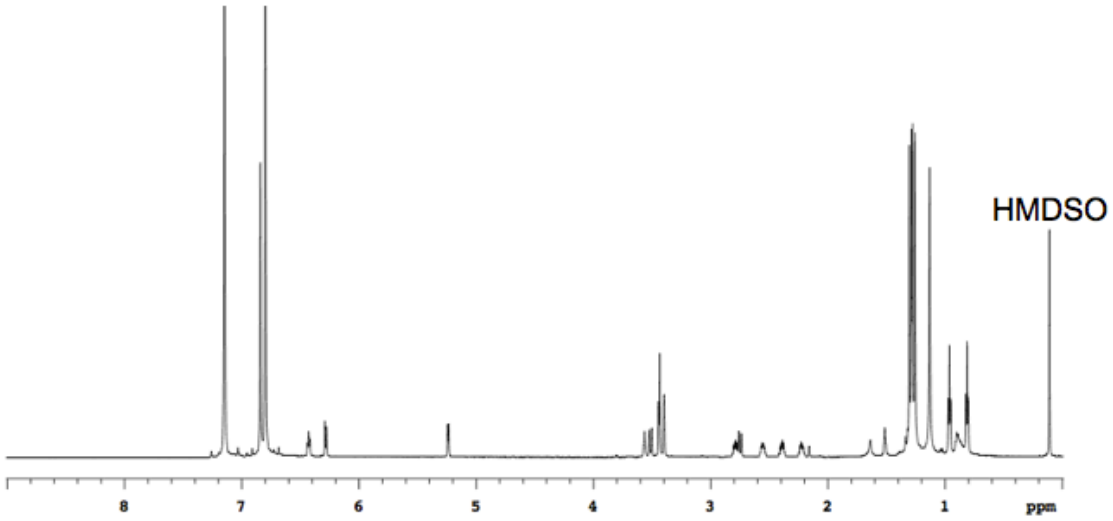

Figure 4.4. ^{1}H NMR Spectrum of **2** in Anisole-d_8 Formed after Adding KO^{t}Bu to **5**

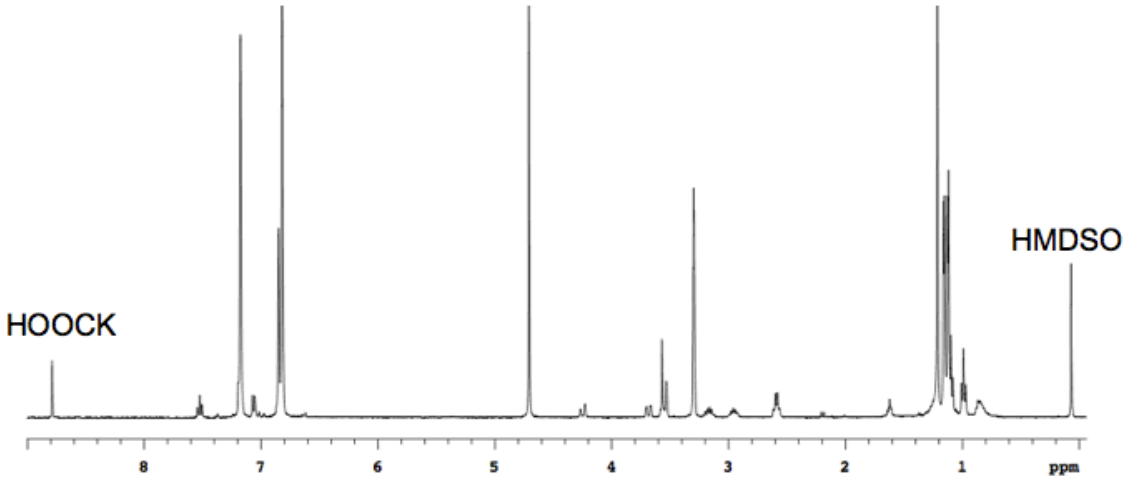

Figure 4.5. ^{1}H NMR Spectrum after Adding CD_3OD

C. Catalytic CO_2 Hydrogenation Studies (Table 4.1 and Table 4.2)

In an N_2-atmosphere dry box, Ru catalyst (0.25 mL of a 2.2 µM solution, 0.554 µmol) was added to a 30 mL glass liner containing base (0.664 mmol, 1200 equiv) and a Teflon octagon magnetic stirbar (5/16 x 1/2 in.). An additional 1.75 mL of solvent was then added to the liner. Before inserting the liner into the well of the pressure vessel, 1.2 mL of solvent was added to the well of the pressure vessel. The vessel was then sealed and removed from the dry box where it was then pressurized with 10 bar CO_2 followed immediately by 30 bar H_2. The reaction was then heated at 120 ºC (using Specview

software, initial set temperature = 90 ºC; this was done to prevent over-shooting the desired temperature) for 4 hours at a stir rate of 800 RPM, and was then allowed to cool to room temperature before venting to atmospheric pressure. The volatiles inside the glass liner were then removed under high vacuum, and 2 mL of D_2O, 50 µL of 12 M HCl, and DMF (internal standard, 40 uL, 0.519 mmol) were added sequentially to the residue. The solution was then analyzed by ^{1}H NMR spectroscopy (see Figure 4.6 for a sample spectrum, and Figure 4.7**Figure 4.8**–Figure 4.9 for time studies using catalysts **2**, **5**, and **6**). All data points are based off 3–5 trials per data point.

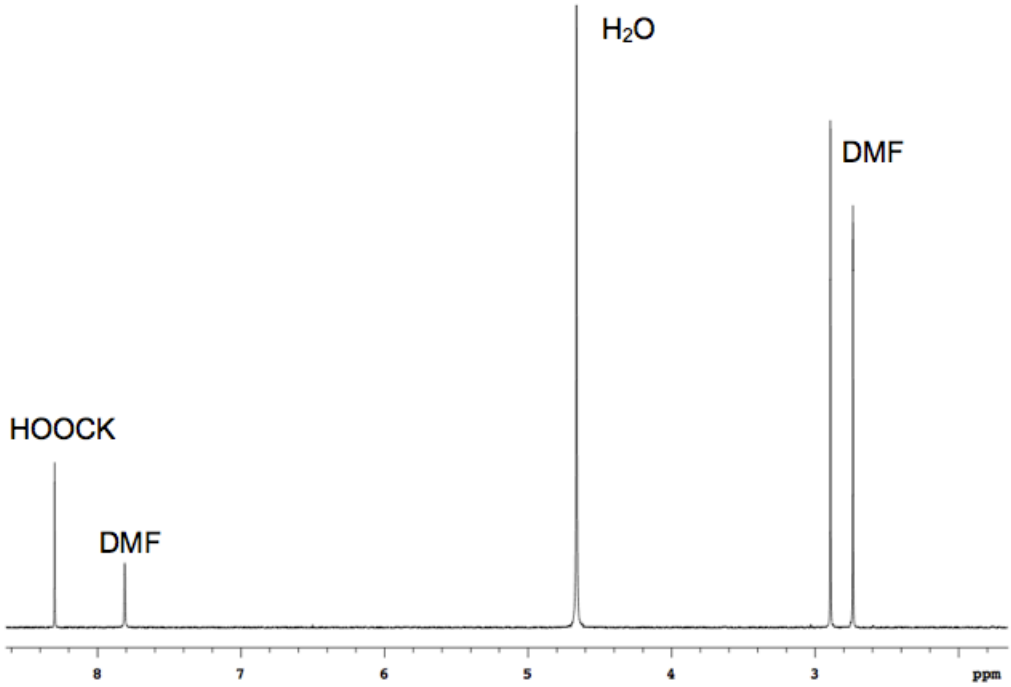

Figure 4.6. ^{1}H NMR Spectrum for Quantitative Analysis of Formate from High Pressure Reactions

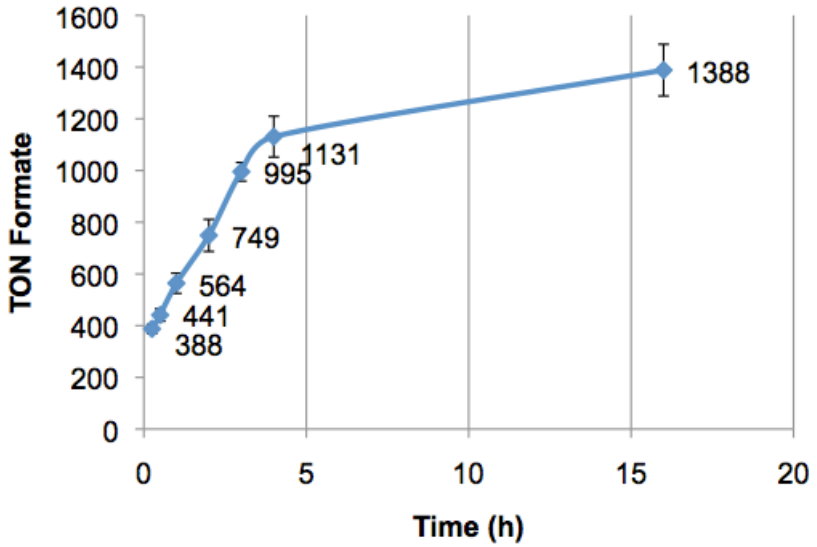

Figure 4.7. Evaluation of Catalytic Activity of **2** for CO_2 Hydrogenation to Formate over Time. Conditions: CO_2 (10 bar), H_2 (30 bar), 0.554 µmol **2**, 0.6648 mmol K_2CO_3 (1200 equiv), 2 mL diglyme, 120 ºC.

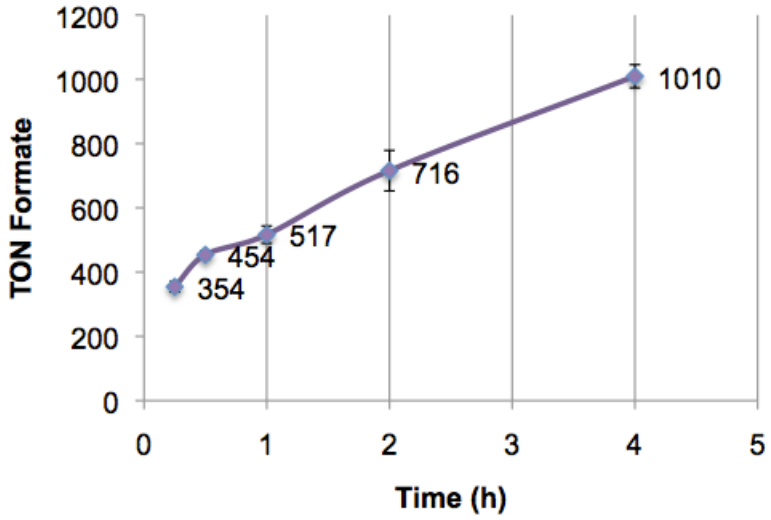

Figure 4.8. Evaluation of Catalytic Activity of **5** for CO_2 Hydrogenation to Formate over Time. Conditions: CO_2 (10 bar), H_2 (30 bar), 0.554 µmol **5**, 0.6648 mmol K_2CO_3 (1200 equiv), 2 mL diglyme, 120 ºC.

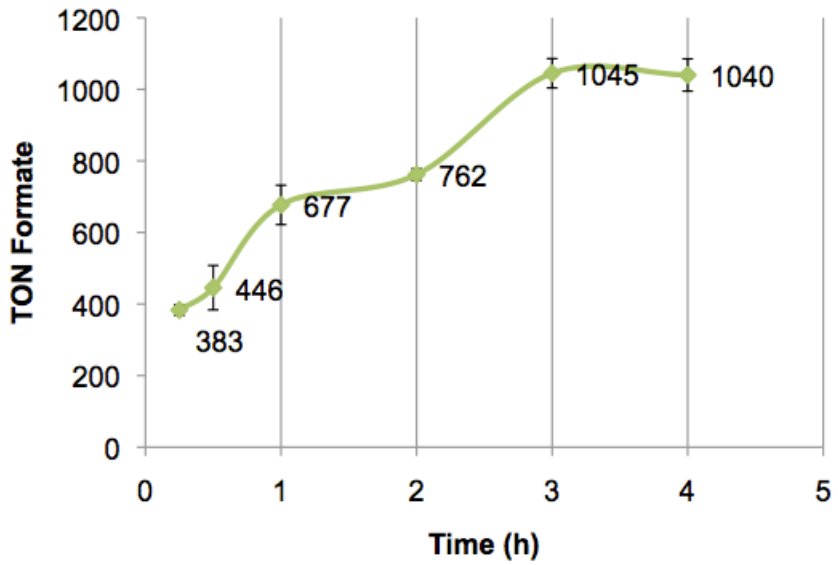

Figure 4.9. Evaluation of Catalytic Activity of **6** for CO_2 Hydrogenation to Formate over Time . Conditions: CO_2 (10 bar), H_2 (30 bar), 0.554 µmol **6**, 0.6648 mmol K_2CO_3 (1200 equiv), 2 mL diglyme, 120 ºC.

D. Procedure for Reversibility Studies of ***6-^{13}C*** *with CO_2 (Table 4.3)*

In an N_2-atmosphere dry box, **6-^{13}C** (1.8 mg, 3.63 µmol) and 0.45 mL of anisole were added to a J-young tube. A ^{13}C NMR spectrum was acquired in order to obtain the initial integral ratio of **6-^{13}C** to anisole. The solution was then frozen in LN_2, the N_2 atmosphere was removed, the tube was sealed while the solution thawed, and 1 bar CO_2 was introduced. The tube was then shaken before heating in an oil bath for 4 hours at the specified temperature (Figure 4.5). A final ^{13}C NMR spectrum was acquired and the amount of $^{13}CO_2$ that exchanged for CO_2 was measured by comparing the initial ratio of **6-^{13}C** : anisole to the final ratio (see Figure 4.10 for an example spectrum).

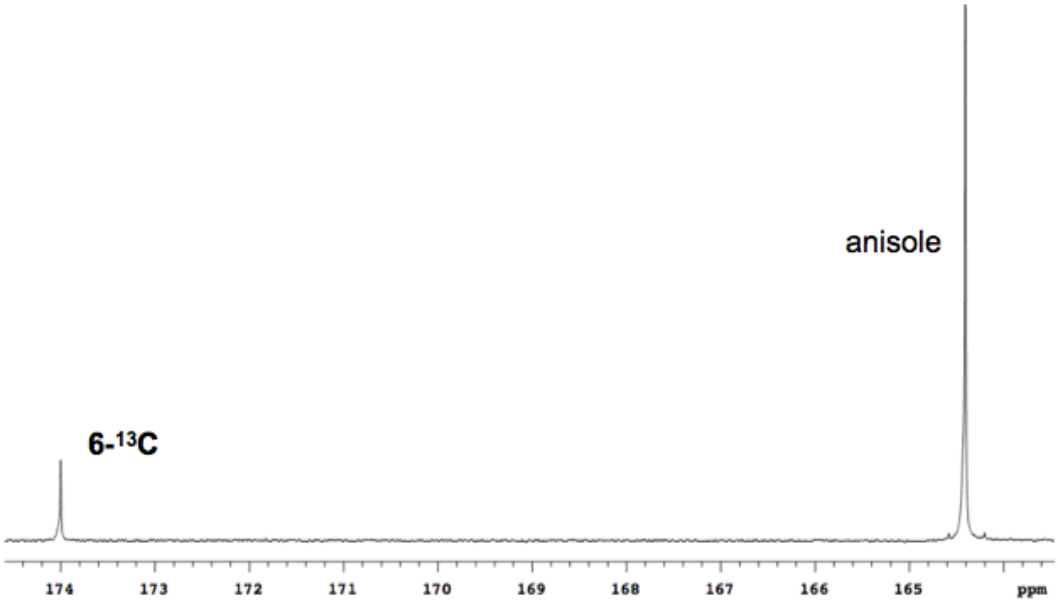

Figure 4.10. ^{13}C NMR for Quantitative Analysis of CO_2 Scrambling at **6-^{13}C**. ^{13}C NMR parameters: decoupled without NOE, 3 second acquisition time, 0.1 second relaxation delay, 100 scans.

II. Synthesis and Characterization of 5 and 7

*A. Synthesis and Characterization of Complex **5***

In an N_2-atmosphere dry box, (PNN)RuH(CO) (**2**, 20 mg, 0.044 mmol) was dissolved in 2 mL THF and added to a 4 mL scintillation vial. Upon the addition of formic acid (50 μL of a 1.1 M solution in THF, 0.053 mmol), there was an immediate color change from a dark red/brown solution to a pale yellow suspension. The suspension was then filtered on a glass frit, the residue was triterated and sonicated with pentanes (5 mL x 2), and finally dried in vacuo to afford **5** as a pale yellow powder (22 mg, 95% yield). X-ray quality crystals (yellow needles) were formed at room temperature by dissolving 5 in a minimal amount of CH_2Cl_2 and layering this solution with benzene (see Table 4.9 for details).

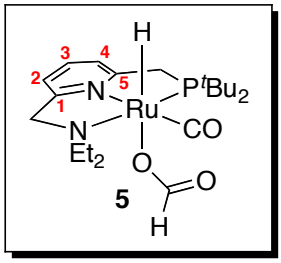

$^{31}P\{^1H\}$ NMR (CD_2Cl_2): δ 109.4 (s).

^1H NMR (CD_2Cl_2): δ -16.53 (d, J_{HP} = 27.8 Hz, 1H, Ru-*H*), 1.10 (t, J_{HH} = 7.3 Hz, 3H, NCH_2CH_3), 1.15 (t, J_{HH} = 6.9 Hz, 3H, NCH_2CH_3), 1.18 (d, J_{HP} = 13.2 Hz, 9H, $PC(CH_3)_3$), 1.29 (d, J_{HP} = 13.3 Hz, 9H, $PC(CH_3)_3$), 2.75 (q, J_{HH} = 5.4 Hz, 2H, NCH_2CH_3), 3.11 (dq, J_{HH} = 7.0 Hz, J_{HH} = 11.7 Hz, 1H, $NCHHCH_3$), 2.84 (dd, J_{HH} = 16.9 Hz, J_{PH} = 8.4 Hz, 1H, CHHP), 3.27 (dq, J_{HH} = 7.0 Hz, J_{HH} = 11.7 Hz, 1H, $NCHHCH_3$), 3.51 (dd, J_{HH} = 16.9 Hz, J_{HP} = 9.9 Hz, 1H, CHHP), 3.76 (dd, J_{HH} = 14.5 Hz, J_{HP} = 2.6 Hz, 1H, NCHHC), 4.59 (d, J_{HH} = 14.5 Hz, 1H, NCHHC), 7.20 (d, J_{HH} = 7.6 Hz, 1H, Py-*H2*), 7.35 (d, J_{HH} = 7.7 Hz, 1H, Py-*H4*), 7.67 (t, J_{HH} = 7.7 Hz, 1H, Py-*H3*), 8.69 (s, 1H, *H*COO).

$^{13}C\{^1H\}$ NMR (CD_2Cl_2): δ 8.34 (s, NCH_2CH_3), 11.29 (s, NCH_2CH_3), 29.15 (d, J_{CP} = 4.3 Hz, $PC(CH_3)_3$), 30.28 (d, J_{CP} = 2.9 Hz, $PC(CH_3)_3$), 35.20 (d, J_{CP} = 24.5 Hz, $PC(CH_3)_3$), 37.16 (d, J_{CP} = 12.7 Hz, $PC(CH_3)_3$), 37.70 (d, J_{CP} = 20.6 Hz, CH_2P), 50.24 (s, NCH_2CH_3), 54.18 (s, NCH_2CH_3), 64.58 (s, CH_2N), 119.94 (s, *C2*), 120.82 (d, J_{CP} = 9.4 Hz, *C4*), 137.71 (s, *C3*), 160.71 (d, J_{CP} = 2.0 Hz, C1), 161.98 (d, J_{CP} = 4.6 Hz, *C5*), 170.56 (s, H*C*OO), 208.65 (dd, $J_{PC/HC}$ = 6.9 Hz, $J_{PC/HC}$ = 14.5 Hz Ru-*C*O).

IR (KBr pellet, cm^{-1}): 2021 (ν (Ru-H)), 1900 (ν(CO)), 1610 (ν (HCOO)).

Anal. Calcd. for $C_{21}H_{38}N_2O_3PRu$•0.25 C_4H_8O (*Note ^1H NMR shows 0.25 equiv THF per equiv* ***5***): C, 51.15; H, 7.80; N, 5.42. Found: C, 51.55, H, 7.51; N, 5.12.

^{31}P NMR Spectrum of 5 (CD_2Cl_2)

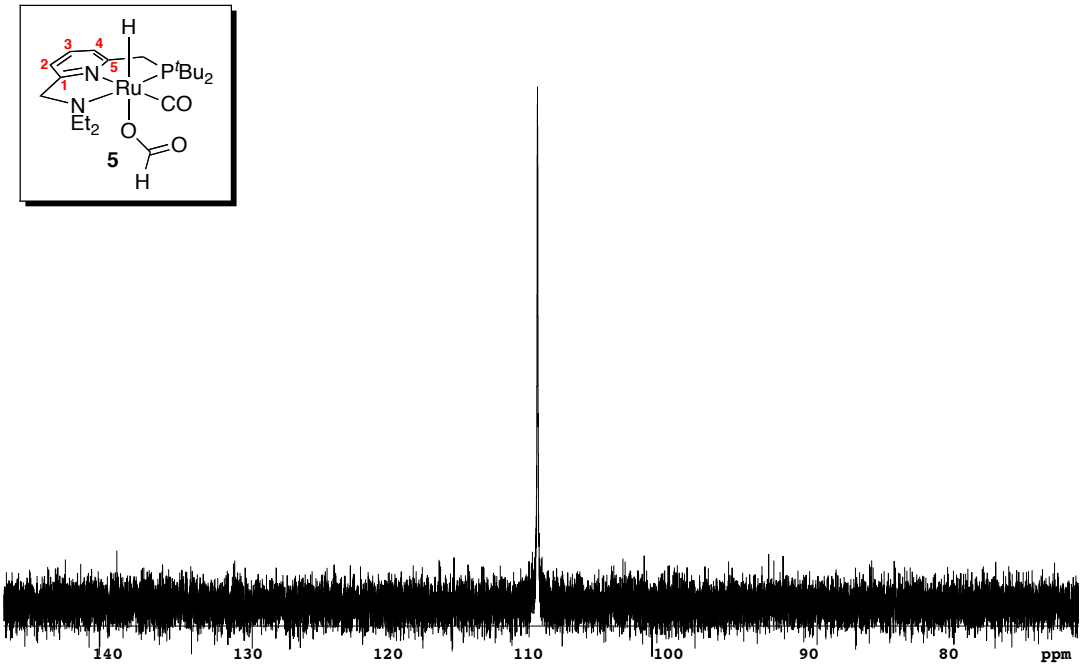

^{1}H NMR Spectrum of 5 (CD_2Cl_2)

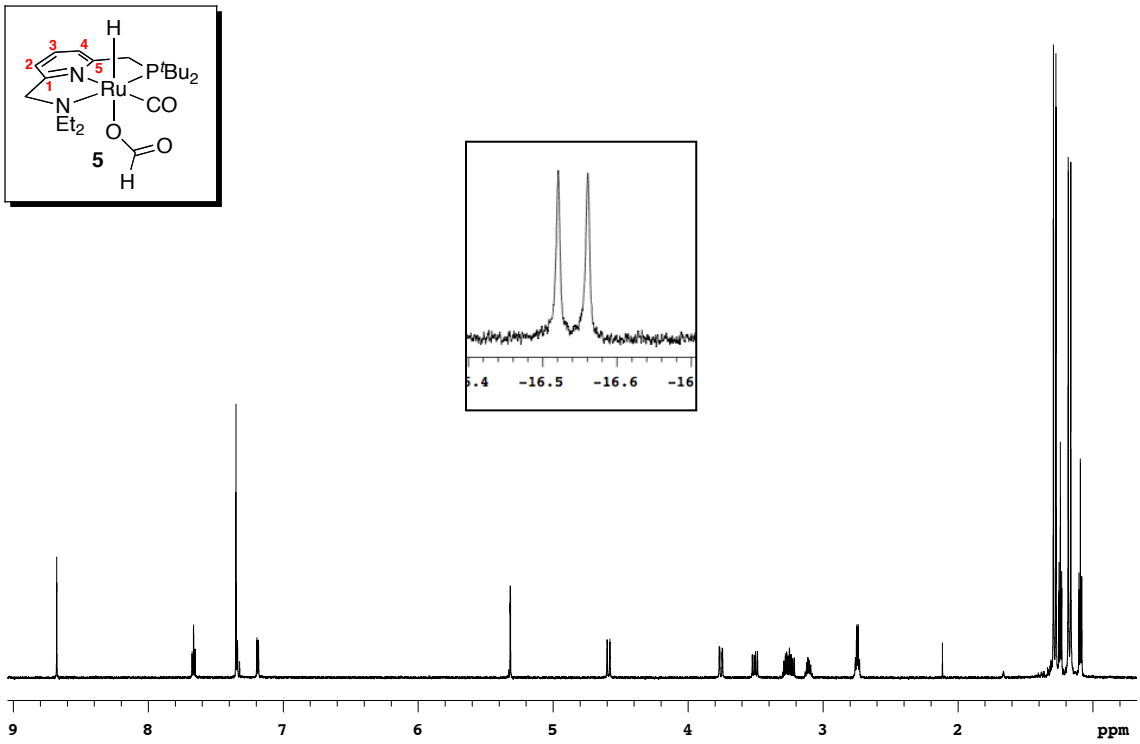

^{13}C NMR Spectrum of 5 (CD_2Cl_2)

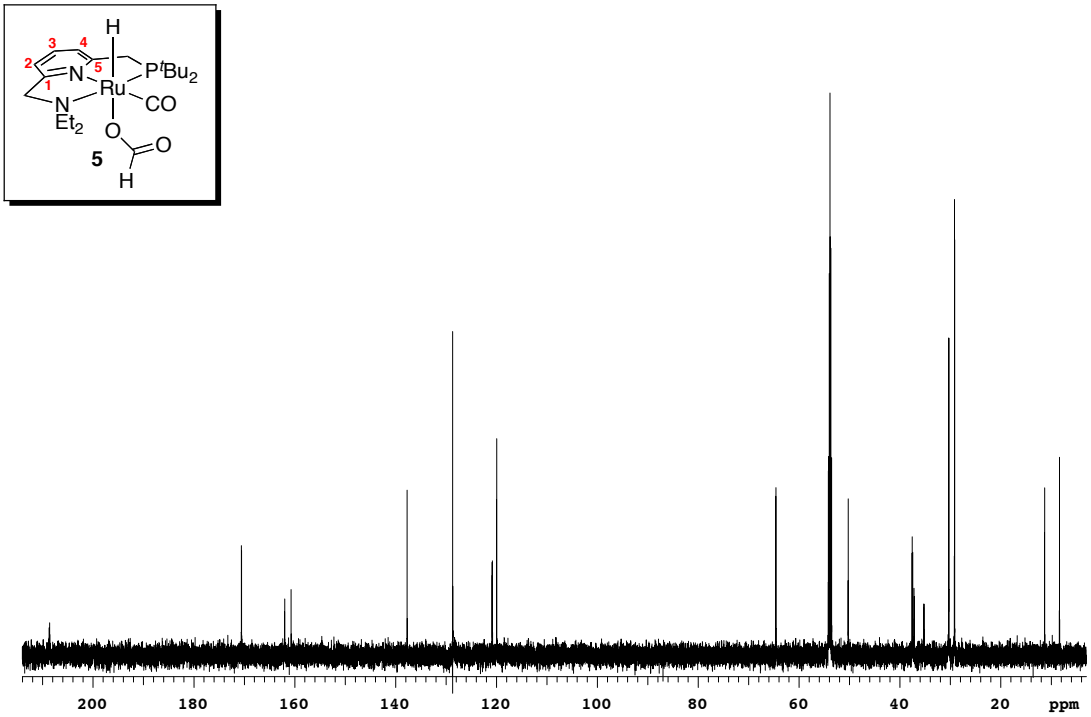

^{1}H-^{1}H gCOSY Spectrum of 5 (CD_2Cl_2)

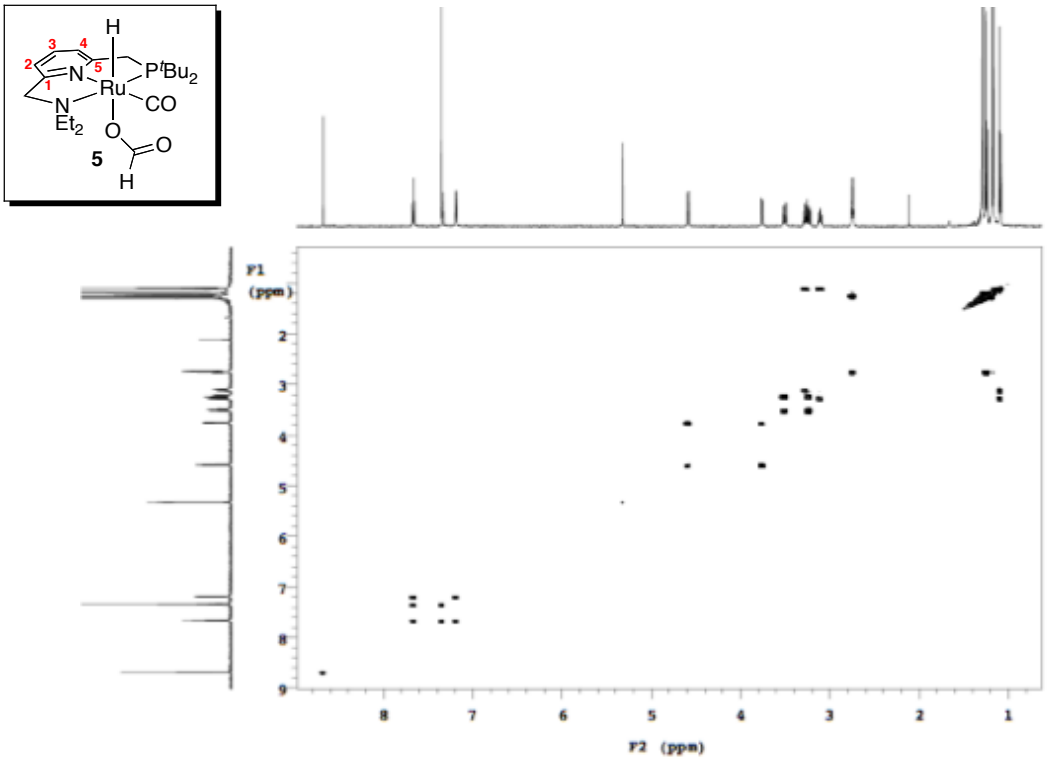

^{1}H-^{13}C gHSQC Spectrum of 5 (CD_2Cl_2)

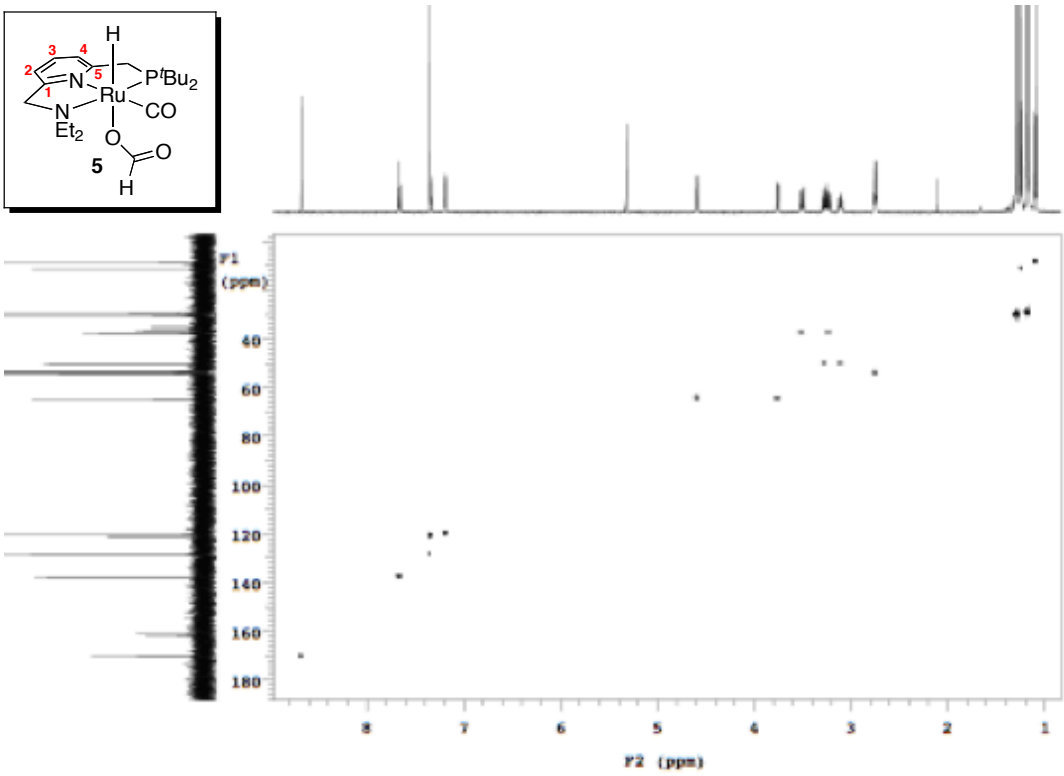

^{1}H-^{13}C gHMBC Spectrum of 5 (CD_2Cl_2)

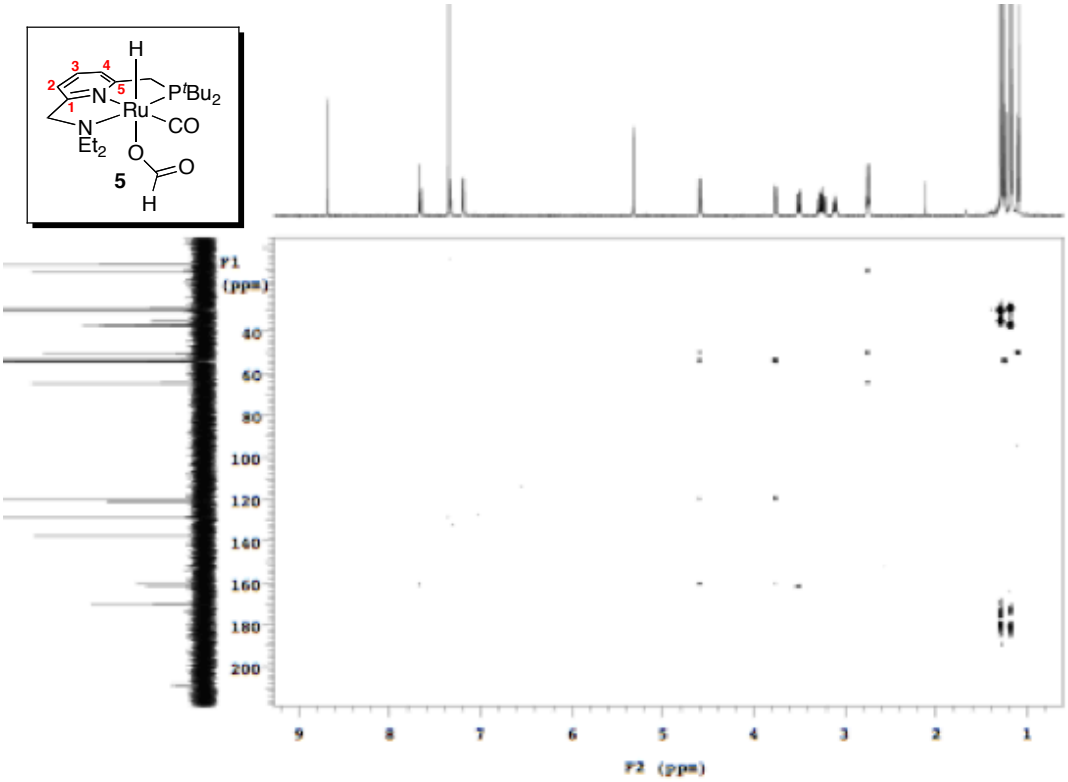

B. X-ray Structure Determination for ***5***

Yellow needles of **5** were grown from a dichloromethane/benzene solution of the compound at 22 ºC. The crystal was mounted on a Rigaku AFC10K Saturn 944+ CCD-based X-ray diffractometer equipped with a low temperature device and Micromax-007HF Cu-target micro-focus rotating anode (l = 1.54187 A) operated at 1.2 kW power (40 kV, 30 mA). The X-ray intensities were measured with the detector placed at a distance 42.00 mm from the crystal. The exposure time was 1 s for the low angle images and 4 s for high angle. The integration of the data yielded a total of 33673 reflections to a maximum 2q value of 136.48°, of which 4619 were independent and 4570 were greater than 2s(I). The final cell constants (Table 4.9) were based on the xyz centroids of 22271 reflections above 10s(I). Analysis of the data showed negligible decay during data collection; the data were processed with CrystalClear 2.0 and corrected for absorption. The structure was solved and refined with the Bruker SHELXTL (version 2008/4) software package.

Table 4.9. Crystal Data and Structure Refinement for **5**

Empirical formula	$C_{21}H_{37}N_2O_3PRu(C_6H_6)_{0.5}$
Formula weight	536.62
Temperature	85(2) K
Wavelength	1.54178 Å
Crystal system	Monoclinic
Space group	C 2/c
Unit cell dimensions	a = 32.0382(6) Å, a = 90º b = 11.1091(2) Å, b = 118.402º c = 16.1622(11) Å, g = 90º
Volume	5060.0(4) $Å^3$
Z	8
Calculated density	1.409 mg/mm^3
Absorption coefficient	5.822 mm^{-1}
F(000)	2248

Crystal size	0.16 x 0.16 x 0.02 mm^3
Theta range for data collection	3.14 to 68.24º
Limiting indices	$-38 \leq h \leq 38$, $-13 \leq k \leq 13$, $-19 \leq l \leq 19$
Reflections collected	33673
Independent reflections	4619 [R(int) = 0.0513]
Completeness to theta	68.24 (99.8 %)
Absorption correction	Semi-empirical from equivalents
Max. and min. transmission	0.891 and 0.552
Refinement method	Full-matrix least-squares on F^2
Data / restraints / parameters	4619 / 53 / 316
Goodness-of-fit on F^2	1.041
Final R indices [I>2s(I)]	R_1 = 0.0283, wR_2 = 0.0757
R indices (all data)	R_1 = 0.0286, wR_2 = 0.0759
Largest diff. peak and hole	0.647 and -0.900 e A^{-3}

C. Synthesis and Characterization of Complex 7

In an N_2-atmosphere dry box, RuH(PNN-CO_2)(CO) (**6**, 40 mg, 0.08 mmol) was dissolved in 0.5 mL DMSO and added to a 4 mL schlenk tube equipped with a Teflon stir bar. Upon the addition of KO^{t}Bu (9 mg, 0.08 mmol, 1 equiv), there was an immediate color change from pale yellow to bright orange. The reaction was allowed to stir for 5 min. at room temperature before the volatiles were removed in vacuo and the residue was triterated with benzene (2 x 1 mL) to afford **7** as a bright orange powder (44 mg, 89% yield, 1.6 equiv DMSO per molecule of **7**).

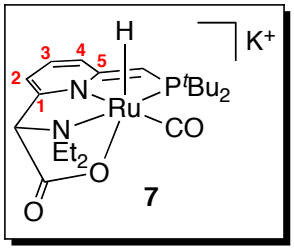

$^{31}P\{^{1}H\}$ NMR (DMSO-d_6): d 105.58 (s).

^{1}H NMR (DMSO-d_6): d -18.24 (d, J_{HP} = 31.2 Hz, 1H, Ru-***H***), 0.95 (t, J_{HH} = 7.2 Hz, 3H, $N(CH_2C\boldsymbol{H}_3)$, 1.15 (t, J_{HH} = 7.2 Hz, 3H, $NCH_2C\boldsymbol{H}_3$), 1.10 (d, J_{HP} = 12.3 Hz, 9H, $PC(C\boldsymbol{H}_3)_3$), 1.16 (d, J_{HP} = 12.6 Hz, 9H, $PC(C\boldsymbol{H}_3)_3$), 2.57 (dq, *overlapping with DMSO*, 1H, $NC\boldsymbol{H}HCH_3$), 2.62 (dq, J_{HH} = 13.5 Hz, J_{HH} = 6.5 Hz, 1H, $NC\boldsymbol{H}HCH_3$), 2.81 (dq, J_{HH} = 12.9 Hz, J_{HH} = 6.7 Hz, 1H, $NC\boldsymbol{H}HCH_3$), 3.00 (dq, J_{HH} = 14.5 Hz, J_{HH} = 7.0 Hz, 1H, $NC\boldsymbol{H}HCH_3$), 3.08 (d, J_{HP} = 1.9 Hz, 1H, C***H***P/CDP*), 3.65 (br s, 1H, $NC\boldsymbol{H}CO_2$), 5.40 (d, J_{HH} = 6.3 Hz, 1H, Py-***H2***), 5.89 (d, J_{HH} = 8.9 Hz, 1H, Py-***H4***), 6.34 (t, J_{HH} = 6.3 Hz, 1H, Py-***H3***).

$^{13}C\{^{1}H\}$NMR (DMSO-d_6): d 9.27 (s, $NCH_2\boldsymbol{C}H_3$), 9.62 (s, $NCH_2\boldsymbol{C}H_3$), 29.68 (d, J_{CP} = 5.6 Hz, $PC(\boldsymbol{C}H_3)_3$), 30.33 (d, J_{CP} = 2.9 Hz, $PC(\boldsymbol{C}H_3)_3$), 34.20 (d, J_{CP} = 32.9 Hz, $P\boldsymbol{C}(CH_3)_3$), 37.73 (d, J_{CP} = 13.6 Hz, $P\boldsymbol{C}(CH_3)_3$), 46.33 (s, $N\boldsymbol{C}H_2CH_3$), 47.20 (s, $N\boldsymbol{C}H_2CH_3$), 62.51 (m, ***C***HP/CDP*), 78.27 (s, ***C***$HNCO_2$), 96.38 (s, ***C2***), 109.85 (d, J_{CP} = 16.1 Hz, ***C4***), 130.82 (s, ***C3***), 153.60 (d, J_{CP} = 1.8 Hz, ***C1***), 165.83 (d, J_{CP} = 16.7 Hz, ***C5***), 171.94 (s, ***C***O_2), 209.08 (d, J_{CP} = 14.7 Hz, Ru-CO).

*Note: The C***H***P H is exchanging with D from DMSO-d_6 (full conversion of CHP to CDP in 2 hours at room temperature). This results in a lower peak intensity for C***H***P in the ^{1}H NMR spectrum, a multiplet for ***C***HP/***C***DP in the ^{13}C NMR spectrum, and reduced or no cross peak for correlations involving C***H***P in the 2D spectra. Scrambled DMSO can also be seen in the spectra.

^{31}P NMR Spectrum of 7 in DMSO-d_6

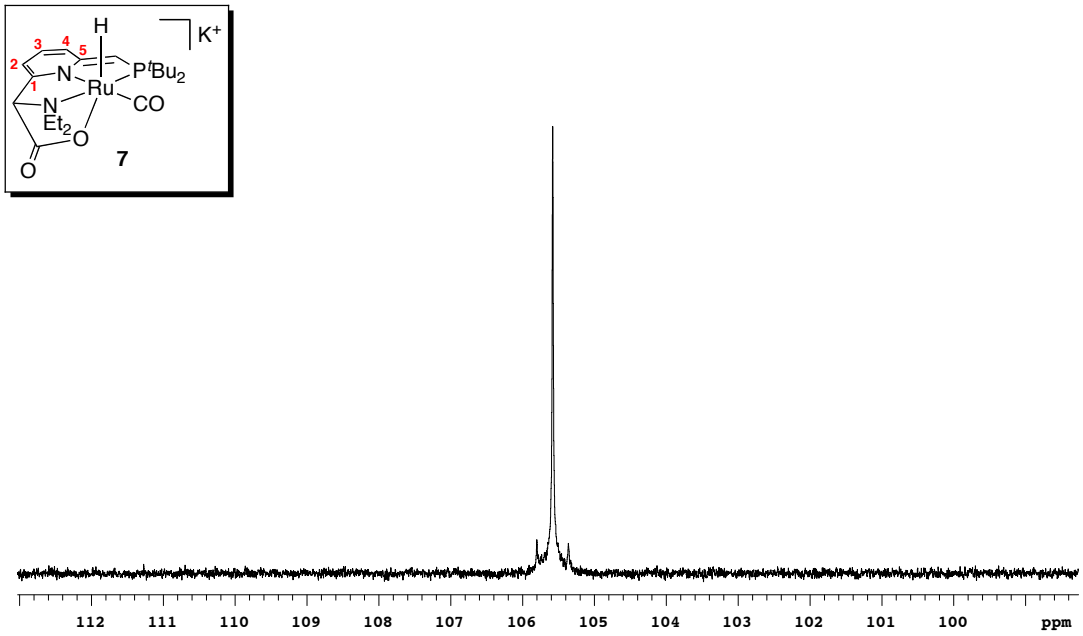

^{1}H NMR Spectrum of 7 in DMSO-d_6

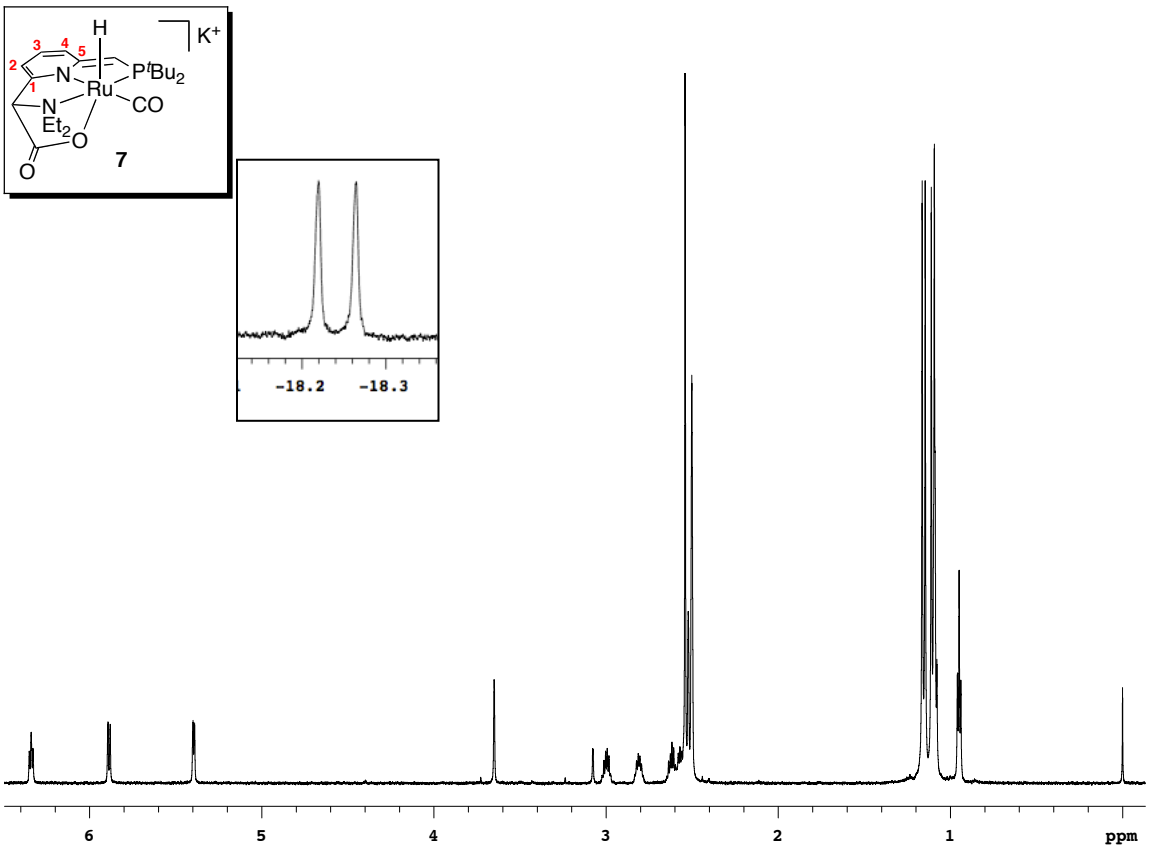

^{13}C NMR Spectrum of 7 in DMSO-d_6

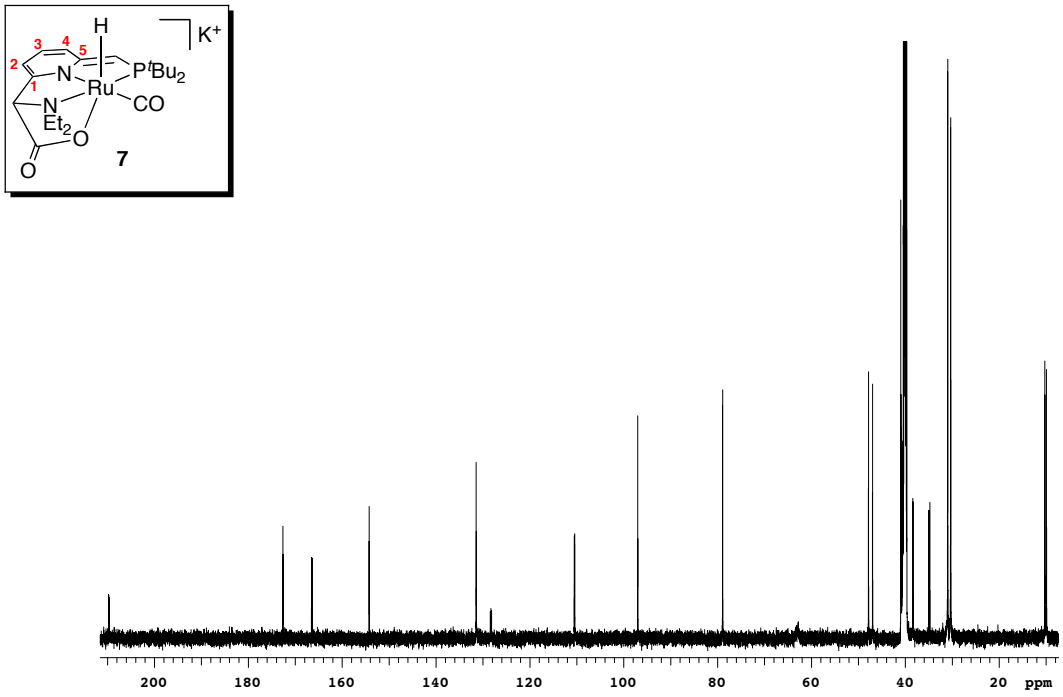

^{1}H-^{1}H gCOSY Spectrum of 7 in DMSO-d_6

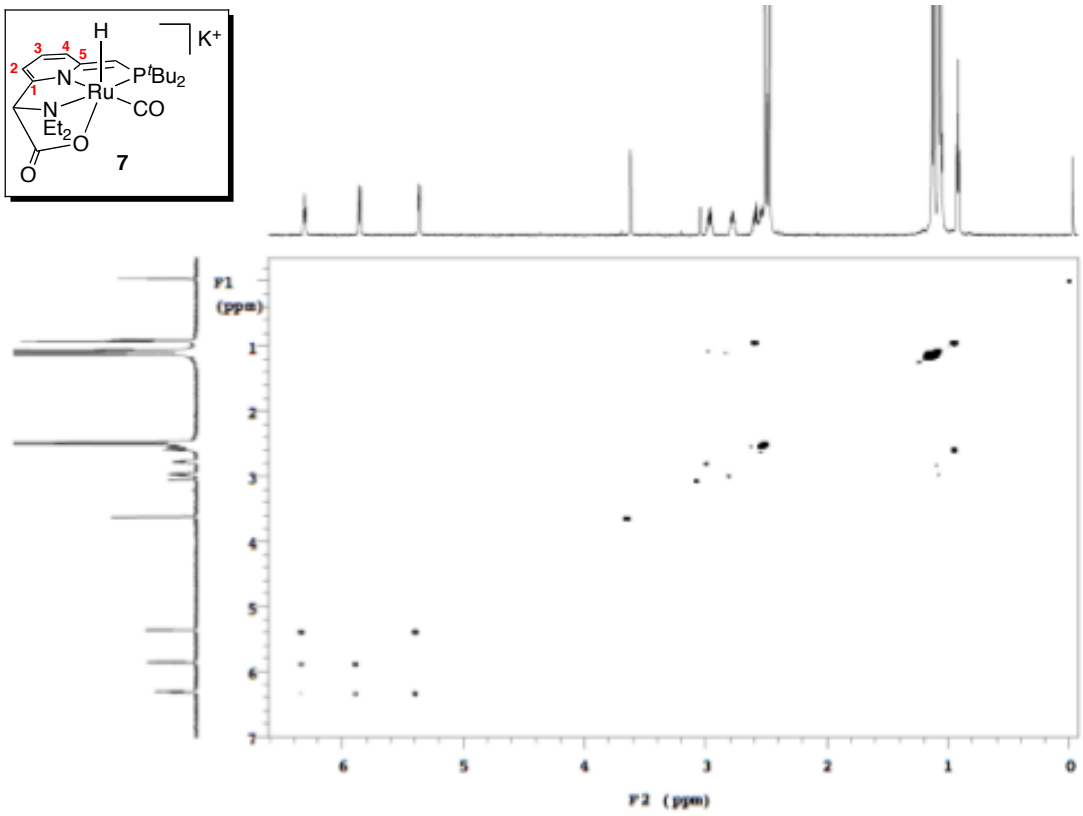

^{1}H-^{13}C gHSQC Spectrum of 7 in DMSO-d_6

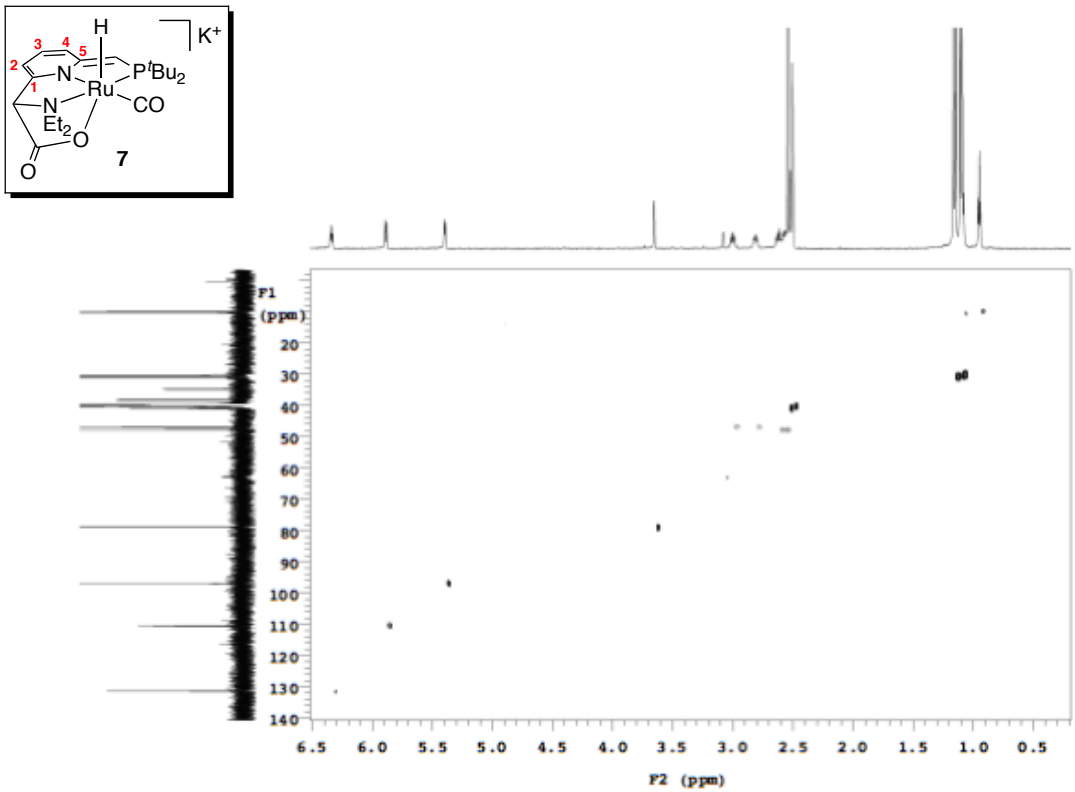

^{1}H-^{13}C gHMBC Spectrum of 7 in DMSO-d_6

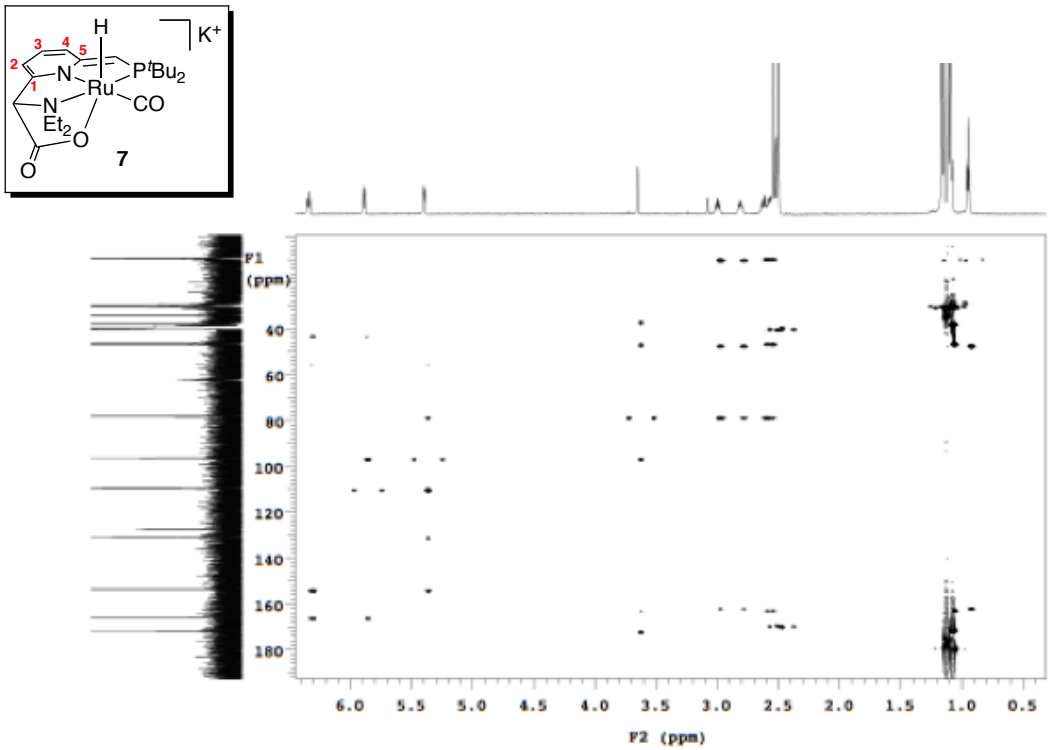

III. Experimental Details for Amide Intermediate Cascade System

A. Procedure for Hydrogenation of CO_2 to CH_3OH (Table 4.6 and Table 4.7)

In an N_2-atmosphere dry box, Ru catalyst (0.0059 mmol, 1 mol%) was dissolved in 2 mL of a solution of $NHMe_2$ in THF (4.6 M, 9.2 mmol, 1600 equiv. relative to Ru), and was added to the metal well of the pressure vessel along with a Teflon octagon magnetic stirbar (5/16 x 1/2 in.). The vessel was sealed and removed from the dry box, where it was then pressurized with 1 bar CO_2 followed immediately by 50 bar H_2. The reaction was heated at 70 ºC for 1 hour before it was ramped to 135 ºC for 18 hours (using Specview software, initial set temperature = 38 ºC and 92 ºC respectively; this was done to prevent over-shooting the desired temperature) at a stir rate of 800 RPM, and then was allowed to cool to room temperature. The vessel was slowly vented using a metering valve through a LN_2-cooled trap. Once the vessel reached atmospheric pressure, the trap was connected to a Schlenk line and the entire system was placed under vacuum, and the liquid contents of the pressure vessel were collected in the trap. The trap was disconnected from the Schlenk line, and allowed to warm to room temperature. 1,3,5-trimethoxybenzene (0.178 mmol, 300 µL of 0.6 M solution in DMSO-d_6) was added as an internal ^{1}H NMR standard, and the contents of the trap were rinsed with DMSO-d_6. 50 µL of this solution was then added to an NMR tube, diluted with DMSO-d_6, and acidified to a pH of 2. The mixture was analyzed by ^{1}H NMR spectroscopy (see Figure 4.11).

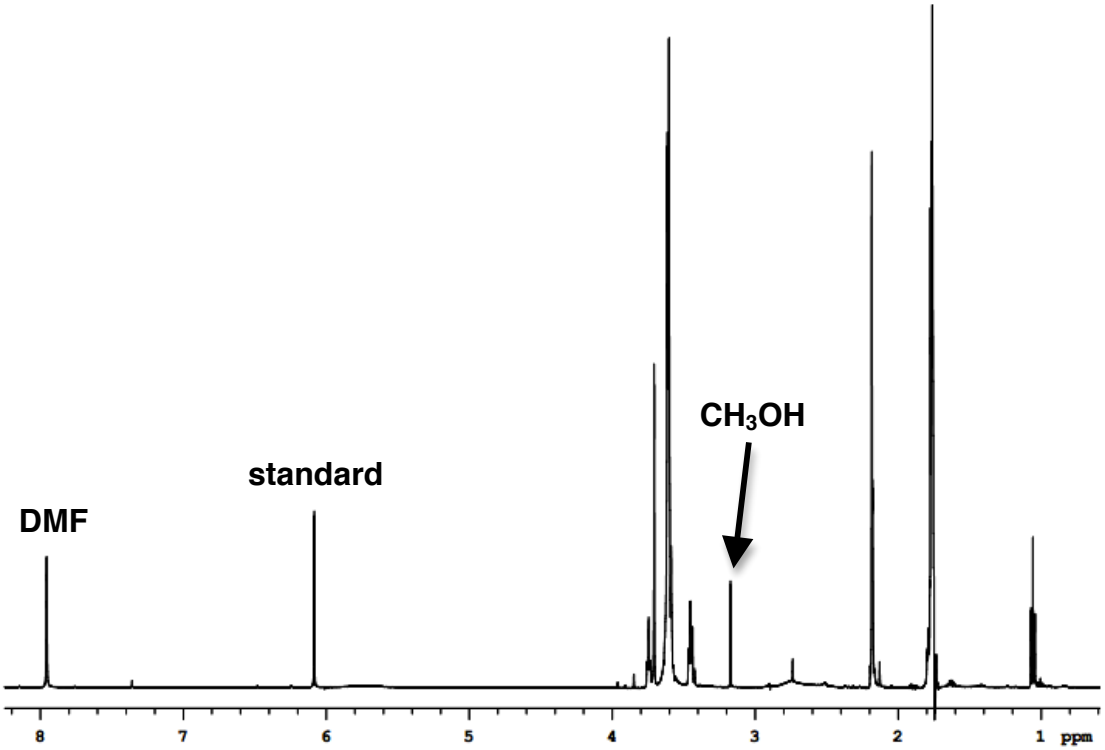

Figure 4.11. Representative ^{1}H NMR Spectrum for Analysis of CH_3OH and DMF in CO_2 Hydrogenation Experiment. NMR experimental details: 10 s relaxation delay, 4 scans acquired, solvent suppression of THF solvent peaks and NH_2Me_2Cl.

*E. Procedure for Reactivity of **10** with CO_2 and H_2*

*I. Synthesis and Characterization of Authentic Sample of **13***

Upon mixing a solution of **10** (2 mg, 4.5 µmol, 1 equiv.) in 0.45 mL toluene-d_8 with FA (1 µL, 0.025 mmol, 6 equiv.) in a J-Young NMR tube, a color change from green/black to red/orange was observed, and red solid precipitated out. An initial ^{1}H NMR spectrum was acquired at room temperature revealing two Ru-H species (Ru–H peaks: –15.77 ppm, br d; –16.52 ppm, br s) where all of the peaks were broad. The NMR spectrometer was then warmed up to 80 ºC for 5 minutes. Upon cooling back to room temperature, a dark brown precipitate had formed and no FA remained in the spectrum. Instead, H_2 was observed, indicating that decomposition of FA to CO_2 and H_2 had occurred.[32] As shown in Figure 4.14, peaks indicative of complex **13** are shown in the ^{1}H NMR spectrum and the gHSQCAD spectrum (Figure 4.13). Note: see Chapter 3 for details on experimental details and analysis for experiment with **2**.

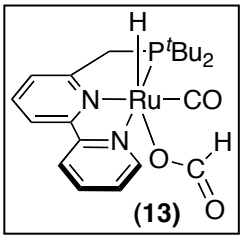

Diagnostic peaks:

^{1}H NMR (toluene-d_8): δ -15.76 (d, J_{HP} = 25.2 Hz, 1H, Ru-*H*), 8.97 (br s, 1H, ***H***COO), 9.16 (br s, 1H, bipyridine-***H***).

^{13}C NMR (toluene-d_8): δ 158.76 (s, bipyridine-***C***), 172.58 (s, H***C***OO).

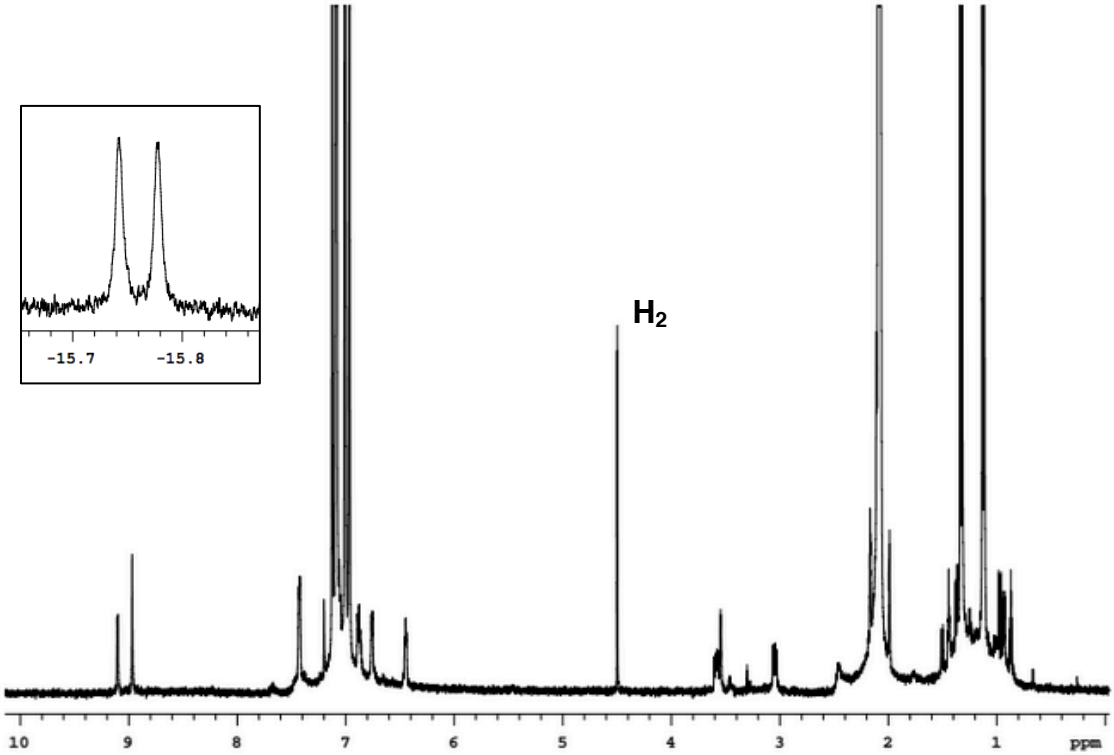

Figure 4.12. ^{1}H NMR Spectrum of **13**: Reaction of **10** with FA

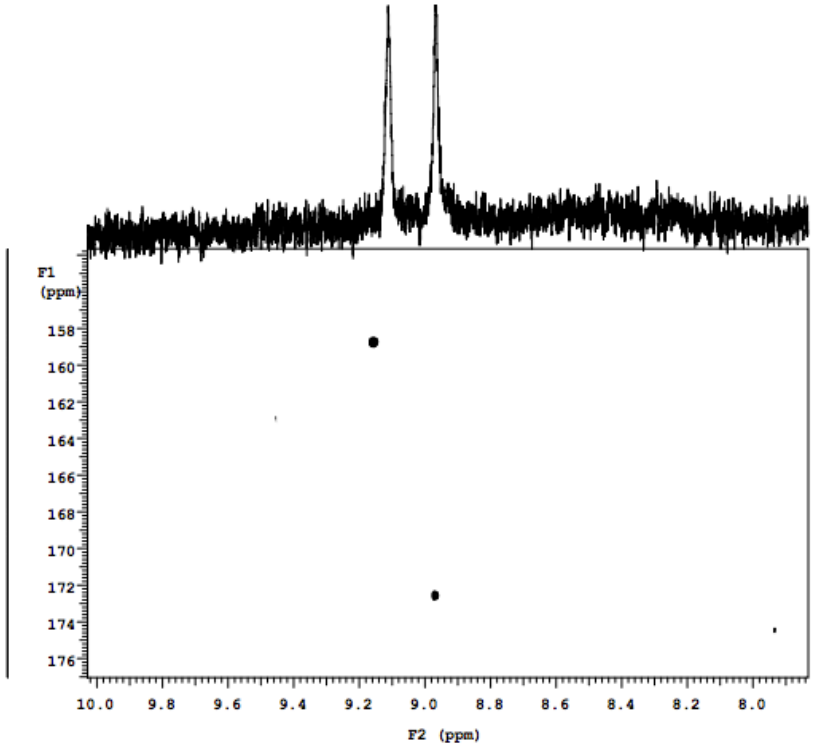

Figure 4.13. gHSQCAD Spectrum of **13**: Reaction of **10** with FA. Experimental details: Band selected: 140-180 ppm, J_{CH} = 220 Hz.

*II. Reaction of **10** with CO_2 and H_2*

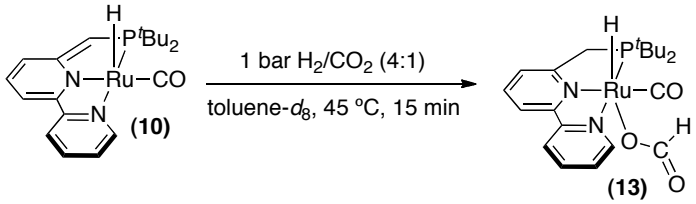

In an N_2-atmosphere dry box, **10** (2.5 mg, 5.6 µmol) and 0.45 mL of toluene-d_8 were added to a J-young tube. The solution was frozen in LN_2, the N_2 atmosphere was removed, the tube was sealed while the solution thawed, and 1 bar H_2/CO_2 (4:1) was then introduced. An initial ^{1}H NMR spectrum was acquired at room temperature revealing two Ru-H species (Ru–H peaks: –15.76 ppm, br d; –16.52 ppm, br s) where all of the peaks were broad. The tube was then heated to 45 ºC in the NMR instrument and cooled back down to room temperature where a dark brown dark precipitate had formed. The complex that remained in solution is shown in Figure 4.14 in a ^{1}H NMR spectrum.

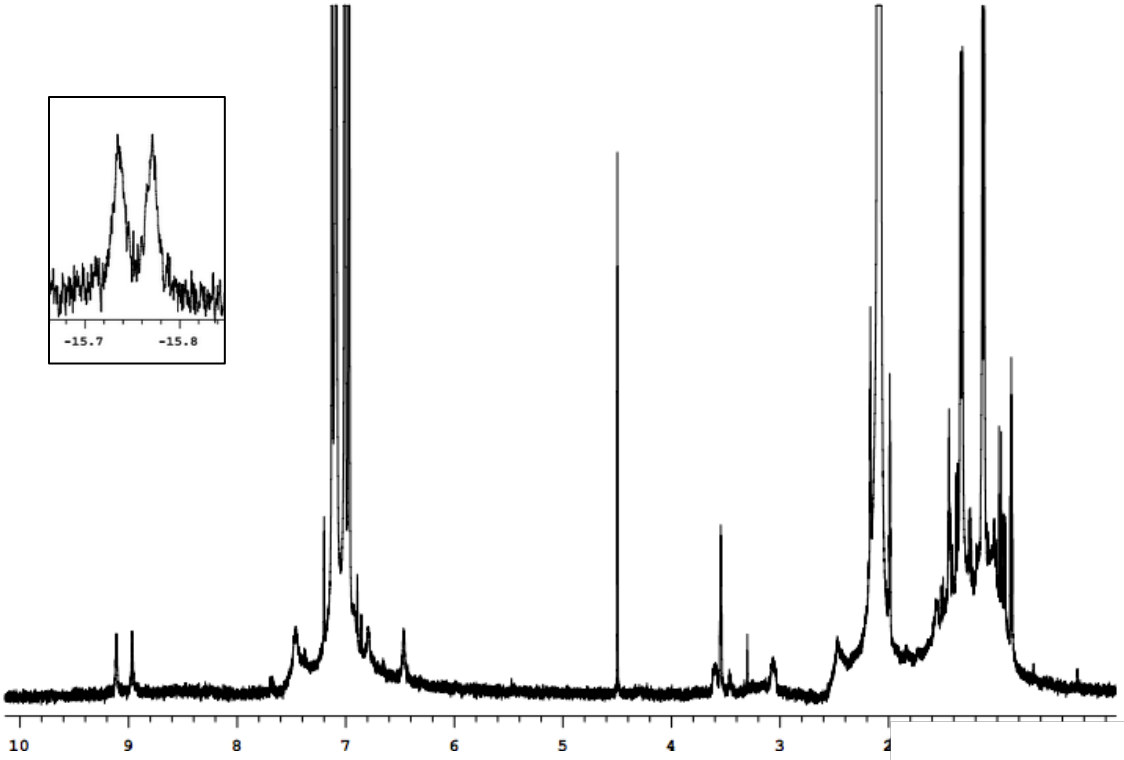

Figure 4.14. ^{1}H NMR Spectrum of **13**: Reaction of **10** with H_2/CO_2

4.6 References

1. Huff, C. A.; Sanford, M. S. Cascade Catalysis for the Homogeneous Hydrogenation of CO_2 to Methanol. *J. Am. Chem. Soc.* **2011**, *133,* 18122.

2. Munshi, P.; Main, A. D.; Linehan, J. C.; Tai, C.-C.; Jessop, P. G. Hydrogenation of Carbon Dioxide Catalyzed by Ruthenium Trimethylphosphine Complexes: The Accelerating Effect of Certain Alcohols and Amines. *J. Am. Chem. Soc.* **2002**, *124*, 7963.

3. For catalytic results: Zhang, J.; Leitus, G.; Ben-David, Y.; Milstein, D. Efficient Homogeneous Catalytic Hydrogenation of Esters to Alcohols. *Angew. Chem., Int. Ed.* **2006**, *45*, 1113; (b) For synthetic procedure: Zhang, G.; Leitus, Y.; Milstein, Ben-David, Y.; Milstein, D. Facile Conversion of Alcohols into Esters and Dihydrogen Catalyzed by New Ruthenium Complexes. *J. Am. Chem. Soc.* **2005**, *127*, 10840.

4. CO_2 hydrogenation to formic acid and/or formate salt: (a) Schaub, T.; Paciello, R. A. A Process for the Synthesis of Formic Acid by CO_2 Hydrogenation: Thermodynamic Aspects and the Role of CO. *Angew. Chem. Int. Ed.* **2011**, *50*, 7278; (b) Wesselbaum, S.; Hintermair, U.; Leitner, W. Continuous-Flow Hydrogenation of Carbon Dioxide to Pure Formic Acid using an Integrated $scCO_2$ Process with Immobilized Catalyst and Base. *Angew. Chem. Int. Ed.* **2012**, *51*, 8585; (c) Zhang, Z.; Xie, Y.; Li, W.; Hu, S.; Song, J.; Jiang, T.; Han, B. Hydrogenation of Carbon Dioxide is Promoted by a Task-Specific

Ionic Liquid. *Angew. Chem. Int. Ed.* **2008**, *47*, 1127; (d) Leitner, W. Carbon Dioxide as a Raw Material: The Synthesis of Formic Acid and Its Derivatives from CO. *Angew. Chem. Int. Ed.* **1995**, *34*, 2207; (e) Jessop, P. G.; Ikariya, T.; Noyori, R. Homogeneous Hydrogenation of Carbon Dioxide. *Chem. Rev.* **1995**, *95*, 259; (f) Jessop, P. G. Homogeneous Hydrogenation of Carbon Dioxide. In *Handbook of Homogeneous Hydrogenation*; Wiley-VCH: Weinheim, Germany, 2007; p 489; (g) Jessop, P. G.; Joo, F.; Tai, C.-C. Recent Advances in the Homogeneous Hydrogenation of Carbon Dioxide. *Coord. Chem. Rev.* **2004**, *248*, 2425; (h) Wang, W.; Wang, S.; Ma, X.; Gong, J. Recent Advances in Catalytic Hydrogenation of Carbon Dioxide. *Chem. Soc. Rev.* **2011**, *40*, 3703; (i) Jeletic, M. S.; Mock, M. T.; Appel, A. M.; Linehan, J. C. A Cobalt-Based Catalyst for the Hydrogenation of CO_2 under Ambient Conditions. *J. Am. Chem. Soc.* Article, **2013**, *135*, 11533; (j) Langer, R.; Diskin-Posner, Y.; Leitus, G.; Shimon, L. J. W.; Ben-David, Y.; Milstein, D. Low-Pressure Hydrogenation of Carbon Dioxide Catalyzed by an Iron Pincer Complex Exhibiting Noble Metal Activity. *Angew. Chem. Int. Ed.* **2011**, *50*, 9948.

5. Werkmeister, S.; Junge, K.; Beller, M. Catalytic Hydrogenation of Carboxylic Acid Esters, Amides, and Nitriles with Homogeneous Catalyisis. *Org. Process Res. Dev.* **2014**, *18*, 289.

6. Tanaka, R.; Yamashita, M.; Nozaki, K. Catalytic Hydrogenation of Carbon Dioxide using Ir(III)-Pincer Complexes. *J. Am. Chem. Soc.* **2009**, *131*, 14168.

7. Computational studies on similar systems suggest that the most likely mechanism involves Ru bound to a tridentate pincer ligand (instead of featuring hemilabity of the pincer ligand). See also ref 8.

8. (a) For a computational study on CO_2 hydrogenation with **1** see: Li, J.; Yoshizawa, K. Catalytic Hydrogenation of Carbon Dioxide with a Highly Active Hydride on Ir(III)-Pincer Complex: Mechanism for CO_2 Insertion and Nature of Metal-Hydride Bond. *Bull. Chem. Soc. Jpn.* **2011**, *84*, 1039; (b) For a computational study on hydrogenation of dimethyl carbonate with **2** see: Yang, X. *ACS Catal.* **2012**, *2*, 964.

9. In Chapter 3 (Scheme 3.14) **2** was treated with H_2 and CO_2 at 120 ºC, whereby a reverse in selectivity for **5**:**6** was observed with <5% yield of **5** and 95% yield of **6**. These data demonstrate that temperature plays an important role in the product distribution for this transformation.

10. For analagous FePNP complex see: Zell, T.; Butschke, B.; Ben-David, Y.; Milstein, D. Efficient Hydrogen Liberation from Formic Acid Catalyzed by a Well-Defined Iron Pincer Complex under Mild Conditions. *Chem. Eur. J.* **2013**, *19*, 8068.

11. For details on the synthesis and characterization of **6**: Huff, C. A.; Kampf, J. W.; Sanford, M. S. Role of a Noninnocent Pincer Ligand in the Activation of CO_2 at (PNN)Ru(H)(CO). *Organometallics* **2012**, *31*, 4643.

12. For binding of CO_2 at a related RuPNP complex see: Vogt, M.; Gargir, M.; Iron, M. A.; Diskin-Posner, Y.; Ben-David, Y.; Milstein, D. A New Mode of Activation of CO_2 by Metal-Ligand Cooperation with Reversible C-C and M-O Bond Formation at Ambient Temperature. *Chem. Eur. J.* **2012**, *18*, 9194.

13. For binding of other carbonyl compounds at **2** see: Huff, C. A.; Kampf, J. W.; Sanford, M. S. Reversible Carbon-Carbon Bond Formation between Carbonyl Comppounds and a Ruthenium Pincer Complex. *Chem. Commun.* **2013**, *49*, 7147.

14. Szmant, H. H. *Organic Building Blocks of the Chemical Industry*; Wiley: New York, 1989, p. 222.

15. Control reactions were performed to probe the direct hydrogenation of K_2CO_3 and $KHCO_3$ to HCOOK (*in the absence* of CO_2) catalyzed by **2**. It was determined that a TON of <5 for K_2CO_3 and 65 for $KHCO_3$ could be detected under the standard conditions "a" described in **Table 4.1**.

16. This value assumes that both K_2CO_3 and $KHCO_3$ can act as bases in the reaction.

17. (a) Federsel, C.; Ziebart, C.; Jackstell, R.; Baumann, W.; Beller, M. Catalytic Hydrogenation of Carbon Dioxide and Bicarbonates with a Well-Defined Cobalt Dihydrogen Complex. *Chem. Eur. J.* **2012**, *18*, 72; (b) Federsel, C.; Boddien, A.; Jackstell, R.; Jennerjahn, R.; Dyson, P. J.; Scopelliti, R.; Laurenczy, G.; Beller, M. A Well-Defined Iron Catalyst for the Reduction of Bicarbonates and Carbon Dioxide to Formates, Alkyl Formates, and Formamides. *Angew. Chem. Int. Ed.* **2010**, *49*, 9777; (c) Ziebart, C.; Federsel, C.; Anbarasan, P.; Jackstell, R.; Baumann, W.; Spannenberg, A.; Beller, M. Well-Defined Iron Catalyst for Improved Hydrogenation of Carbon Dioxide and Bicarbonates. *J. Am. Chem. Soc.* **2012**, *134*, 20701.

18. In all cases, the TOF was calculated using the number of turnovers of formate detected at ~35% conversion. The time required to reach ~35% conversion varied with the catalyst and conditions. Importantly, 35% conversion represents 35% of the maximum observed conversion rather than 35% of the maximum possible conversion.

19. Alternative structures for **8** and **9** involve dissociation of the hemilabile NEt_2 arm, where the anionic oxygen tethered to the ligand could then coordinate to the Ru metal center. However, we cannot determine which structure is the preferred one given our data.

20. The product was isolated in 89% yield, but the isolated material contained ~10% of starting material **6** (presumably generated by protonation).

21. The low yield is thought to be due to the water sensitivity of **7**.

22. (a) Jessop, P. G.; Hsiao, Y.; Ikariya, T.; Noyori, R. Homogeneous Catalysis in Supercritical Fluids: Hydrogenation of Supercritical Carbon Dioxide to Formic Acid, Alkyl Formates, and Formamides. *J. Am. Chem. Soc.* **1996**, *118*, 344; (b) Kröcher, O.: Köppel, R. A.; and Baiker, A. Highly Active Ruthenium Complexes with Bidentate Phosphine Ligands for the Solvent-Free Catalytic Synthesis of *N*,*N*-Dimethylformamide and Methyl Formate. *Chem. Commun.* **1997**, 453.

23. (a) For complex **10**: Balaraman, E.; Gnanaprakasam, B.; Shimon, L. J. W.; Milstein, D. Direct Hydrogenation of Amides to Alcohols and Amines under Mild Conditions. *J. Am. Chem. Soc.* **2010**, *132*, 16756; (b) for analogue of **10**: Barrios-Francisco, R.; Balaraman, E.; Diskin-Posner, Y.; Leitus, G.; Shimon, L. J. W.; Milstein, D. PNN Ruthenium Pincer Complexes Based on Phosphinated 2,2′-Dipyridinemethane and 2,2′-Oxobispyridine. Metal–Ligand Cooperation in Cyclometalation and Catalysis. *Organometallics* **2013**, *32*, 2973.

24. For **12**: John, J. M.; Bergens, S. H. A Highly Active Catalyst for the Hydrogenation of Amides to Alcohols and Amines. *Angew. Chem. Int. Ed.* **2011**, *50*, 10377.

25. Núñez Magro, A. A.; Eastham, G. R.; Cole-Hamilton, D. J. The Synthesis of Amines by the Homogeneous Hydrogenation of Secondary and Primary Amides. *Chem. Commun.* **2007**, 3154.

26. Balaraman, E.; Gunanathan, C.; Zhang, J.; Shimon, L. J. W.; Milstein, D. Efficient Hydrogenation of Organic Carbonates, Carbamates and Formates Indicates Alternative Routes to Methanol Based on CO_2 and CO. *Nature Chemistry* **2011**, *3*, 609.

27. For catalytic results with **11**: Kuriyama, W.; Matsumoto, T.; Ogata, O.; Ino, Y.; Aoki, K.; Tanaka, S.; Ishida, K.; Kobayashi, T.; Sayo, N.; Saito, T. Catalytic Hydrogenation of Esters. Development of an Efficient Catalyst and Processes for Synthesising (R)-1,2-Propanediol and 2-(l-Menthoxy)ethanol. *Org. Process Res. Dev.* **2012**, *16*, 166.

28. (a) Dub, P. A.; Ikariya, T. Catalytic Reductive Transformations of Carboxylic and Carbonic Acid Derivatives Using Molecular Hydrogen. *ACS Catal.* **2012**, *2*, 1718. (b) Greenberg, A.; Chiu, Y.-Y.; Johnson, J. L.; Liebman, J. F. The Resonance Energy of Amides, the Structure of Aziridinone, and Its Relationship to Other Strained Lactams. *Structural Chemistry* **1991**, *2*, 117.

29. An additional difference in reaction conditions between **Table 4.4** and the reported procedure is that 4 mol% of strong base $KN[(SiCH_3)_3Si]_2NK$ was required for appreciable turnover.

30. This peak likely corresponds to Ru-CO_2 adduct on the P-side of **10**. ^{1}H NMR spectrum of **10** treated with CO_2 in THF-d_8 provided a spectrum with broad peaks, and a broad s at –16.83 ppm.

31. Peaks in ^{1}H NMR spectrum at 45 ºC were very broad.

32. At the end of the reaction (after heating to 80 ºC), no FA was observed in the spectrum, and instead H_2 was present. This indicates that **10** acts as a catalyst to facilitate the decomposition of FA into H_2 and CO_2. See the following for a review on similar reports of catalytic decomposition of FA: Loges, B.; Boddien, A.; Gärtner, F.; Junge, H.; Beller, M. Catalytic Generation of Hydrogen from Formic Acid and its Derivatives: Useful Hydrogen Storage Materials. *Top. Catal.* **2010**, *53*, 902.

33. Excerpts of Chapter 4 reprinted with permission from Huff, C. A.; Sanford, M. S. Catalytic CO_2 Hydrogenation to Formate by a Ruthenium Pincer Complex. *ACS Catal.* **2013**, *3*, 2412. Copyright 2013. American Chemical Society.

34. Mainz, V. V.; Andersen, R. A. Preparation of $RuCH_2PMe_2(PMe_3)_3Cl$, $Ru(CH_2PMe_2)_2(PMe_3)_2$, and $Rh_2(CH_2PMe_2)_2(PMe_3)_4$ and Their Reactions with Hydrogen. *Organometallics* **1984**, *3*, 675

35. Young, R.; Wilkinson, G. 85. Dihydrotetrakis(triphenylphosphine)-Ruthenium(II) *Inorg. Synth.* **1990**, *28*, 337.

CHAPTER 5

Cascade Homogeneous and Heterogeneous Catalysis for the Hydrogenation of Carbon Dioxide to Methanol

5.1 Introduction

Anthropogenic CO_2 emissions have begun to offset the natural carbon cycle and are a significant contributing factor to global warming and climate change.[1] For this reason, mitigating CO_2 emissions is an important challenge to be faced in coming decades as the global population continues to grow. One approach to reducing atmospheric CO_2 concentrations is to use abundantly available CO_2 as a C1 building block to synthesize more valuable commodity chemicals. An example of a desirable target commodity chemical is methanol, which has a current global demand of 30 million metric tonnes and serves as an important chemical feedstock,[2] as well as a potential gasoline replacement.[3] Methanol is currently produced from methane-derived synthesis gas (syngas), or CO and H_2, from which the synthesis (equation 1) requires elevated temperatures (220–270 ºC) and pressures (50–100 bar) with a $Cu/Al_2O_3/ZnO$ heterogeneous catalyst.[4] However, there is also precedent for synthesizing CH_3OH from CO_2 and H_2 (equation 2) using similar Cu catalysts. A pilot plant scale operation for CO_2 hydrogenation to CH_3OH was established using the heterogeneous catalyst $Cu/Al_2O_3/ZnO/ZrO_2/Ga_2O_3$ at 250 ºC, thus demonstrating the viability for this process.[5]

$$CO + 2H_2 \rightarrow CH_3OH \quad (1)$$

$$CO_2 + 3H_2 \rightarrow CH_3OH + H_2O \quad (2)$$

Examining the thermodynamics of equation 2, reveals that this reaction is entropically disfavored with $\Delta S^o = -97.8$ calmol^{-1}K^{-1}. Operating at high temperatures with

a negative entropy of a reaction magnifies a negative TΔS term, thus disfavoring the overall reaction, where $\Delta G^o = \Delta H^o - T\Delta S^o$ and $\Delta G^o = 0$ at 47 ºC. This negative affect on the reaction can further be demonstrated by considering the equilibrium constant at 250 ºC where $K_{eq} = 1 \times 10^{-8}$. Therefore, it is desirable to conduct this reaction at lower temperatures in order to achieve an overall higher theoretical yield of methanol. However, reducing the reaction temperature below 220 ºC is kinetically undesirable when using reported heterogeneous catalysts and results in low reaction rates.[4]

In order to address this challenge, we implemented homogeneous catalysis for this reaction, where this system operates at lower reaction temperatures. The cascade system shown in Scheme 5.1 is the first example demonstrating homogeneously catalyzed hydrogenation of CO_2 to CH_3OH. Multiple homogeneous catalysts are employed, where a combination of **A-1**, **B-1**, and **C-1** were most successful operating at 135 ºC.[6] The first step entails conversion of CO_2 to formic acid (FA) using catalyst **A** (step i). This step is followed by an exothermic esterification reaction catalyzed by **B** (step ii), forming a formate ester. The ester is hydrogenated using catalyst **C** and H_2 to CH_3OH and the corresponding ester-derived alcohol (ROH, step iii). Using this system, a TON (turnover number) of 25 was obtained for CH_3OH.

Scheme 5.1. Cascade System for CO_2 Conversion to CH_3OH

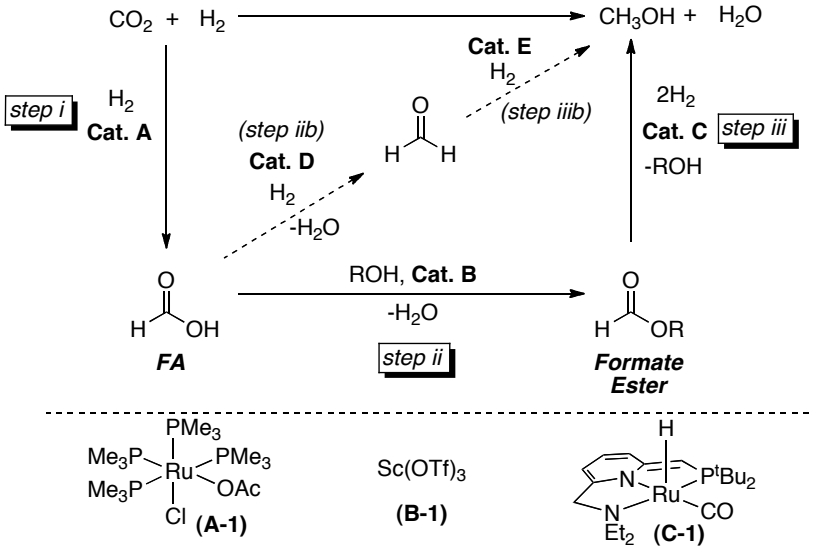

Employing homogeneous catalysts for this reaction provided a route to low temperature CH_3OH synthesis; however, a major challenge for this cascade system was catalyst and reaction component incompatibilities (e.g. **C-1** with CO_2).[7] In an attempt to address this incompatibility, heterogeneous catalysts were considered for substitution into the cascade system. The primary limitation for using heterogeneous catalysts at low temperatures is the rate of the reaction is substantially reduced. To overcome sluggish reaction rates: i) the rate-determining step was identified for the heterogeneous catalyst, ii) a homogeneous catalyst capable of performing the rate determining step at low temperatures was selected; and iii) the homogeneous and heterogeneous catalysts were combined to perform catalysis in tandem (Scheme 5.2). Using this approach, a variety of homogeneous and heterogeneous catalysts were tested together in this cascade system. Furthermore, an added benefit of this approach is that new chemical pathways otherwise not feasible using solely homogeneous catalysts are now available. For example, direct hydrogenation of FA to formaldehyde (Scheme 5.1 step iib) using homogeneous catalysts is not known; however, this reactivity has been demonstrated at heterogeneous Cu surfaces.[8] Hydrogenation of formaldehyde to CH_3OH (step iiib) would complete the cycle, where both homogeneous and heterogeneous systems are precedented for the transformation.

Scheme 5.2. Cascade Homogeneously and Heterogeneously Catalyzed Conversion of CO_2 to CH_3OH

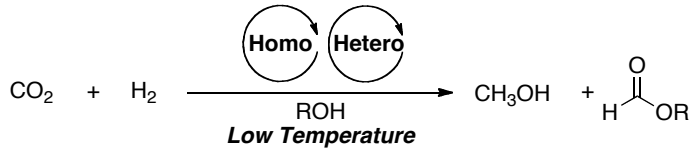

5.2 Literature Reported Heterogeneous Catalysts for CO_2 Hydrogenation to CH_3OH

Commercially available heterogeneous Cu catalysts reported for CO_2 and formate ester hydrogenation were evaluated for the cascade conversion of CO_2 to CH_3OH at 135 ºC, using ethanol (EtOH) as solvent, 10 bar CO_2, and 30 bar H_2. This work was conducted in collaboration with Yuan Chen, a graduate student in UM Chemical

Engineering. Yuan prepared all of the heterogeneous catalysts for these studies. Prior to use, the commercial heterogeneous materials were reduced from Cu–O to Cu[9] through treatment with H_2 at elevated temperatures (between 200–210 ºC). Furthermore, in order to calculate the turnover number (TON) when using a heterogeneous catalyst, a value representing the number of active sites for each catalyst was required. These values were estimated for each catalyst using CO or N_2O uptake studies.[10]

As shown in Table 5.1, **$Cu/Al_2O_3/ZnO$** (**Cu/Al/ZnO**), an analogous material to that used industrially to produce CH_3OH from syngas, yielded a TON of just 2 for the conversion of CO_2 to CH_3OH at 135 ºC (entry 1). This is likely due to reduced kinetics at this lower temperature. $Cu_2Cr_2O_4$ has been demonstrated as a hydrogenation catalyst for formate esters[11] and CO_2[12] and was shown to yield 33 turnovers for CH_3OH and 24 turnovers of ethyl formate (EF) under the reaction conditions (entry 2). To test if steps iib and iiib (Figure 5.1) were operative, EtOH was removed from the system and dioxane was instead used as the reaction solvent. Under these conditions, a TON of just 8 was obtained (entry 3), indicating that ethyl formate is likely an important intermediate in this system.

Table 5.1. Hydrogenation of CO_2 to CH_3OH with Commercially Available Cu Catalysts

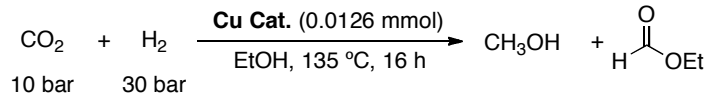

Entry[a]	Catalyst	Active Sites[b] (mmol/g)	Modified Conditions	TON CH_3OH	TON EF
1	**33 wt% Cu/Al/ZnO**	0.133	--	2	5
2[c]	**36 wt% $Cu_2Cr_2O_4$**	0.053	--	33	24
3	**36 wt% $Cu_2Cr_2O_4$**	0.053	dioxane	8	n/a

[a] Conditions: CO_2 (10 bar), H_2 (30 bar), **Cu catalyst** (0.0126 mmol active sites), EtOH (1.5 mL), 135 ºC, 16 h; [b] Active sites per volume of weight of material approximated through surface CO adsorption studies; [c] Dioxane (1.5 mL) was used instead of EtOH.

5.3 Tandem Homogeneous and Heterogeneous Catalysis

Homogeneous catalysts shown in Figure 5.1 were previously tested as catalysts for the homogeneously catalyzed cascade hydrogenation system (Figure 5.1). Ru and Fe complexes/systems **A-1**–**A-3** have been reported to catalyze the conversion of CO_2 to FA

and formate esters (step i and step i/ii),[13] **B-1** and **B-2** are both effective at catalyzing the conversion of FA to EF (step ii)[14], and **C-1** and **C-2** have been demonstrated as catalysts for both step i[15] and step iii[16]. A variety of combinations of these homogeneous catalysts were tested herein with different heterogeneous catalysts in the cascade CO_2 hydrogenation system. Again, the heterogeneous catalysts were prepared by Yuan Chen in UM Chemical Engineering.

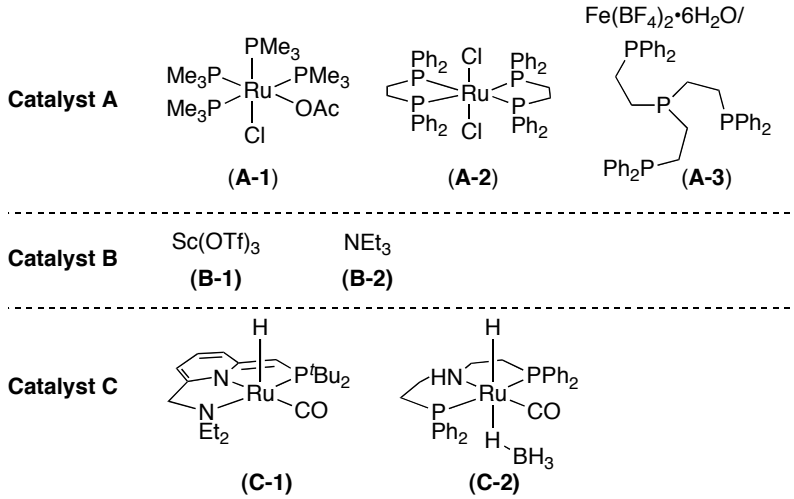

Figure 5.1. Homogeneous Catalysts for Application to the Cascade System

5.3.1 Commercial Heterogeneous Cu Catalysts

Cu/Al/ZnO performed poorly for hydrogenation of CO_2 to CH_3OH, yielding just 4 turnovers for CH_3OH under the standard reaction conditions (Table 5.1, entry 1). Thus homogeneous catalysts were introduced to determine if a synergistic effect could be obtained. Hypothesizing that the slow step for this catalyst is formation of EF, **A-1** was introduced into the reaction conditions. Production of EF significantly increased (Table 5.2, entry 1, TON = 55 vs TON = 5 in Table 5.1, entry 1) when including this CO_2 hydrogenation catalyst; however, conversion to CH_3OH was still low. To address this, ester hydrogenation catalyst **C-1** was added along with **A-1**; however, this resulted in a decrease in the amount of EF formed in the reaction and yielded no increase in CH_3OH generation (entry 2). The combination of **C-1** and **Cu/Al/ZnO** provided the highest TON for CH_3OH at 6; however, catalyst incompatibility does still seem to be an issue, as demonstrated by reduced turnover for EF (entry 3). **$Cu_2Cr_2O_4$** was also tested with **A-1**

(entry 4) and **C-1** (entry 5), but in both cases reduced yields of CH_3OH and EF were observed compared with the unaided heterogeneous catalyst.

Table 5.2. Tandem Homogenous and Heterogeneous Catalysis: Commercial Cu Catalysts

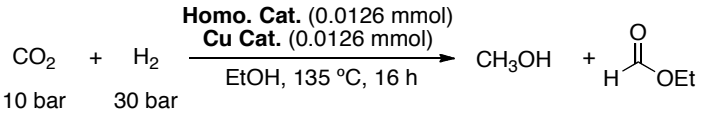

Entry[a]	Homogeneous Catalyst(s)	Heterogeneous Catalyst	TON CH_3OH	TON EF
1	**A-1**	**33 wt% Cu/Al/ZnO**	<1	55
2	**A-1/C-1**	**33 wt% Cu/Al/ZnO**	<1	16
3	**C-1**	**33 wt% Cu/Al/ZnO**	6	25
4	**A-1**	**36 wt% $Cu_2Cr_2O_4$**	<1	32
5[b]	**C-1**	**36 wt% $Cu_2Cr_2O_4$**	2	39

[a] Conditions: CO_2 (10 bar), H_2 (30 bar), **Cu catalyst** (0.0126 mmol active sites), **A-1**, **B-1**, and/or **C-1** (0.0126 mmol), EtOH (1.5 mL), 135 ºC, 16 h. [b] A separate batch of **$Cu_2Cr_2O_4$** was used for this entry.

5.3.2 Mo_2C Supported Metal Catalysts

Commercial Cu supported heterogeneous catalysts do show activity at lower temperatures (135 ºC); however, they are prone to deactivation by components of homogeneous systems. Therefore, we aimed to identify heterogeneous catalysts that would be less prone to deactivation. Molybdenum carbide supported catalysts have been demonstrated to be catalytically active for hydrogenolysis reactions,[17] and furthermore have been reported to be more tolerant of catalyst poisons like H_2S when compared with the Al_2O_3 supported analogue in the Ni catalyzed hydrogenation of arenes.[18]

$CuMo_2C$ was prepared and evaluated for CO_2 conversion to CH_3OH.[19] A turnover number[20] of 13 was observed for CH_3OH and 6 for EF under our standard conditions at 135 ºC (Table 5.3, entry 1). A variety of different homogeneous catalysts and systems for step i were tested (entries 2–4), where **A-1** resulted in an increase in yield for CH_3OH with a TON = 16, accompanied by an increased turnover of EF (entry 2). It was previously demonstrated that combining **A-1** with **B-1** or **B-2** under similar conditions provided significant quantities of formate ester;[6] however, when tested in this system, reduced turnovers were observed (entries 5 and 7). In particular, **B-1** ($Sc(OTf)_3$)

significantly reduced catalytic activity. To address potential Cu deactivation by Sc, a solid supported $Sc(OTf)_3$ was tested. While the deactivation was reduced, the overall yield did not improve (entry 6). **C-1** and **C-2** yielded similar activity to that of the **$CuMo_2C$** alone (entries 8 and 9). Overall, moderate improvement in TON was observed when combining **A-1** with **$CuMo_2C$**. Promisingly, minimal deactivation of the heterogeneous catalyst was observed when treating **$CuMo_2C$** with a number of homogeneous catalysts.

Table 5.3. Tandem Homogenous and **$CuMo_2C$** Catalysis

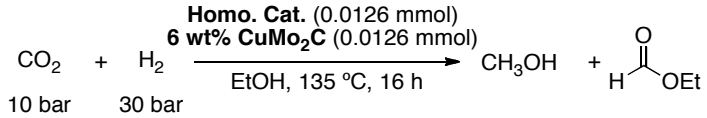

Entry[a]	Homogeneous Catalyst(s)	TON CH_3OH	TON EF
1	--	13	6
2	**A-1**	16	13
3	**A-2**	4	2
4	**A-3**	3	2
5	**A-1 / B-1**	4	11
6[b]	**A-1 / B-1 Polymer**	10	14
7[c]	**B-2**	12	7
8	**C-1**	12	8
9	**C-2**	13	6

[a] Conditions: CO_2 (10 bar), H_2 (30 bar), **Cu catalyst** (0.0126 mmol active sites), **A**, **B**, and/or **C** (0.0126 mmol), EtOH (1.5 mL), 135 ºC, 16 h. [b]0.5-1.5 mmol/g $Sc(OTf)_3$ on 30-60 mesh; [c]115 equiv. **B-2**.

It has been reported that native Mo_2C itself is reactive, where carbides can spontaneously oxidize in the presence of O_2,[21] so as a control study the catalytic activity of **Mo_2C** was tested for this reaction. Interestingly, the Mo_2C native support was highly active under the reaction conditions, yielding a TON = 31 for CH_3OH (Table 5.4, entry 1). However, upon adding **A-1** to improve generation of EF, substantial catalyst poisoning was observed (entry 2). Upon testing other metal supported Mo_2C catalysts, Pd supported Mo_2C[19] was found to yield similar activity to **Mo_2C** (entry 3). Further compatibility tests with a variety of homogeneous catalysts, aimed at promoting steps i

and iii of the cascade system, still gave rise to catalyst poisoning (entries 4–7), albeit to a lesser degree than what was observed with **Mo_2C**. The most successful combination of catalysts was **$PdMo_2C$** with **A-1** (entry 4) or with **C-1** (entry 6), providing TONs of 21 and 22 for CH_3OH, respectively.

Table 5.4. Tandem Homogenous and Heterogeneous Catalysis: Commercial Cu Catalysts

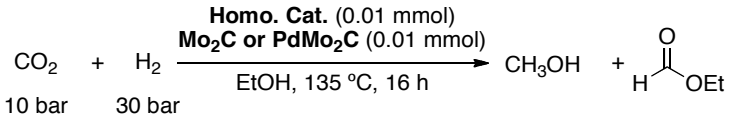

Entry[a]	Homogeneous Catalyst(s)	Heterogeneous Catalyst	Modified Conditions	TON CH_3OH	TON EF
1	--	**Mo_2C (untreated)**	--	31	8
2	**A-1**	**Mo_2C (untreated)**	--	7	9
3[b]	--	**6 wt% $PdMo_2C$**	--	31	7
4	**A-1**	**6 wt% $PdMo_2C$**	--	21	9
5	**A-2**	**6 wt% $PdMo_2C$**	--	9	4
6	**C-1**	**6 wt% $PdMo_2C$**	--	22	10
7	**C-2**	**6 wt% $PdMo_2C$**	--	18	10

[a] Conditions: CO_2 (10 bar), H_2 (30 bar), **Mo_2C** or **$PdMo_2C$** (0.01 mmol active sites), **A** or **C** (0.01 mmol), EtOH (1.5 mL), 135 ºC, 16 h.

5.4 Additional Experiments

5.4.1 Influence of Supplemental Cascade Intermediate on CO_2 Hydrogenation

Promising data was obtained when combining a homogeneous catalyst for step i with a heterogeneous function as a catalyst for steps ii and iii (e.g. Table 5.2, entry 3 and Table 5.3, entry 2). To obtain a better understanding of the influence that significantly increased rates of FA or EF production would have on the reaction, a study was conducted where these cascade intermediates (FA and EF) were added to a heterogeneously catalyzed reaction. With **$CuMo_2C$** as the catalyst, 100 equivalents of FA was added at the onset of the reaction, and a TON of 32 for CH_3OH and 14 for EF was observed (Table 5.5, entry 1). Importantly, the equilibrium for the reaction of catalyst with FA lies far towards CO_2; thus as expectedas approximately 60% of the FA added underwent decarboxylation to form CO_2 and H_2.[22] Further testing the influence of adding EF at the onset of the reaction, provided 83 turnovers for CH_3OH and 27 turnovers for EF (entry 2). Likewise, this experiment was repeated with Mo_2C and similar results were

obtained (entry 3, TON = 92 for CH_3OH). These results indicate that formation of EF during cascade catalysis largely influences the yield of CH_3OH, and that if more EF could be produced at a faster rate under catalytic conditions, the potential yield of CH_3OH is high.

Table 5.5. Hydrogenation of CO_2 to CH_3OH with **$CuMo_2C$**: Affect of Cascade Intermediate

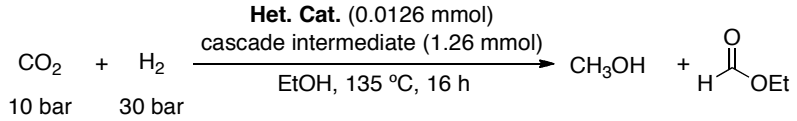

Entry[a]	Heterogeneous Catalyst	Cascade Intermediate	TON CH_3OH	TON EF
1	**6 wt% $CuMo_2C$**	FA	32	14
2	**6 wt% $CuMo_2C$**	EF	83	27[b]
3	**Mo_2C (untreated)**	EF	92	12[b]

[a] Conditions: CO_2 (10 bar), H_2 (30 bar), $CuMo_2C$ (42 mg, 0.0126 mmol), EtOH (1.5 mL), FA or EF (1.26 mmol, 100 equiv. relative to $CuMo_2C$), 135 ºC, 16 h; [b] Represents summation of EF produced in the reaction and recovered EF.

5.5 Potential Deactivation Modes for Mo_2C Heterogeneous Catalysts

The primary limitation to combining homogeneous and heterogeneous catalysis for the CO_2 hydrogenation to CH_3OH, is catalyst incompatibility. In order to understand potential deactivation pathways, the heterogeneous catalyst was collected and examined after the tandem homogeneously/heterogenously catalyzed reaction was complete. Through ICP (inductively coupled plasma) analysis of the atomic composition of the material, insight into modes of deactivation at the heterogeneous active sites could be evaluated.

After washing the residue recovered from the **Mo_2C** and **A-1** catalyzed reaction (Table 5.4, entry 2) with THF (tetrahydrofuran), to remove any residual homogeneous catalyst, ICP analysis was conducted. As shown in Table 5.6, 7 μmol of P and 1 μmol Ru were deposited on the heterogeneous catalyst surface during the reaction (entry 1). Considering that the **Mo_2C** catalyst used in this reaction contains 10 μmol of active sites, 70% of these sites are potentially poisoned by the homogeneous PMe_3 ligand. Similarly, the combination of **$PdMo_2C$** with **A-1** (Table 5.4, entry 4) yielded significant P

adsorption (entry 2, 6 μmol P), but demonstrated less deposition of Ru compared with **Mo_2C**. We anticipated that the binding of P to the heterogeneous surface would be reduced using **C-1** since the tridentate pincer ligand is expected to be less prone to dissociation from the Ru metal center compared with monodentate PMe_3 ligands. Furthermore, the *tert*-butyl substitution provides a bulkier and less nucleophilic P. Indeed, upon combining **$PdMo_2C$** with **C-1** (Table 5.4, entry 6), just 1 μmol P was adsorbed to the surface; however, 1 μmol Ru still deposited on the catalyst surface (entry 3). Based on the data inferred from ICP analysis, it appears that both phosphines and Ru could be the source of deactivation of **Mo_2C** and metal supported **Mo_2C** heterogeneous catalysts, although P poisoning can be attenuated through the use of bulky multidentate phosphine ligands. Further studies will be required to deconvolute the specific deactivation roles of each Ru and P.

Table 5.6. ICP Analysis for Determination of Mechanism for Heterogeneous Catalyst Deactivation

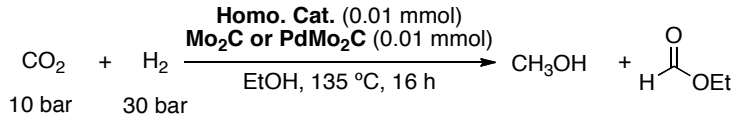

Entry[a]	Homogeneous Catalyst	Heterogeneous Catalyst	%Ru	μmol Ru	%P	μmol P
1	**A-1**	**Mo_2C (untreated)**	12	1	17	7
2	**A-1**	**6 wt% $PdMo_2C$**	4	<1	14	6
3[b]	**C-1**	**6 wt% $PdMo_2C$**	11	1	12	1

[a] Conditions: CO_2 (10 bar), H_2 (30 bar), **Mo_2C** or **$PdMo_2C$** (0.01 mmol active sites), **A-1** or **C-1** (0.01 mmol), EtOH (1.5 mL), 135 °C, 16 h. Note: Percentages of P and Ru are calculated relative to the amount of Mo detected and are represented as a fraction of the total atom added at the onset of the reaction.

5.6 Conclusions and Outlook

The feasibility of combining homogeneous and heterogeneous catalysts together for low-temperature cascade hydrogenation of CO_2 to CH_3OH was demonstrated. Commercially available Cu catalysts like **$Cu/Al_2O_3/ZnO$** and **$Cu_2Cr_2O_4$** were shown to be more prone to poisoning by homogeneous catalysts compared with metal supported **XMo_2C** catalysts (X = Cu or Pd). Overall, catalyst incompatibilities between

homogeneous and heterogeneous components of the system remain the primary limitation to this system.

Moving forward, evaluating poisoning of heterogeneous catalysts by homogeneous ligands and metals will provide a better understanding of the general tolerance of the heterogeneous catalyst toward homogeneous systems and reduce superfluous catalyst synthesis. Some ligands and metals that are of particular interest, due to their frequent use in hydrogenation catalysis, are shown in Figure 5.2. Additionally, increasing ethyl formate production in the cascade system was demonstrated to greatly increase the TON for CH_3OH. Therefore, other homogeneous and heterogeneous catalysts for steps i and ii will be considered.

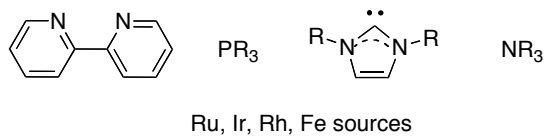

Figure 5.2. Potential Homogeneous Ligands and Metal Sources for Application in the Tandem Homogeneous/Heterogeneously Catalyzed System. R = Alkyl Group

5.7 Experimental Procedures and Characterization of Data

General Procedures

NMR spectra were obtained on a Varian VNMRs 500 MHz (499.90 MHz for ^1H; 125.70 MHz for ^{13}C) spectrometer. Chemical shifts were referenced to an internal standard (tetramethylsilane for ^1H). All high-pressure reactions were carried out using a Parr Model 5000 Multiple Reactor system that includes six 50 mL vessels equipped with flat-gaskets and head mounting valves. The system was operated with a 4871 process controller and SpecView version 2.5 software. A Swagelok SS Medium-Flow metering valve was used during the collection of volatile products from the pressurized reaction vessels. ICP-OES data was obtained on a Perkin-Elmer Optima 2000 DV or a Varian 710-ES analyzer with Winlab software. A quartz flow-through reactor with a mass flow controller was used to reduce and synthesize heterogeneous materials. X-ray diffraction (XRD, Miniflex 600) was utilized to determine the phases of the reduced catalysts. Surface areas (BET) were measured using N_2 physisorption equipped with Micromeritics ASAP 2010 analyzer.

Materials and Methods

All experiments were conducted under an oxygen-free atmosphere in either a glovebox or using Schlenk line technique, and all liquids were degassed using three freeze-pump-thaw cycles. $Ru(PMe_3)_4(OAc)Cl$ (**A-1**),[23] $Ru(dppe)_2Cl_2$ (**A-2**),[24] (PNN)Ru(H)(CO) (**C-1**),[25] Mo_2C,[19] $CuMo_2C$,[19] and $PdMo_2C$[19] were prepared according to a literature procedure. All the heterogeneous samples were used stored and transferred in an oxygen/moisture free environment after the pretreatment and were degassed (< 5 mm Hg) at elevated temperature for 4 hours (Cu-based commercial catalysts at 200 °C and Mo_2C-based catalysts at 350 °C) prior to the BET measurements. Dry carbon dioxide (99.8%) and ultra high purity hydrogen (99.999%) were purchased from Metro Welding. Ethyl formate (Acros) was purified by distillation from P_2O_5. Scandium triflate, iron tetrafluoroborate hexahydrate, and tris[2-(diphenylphosphino)ethyl]phosphine, and scandium triflate polymer-bound were purchased from Sigma Aldrich and used as is. Ethanol (VWR) was dried over magnesium turnings and triethylamine (Acros) was dried over CaH_2. DMSO-d_6 (Cambridge Isotopes Laboratories), *N,N*-dimethylformamide (Alfa Aesar, 99.8%) , formic acid (Aldrich), anhydrous dioxane (Acros, 99%), and Carbonylchlorohydrido[bis(2-(diphenylphosphinoethyl)amino]ruthenium(II) or Ru-MACHO (**C-2**) (Strem) were used as is. CuO/Cr_2CuO_4 (62-64% Cr_2CuO_4, 22-24% CuO, 6% BaO, 0-4% Graphite, 1% CrO_3, 1% Cr_2O_3) was purchased from Strem and $CuO/Al_2O_3/ZnO$ ("Megamax 700" 33 wt% Cu as determined by ICP analysis) was purchased from Süd-Chemie. ICP standards were purchased from the following vendors: Mo, Pd (GFS Chemicals), Ru (Fisher Scientific), Y (Ricca Chemicals), and P (Aldrich).

Experimental Details

I. Preparation and Characterization of Heterogeneous Catalysts

A. Reduction of Commercial Heterogeneous Cu Catalysts using H_2

CuO/Cr_2CuO_4 or $CuO/Al_2O_3/ZnO$ were acquired commercially as pellets and were crushed and sieved to a particle size range of 125-250 μm. 200 grams of powder was supported in a tubular quartz reactor with catalysts loaded on a quartz wool bed and placed in a vertical furnace. The powder was exposed to 4% H_2 in N_2 flowing at 50

mL/min where the temperature was ramped from 25 ºC to 200 ºC for $Cu/Al_2O_3/ZnO$ and 210 ºC for CuO/Cr_2CuO_4 at a rate of 4 ºC/min. Once at 200 ºC or 210 ºC, the temperature was held for 4 hours. XRD (X-ray diffraction) analysis was used to verify that the CuO was completely reduced to metallic Cu. BET (Brunauer-Emmett-Teller) measurements were acquired to obtain surface area measurements and ICP analysis was conducted to determine the Cu composition (Note: these experiments were performed by Yuan Chen).

Table 5.7. BET Analysis of Heterogeneous Catalysts

Entry[a]	Heterogeneous Catalyst	BET Surface Area (m^2/g)	Cu Composition (wt%)
1	**Cu/Al/ZnO**	59.6	32.6
2	**$Cu_2Cr_2O_4$**	46.2	35.7
3	**$CuMo_2C$**	135.1	5.8
4	**Mo_2C**	150.8	<1

II. CO_2 Hydrogenation

A. Procedure for CO_2 Hydrogenation to CH_3OH

In an N_2-atmosphere dry box, a solution of homogeneous catalyst(s) (0.01 mmol, 1 equiv.) in 1.5 mL EtOH was added to a 30 mL glass liner containing heterogeneous catalyst (0.01 mmol, 1 equiv.) and a Teflon octagon magnetic stirbar (5/16 x 1/2 in.). Before inserting the liner into the well of the pressure vessel, 1.5 mL of EtOH was added to the well of the pressure vessel. The vessel was sealed and removed from the dry box, where it was pressurized with 10 bar CO_2 followed immediately by 30 bar H_2. The reaction was then heated at 135 ºC (using Specview software, initial set temperature = 92 ºC; this was done to prevent over-shooting the desired temperature) for 16 hours at a stir rate of 800 RPM (rotations per minute), and was then allowed to cool to room temperature. It was next slowly vented using a metering valve through a LN_2-cooled trap. Once the vessel reached atmospheric pressure, the trap was connected to a Schlenk line and the entire system was placed under vacuum, and the liquid contents of the pressure vessel were then collected in the trap. The trap was disconnected from the Schlenk line, and allowed to warm to room temperature. DMF (0.519 mmol, 40 µL, 52 equiv.) was added as an internal ^1H NMR standard and the contents of the trap were rinsed with DMSO-d_6. 50 µL of this solution was then added to an NMR tube, and diluted with

DMSO-d_6. The mixture was analyzed by ^{1}H NMR spectroscopy (see Figure 5.3). The error associated with these reactions is on the order of +/-5 TONs when using the same batch of heterogeneous catalyst and +/- 3 TONs between batches of heterogeneous catalyst.

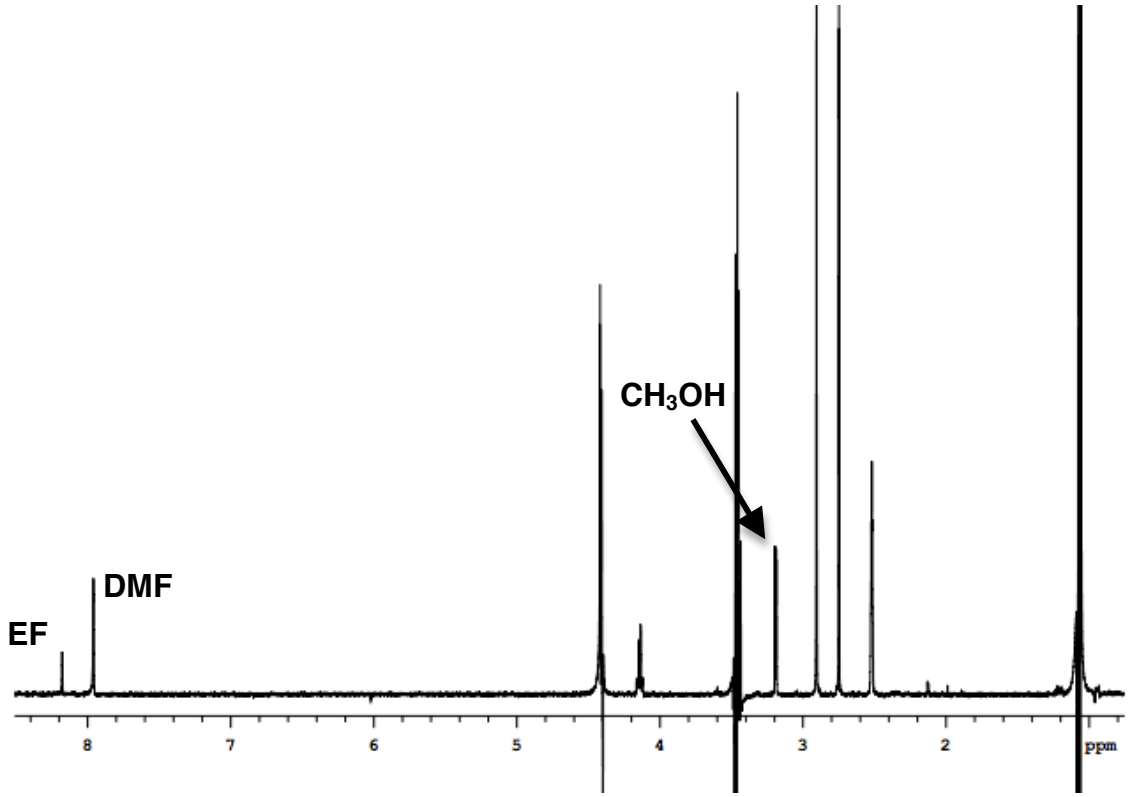

Figure 5.3. Representative ^{1}H NMR spectrum for CO_2 Hydrogenation to CH_3OH. NMR experimental details: 10 s relaxation delay, 4 scans acquired, solvent suppression of EtOH solvent peaks.

B. ICP Analysis On Heterogeneous Catalysts

ICP Sample Preparation: The work-up described in section A above was performed on the tandem homogeneously/heterogeneously catalyzed reaction, where during the last step before disconnecting the trap from the schlenk line, the pressure vessel was filled with N_2. The vessel was then opened in air and the solid residue remaining in the glass liner was quickly transferred to a 4 mL vial and immediately pumped into a N_2-atmosphere dry box. Once inside the dry box, the solid was washed with dry THF (3 x 3 mL) to remove any homogeneous catalyst from the residue. The material was removed

from the glovebox and allowed to dry in air before approximately 4 mg of the solid material was digested with 1.5 mL of a 3:1 $HCl:HNO_3$ solution. An ytterium ICP standard (1 ppm) was added to the solution.

Calibration Curve: Varying concentrations of standard solutions of Y (internal standard), Mo, Ru, Pd, and P atoms were analyzed in order to generate calibration curves using the selected atomic spectral lines listed for each atom shown in Table 5.8. Note: the P spectral line at 213.617 nm is close to a spectral Mo line at 213.620 nm. In order to quantify any resulting interference, a 250 ppm sample of Mo (similar concentration to experimental samples that were analyzed) was analyzed for P. A concentration of 0.085 ppm for P was determined for this sample and the spectral interference may attribute 1–4% error in the P yield calculation in the experimental samples.

Table 5.8. Concentration of Calibration Standards for ICP Analysis

	Concentration of Analyte (ppm)				
Calibration Sample	**Y (371.029 nm)**	**Mo (202.031 nm)**	**Ru (240.272 nm)**	**Pd (340.458 nm)**	**P (213.617 nm)**
Blank	1	--	--	--	--
A	1	200	1	1	1
B	1	250	5	5	5
C	1	300	10	10	10

Determination of Atomic Concentrations: Using the calibration curve, the concentration of each atom in the experimental sample could be determined. Assuming all Mo that was initially added was recovered at the end of the reaction, the molar ratio of Mo to Ru or P was quantified. Furthermore, the moles of Ru and P calculated can be compared with the initial moles of Ru and P added in the reaction in order to determine the percentage of each atom that adsorbed to the heterogeneous surface.

5.8 References

1. Prentice, I. C. The Carbon Cycle and Atmospheric Carbon Dioxide. In *Climate Change 2001: The Scientific Basis*. Cambridge Univeristy Press, 2001, pp. 183.

2. Methanol Utilisation Technologies. In *Methanol: The Basic Chemical and Energy Feedstock of the Future: Asinger's Vision Today.* Bertau, M.; Offermanns, H.; Plass, L.; Schmidt, F.; Wernicke, H.-J., Eds.; Wiley, 2014, pp. 327.

3. Olah, G. A.; Goeppert, A.; Prakash, G. K. S. Beyond Oil and Gas: The Methanol Economy. Weinheim: Wiley, 2006; pp 193.

4. Lee, S. Methanol Synthesis from Syngas. In *Handbook of Alternative Fuel Technologies*. CRC Press, 2007, pp 297.

5. Ushikoshi, K.; Moria, K.; Watanabe, T.; Takeuchi, M.; Saito, M. A 50 kg/day Class Test Plant for Methanol Synthesis from CO_2 and H_2. *Stud. Surf. Sci. Catal.* **1998**, *114*, 357.

6. Huff, C. A.; Sanford, M. S. Cascade Catalysis for the Homogeneous Hydrogenation of CO_2 to Methanol. *J. Am. Chem. Soc.* **2011**, *133,* 18122.

7. Huff, C. A.; Kampf, J. W.; Sanford, M. S. Role of a Noninnocent Pincer Ligand in the Activation of CO_2 at (PNN)Ru(H)(CO). *Organometallics* **2012***, 31*, 4643.

8. Weigel, J.; Koeppel, R. A.; Baiker, A.; Wokaun, A. Surface Species in CO and CO_2 Hydrogenation over Copper/Zirconia: On the Methanol Synthesis Mechanism. *Langmuir* **1996**, *12*, 5319.

9. Cu supported heterogeneous catalysts sold as Cu-O not reduced Cu. Cu–O is stable toward O_2, and thus safer and more stable to store and distribute.

10. For experiments determining the active sites for Cu heterogeneous material using CO or N_2O uptake experiments: (a) Cu/Al/ZnO: Schaidle, J. A.; Lausche, A. C.; Thompson, L. T. Effects of Sulfur on Mo_2C and Pt/Mo_2C Catalysts: Water Gas Shift Reaction. *J. Catal.* **2010**, *272*, 235; (b) $Cu_2Cr_2O_4$: Gormley, R. J.; Rao, V. U. S.; Soong, Y. Methyl Formate Hydrogenolysis for Low-Temperature Methanol Synthesis. *Appl. Catal. A-Gen.* **1992**, *87*, 81.

11. Evans, J. W.; Casey, P. S.; Wainwright, M. S.; Trimm, D. L.; Cant, N. W. Hydrogenolysis of Alkyl Formates over a Copper Chromite Catalyst. *Appl. Catal.* **1983**, *7*, 31.

12. Ma, L.; Tran, T.; Wainwright, M. S. Methanol Synthesis from CO_2 using Skeletal Copper Catalyst Containing Co-Precipitated Cr_2O_3 and ZnO. *Top. in Catal.* **2003**, *22*, 295.

13. For catalytic results for step i: (a) **A-1**: Munshi, P.; Main, A. D.; Linehan, J. C.; Tai, C.-C.; Jessop, P. G. Hydrogenation of Carbon Dioxide Catalyzed by Ruthenium Trimethylphosphine Complexes: The Accelerating Effect of Certain Alcohols and Amines. *J. Am. Chem. Soc.* **2002**, *124*, 7963; (b) **A-2**: Kröcher, O.; Köppel, R. A.; Baiker,

A. Highly Active Ruthenium Complexes with Bidentate Phosphine Ligands for the Solvent-Free Catalytic Synthesis of *N*, *N*-Dimethylformamide and Methyl Formate. *Chem. Commun*. **1997**, 453; (c) **A-3**: Federsel, C.; et al. A Well-Defined Iron Catalyst for the Reduction of Bicarbonates and Carbon Dioxide to Formates, Alkyl Formates, and Formamides. *Angew. Chem., Int. Ed.* **2010**, *49*, 9777.

14. (a) **B-1**: Barrett, A. G. M.; Braddock, D. C. Scandium(III) or Lanthanide(III) Triflates as Recyclable Catalysts for the Direct Acetylation of Alcohols with Acetic Acid. *Chem. Commun.* **1997**, 351; (b) **B-2**: Jessop, P. G.; Hsiao, Y.; Ikariya, T.; Noyori, R. Homogeneous Catalysis in Supercritical Fluids: Hydrogenation of Supercritical Carbon Dioxide to Formic Acid, Alkyl Formates, and Formamides. *J. Am. Chem. Soc.* **1996**, *118*, 344.

15. For catalytic results for step i: (a) **C-1**: Huff, C. A.; Sanford, M. S. Catalytic CO_2 Hydrogenation to Formate by a Ruthenium Pincer Complex. *ACS Catal.* **2013**, *3*, 2412; (b) **C-2**: see Chapter 4.3 of this dissertation.

16. For catalytic results for step iii: (a) **C-1**: Zhang, J.; Leitus, G.; Ben-David, Y.; Milstein, D. Efficient Homogeneous Catalytic Hydrogenation of Esters to Alcohols. *Angew. Chem., Int. Ed.* **2006**, *45*, 1113; (b) **C-2**: Kuriyama, W.; Matsumoto, T.; Ogata, O.; Ino, Y.; Aoki, K.; Tanaka, S.; Ishida, K.; Kobayashi, T.; Sayo, N.; Saito, T. Catalytic Hydrogenation of Esters. Development of an Efficient Catalyst and Processes for Synthesising (R)-1,2-Propanediol and 2-(l-Menthoxy)ethanol. *Org. Process Res. Dev.* **2012**, *16*, 166.

17. Lee, J. S.; Locatelli, S.; Oyama, S. T.; Boudart, M. Molybdenum Carbide Catalysts 3. Turnover Rates for the Hydrogenolysis of *n*-Butane. *J. Catal.* **1990**, *125*, 157.

18. Frauwallner, M.-L.; López-Linares, Lara-Romero, J.; Scott, C. E.; Vieman, A.; Hernández, E.; Pereira-Almao, P. Toluene Hydrogenation at Low Temperature using a Molybdenum Carbide Catalyst. *Appl. Catal. A-Gen.* **2011**, *394*, 62.

19. For preparation of Mo_2C, $CuMo_2C$, and $PdMo_2C$ see: Schaidle, J. A.; Schweitzer, N. M.; Ajenifujah, O. T.; Thompson, L. T. On the Preparation of Molybdenum Carbide-Supported Metal Catalysts. *J. Catal.* **2012**, *289*, 210.

20. Note: number active sites used for $CuMo_2C$ and $PdMo_2C$ were approximated by using experimental value determined for Mo_2C = 0.3 mmol/g. See ref 10a.

21. Schweitzer, N. M.; Schaidle, J. A.; Ezekoye, O. K.; Pan, X.; Linic, S.; Thompson, L. T. High Activity Carbide Supported Catalysts for Water Gas Shift. *J. Am. Chem. Soc*. **2011**, *133*, 2378.

22. This value was estimated based on there being no FA was observed at the end of the reaction.

23. Synthesis of **A-1**: Mainz, V. V.; Andersen, R. A. Preparation of $RuCH_2PMe_2(PMe_3)_3Cl$, $Ru(CH_2PMe_2)_2(PMe_3)_2$, and $Rh_2(CH_2PMe_2)_2(PMe_3)_4$ and Their Reactions with Hydrogen. *Organometallics* **1984**, *3*, 675.

24. Synthesis of **A-2**: Mason, R.; Meek, D. W.; Scollary, G. R. Polyphosphine Complexes of Ruthenium(II). *Inorg. Chim. Acta*, **1976**, *16*, L11.

25. Synthesis of **C-1**: Zhang, G.; Leitus, Y.; Milstein, Ben-David, Y.; Milstein, D. Facile Conversion of Alcohols into Esters and Dihydrogen Catalyzed by New Ruthenium Complexes. *J. Am. Chem. Soc.* **2005**, *127*, 10840.